

4 Safety Evaluation Review supplemental notes

Objective: This section collects and formalizes several analyses that I developed as personal notes during the early stages of the safety evaluation review of the Yucca Mountain (YM) license application. These analyses provide supplemental information related to the interaction between uncertainty, variability, transport, and performance assessment calculations. The original analyses, completed in March, 2009, were intended to guide me in understanding which aspects of the natural system have substantial impacts on performance assessment calculations. If there are additional annotations added for completeness, the annotations are indicated and dated for clarity.

06/15/10 TSPA realization dose histories.



Annotation dated 06/15/10: This section is reproduced almost verbatim from my personal notes last modified on March 30, 2009, with some formatting alterations. In this section, I first looked at the set of dose histories calculated by the TSPA code that DOE provided as part of the license application. DOE uses the nominal scenario to represent undisturbed conditions, but considers the seismic scenario to be the most representative. The seismic and igneous scenarios represent the two disruptive scenarios that have the largest dose consequences.



Figures 4-1, 4-2, and 4-3 plot individual realization histories extracted from TSPA for different disruptive scenarios. The histories are color-coded according to the infiltration scenario used in the realization. Heavy lines represent the mean concentration for all of the realizations with the same scenario. Symbols represent the expected value of the maximum dose and the maximum expected dose for each infiltration scenario. Figures 4-4, 4-5, and 4-6 plot the same realizations represented in a different way.

Annotation dated 06/15/10: The first set of three figures show calculated dose, the second set shows dose normalized by the regulatory dose standard. In the second set, there is a precipitous drop in dose at 10,000 years (10 ky) because the dose standard changes from 15 to 100 millirem at that point in time. I indicated the climate states as a background color. Things I noted from these figures:

- *The individual realizations have a wide range in doses at any point in time relative to the mean curve*
- *The wetter mean curves tend to have somewhat larger values than the drier mean curves*

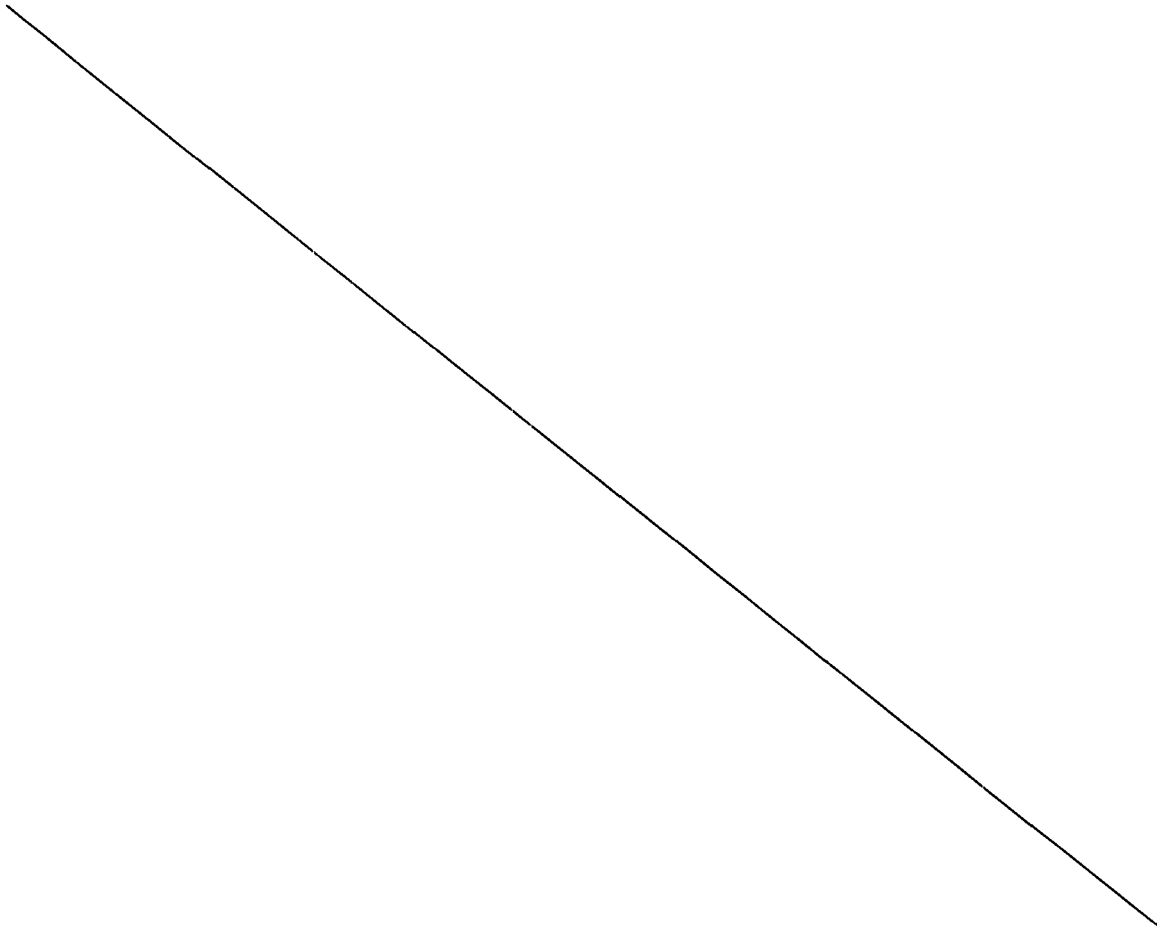
Annotation dated 4/19/11:

Figures 4-1 through 4-6 display "hair" plots of realizations from the TSPA-LA nominal, seismic, and igneous scenarios. These plots report maximum expected values and expected maximum values for the infiltration scenarios, given a disruption scenario. The regulatory dose limit is provided as a reference curve in Figures 4-1 through 4-3. In Figures 4-4 through 4-6 I normalized by the regulatory dose limit to visually examine the relative influence of the step change in the dose standard at 10,000 years (i.e., does a maximum with respect to the limit occur in the first 10,000 years or in the post-10,000-year period).

I used the figures to provide insight into the effects of infiltration on calculated dose under different infiltration and disruption scenarios. Each infiltration scenario has a different conditional probability, as does each disruption scenario. Each of the reported expected values in the figures represents just the realizations included in the combination of infiltration and disruption scenario without adjusting for the probability of the scenario. The reported expected values would be more precisely labeled as conditional expected values given both the infiltration scenario and the disruption scenario.

Note that if one wanted to combine the expected values for a regulatory comparison to the dose limit, one would need to multiply the expected values by the scenario probabilities.

SAS



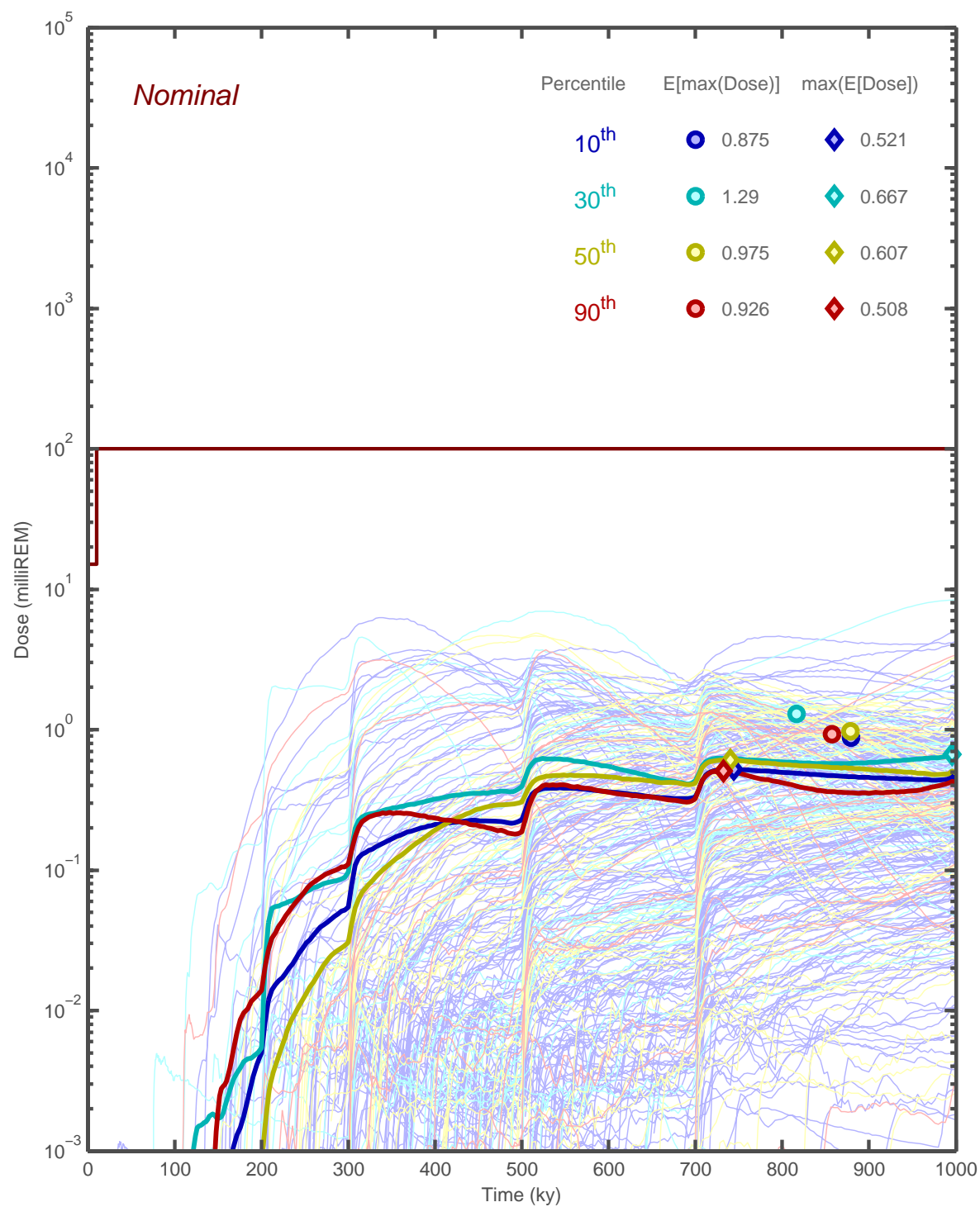


Figure 4-1: Nominal scenario realizations and expected values from TSPA LA simulations, partitioned according to infiltration scenario. Expected peak doses and maximum expected doses are indicated.

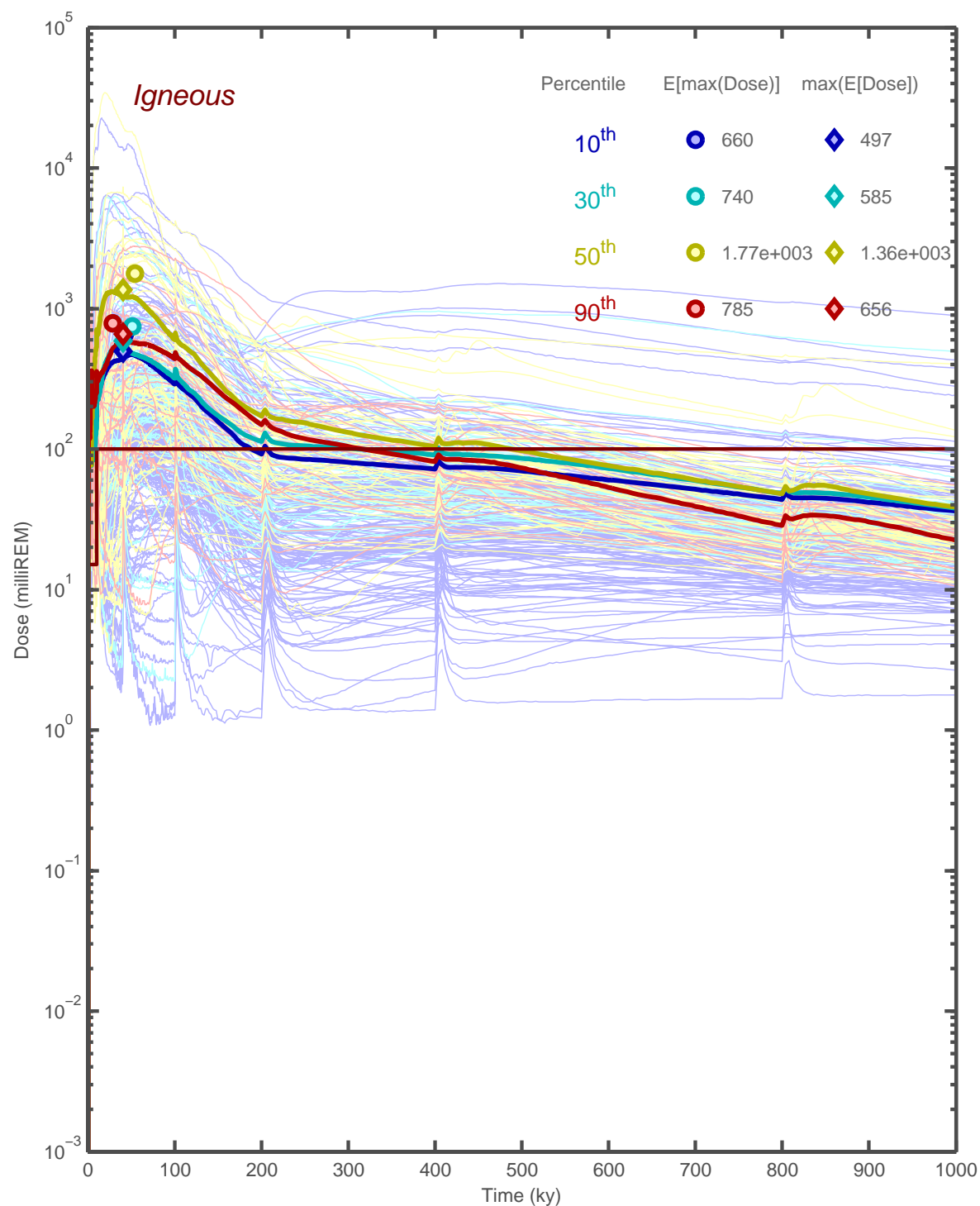


Figure 4-2: Igneous scenario realizations and expected values from TSPA LA simulations, partitioned according to infiltration scenario. Expected peak doses and maximum expected doses are indicated.

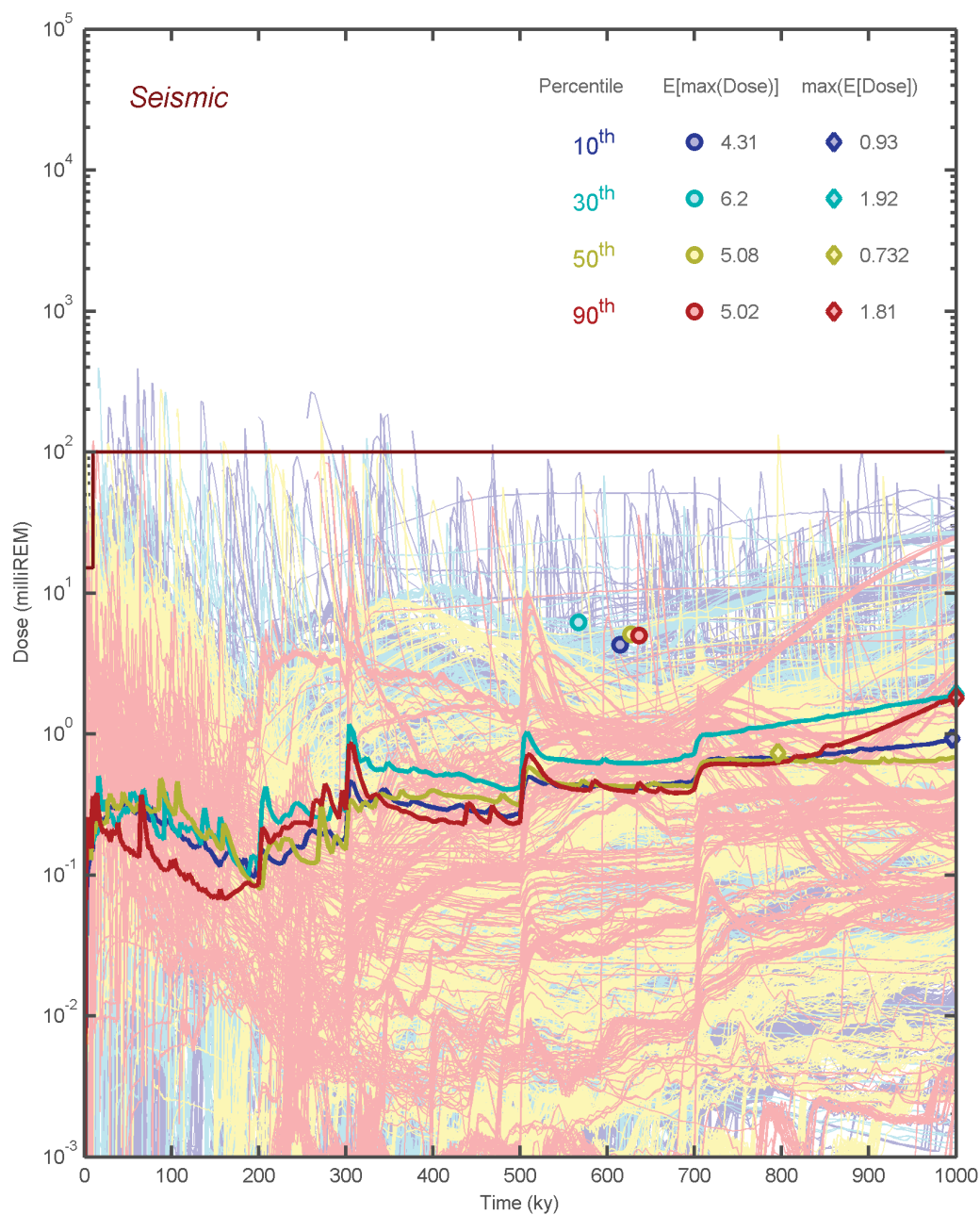


Figure 4-3: Seismic scenario realizations and expected values from TSPA LA simulations, partitioned according to infiltration scenario. Expected peak doses and maximum expected doses are indicated.

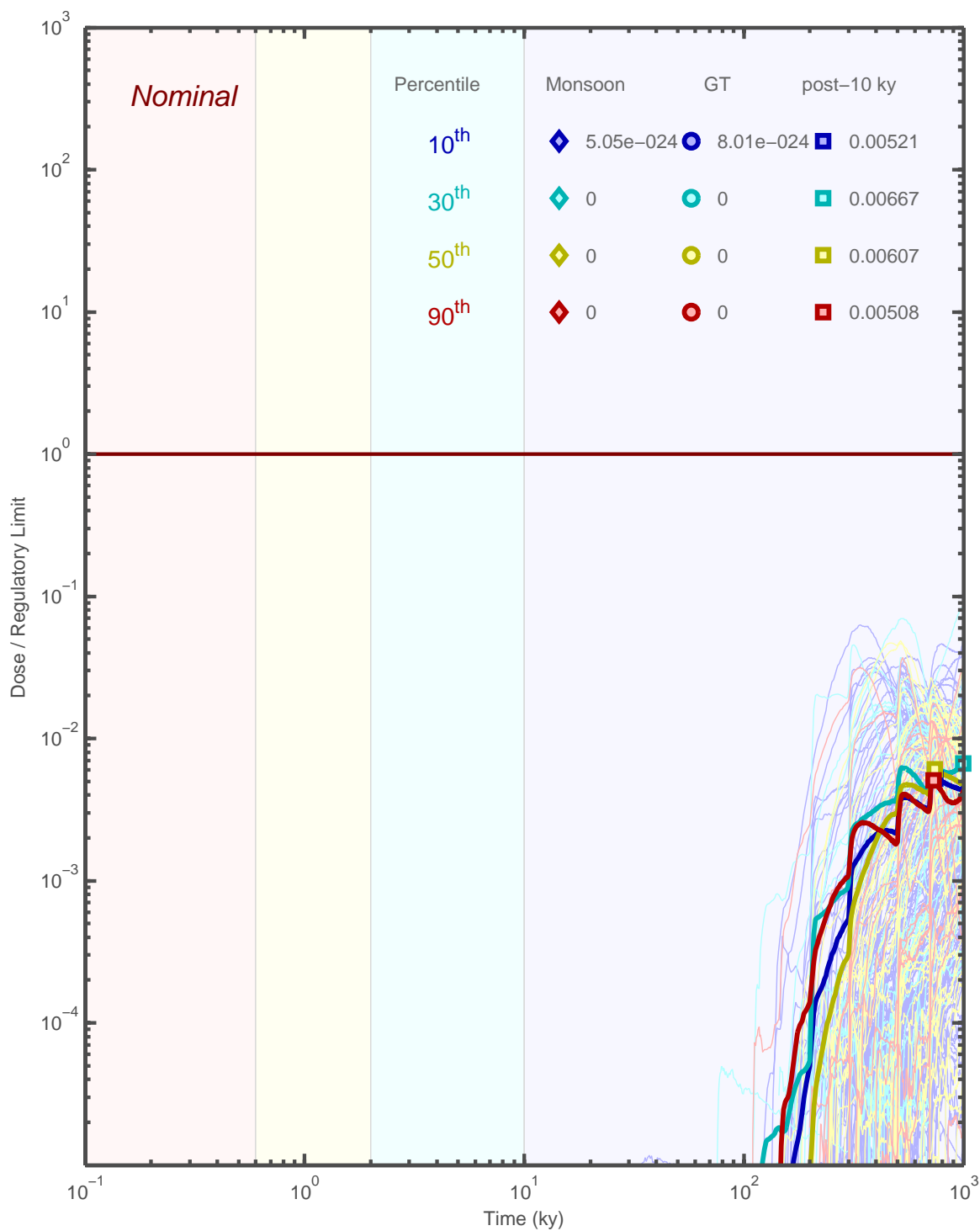


Figure 4-4: Nominal scenario realizations and expected values from TSPA LA simulations, partitioned according to infiltration scenario and normalized to the regulatory limit. Expected peak doses and maximum expected doses are indicated.

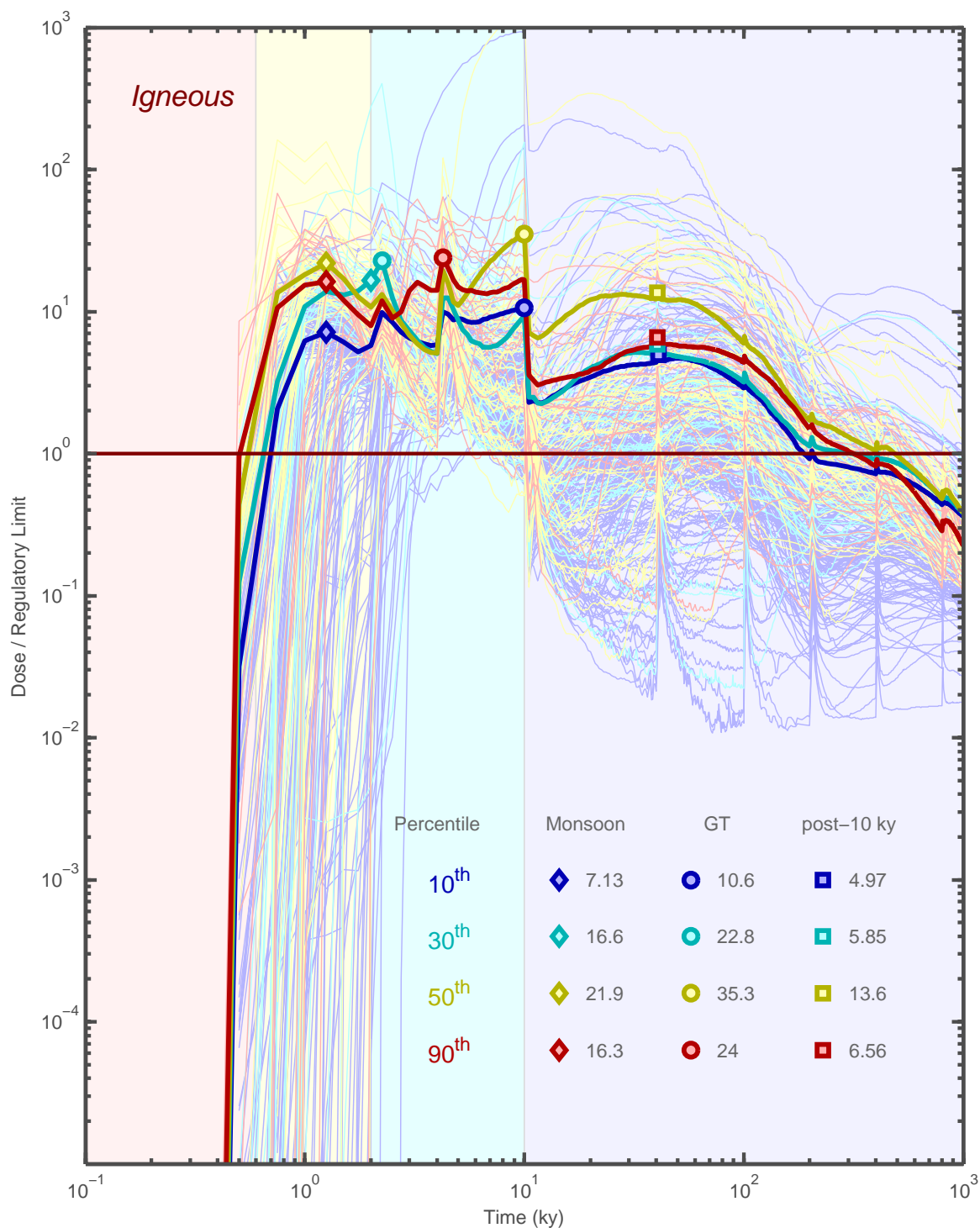


Figure 4-5: Igneous scenario realizations and expected values from TSPA LA simulations, partitioned according to infiltration scenario and normalized to the regulatory limit. Expected peak doses and maximum expected doses are indicated.

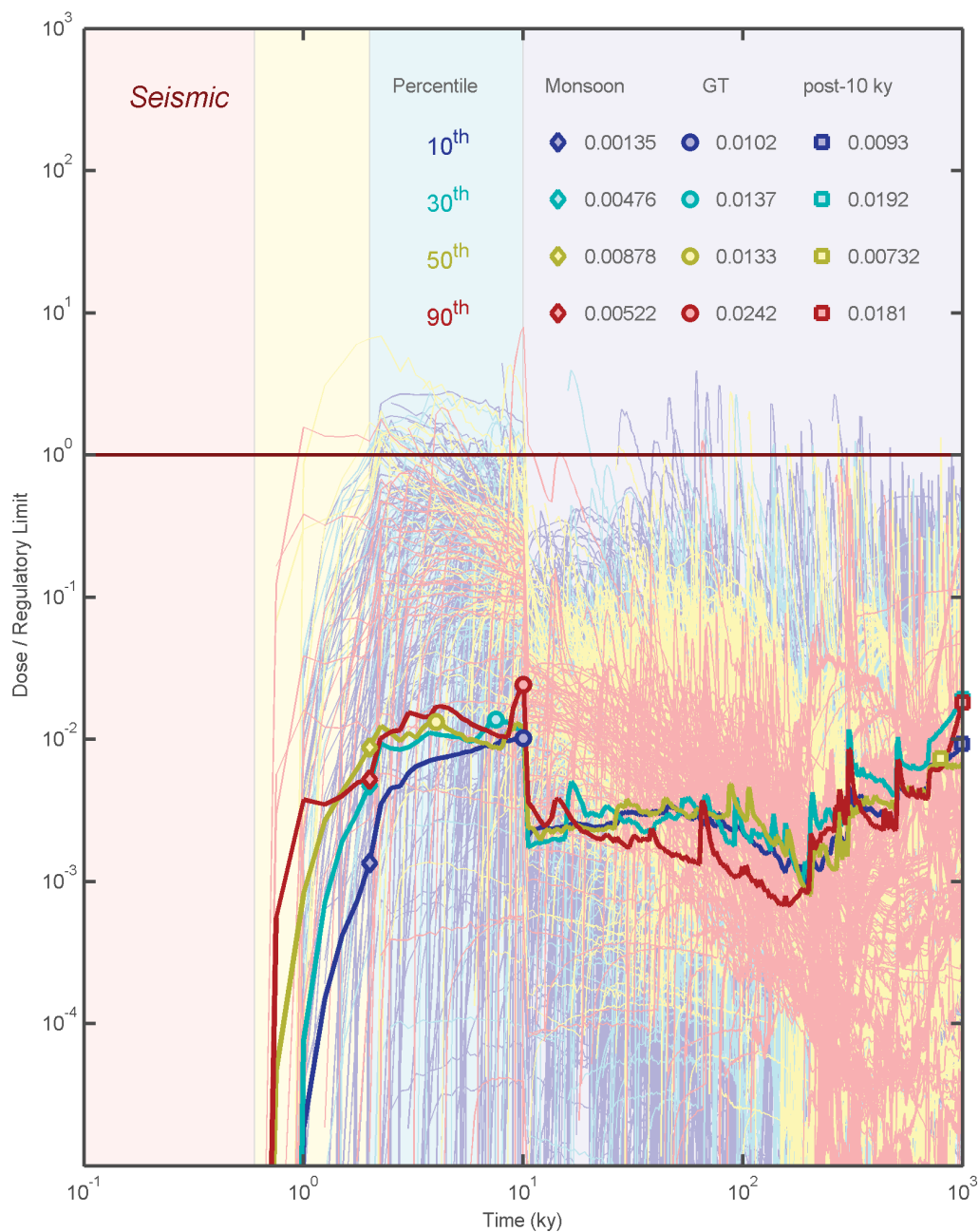
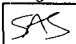


Figure 4-6: Seismic scenario realizations and expected values from TSPA LA simulations, partitioned according to infiltration scenario and normalized to the regulatory limit. Expected peak doses and maximum expected doses are indicated.


- *The mean curves do not necessarily track the infiltration scenario at any particular point in time, nor does the maximum expected value*
- *There are many fewer realizations for the high-infiltration scenarios than the 10th-percentile scenario*
- *There does not appear to be any large systematic change in dose associated with a change to a different climate state*

The seismic figures have a little different appearance because the postscript files created from the realizations are very large, so I used Illustrator to convert PNG files to postscript.

A few weeks after extracting the previous results, I did a regression analysis on the effects of net infiltration on the maximum expected value of calculated dose for the two disruptive scenarios. I didn't use the present-day climate state because it is dominated by thermal effects. I did the regression two ways: (i) weighting the average dose equally for each infiltration percentile, and (ii) weighting the average dose according to the number of realizations in the infiltration percentile. The regression results are plotted in Figure 4-7, with the size of the symbol proportional to the number of realizations. The regression indicates that, for both the igneous and seismic scenarios, calculated maximum expected dose is systematically dependent on net infiltration but is less than linearly proportional to net infiltration. A linear relationship would be indicated by the exponent $\alpha = 1$. There is sufficient scatter that it is difficult to make strong conclusions. 

06/15/10 Transport and release supplemental simulations.



Annotation dated 06/15/10: The next set of figures describes an analysis using my own calculations rather than DOE calculations. In this series, I was trying to understand the effect of travel time variability with respect to performance measures. I selected a lognormal travel time distribution as generally representative of natural media. 

Figures 4-8, 4-9, 4-10, and 4-11 represent the implications from travel time variability and uncertainty. All of the figures consider travel time to be lognormally distributed, with the color coding according to the coefficient of variation (standard deviation divided by mean). The curves represent the analytic representation of the probability density function [Figure 4-8 (top)] and cumulative density function [Figure 4-8 (bottom) through 4-11]. The time axis is normalized by the median travel time (T_{median}) in all figures.

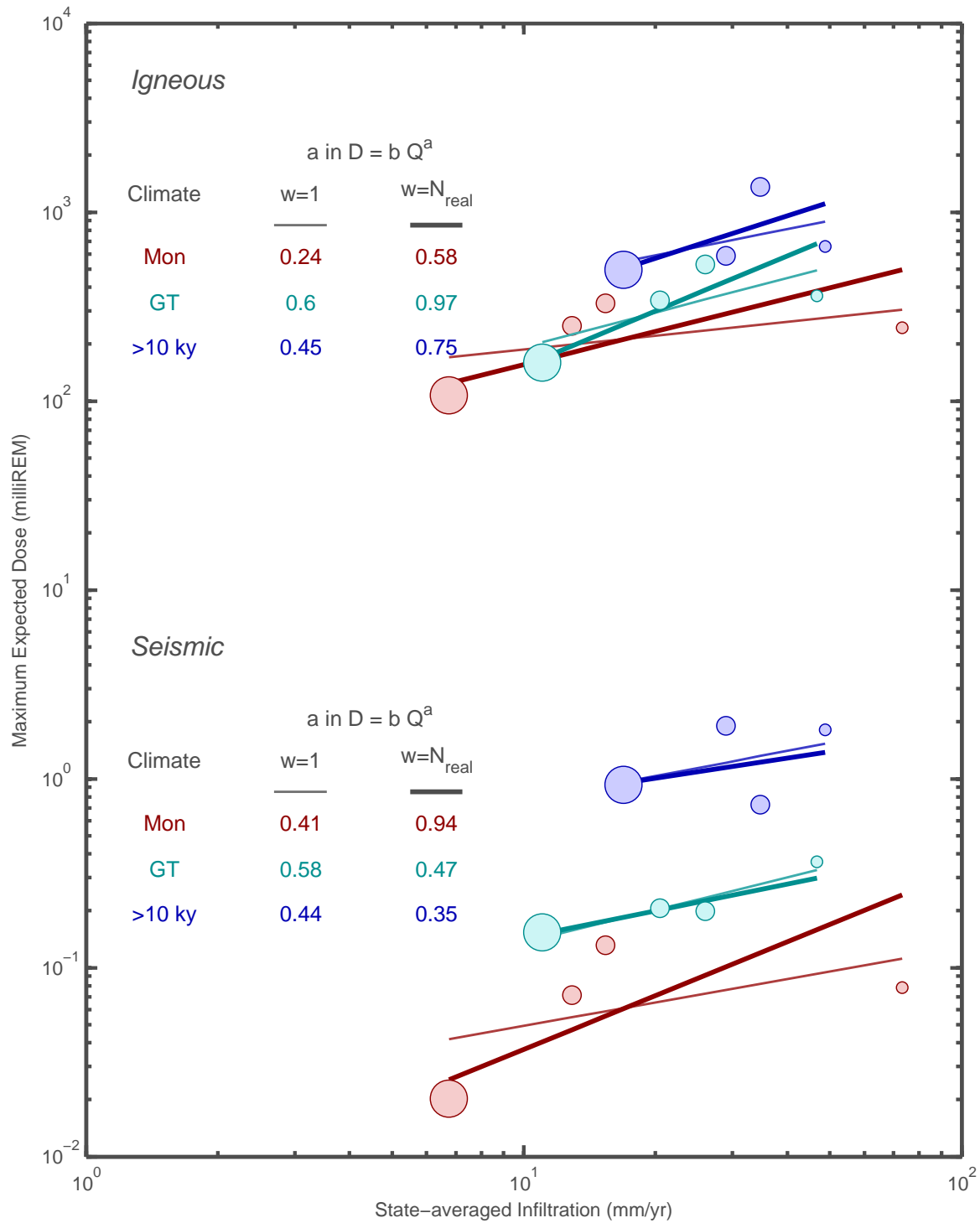


Figure 4-7: Regression of maximum expected dose within a climate state to areal-average net infiltration.

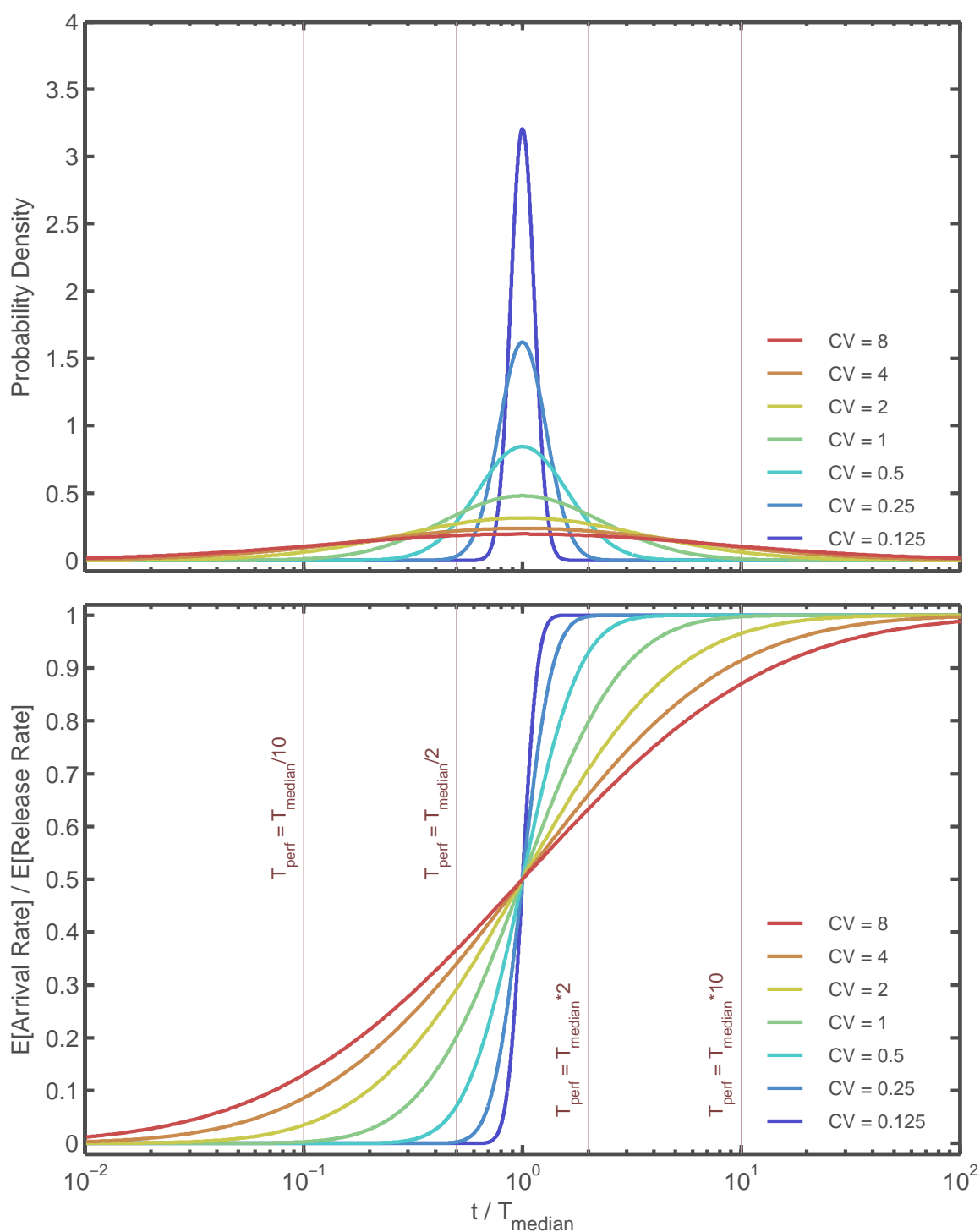


Figure 4-8: Expected arrival rate normalized by source emission rate for a lognormal travel time distribution, assuming the source is constant in time once initiated but the source initiation time is uniformly distributed in time.

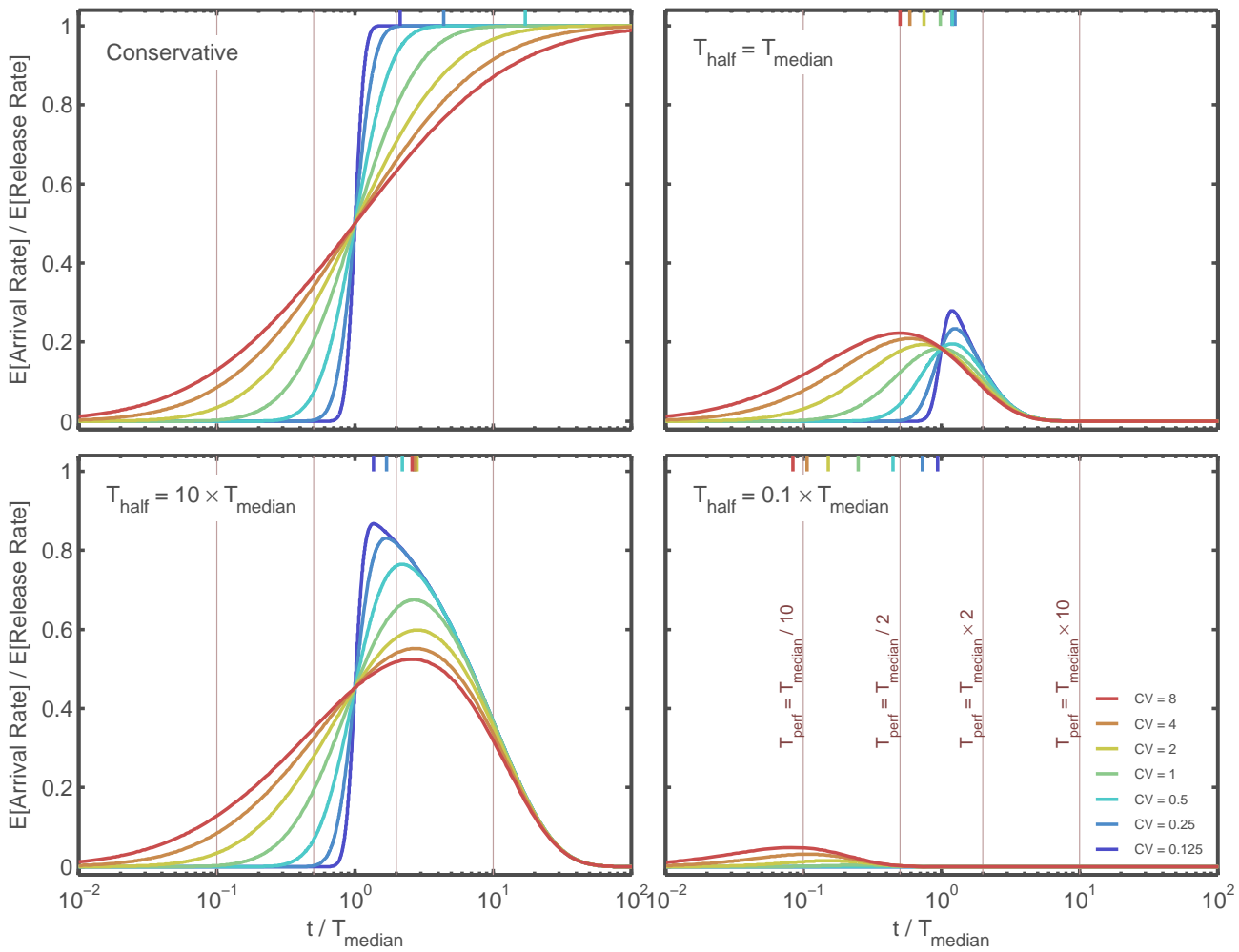


Figure 4-9: Expected arrival rate normalized by source emission rate for a lognormal travel time distribution, assuming the expected source is constant in time and the inventory decays in time.

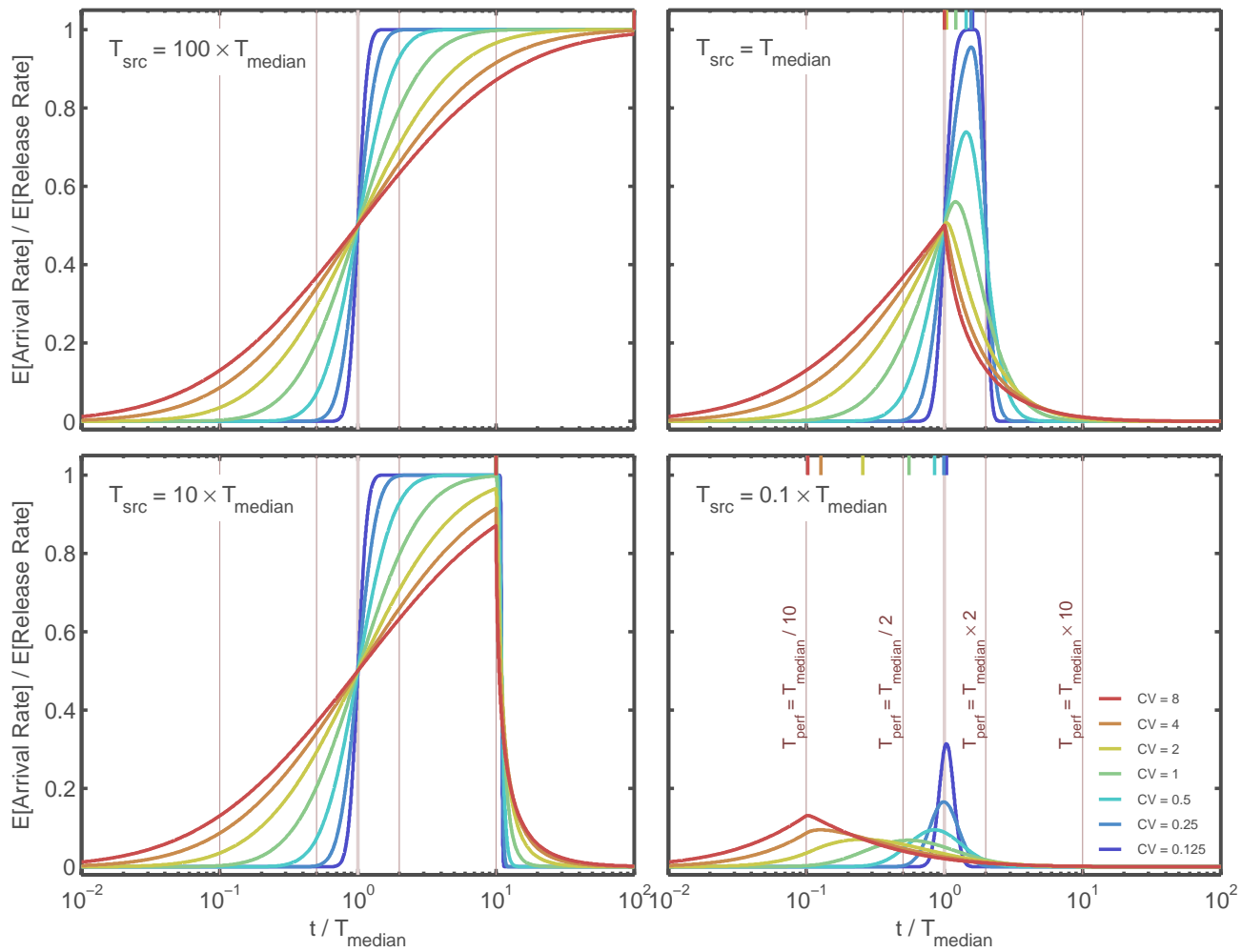


Figure 4-10: Expected arrival rate normalized by source emission rate for a lognormal travel time distribution, assuming the expected source is constant in time for a fixed period.

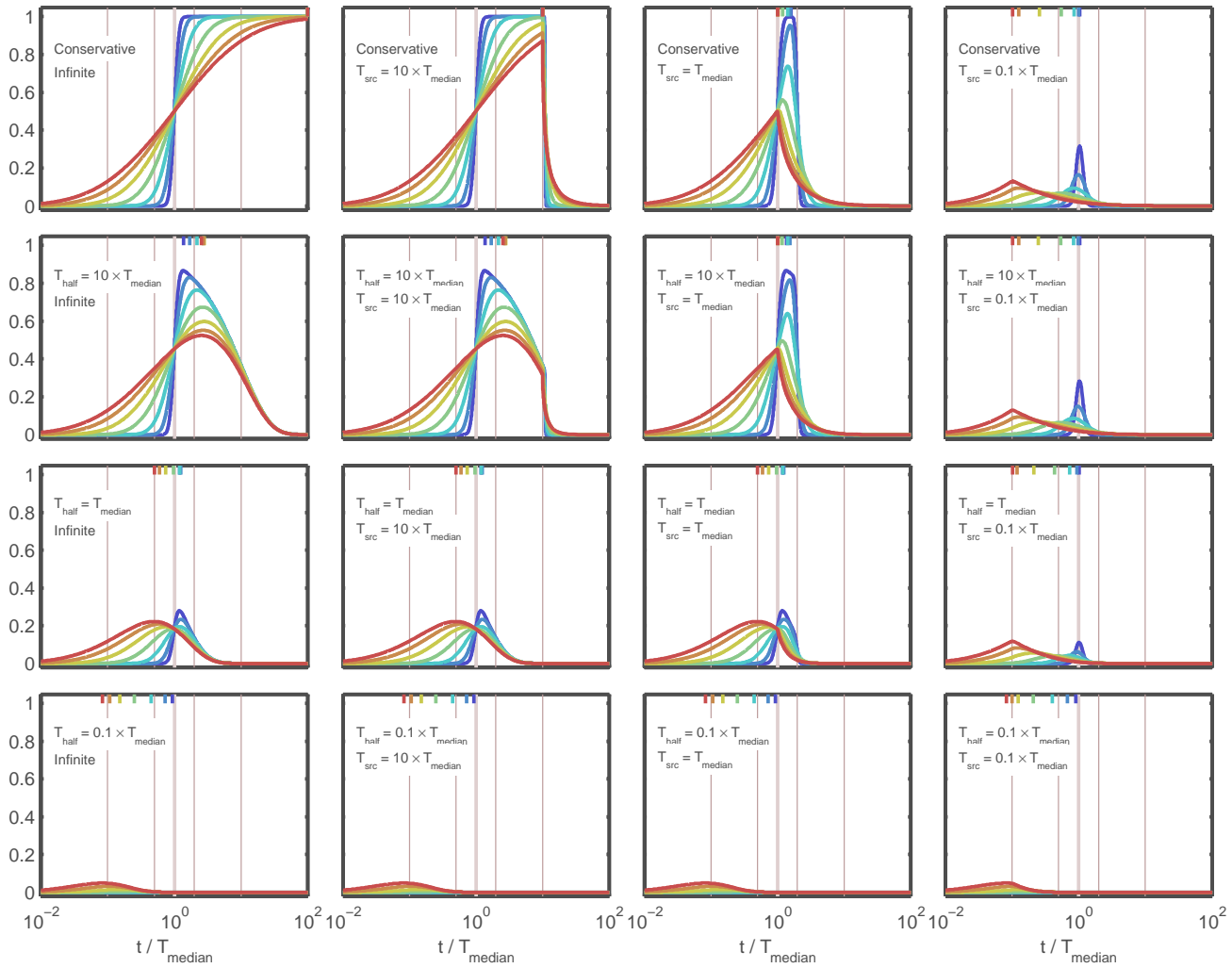
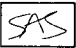


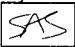
Figure 4-11: Expected arrival rate normalized by source emission rate for a lognormal travel time distribution, assuming the expected source is constant in time for a fixed period and the inventory decays in time.

Figure 4-8 (bottom) represents the expected rate of mass arrival as a function of time relative to the expected rate of mass release, assuming a conservative species is released at a constant expected rate. Vertical lines represent particular performance periods. For example, the vertical line at $t/T_{\text{median}} = 10$ represents a performance period that is ten times the median travel time. The largest expected dose occurs when the largest fraction of the possible travel times have occurred at the end of the performance period. For median travel times shorter than the performance period, a larger expected peak arrival rate results from a smaller spread in travel times, but generally the peak rate differs by less than a factor of two regardless of variability. For median travel times longer than the performance period, a larger expected peak arrival rate results from a larger spread in travel times and high variability in travel times can result in peak arrival rates that are orders of magnitude larger than result when travel times have low variability.

Figure 4-9 uses the same release and travel time assumptions as Figure 4-8, but with different radionuclide decay rates (T_{half}). The analytic solution is multiplied by the exponential decay term. The top left figure reprises Figure 4-8 (bottom). The peak arrival time occurs sooner as the radionuclide decays faster. Further, the peak arrival rate is less affected when the travel times are more variable.

Figure 4-10 considers the same release and radionuclide decay rate assumptions as Figure 4-8, but with different durations for the source (T_{src}). After the termination of the source, the cumulative density function from all travel times is reduced by the cumulative density function corresponding to times after the source ceases emitting. Again the top left figure reprises Figure 4-8 (bottom). Figure 4-11 provides all combinations of finite source duration and half life.

Annotation dated 06/15/10: Based on these figures, it appears that a radionuclide with a half-life short relative to the performance period requires high variability or high velocities for much of the released radionuclide to reach the compliance point. 

Annotation dated 06/15/10: The next set of figures continues the analysis using my own calculations. In this series, I was trying to understand the interplay between waste package failure rates, waste depletion given failure, and decay in affecting the expected release patterns. These factors affect the insights from the preceding analysis, which assumes that release occurs as a single pulse over a finite time. The highly abstracted representation assumes that (i) a failure event may occur randomly at any moment during the failure period and (ii) expected release rates given a failure are constant over a finite duration. The factors varied include (i) failure period duration, (ii) depletion rate given failure, and (iii) radionuclide half life. The plotted results represent the aggregate from many waste packages. 

There may be known finite-duration periods over which failures are known to occur. The expected release during and after such periods is indicated in Figure 4-12 when the period with failures occurring starts at time 0 and ends at time T_{allf} . Once a waste package fails, it is assumed to release at a uniform rate over a finite duration, T_{src} .

These curves are calculated using the cumulative density functions for begin of release (*i.e.*, failure time) and end of release (*i.e.*, failure time plus duration of release given a failure). The fraction of waste packages releasing is simply the difference between cumulative failures and cumulative end of releases. The expected release rate is normalized by the release rate when all mass is released over T_{allf} . The effect of inventory decay is illustrated by multiplying all release rates by the exponential decay term with half-life T_{half} .

A plateau arises in situations where the release duration is less than or equal to the arrival rate of failures. This plateau arises after a period of T_{src} , and is not reached if the release period after a failure is longer than the period in which failures occur.

Figure 4-12 indicates the situation where failures can start immediately, such as the igneous intrusion and seismic failure scenarios. The effect of a delayed onset of failures, such as failures from corrosion, is illustrated in Figure 4-13. The failure period becomes shorter from left to right and the half-life becomes shorter from top to bottom. The height of the plateau is greater than one, because of the normalization relative to a period of T_{allf} .

06/16/10 Direct seepage effects on diffusive releases.



Annotation dated 06/16/10: This section is reproduced almost verbatim from my personal notes last modified on March 30, 2009, with some formatting alterations. The section describes independent abstracted calculations rather than DOE calculations. In this analysis, I was trying to understand the essential effects of the interplay between seepage and diffusion for a solubility-limited conservative species. The behavior of a dissolution-limited species, in which the dissolution of the source material controls the upstream flux, can be rather different because the upstream concentration “floats” in order to meet the specified flux. Note that the two cases may have similar characteristics in the important case where the dissolution of the source exponentially decays with time.



The DOE Engineered Barrier System (EBS) release model calculates mass release rates to the matrix and fractures of the far field using a network model. The model has separate “boxes” for the waste package, invert, and 3 columns each of matrix and fractures. Links between boxes represent the legs between (i) waste package and invert, (ii) invert and underlying matrix and fracture

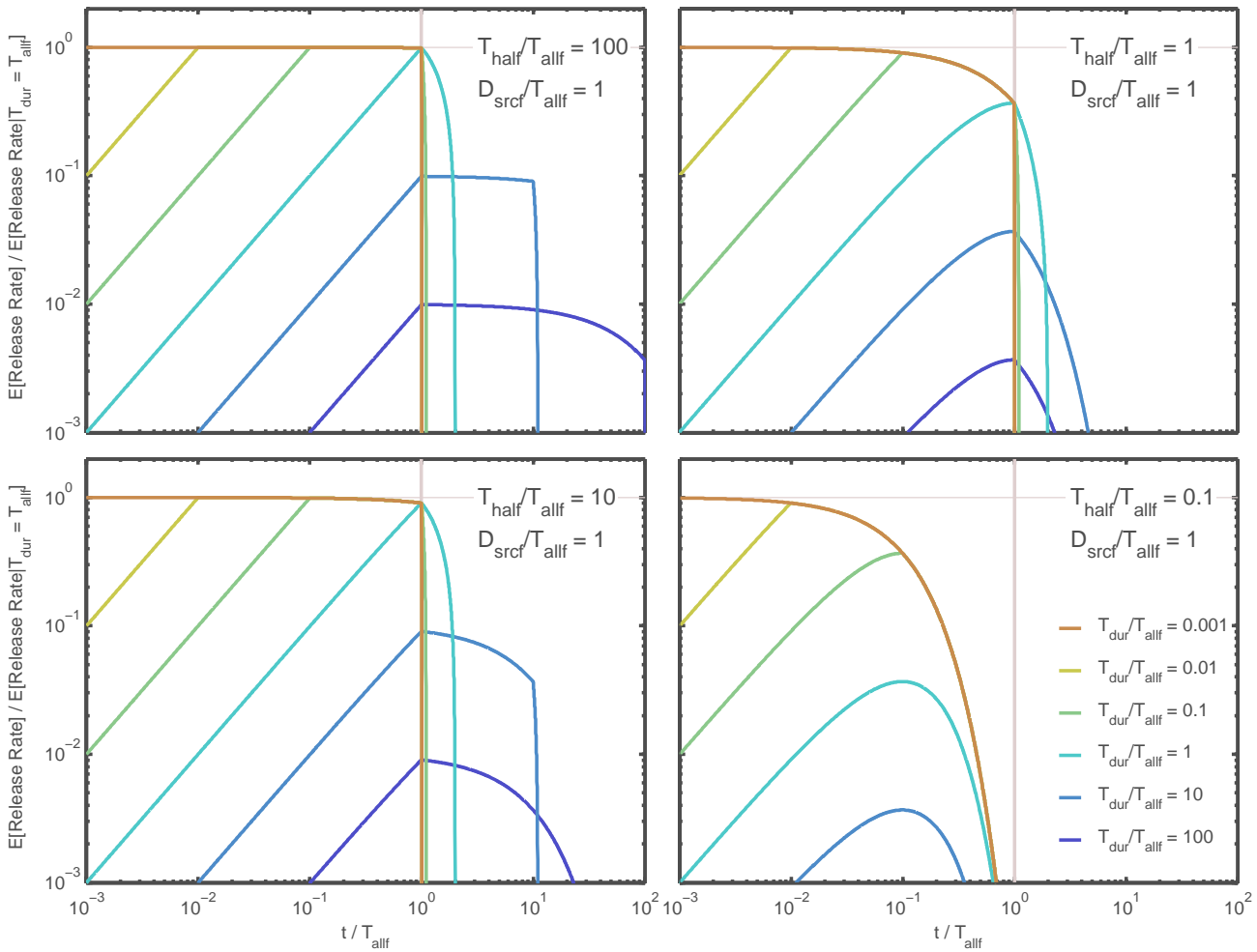


Figure 4-12: Expected release rate when releases occur at a steady rate for a finite duration T_{src} and failures are spread uniformly in time between time 0 and time T_{allf} .

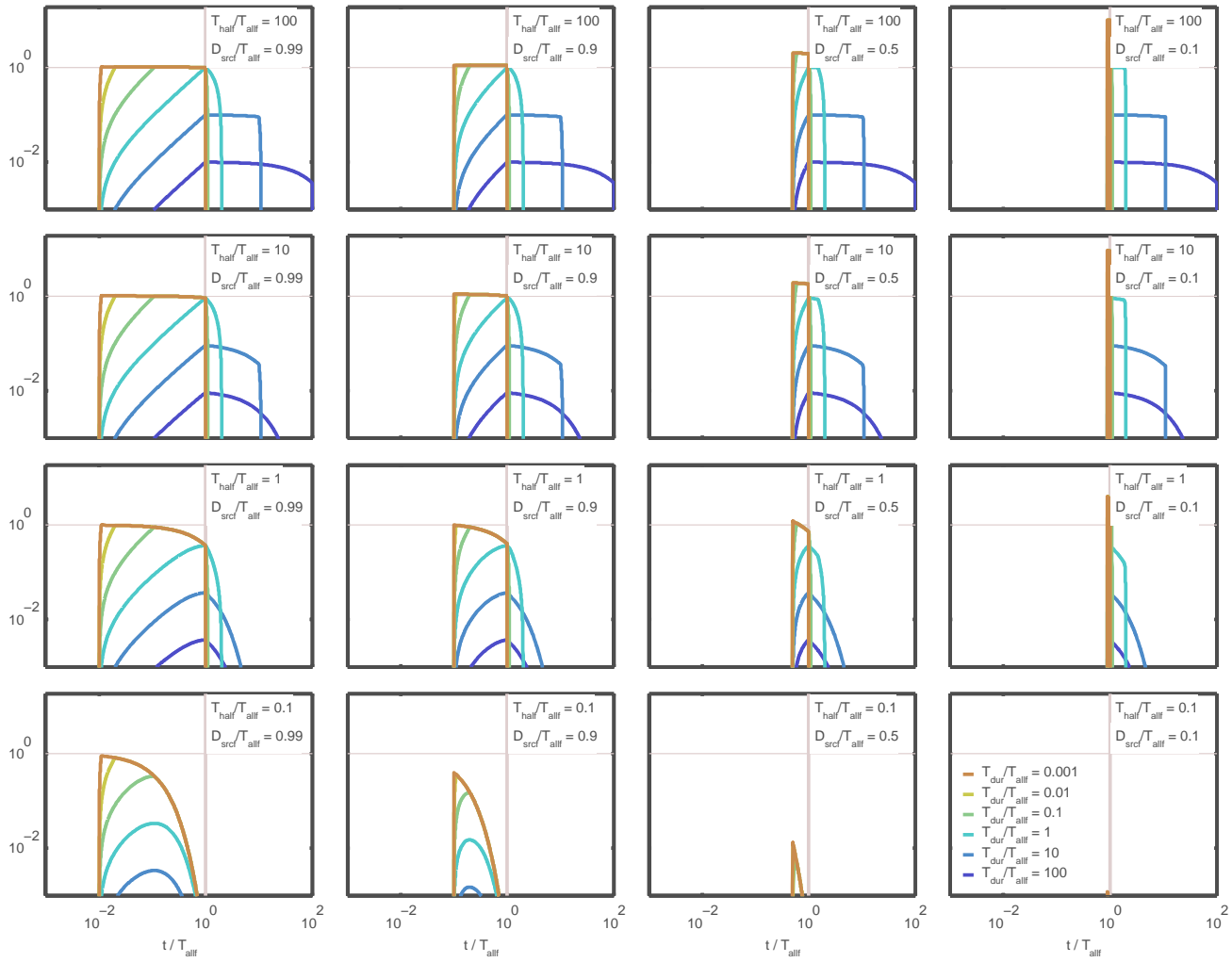


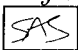
Figure 4-13: Expected release rate when releases occur at a steady rate for a finite duration T_{src} and failures are spread uniformly in time between a starting time later than time 0 and time T_{allf} .

boxes, (iii) matrix-to-matrix connections, (iv) fracture-to-fracture connections, and (v) matrix-to-fracture connections. The far field boundary condition is assigned a zero concentration.

A simplified 4-link representation of the EBS model contains links representing the waste package, invert, underlying matrix, and underlying fracture system. Assuming that (i) advective fluxes are approximated by water flux times the concentration at the upstream end of each box and (ii) diffusive fluxes are approximated by a linear gradient over the link yields an approximate analytical solution describing the steady-state release for a radionuclide with a fixed concentration inside the waste package and zero concentration in the far field. The analytical solution to this problem is

$$Q = \left[\frac{(K_w + F_w)(K_i + F_i)(K_m + K_f + F_m + F_f)}{(K_w + K_i + F_i)(K_m + K_f + F_m + F_f) + K_i K_w} \right] C_w \quad (4-1)$$

where subscripts w , i , m , and f represent waste package, invert, matrix, and fracture legs; Q represents mass release rate; K represents (AD/LR) ; F represents AV ; and C represents concentration. The coefficients A , D , L , R , and V represent the area for diffusive flow, the diffusion coefficient, the length over which diffusion occurs, the retardation coefficient, and the fluid velocity, respectively.

Annotation dated 06/16/10: The use of the retardation coefficient is, strictly speaking, not appropriate for a steady-state problem because it multiplies the storage term. In the remainder of this section, consider $R = 1$ for a true steady state and discussion with $R > 1$ as representing approximate "early" conditions. Also note that the analytic solution represents both advection and diffusion as constant across a link, and will over-estimate total flux because the concentration profile does not vary linearly across a link for two fixed concentration conditions when both advection and diffusion occur. 

In most situations, K_f and F_m are essentially zero in the DOE model and F_i equals F_f . When dripping fluxes also do not exist, F_i and F_f are both zero. One representative case considers the situation where the waste package undergoes diffusive releases only (advective fluxes through the waste package would act like increasing the diffusion coefficient) but dripping fluxes move through the invert and pass into the fracture system.

The analytical solution suggests that there are two limiting regimes for releases: (i) waste-package limited, where movement through the waste package limits releases; and (ii) far-field limited, where the invert and far field cannot carry away the waste at the peak release rate from the package. Concentrations at the outside of the waste package are close to zero in the regime that release is limited by the waste package (*e.g.*, few holes for diffusion or strong retardation) and close to the interior concentration in the regime that release is limited by far-field transport. Given a far-field transport capacity, there is a relatively narrow band of waste-package conditions for which

both the waste package and far field limit releases.

The simplified representation of the model shown in Figure 4-14 uses parameters that are comparable to the EBS model with no advective transport through the waste-package leg. The vertical axis in each of the subfigures represents the flux rates for fracture, matrix, and total release from the invert, normalized by a nominal diffusive flux rate. The nominal diffusive flux rate occurs when the concentration outside the waste package is set to zero, the diffusive area is the same as the invert diffusive area, the diffusion coefficient is the nominal free diffusion coefficient (no restrictions from porosity, saturation, or tortuosity), there is no retardation, and a nominal waste package thickness is used. Each subfigure in the third row of Figure 4-14 uses this set of diffusive characteristics in the invert and matrix. The horizontal axis represents the waste package conductance (diffusion coefficient times diffusion area, divided by diffusion length times retardation coefficient) normalized by the far field conductance assuming that the invert and matrix have the nominal diffusive properties. Each column of subfigures represents a different dripping flux, increasing by an order of magnitude in each subfigure from left to right. Each row of subfigures represents a different far-field diffusion coefficient, increasing by an order of magnitude in each subfigure from top to bottom.

Dripping fluxes have little effect on total release at steady state when the effective diffusion coefficient (AD/R) across the waste package wall is less than approximately 4 orders of magnitude smaller than the effective diffusion coefficient for the invert and matrix. The coefficients A , D , and R denote the area for diffusion to occur, the diffusion coefficient, and the retardation coefficient, respectively. The ratio in diffusion-path length determines the ratio between waste package and far field effective diffusion coefficients that just limits diffusion only release (*i.e.*, without dripping). Even though dripping fluxes don't affect total release when the waste package limits release, the proportion of release to the fractures increases as the far-field diffusion coefficient decreases or the dripping flux increases. When the waste package wall is not limiting, then changes in dripping fluxes increase total release and fracture release proportionately.

When tortuosity and water content are factored into the diffusion coefficient, the effective diffusion coefficient may drop by orders of magnitude, implying that (i) $D/D_o \ll 1$ and (ii) a little seepage goes a long way to modifying releases. For the upstream boundary, flux rates from diffusion are smallest at steady state and may be orders of magnitude larger at early times. Also note that advective fluxes may be limited to discrete pathways (*e.g.*, fingers or rivulets), which may reduce the effectiveness of advection for transporting radionuclides.

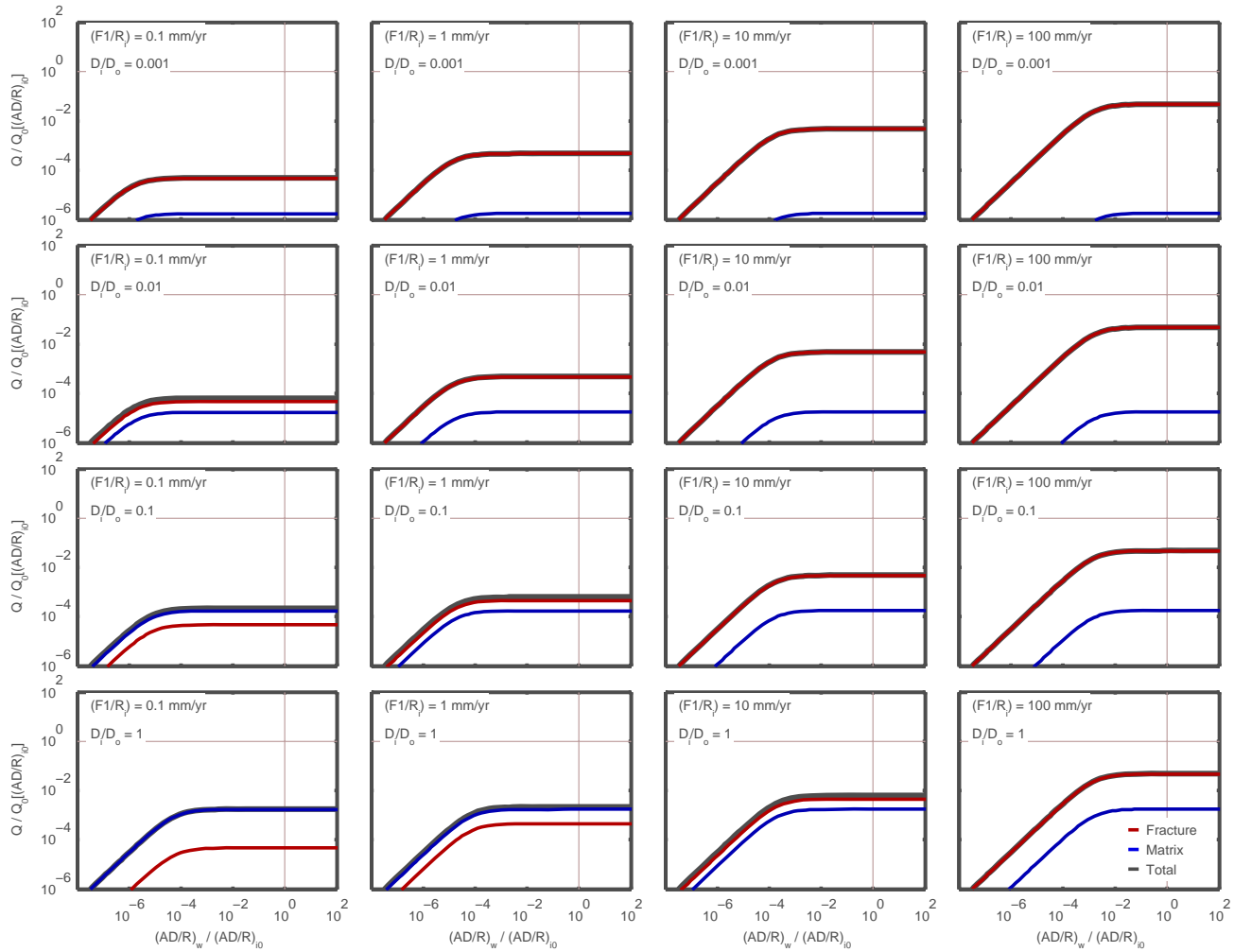


Figure 4-14: Release rate as a function of diffusion coefficients and seepage/condensation fluxes. Normalizing is relative to the case with an invert and matrix diffusion coefficient of 2×10^{-9} m²/s without effects from volumetric water content, retardation, or tortuosity.

06/18/10 Direct seepage effects from parameters.

Annotation dated 06/18/10: This section expands on my personal notes last modified on March 30, 2009. The section describes independent abstracted calculations rather than DOE calculations. In this analysis, I was trying to understand the essential effects of the interplay between uncertainty, variability, percolation flux, and seepage. This analysis serves as a digression to present the seepage models in more detail before returning to release. The methods in this section were developed in March, 2009, but the coding was generalized and streamlined late in 2009. I recently augmented the coding to make the plots more informative.



I created a series of comparison cases based on different representations for areal-average percolation, seepage and flow focusing.

The three abstractions for seepage based on the DOE detailed seepage model results provide one set of representations. The abstraction using trilinear interpolation, which is my independent implementation of the DOE abstraction, includes a “tri” label in the supporting figures. In the trilinear interpolation procedure, sampled values of $1/\alpha$, mean $\log(k_f)$, and Q_p are interpolated within a lookup table to calculate Q_s . The trilinear procedure is described in Section 2. The abstraction using bilinear interpolation, which is another implementation of the DOE abstraction using the same method that DOE used to fill out the trilinear-interpolation table, includes a “bi” label in the supporting figures. In the bilinear interpolation procedure, sampled values of $1/\alpha$ and $\log(k_f/Q_p)$ are interpolated within a lookup table to calculate Q_s . Note that the trilinear interpolation procedure will tend to yield larger estimates for Q_s than the bilinear procedure, all else being equal, because linear interpolation in Q_p places a larger weight on large flux values than logarithmic interpolation. DOE refers to the $1/\alpha$ parameter as a capillary strength parameter in the Safety Analysis Report (SAR). A final abstraction method, based on fitting a function to the detailed process-level simulation results, includes a “fit” label in the supporting figures. The fitted function is described in Section 2.

Figure 4-15 illustrates the seepage model representation of the trilinear approximation. The figure provides the cumulative distribution of seepage flux for all combinations of (i) three average percolation fluxes, (ii) two hydrogeologic units and the weighted average of the units within the repository footprint, and (iii) two drift-scale flow focusing models. The percolation flux of 100 mm/yr is larger than any repository-average or percolation-bin-average flux.

The following discussion describes Figure 4-15 in some detail, because other figures have similar characteristics.

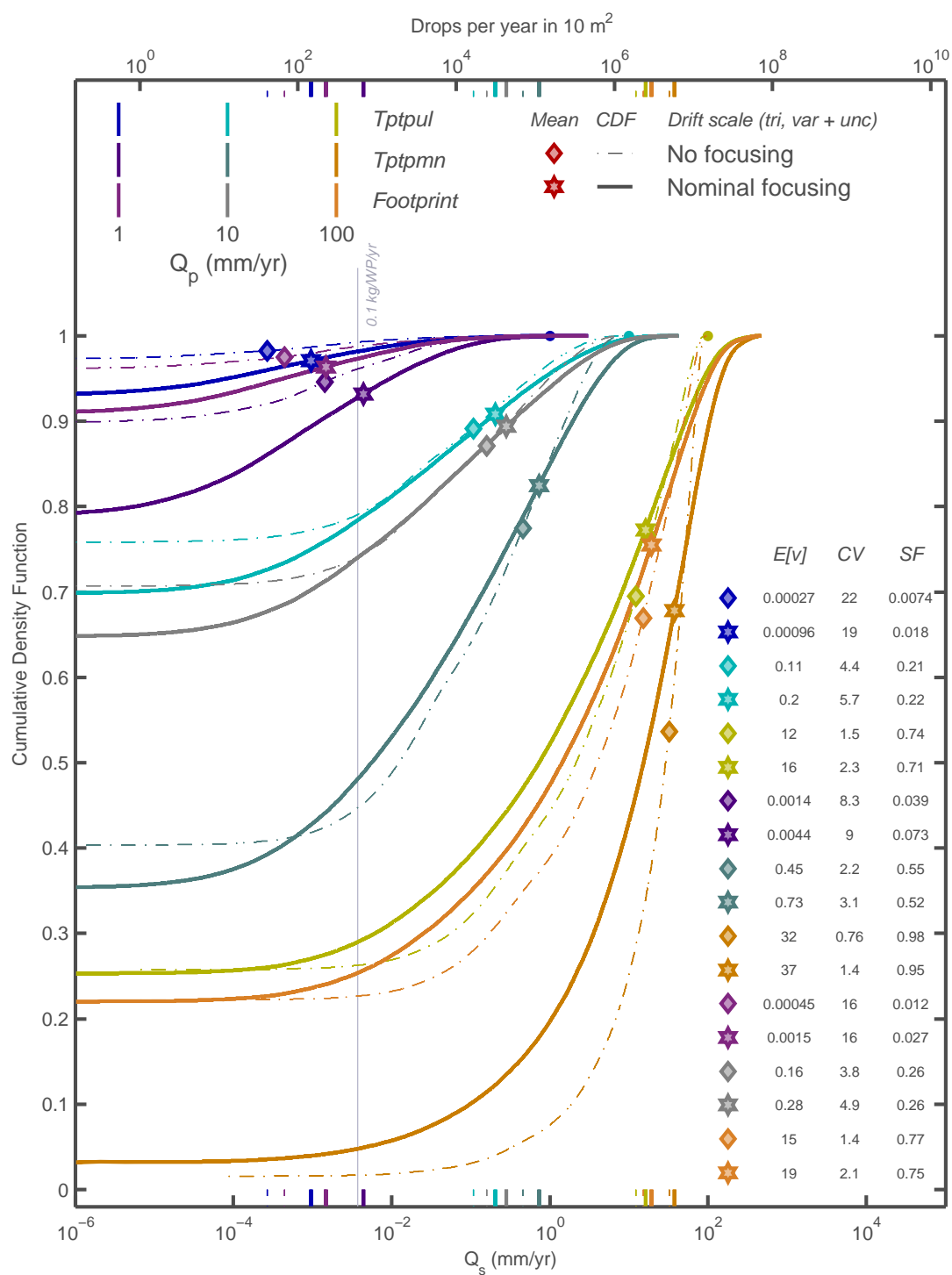


Figure 4-15: Cumulative seepage distribution for representative units and percolation fluxes, with seepage abstracted using trilinear interpolation.

The repository footprint consists of approximately 85 percent lithophysal and 15 percent nonlithophysal units. The Tptpul unit represents the Topopah Spring upper lithophysal unit, which is the dominant lithophysal unit in the footprint. The Tptpmn unit represents the Topopah Spring middle nonlithophysal unit, which is the dominant nonlithophysal unit in the footprint. The curves labeled “footprint” randomly select 85 percent of the realizations from the Tptpul unit and 15 percent from the Tptpmn unit. The Tptpmn unit is more densely fractured, thus has greater seepage for a given percolation flux. The weighted average curves are similar to the Tptpul unit curves but have slightly larger seepage.

The two representations for flow focusing account for local patterns of drift-scale flow variability. This is the variability in flow averaged over the drift area that DOE used in the detailed process-level calculations, approximately corresponding to the width of a drift. The “no focusing” case represents spatially uniform drift-scale flow and the “nominal focusing” case represents the nominal DOE flow focusing abstraction, which has the largest flows approximately 5 times larger than the average flows. Other abstractions in subsequent figures consider a similar independent lognormal approximation. For this approximation, the standard deviation denoted by σ has the same coefficient of variation as the DOE abstraction. More extreme variability is readily considered by modifying the standard deviation; I use 2σ to represent very large variability.

The heading above the labels for the symbols and curves summarizes the abstraction options. The “Drift scale” label indicates that the curves represent drift-scale variability; in subsequent figures I use “Averaged” to represent the average over all drifts. Inside the parentheses, the “tri” represents the trilinear approximation; a “bi” or “fit” represents the bilinear and fitted approximations. The “var” indicates that parameter variability is set to the nominal values for each unit and the “unc” indicates that uncertainty in the model parameters is considered. These can be turned off.

The columns of symbols and values in the bottom right-hand corner represent the expected (mean) values, coefficient of variation, and seepage fraction for each of the $3 \times 3 \times 2 = 18$ cases. The expected values are graphically indicated by colored bars at the top and bottom x axes as well as the symbols on the curves.

DOE sets seepage to zero when the calculated value falls below a threshold of 0.1 kg/WP/yr. The thin gray vertical line labeled 0.1 kg/WP/yr indicates the DOE cutoff value for zero seepage.

The secondary x axis on the top of the figure indicates seepage in terms of the number of drops of water per year falling on a waste package assuming that a drop has a diameter of 5 mm.

06/21/10 More direct seepage effects from parameters.

Annotation dated 06/21/10: This section completes the analysis from the previous entry.



Placing Figure 4-15 into context, DOE describes the repository footprint using four hydrogeologic units. The units are stratigraphically located from bottom (oldest) to top (youngest) as: (i) the Topopah Spring Tuff lower nonlithophysal unit (Tptpln, 2.6 percent of the footprint), (ii) the Topopah Spring Tuff lower lithophysal unit (Tptpll, 80.5 percent), (iii) the Topopah Spring Tuff middle nonlithophysal unit (Tptpmn, 12.4 percent), and (iv) the Topopah Spring Tuff upper lithophysal unit (Tptpul, 4.5 percent) (Bechtel SAIC Company, LLC, 2007, Section 6.3.1). Because the units dip to the east and DOE plans for the emplacement drifts to be horizontal in a generally east-west orientation, the units form generally north-south bands that are ordered from oldest (Tptpln) in the west to youngest (Tptpul) in the east. DOE considers the two lithophysal units to be similar and represents the Tptpul unit using the Tptpll properties. DOE considers the two nonlithophysal units to be similar and represents the Tptpln unit using the Tptpmn properties.

DOE calculates releases for representative waste packages using the expected value and seepage fraction. The calculations are performed separately for representative waste packages in seeping environments and nonseeping environments. DOE uses the seepage fraction to estimate the fraction of packages that would occur in the seeping environment. DOE applies an average seepage flux to the representative waste package that is calculated by dividing the expected flux by the seepage fraction. For a fixed expected seepage flux, increasing the seepage fraction means that more waste packages are considered seeping but the seepage flux for the representative package decreases. The DOE procedure actually takes an additional step of partitioning the percolation fluxes into 5 bins, and separately applying the procedure to each bin.

Figure 4-15 illustrates several characteristics of the DOE seepage model for the repository hydrogeologic units. In general, the Tptpmn unit has both a larger expected value for seepage and a larger seepage fraction than the Tptpul unit. The repository-weighted seepage statistics are intermediate between the statistics for the two units, but more similar to the Tptpll unit because the repository footprint has nearly six times as much lithophysal rock than nonlithophysal rock. At the intermediate flux (10 mm/yr), the nonlithophysal unit has roughly 4 times as much seepage than the lithophysal unit. The ratio of nonlithophysal to lithophysal flux is smaller for larger percolation flux and larger for smaller percolation flux.

Figure 4-15 also illustrates the effect on seepage when flow focusing is included. The nominal focusing curve represents the DOE flow focusing factor distribution. DOE used a set

of intermediate-scale simulations to estimate the flow focusing factor, which has the effect of locally varying the drift-scale percolation flux above or below the nominal average value. The DOE flow focusing factor ranges from 0.116 to 5.016 with an expected value of 1. DOE expresses the nominal relationship as a cumulative distribution,

$$\text{CDF} = [a_0 + x(a_1 + x(a_2 + x(a_3 + xa_4)))]/100 \quad (4-2)$$

where CDF is the cumulative distribution (0 to 1), x is the ratio of focused to background percolation flux, and the a parameters are calibration parameters. The coefficients have the values $a_0 = -11.434$, $a_1 = 102.3$, $a_2 = -35.66$, $a_3 = 5.4998$, and $a_4 = -0.3137$. I added the factor of 100 to convert the DOE representation in terms of a 0 to 100 percentage to a 0 to 1 cumulative distribution. I implemented flow focusing by first creating a table for CDF as a function of x , then sampled values for CDF and used table lookup. The flow focusing factor distribution implies that most locations experience percolation flux that is less than the nominal background flux.

Figure 4-15 indicates that including the nominal flow focusing factor distribution increases repository-average expected seepage by less than a factor of 2 and has no effect on the seepage fraction for a background flux of 10 mm/yr. For larger background fluxes, the nominal flow focusing factor distribution causes smaller relative increase in seepage and slightly decreases the seepage fraction. For smaller background fluxes, the nominal flow focusing factor distribution causes larger relative increase in seepage and increases the seepage fraction. Note that larger background fluxes have larger absolute changes in repository-average seepage even though the relative changes are smaller.

As discussed in the previous entry, I considered three different representations for the seepage abstraction. Figure 4-16 compares the cumulative distributions for seepage for the three representations. The three distributions are essentially identical for large fluxes but differ at the end of the distribution for small fluxes. The expected values are quite similar because the expected value is dominated by the realizations with large fluxes. The seepage fraction, which is determined by an arbitrary value for the seepage cutoff, varies more between abstractions. Consistent with the discussion in the previous entry, the bilinear interpolation procedure consistently has a smaller seepage fraction than the trilinear interpolation procedure and at very small percolation fluxes has a slightly smaller expected value. The fitted function estimates larger seepage for low seepage values than the interpolated functions, thus has a consistent trend to larger expected seepage and larger seepage fraction compared to the others.

I considered the effects of uncertainty and variability for the bilinear scheme by separately turning on and off uncertainty and variability. Figure 4-17 compares the flow focusing factor effects,

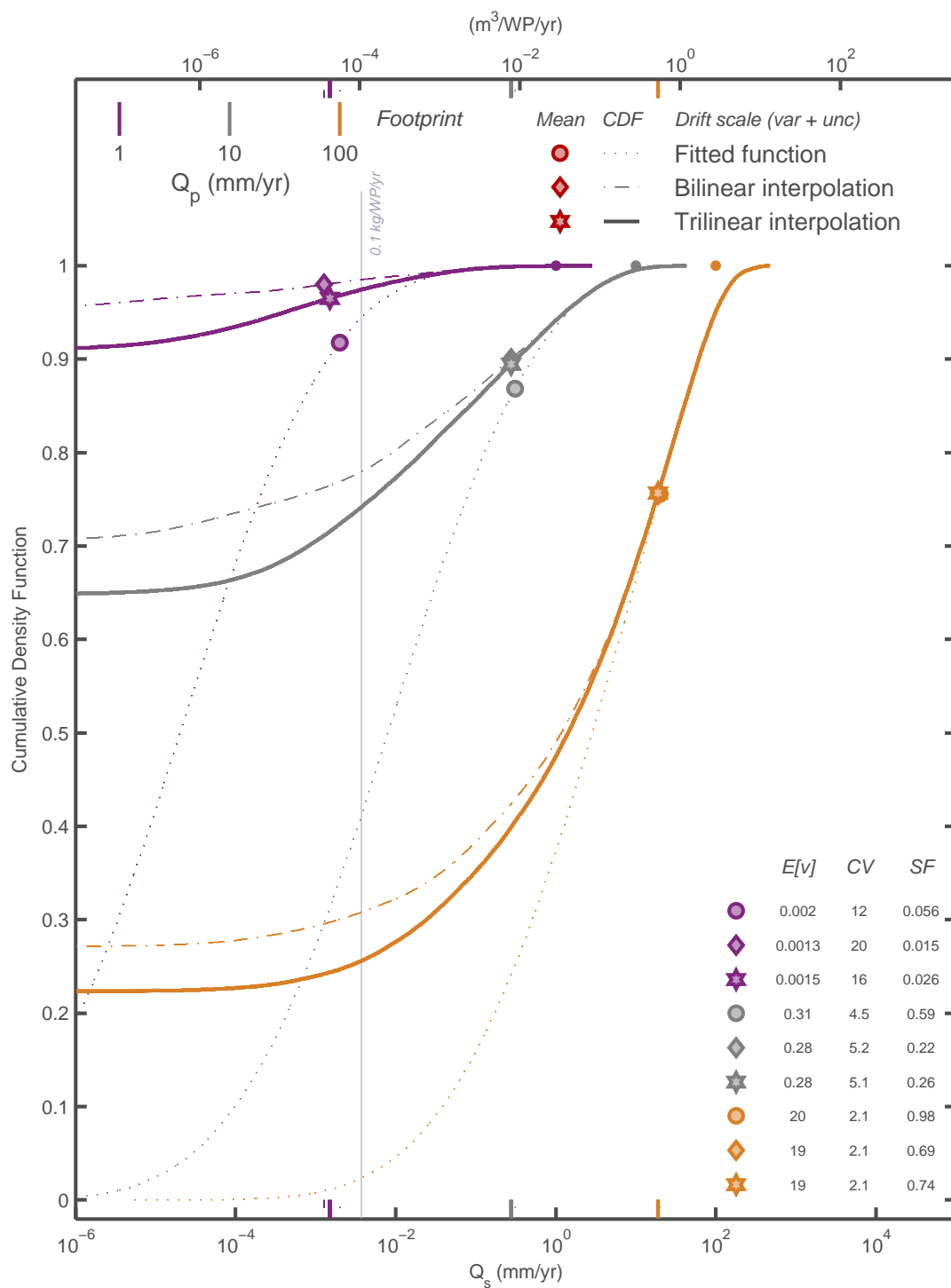


Figure 4-16: Cumulative seepage distribution with units weighted by footprint fraction, comparing percolation flux abstractions.

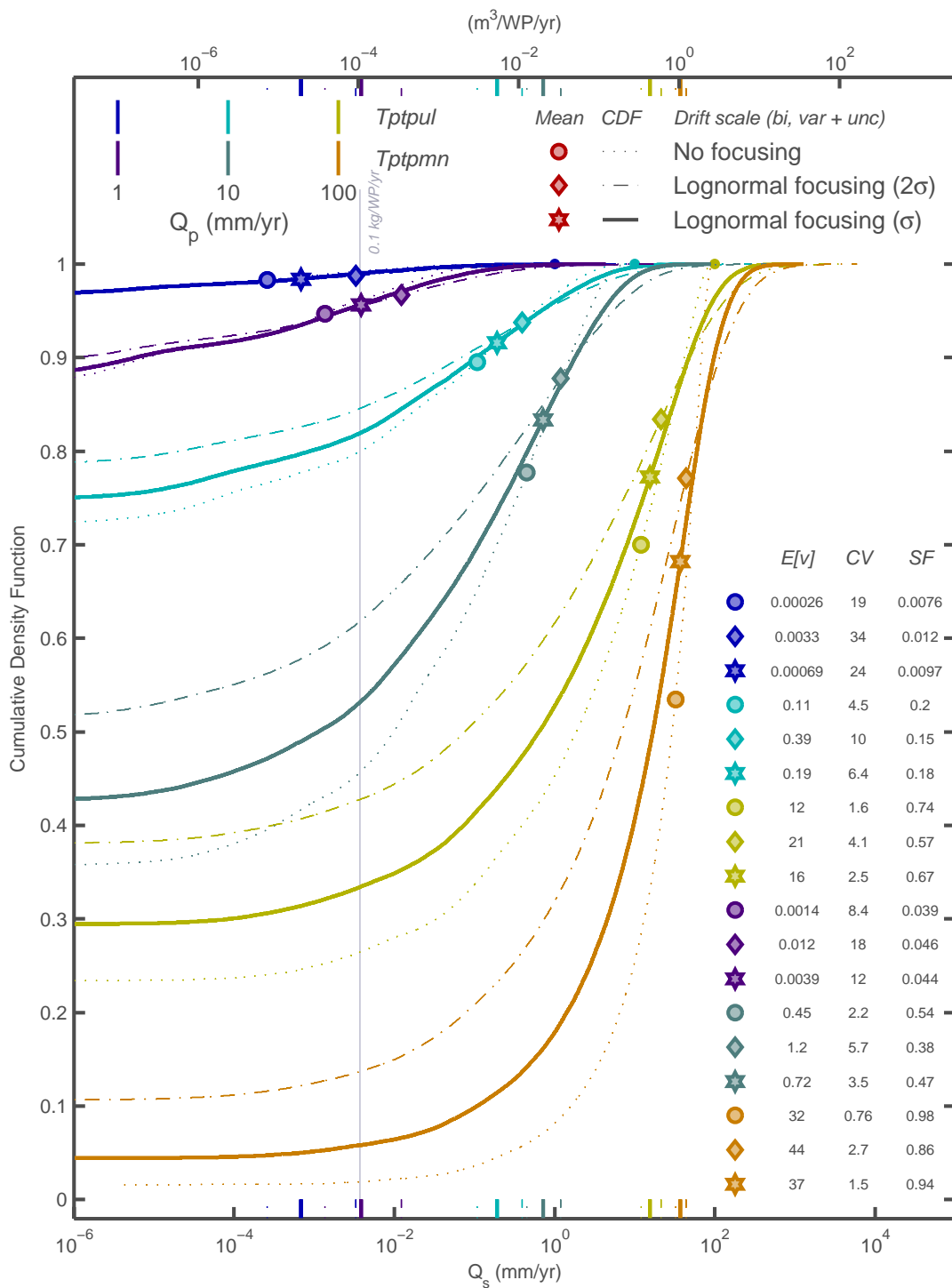


Figure 4-17: Cumulative seepage distribution including uncertainty and variability.

with uncertainty and variability both having their nominal distribution. Figure 4-18 is identical except that variability is turned off by setting variable parameters to their mean values. Figure 4-19 includes variability with the nominal distribution and turns off uncertainty by setting uncertain parameters to their mean values. The lognormal focusing case with σ is similar to the nominal relationship. The lognormal focusing case with 2σ is like doubling the variability relative to the nominal relationship.

Figures 4-17 through 4-19 suggest that variability and uncertainty both tend to increase the expected seepage, with the relative increase dropping as the percolation flux increases. The figures suggest that the effect on seepage fraction depends on the percolation flux, with increased variability acting to increase the seepage fraction for low Q_p and decreasing the seepage fraction for large Q_p . Variability and uncertainty have similar tendencies; for the functional representations considered here, variability has a larger influence on the results than uncertainty. Variability is described using a uniform distribution for $1/\alpha$ and a truncated lognormal distribution for k_f . Uncertainty is described using a triangular distribution for both parameters.

The figures with cumulative seepage distributions presented thus far assume that $1/\alpha$ and $\log(k_f)$ are independent random variables. Insofar as both of these parameters are affected by fracture aperture, the variables may be correlated. DOE does not expect the correlation to be perfect, because both parameters account for factors other than aperture. Further, the relationships among aperture, $1/\alpha$, and $\log(k_f)$ are monotonic but not necessarily linear. Two limiting cases are displayed in Figure 4-20 and Figure 4-21, with perfect negative ($\rho = -1$) and positive ($\rho = 1$) correlations between $1/\alpha$ and $\log(k_f)$, respectively, to bound this effect. The case with no correlation is shown in Figure 4-17. These figures indicate that expected Q_s decreases as the correlation coefficient drops from 1 to 0 to -1 . The seepage fraction tends to a wider distribution (large fluxes increase in seepage fraction, small fluxes decrease in seepage fraction) for the same changes in correlation coefficient.

The final comparison in this entry demonstrates the effect of averaging from the drift scale to the areal-average scale (the average over many realizations of the drift scale). In drift-scale calculations, I combined parameter uncertainty and variability to provide parameter inputs to table lookup. The same procedure, followed by averaging, could be used to calculate areal-average seepage distributions. For computational expediency, I instead created a table of expected seepage as a function of median $1/\alpha$ and $\log(k_f)$, with seepage averaged over the variability in $1/\alpha$ and $\log(k_f)$. When calculating areal-average seepage using this table, I did not include parameter variability in $1/\alpha$ and $\log(k_f)$, only including uncertainty.

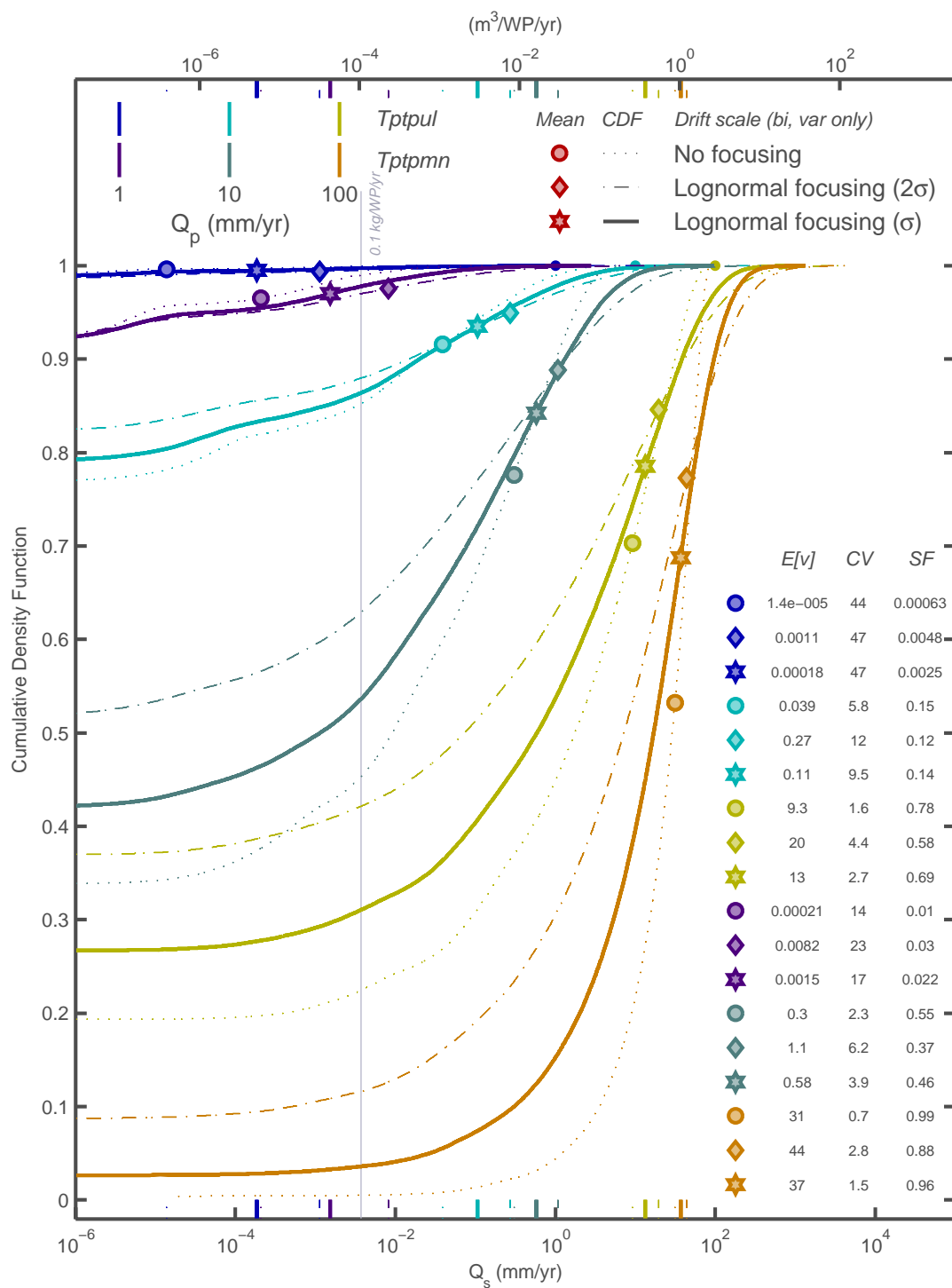


Figure 4-18: Cumulative seepage distribution setting uncertain inputs to the median value and including variability.

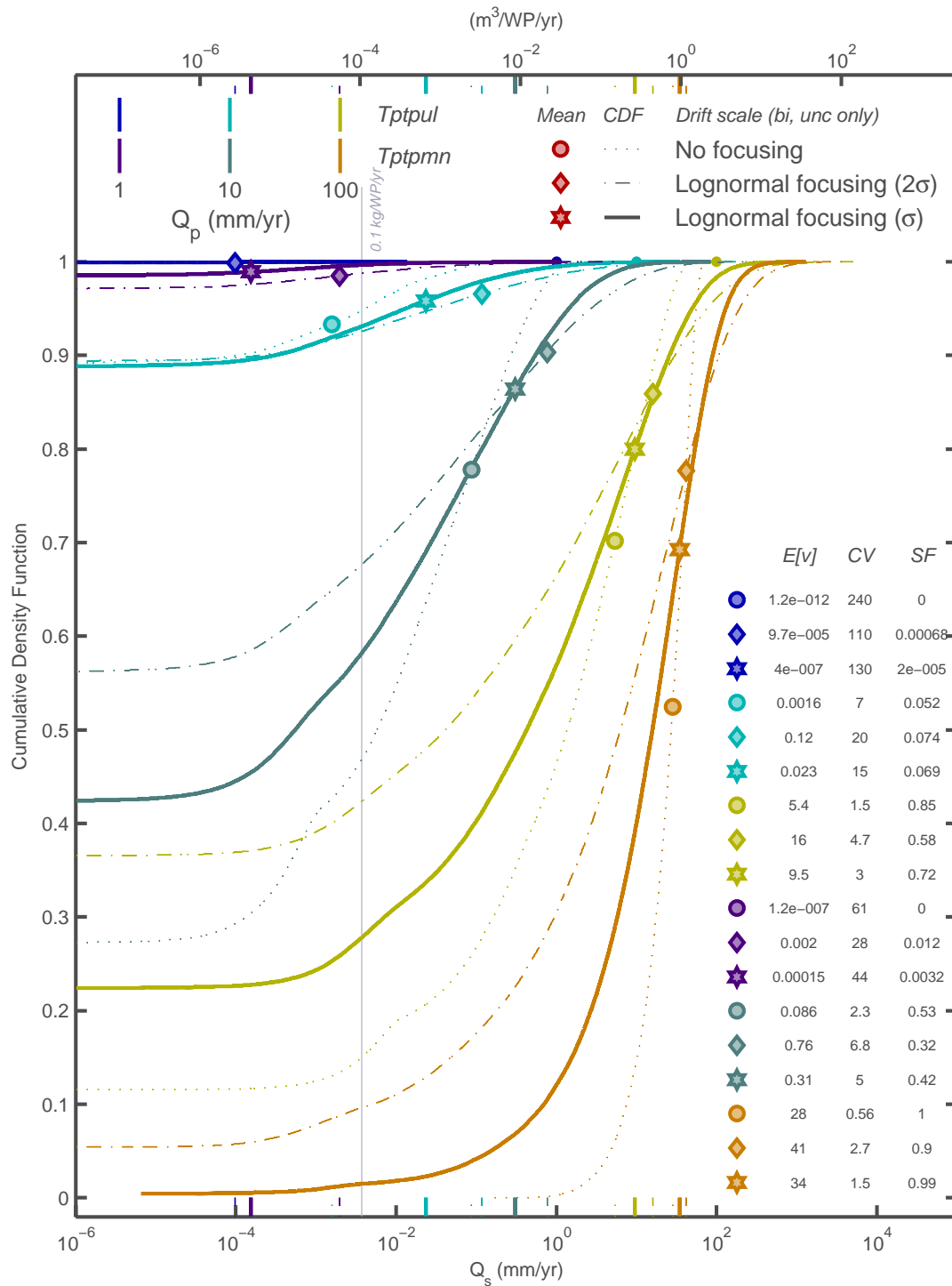


Figure 4-19: Cumulative seepage distribution setting variable inputs to the median value and including uncertainty.

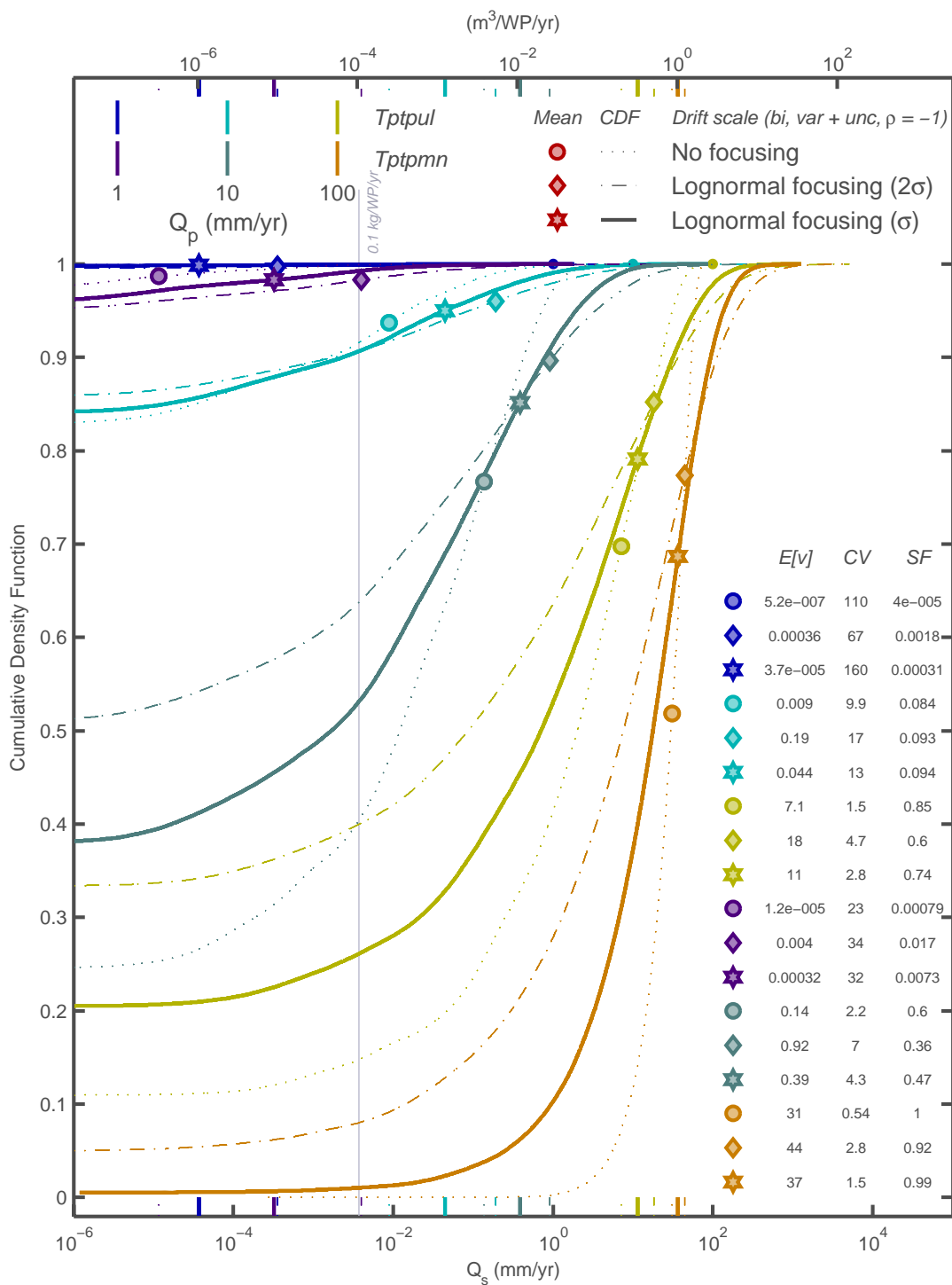


Figure 4-20: Cumulative seepage distribution with perfect negative correlation between $1/\alpha$ and $\log(k_f)$.

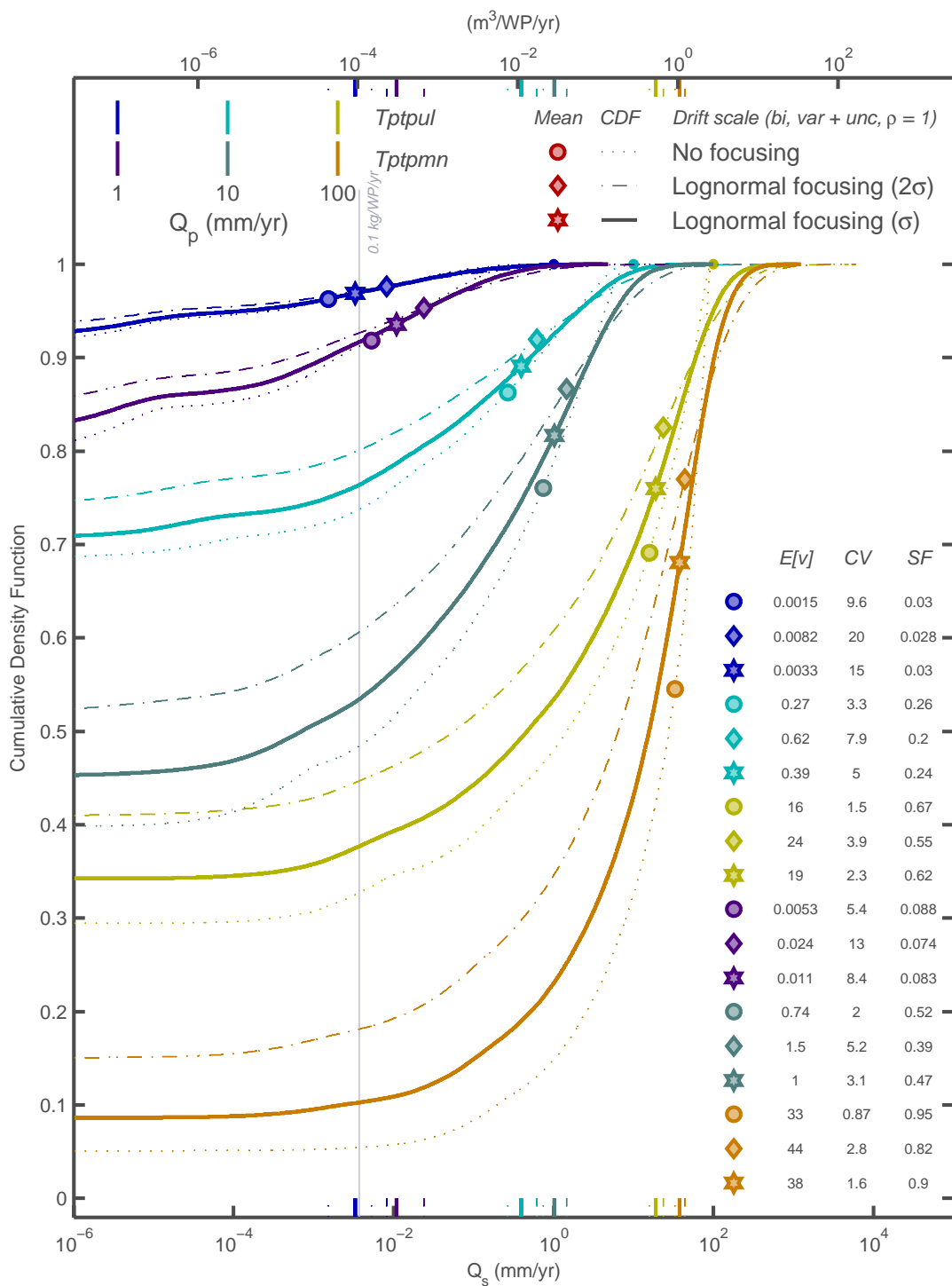


Figure 4-21: Cumulative seepage distribution with perfect positive correlation between $1/\alpha$ and $\log(k_f)$.

Figure 4-22 demonstrates the effect of averaging on the cumulative distribution of seepage. The cumulative distribution of expected seepage is much narrower than the cumulative distribution of drift-scale seepage, although the mean values are identical (to within sampling and roundoff tolerances). Note that the peak areal-average values are less than the average percolation flux over the entire distribution, even though the drift-scale distribution may have a component larger than the average percolation flux.

06/22/10 Return to seepage effects on diffusive releases.



Annotation dated 06/22/10: This section returns to the analysis on releases dated June 16, 2010. The section is based on my personal notes last modified on March 30, 2009. The section describes independent abstracted calculations rather than DOE calculations.



Figure 4-23 considers releases assuming that (i) the matrix, invert, and waste package have the same diffusion coefficient, reduced by four orders of magnitude from free water to account for porosity, saturation, and tortuosity; (ii) the solute is unretarded; (iii) no advective releases occur through the waste package leg; and (iv) the area of the waste package for diffusion is 1/10th of the area of the invert cross section. This is a solubility-limited model, with a fixed concentration inside the waste package, a 3-cm leg from the waste package interior to the invert, a 0.934-m leg in the invert, and zero concentration imposed 15.5 m into the host rock. This situation might represent a waste package that has largely failed but dripping fluxes completely bypass the breach. Figure 4-24 provides the same analysis for seepage weighted by the units found in the repository footprint. Figure 4-24 includes a limiting Q_p that is order of magnitude larger than the largest percolation flux bin considered by DOE, approximately representing a process-level seepage model that over-estimates capillary diversion. In this situation, a increase of three orders of magnitude in average percolation flux results in approximately 1.5 orders of magnitude in release, and a wider range would not substantially increase release (corresponding to the plateaus in Figure 4-14). The effect of flow focusing is minor relative to changes in average percolation flux, especially for low and high average fluxes.

Figure 4-25 compares total steady-state release when the invert diffusion coefficient differs by two orders of magnitude. The left-hand graph in Figure 4-25 considers the same situation as Figure 4-24, except that only 0.001 of the invert area is breached in the waste package. Total release is essentially insensitive to average percolation flux with the small breach, corresponding to the waste-limited regimes in Figure 4-14. The effect of the path length is inversely proportional to the area because the path length always divides the area. The right-hand graph indicates that

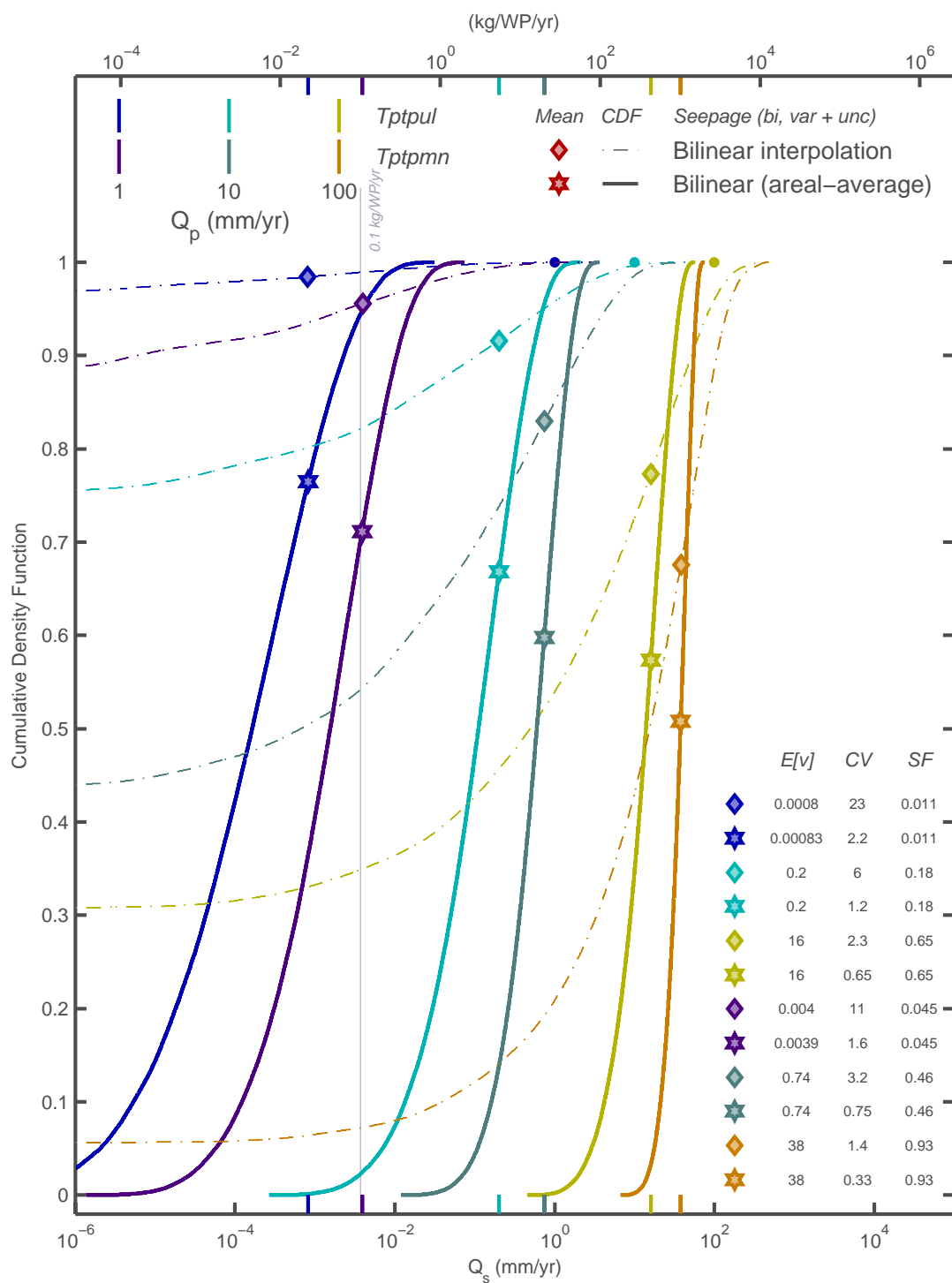


Figure 4-22: Cumulative seepage distribution, including uncertainty and variability, at the drift scale and the expected areal average.

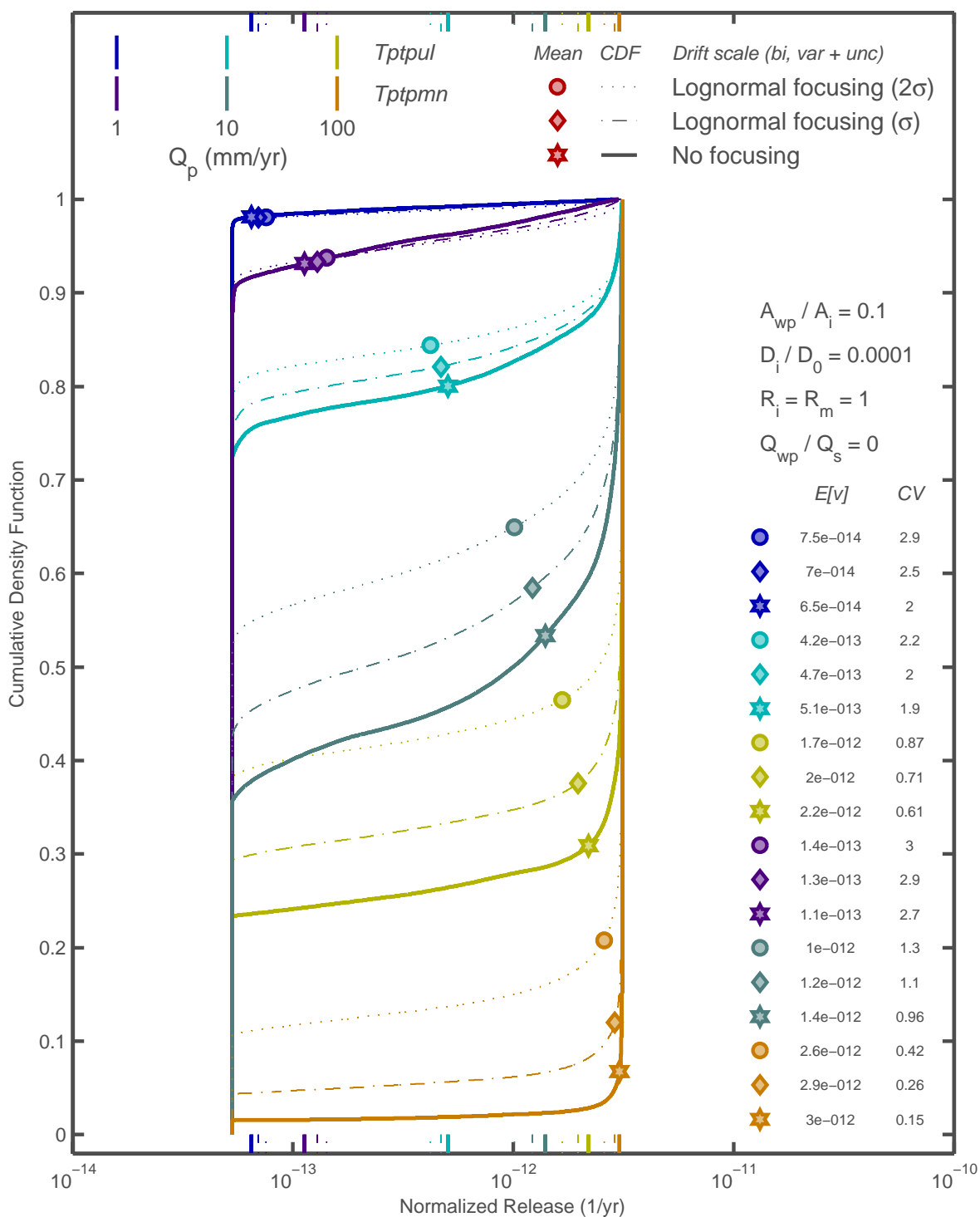


Figure 4-23: Steady-state release for individual units with large failed area, small diffusion coefficient, no water through the waste package, and no retardation.

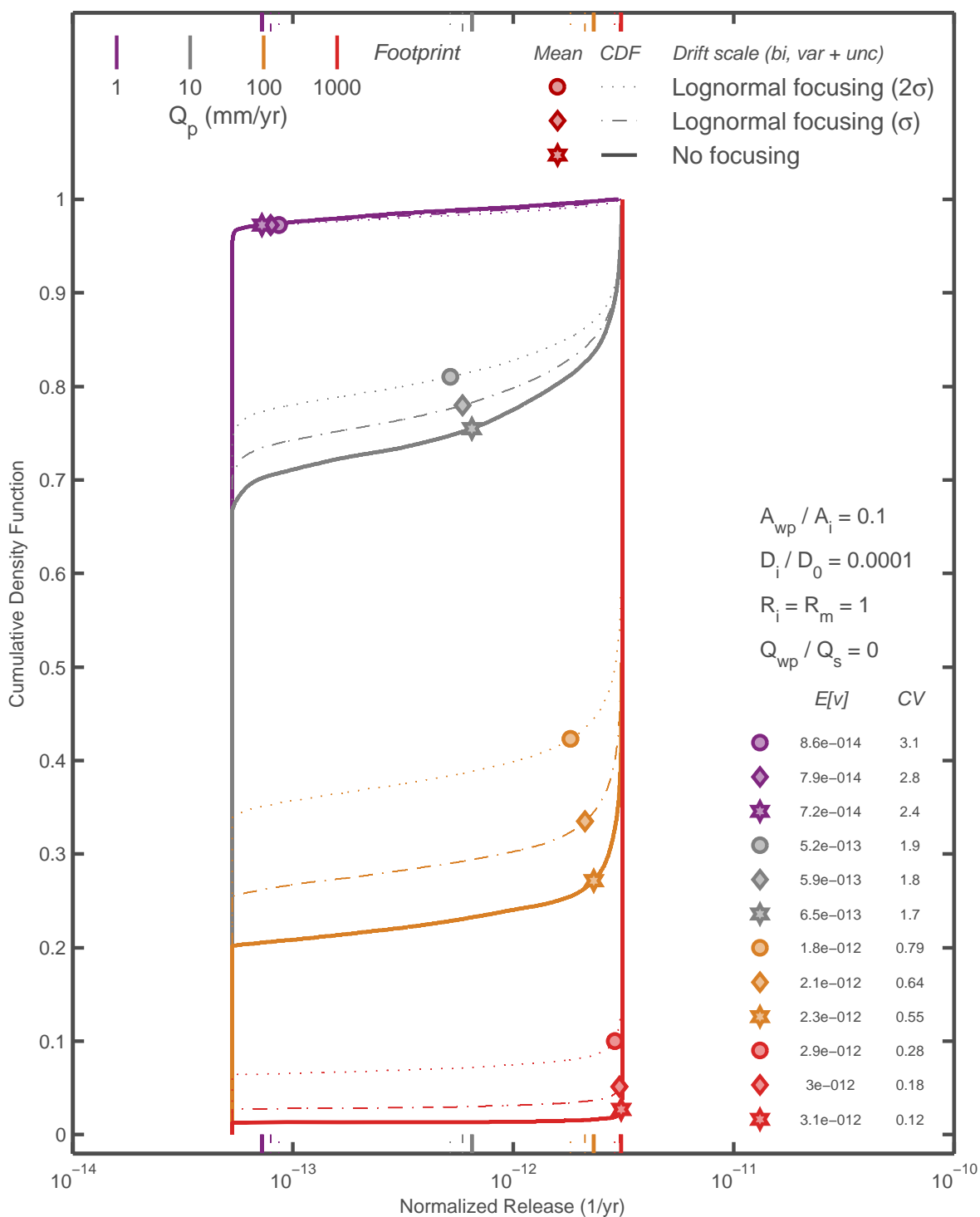


Figure 4-24: Steady-state release with large failed area, small diffusion coefficient, no water through the waste package, and no retardation.

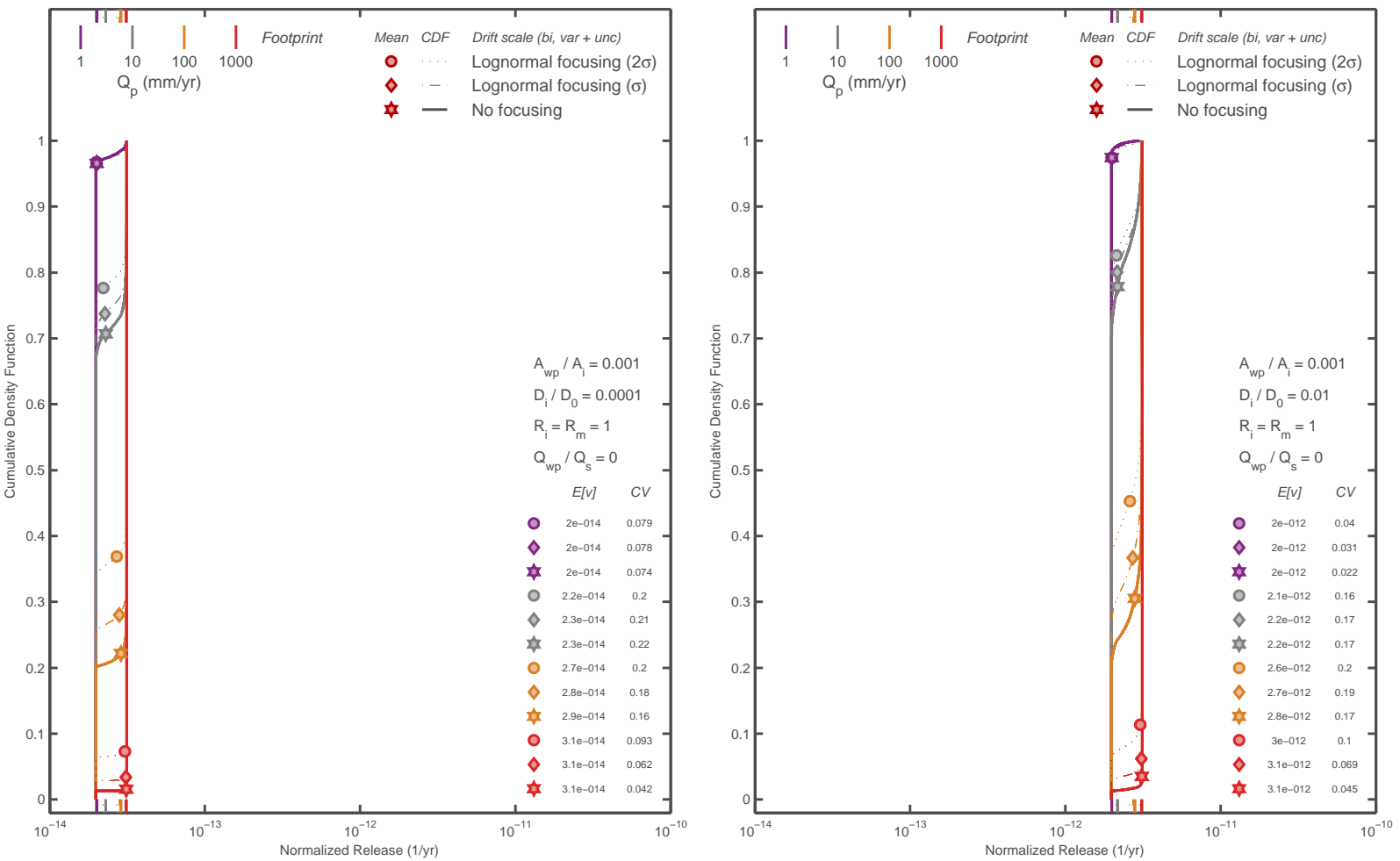


Figure 4-25: Steady-state release with small failed area, small and large invert diffusion coefficient, no water through the waste package, and no retardation.

increasing the diffusion coefficient proportionally increases release when no flow through the waste package occurs.

Figure 4-26 compares the ratio of fracture to matrix releases if water flows through the breach. In this comparison, the breach area differs by two orders of magnitude and the water flowing through the breach is proportional to the breach area. For this case, I assume that the breach is 90 percent effective at repelling water, so that the fraction of the seeping water passing through the breach is 0.1 times the breach area fraction. With a small breach (1/1000th of the waste package area), total release remains essentially insensitive to average percolation flux at low average percolation rates, but an order of magnitude increase in average percolation induces more than an order of magnitude increase in total release at large seepage rates. With a large breach (1/10th of the waste package area), steady releases increase by approximately 1.5 orders of magnitude for each order of magnitude increase in percolation. Note that the x axis in the right-hand figure has a different scale than the other release figures.

Finally, Figure 4-27 provides a case where retardation is implemented by dividing the invert and matrix fluxes by the retardation coefficient. Retardation is not really appropriate for a steady-state solution, because the retardation coefficient multiplies the time derivative. The comparison provides a first-order approximation of early-time releases compared to late-time releases. The effect of retardation in this case appears to be inversely proportional to the effect of the invert diffusion coefficient.

The abstracted model separately considers matrix and fracture release pathways, assuming that all water flux enters the fracture system. The calculated ratio of fracture to matrix release corresponding to Figures 4-23 and 4-24 are shown in Figures 4-28 and 4-29, respectively. Note that the assumption that all seeping water enters the fractures is a first approximation and overestimates the water moving into the fracture system, because the matrix will accept some dripping water. Most of the dripping water will likely enter the matrix at seepage fluxes that are small compared to the matrix hydraulic conductivity. The transition may be less than 0.1 mm/yr for the nonlithophysal units and as large as 10 mm/yr for the lithophysal units, based on the upscaled matrix properties developed from core data presented in SAR Table 2.3.2-3.

Figure 4-30 compares the ratio of fracture to matrix releases for a small breach with invert diffusion coefficients differing by two orders of magnitude, corresponding to Figure 4-25. The total release is larger by two orders of magnitude with the larger invert diffusion coefficient. Based on Figure 4-30, which shows that the expected release ratio for the larger invert diffusion coefficient is two orders of magnitude larger than the expected release ratio with the smaller diffusion coefficient,

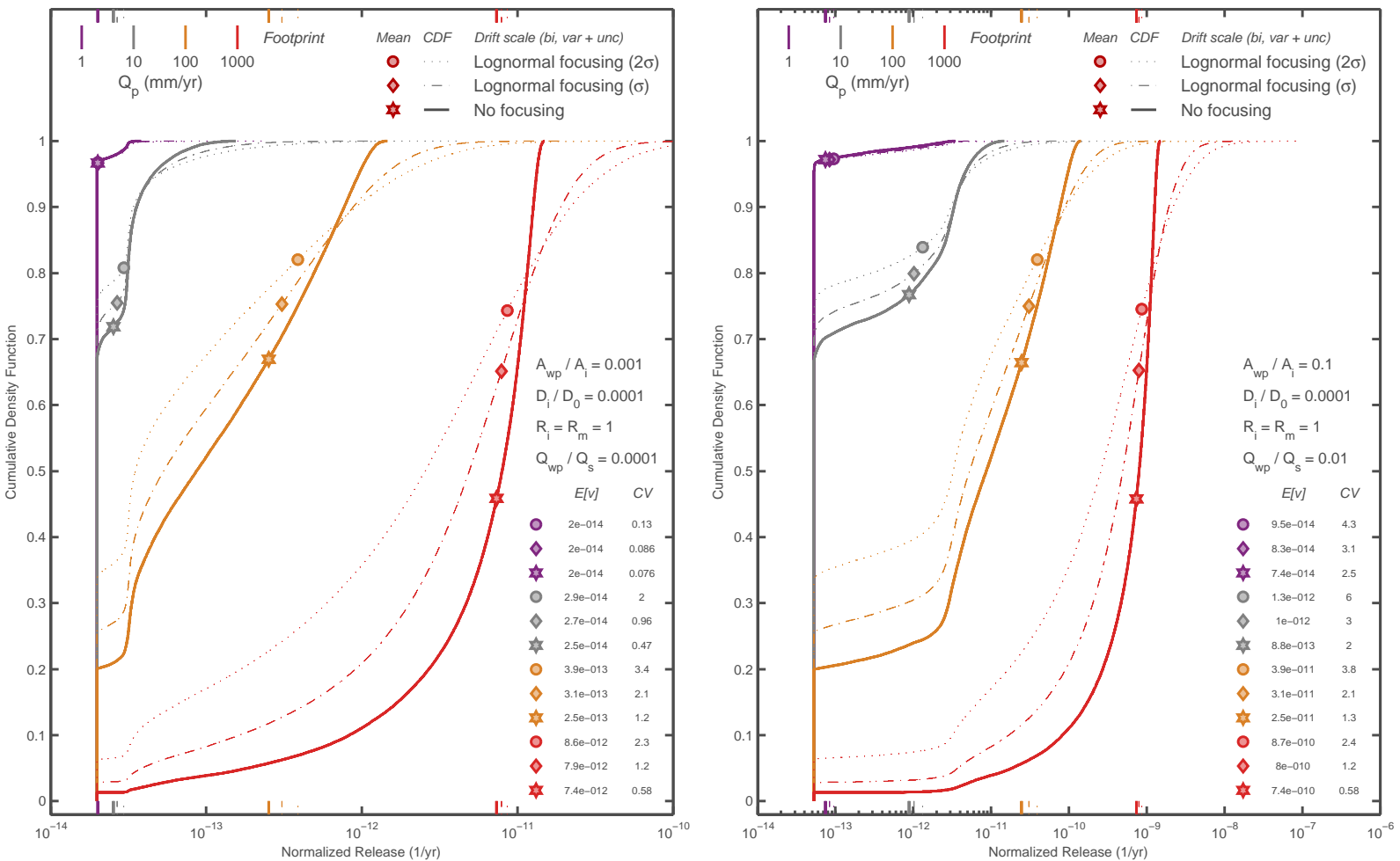


Figure 4-26: Steady-state release with small and large failed area, small diffusion coefficient, water through the waste package proportional to failed area, and no retardation.

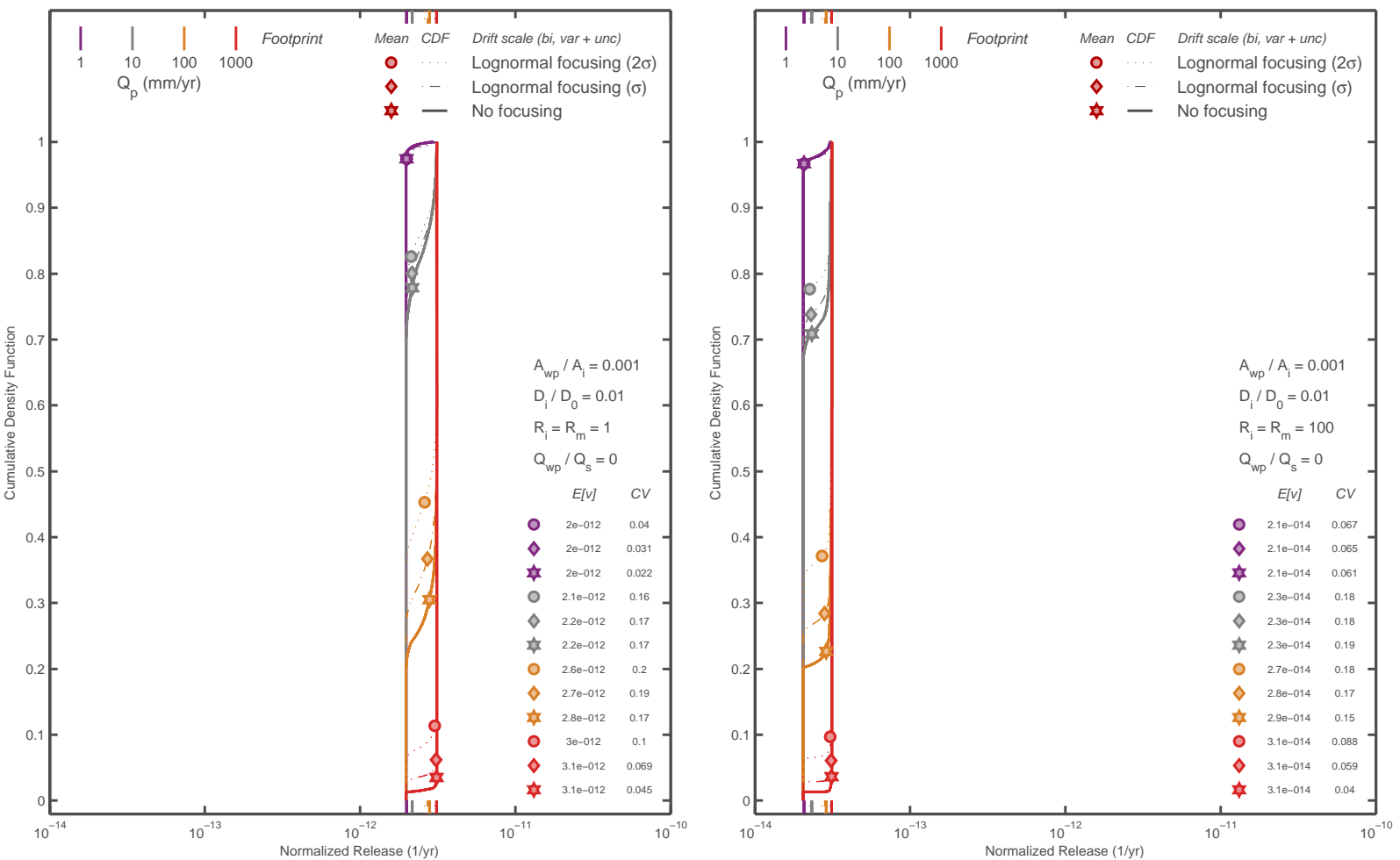


Figure 4-27: Steady-state release with small failed area, large diffusion coefficient, no water through the waste package, comparing no invert/matrix retardation to some retardation.

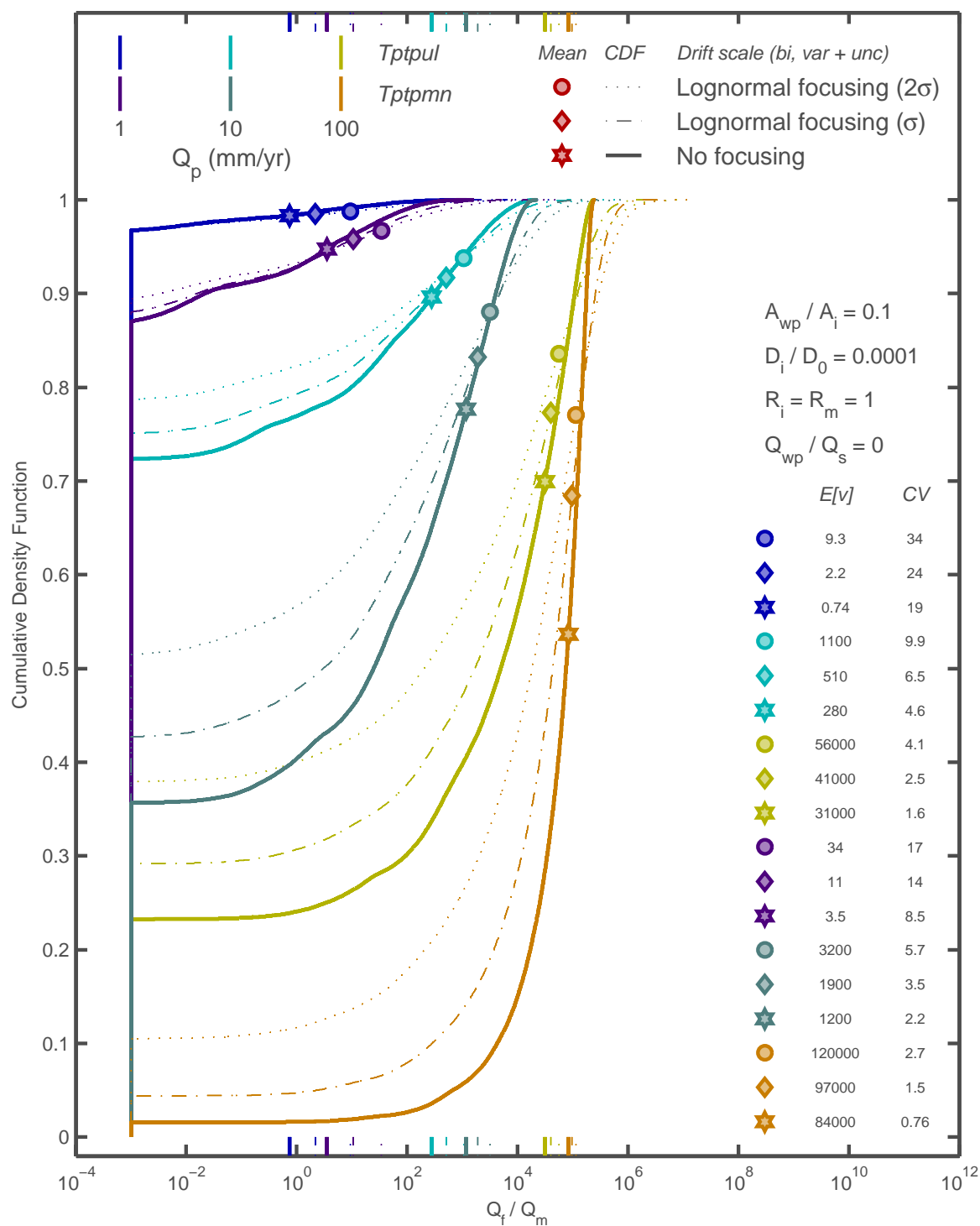


Figure 4-28: Ratio of fracture to matrix release for individual units with large failed area, small diffusion coefficient, no water through the waste package, and no retardation.

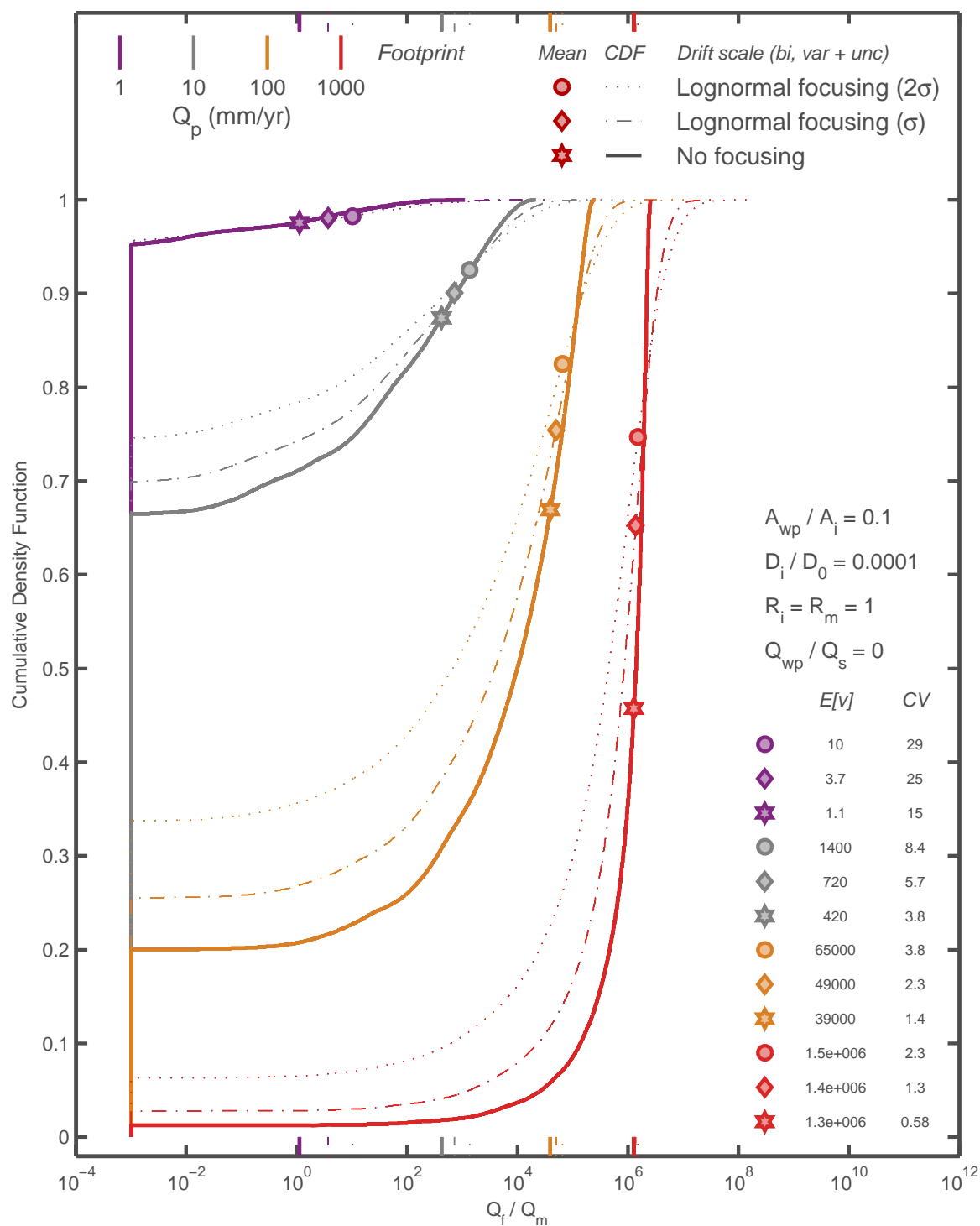


Figure 4-29: Ratio of fracture to matrix release with large failed area, small diffusion coefficient, no water through the waste package, and no retardation.

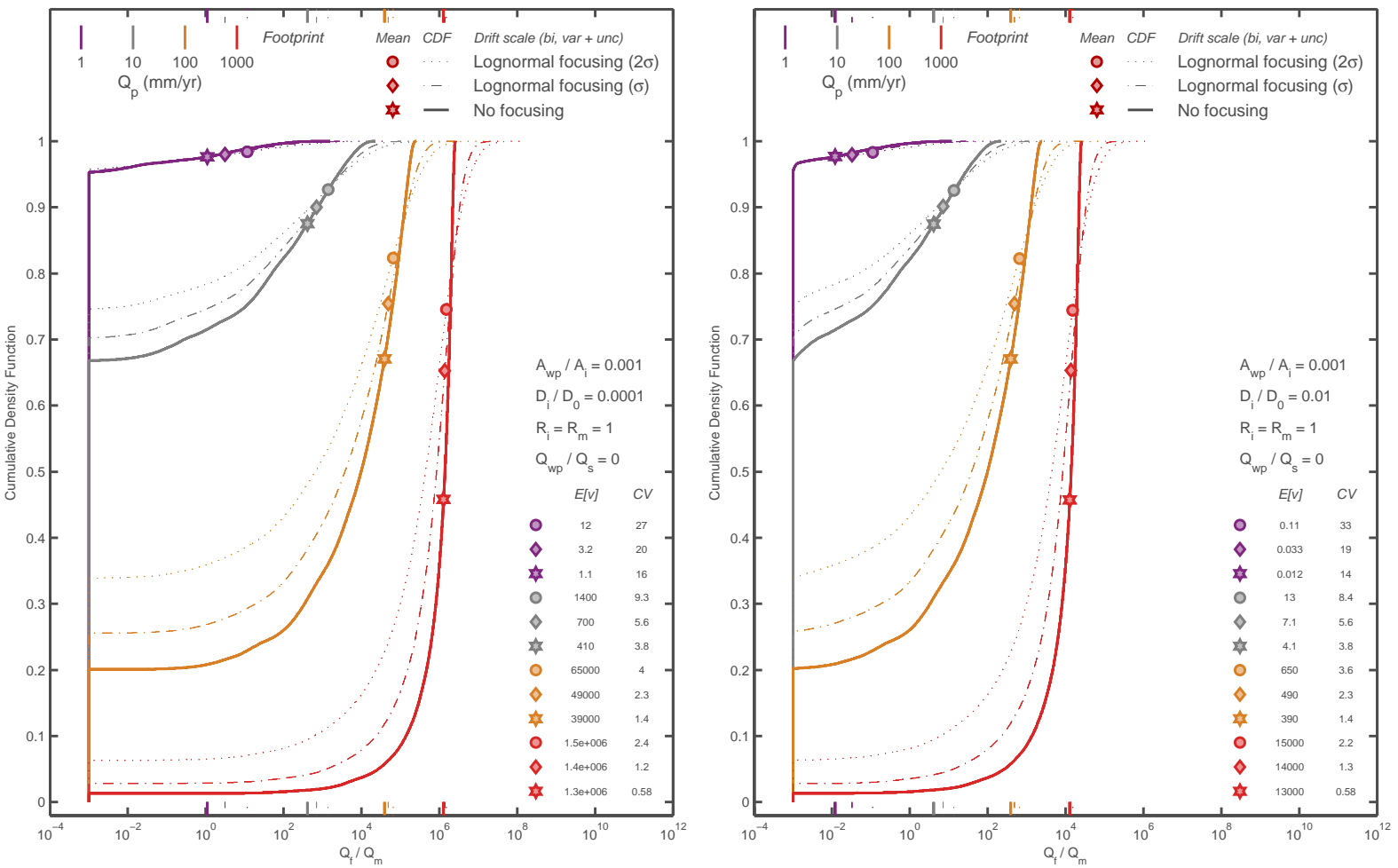


Figure 4-30: Ratio of fracture to matrix release with small failed area, small and large diffusion coefficient, no water through the waste package, and no retardation.

the ratio of fracture to matrix release is proportional to the diffusion coefficient whenever seepage occurs. With no seepage, all release is to the matrix (note that the model includes diffusive release for the fracture pathway over a very small fraction of the host rock area).

Figure 4-31 compares the ratio of fracture to matrix releases if water flows through the breach, corresponding to Figure 4-26. In this comparison, the breach area differs by two orders of magnitude and the water flowing through the breach is proportional to the breach area. For this case, I assume that the breach is 90 percent effective at repelling water, so that the fraction of the seeping water passing through the breach is 0.1 times the breach area fraction. The two cases have essentially the same fracture to matrix release ratios, even though the total release differs considerably between the two cases.

Comparing Figures 4-30, 4-31, and 4-29 (different waste package area and flow-through characteristics, same invert diffusion coefficient) indicates that the partitioning between matrix and fracture is not sensitive to the nature of waste package release even though total release may vary dramatically.

Figure 4-32 compares the ratio of fracture to matrix releases when invert and matrix retardation changes by two orders of magnitude, corresponding to Figure 4-27. Again, retardation is not really appropriate for the steady-state solution and the comparison provides a first-order indication of early-time conditions. As with total release, retardation has the inverse effect that the invert diffusion coefficient has on ratio of fracture to matrix releases whenever seepage occurs. Unlike the total release, however, retardation also proportionally scales the release ratio when seepage fluxes are negligibly small.

06/23/10 More seepage effects on releases.



An additional set of comparisons provides a qualitative look at the effect of a distribution of breaches without flow through the breach. These comparisons reprise cases illustrated before with the additional assumption that the breach area is lognormally distributed in the form

$$\frac{A_{wp}}{A_i} = R_0 10^{\sigma_{\log} N[0,1]} \quad (4-3)$$

where R_0 is the median value (reported as A_{wp}/A_i in the figures), σ_{\log} is the standard deviation of the base-10 logarithm, and $N[0, 1]$ is a zero-mean unit-variance normal distribution. Only total releases are shown in the comparisons, because corresponding figures with the ratio of fracture to matrix release correspond directly to the case without variable breach areas (consistent with the

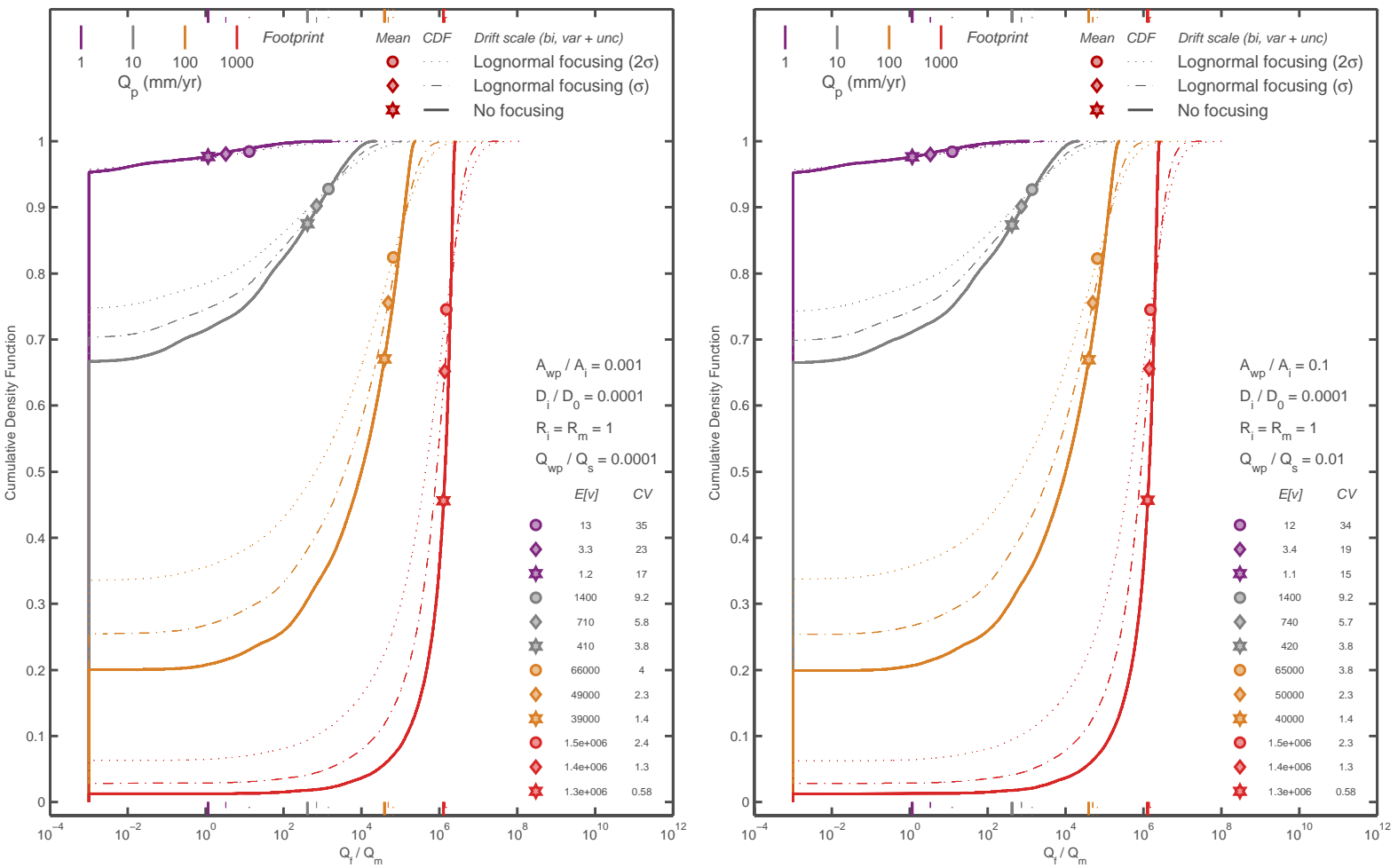


Figure 4-31: Ratio of fracture to matrix release with small and large failed area, small diffusion coefficient, water through the waste package proportional to failed area, and no retardation.

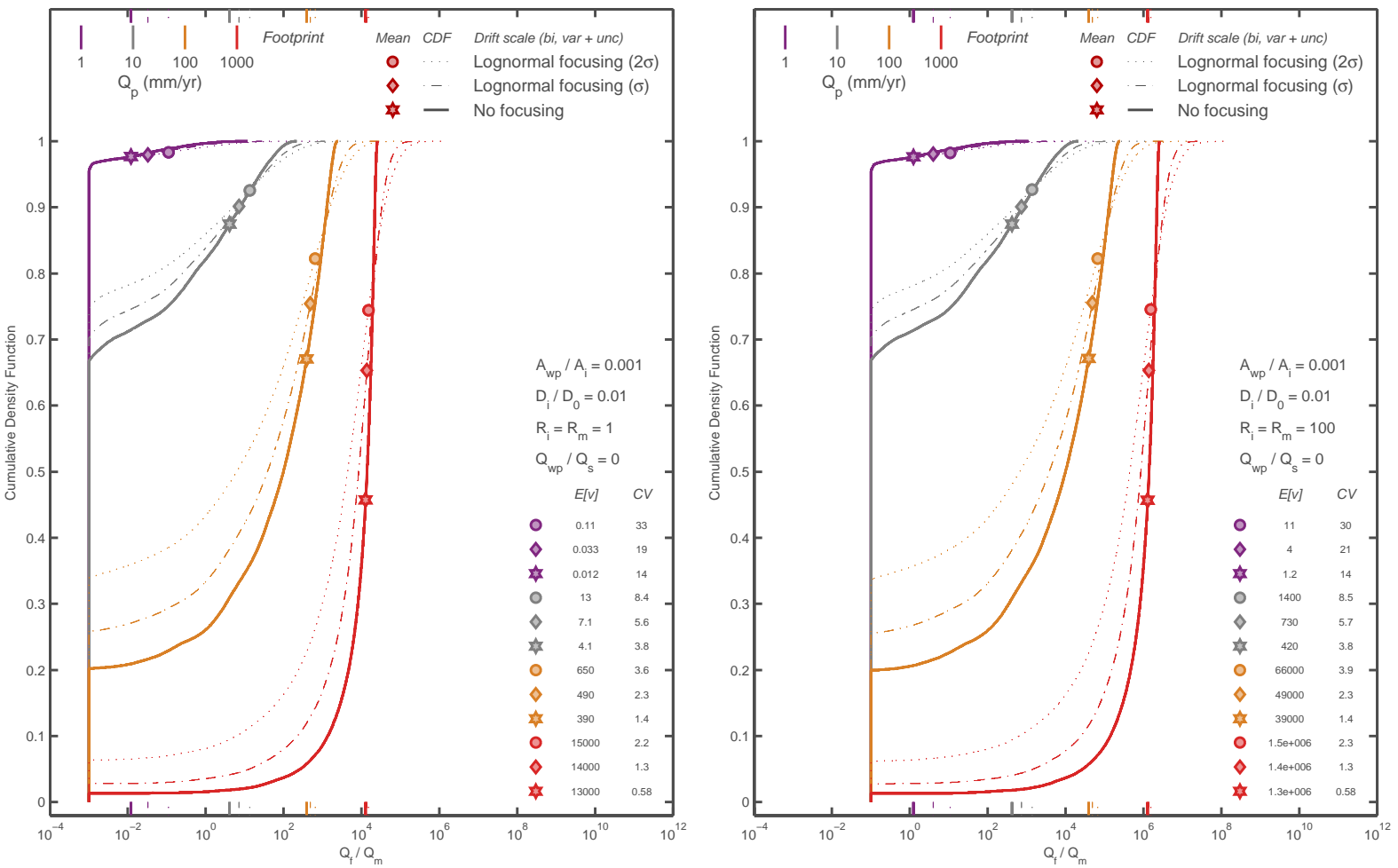


Figure 4-32: Ratio of fracture to matrix release with small failed area, large diffusion coefficient, no water through the waste package, and small and large retardation.

conclusion that waste-package characteristics do not affect the fracture to matrix release ratio). In the comparisons, I use $\sigma_{\log} = 0.5$, for which $E[A_{wp}/A_i] = 1.94R_0$.

Figure 4-33 compares releases with the large breach area and Figure 4-34 compares releases with the small breach area. In both cases, the right-hand figure displays the realizations with lognormally distributed area. The cases with large Q_p are most sensitive to σ_{\log} and the cases with small Q_p are least sensitive. For both the large and small breach cases, the expected release is essentially proportional to $E[A_{wp}/A_i]$ for the highest Q_p and changes little for the lowest Q_p . For all fluxes, the coefficient of variation increases when variability in A_{wp} is included, with the relative change increasing with Q_p in both cases. Increased flow focusing tends to slightly reduce the sensitivity of release to variability in A_{wp} .

Figure 4-35 compares releases with small breach area and large invert diffusion coefficient. The trends are consistent with Figures 4-25 and 4-34.

Figures 4-36 and 4-37 compare releases with small and large breach area, respectively, with water passing through the waste package. For these figures, I fixed the fraction of seeping water passing through the breach to the same value in all cases. With water flowing through the waste packages, variability in breach area slightly increases total release and variability for small percolation fluxes, smoothing the distribution, but variability has little or no effect at large percolation fluxes. This is in contrast to the sensitivity patterns found with variable area but no waste-package water fluxes. Figures 4-38 and 4-39 repeat the same cases except that the breach area is fixed and the fraction of seeping water is variable. In this case, the response is similar to the sensitivity patterns found with variable area and no waste-package water fluxes, with the sensitivity to area replaced by sensitivity to water flux. Note that the lognormal distribution for the fraction of seepage water passing through the waste package tends to make the high end of the release distribution more similar for the different flow focusing cases. Also note that total expected release increases by including the variability in flux through the waste package (with a standard deviation for the log-transformed flux of 0.5), increasing by almost two-fold for large Q_p . In contrast, $2\sigma \approx 2.6$ for the flow focusing factor, yet there is only a nominal change in release for different σ values for the flow focusing factor.

Figure 4-40 compares releases with small breach area and large invert diffusion coefficient, with retardation variable and no flux through the waste package. Again the caveat is that this is an approximation for early releases. The release distribution becomes nearly lognormal, reflecting the distribution for the retardation coefficient. A similar effect should be observed if the diffusion coefficient were sampled instead of the retardation coefficient, because the two have essentially

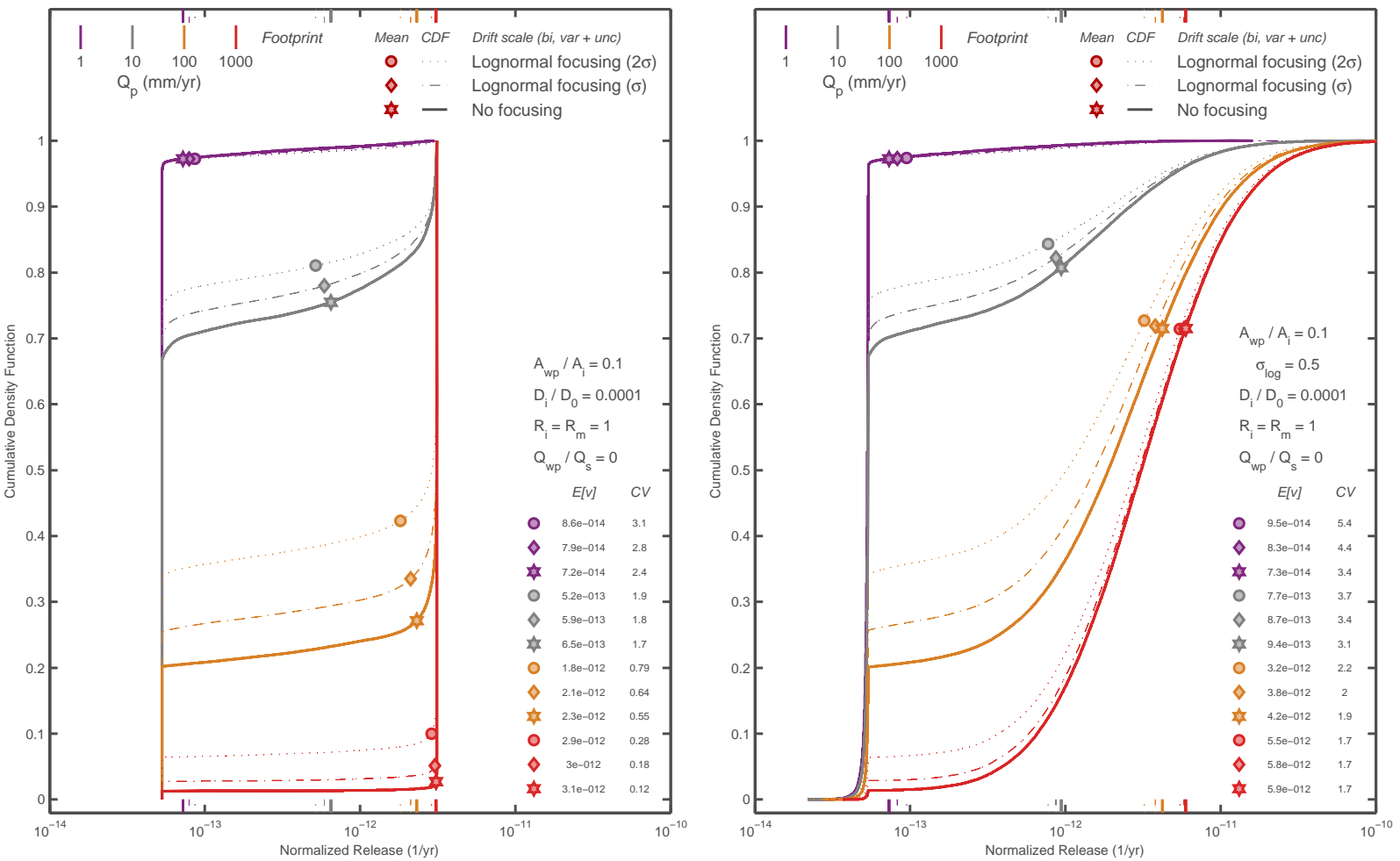


Figure 4-33: Steady-state release with large fixed and variable failed area, small invert diffusion coefficient, no water through the waste package, and no retardation.

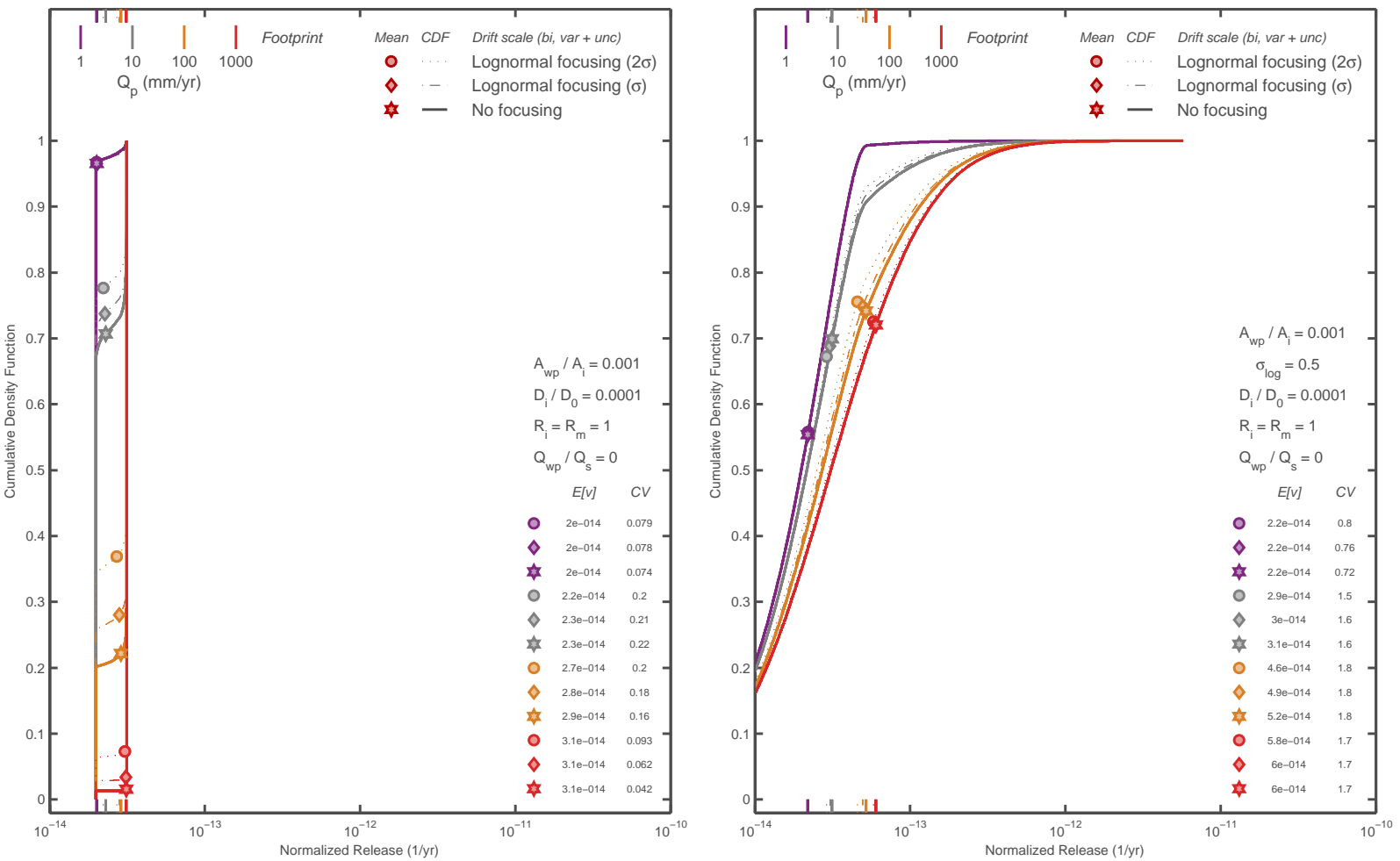


Figure 4-34: Steady-state release with small fixed and variable failed area, small invert diffusion coefficient, no water through the waste package, and no retardation.

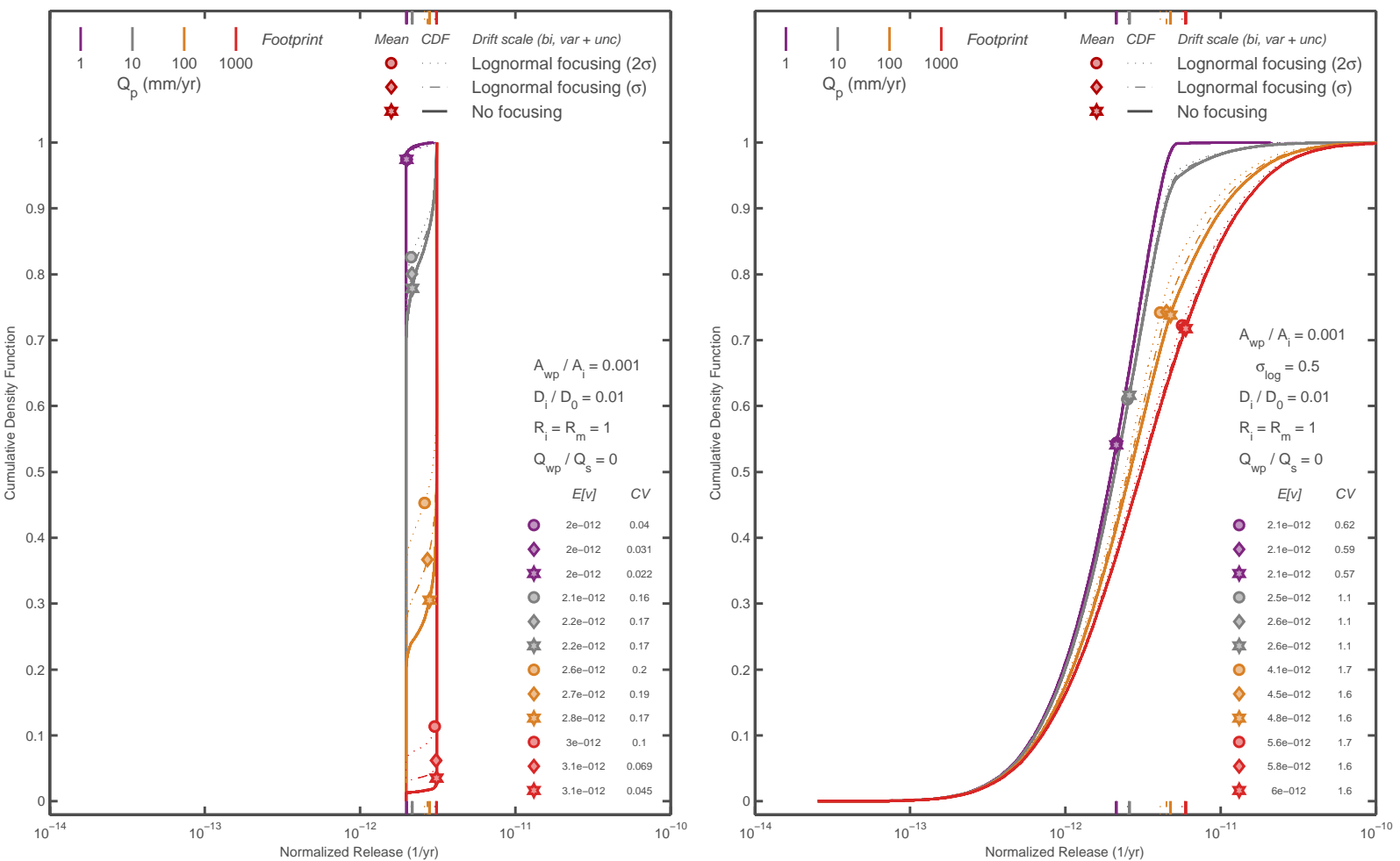


Figure 4-35: Steady-state release with small fixed and variable failed area, large invert diffusion coefficient, no water through the waste package, and no retardation.

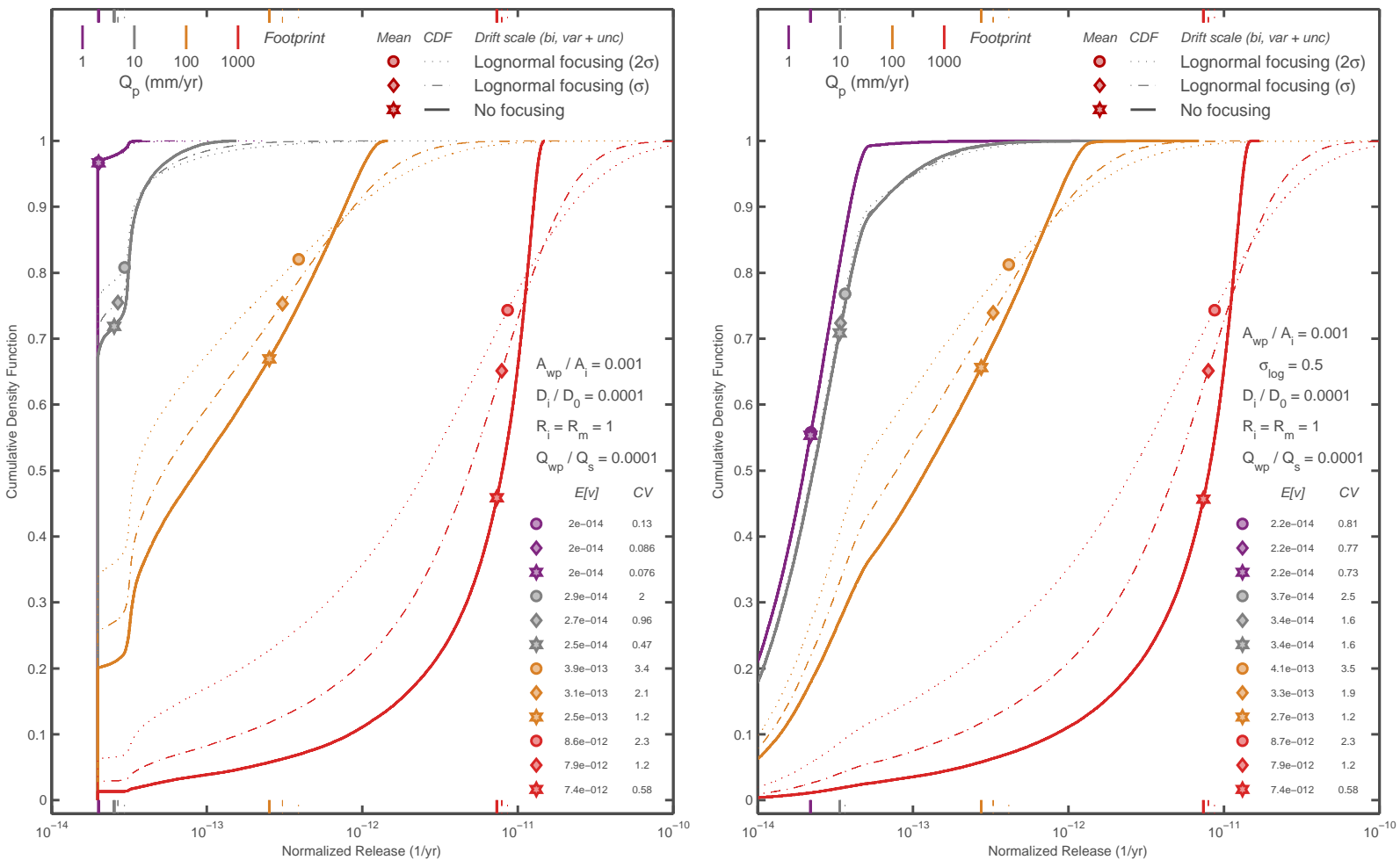


Figure 4-36: Steady-state release with small fixed and variable failed area, small invert diffusion coefficient, water through the waste package, and no retardation.

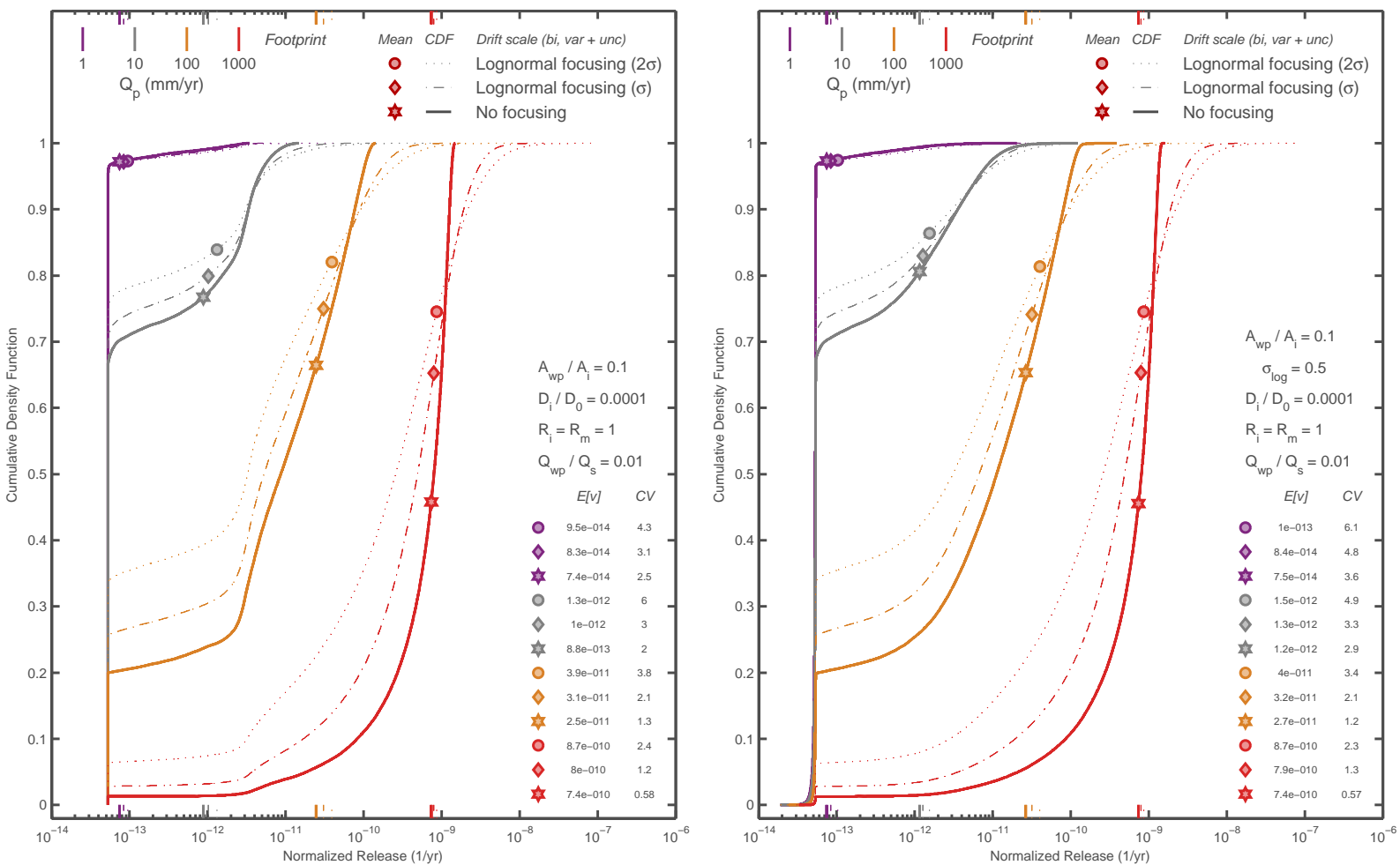


Figure 4-37: Steady-state release with large fixed and variable failed area, small invert diffusion coefficient, water through the waste package, and no retardation.

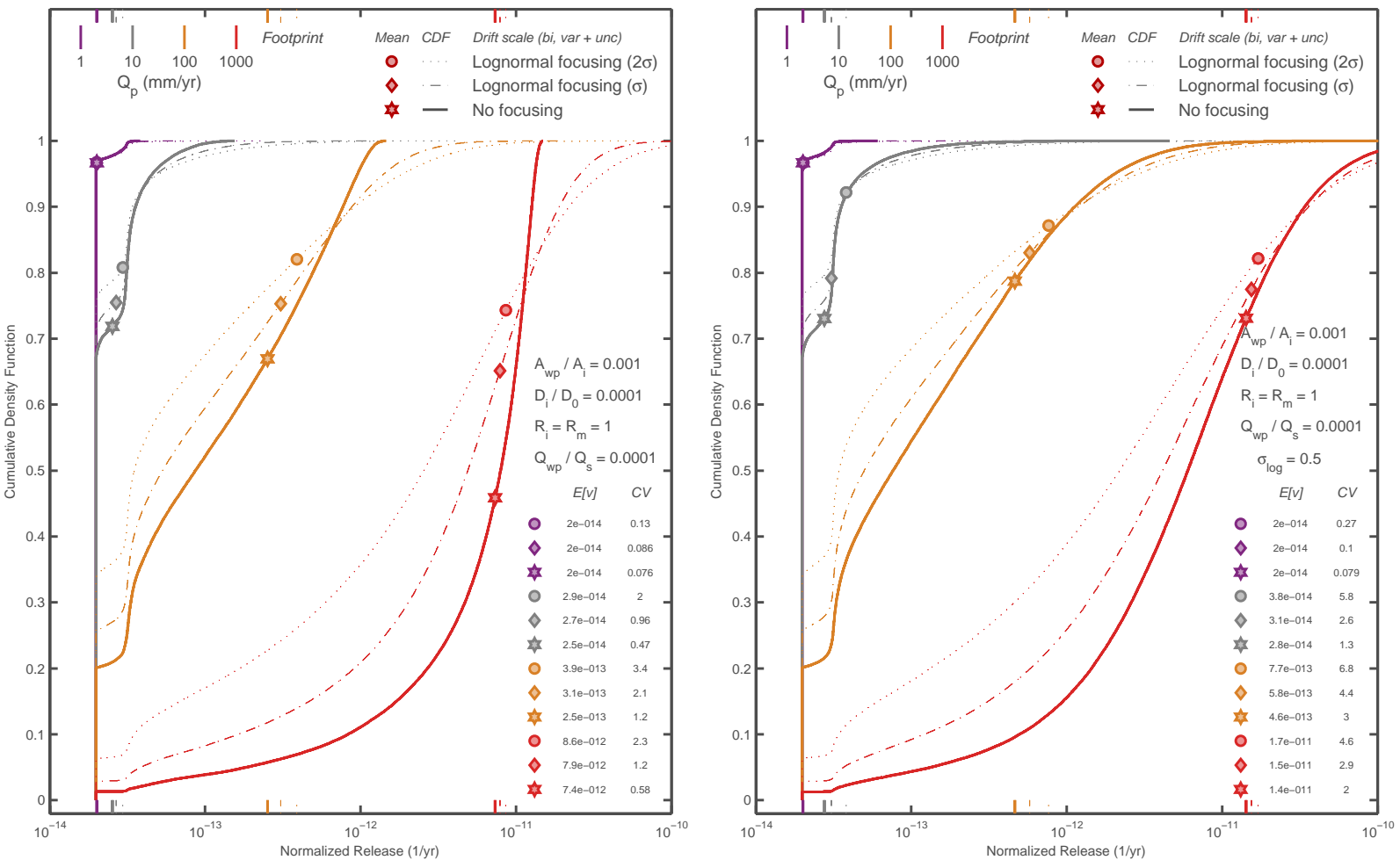


Figure 4-38: Steady-state release with small failed area, small invert diffusion coefficient, fixed and variable water through the waste package, and no retardation.

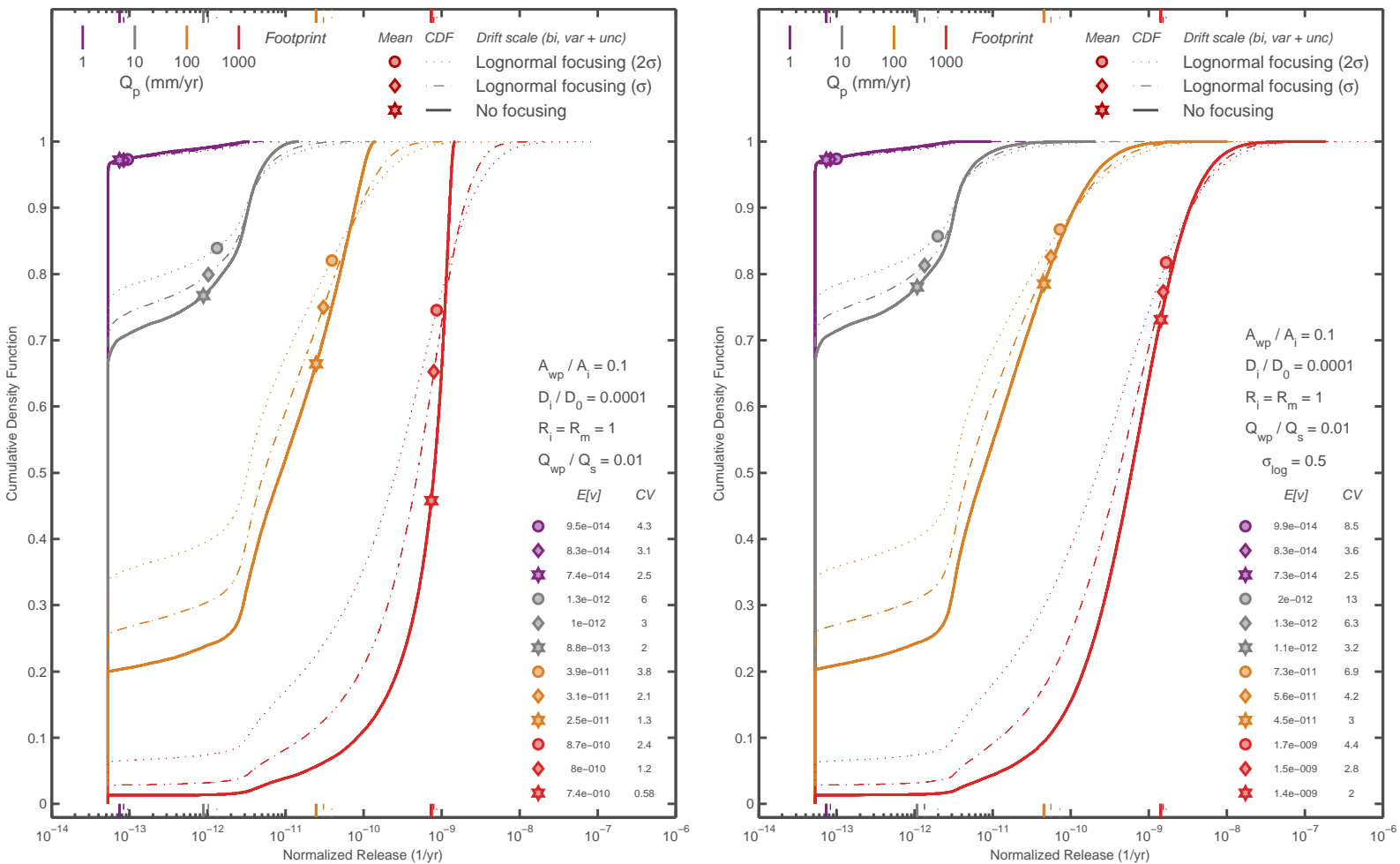


Figure 4-39: Steady-state release with large failed area, small invert diffusion coefficient, fixed and variable water through the waste package, and no retardation.

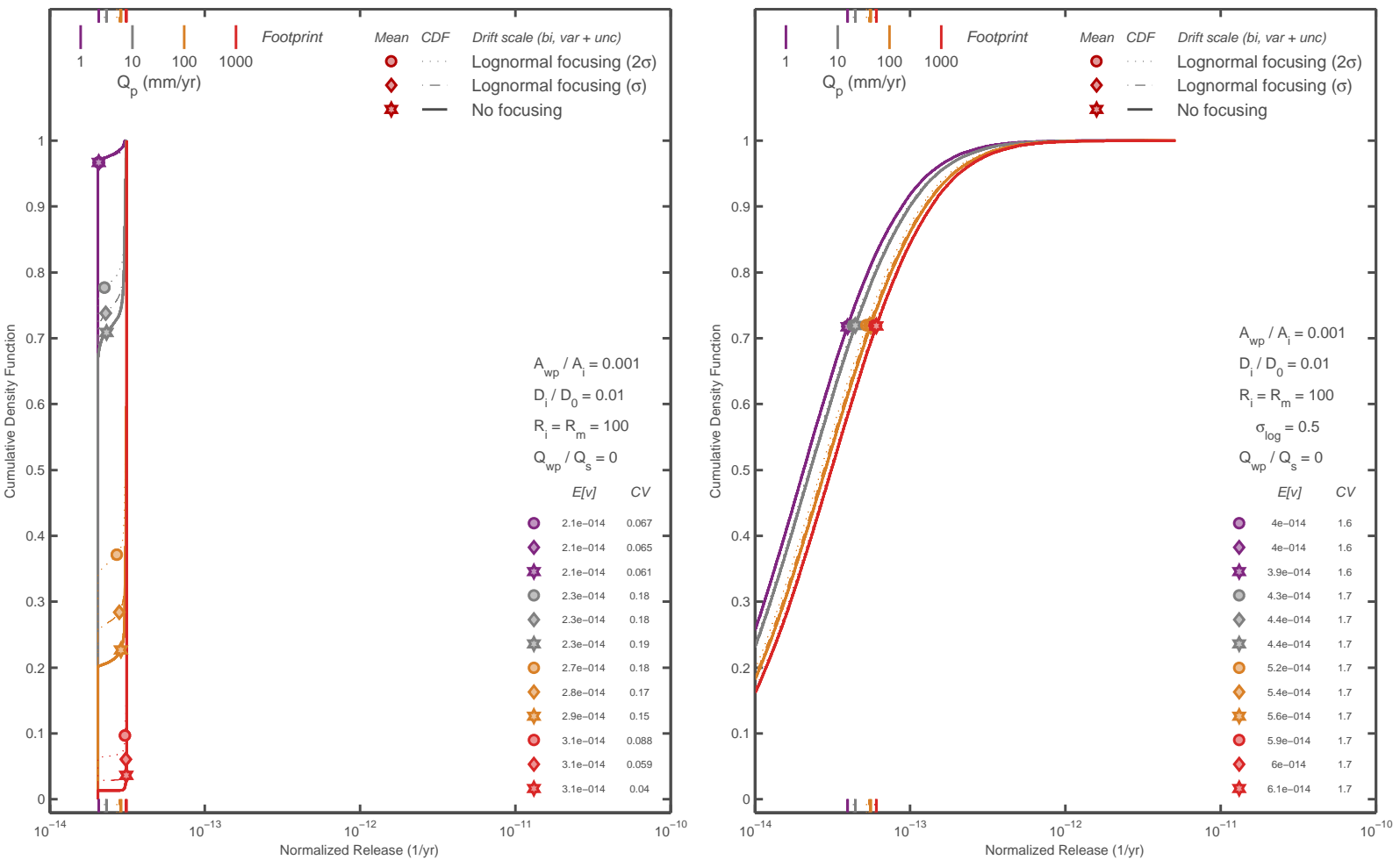


Figure 4-40: Steady-state release with small failed area, large invert diffusion coefficient, no water through the waste package, and fixed and variable retardation.

inversely proportional effects.

As a final example case, Figure 4-41 considers the case where both the breach area and fraction of seepage passing through the waste package are variable with independent lognormal distributions. For this case, the mean fluxes in the five percolation-flux bins of the DOE 10th percentile glacial transition are used. The yellow curves represent the cumulative distribution over all bins, with each bin weighted according to the DOE weighting (0.05, 0.25, 0.4, 0.25, and 0.05, respectively). I also assume here that the mean fraction of seepage water passing through the waste package is the same as the mean breach area. The release distributions have a clear kink corresponding to the transition between realizations with diffusion-limited and advection-limited transport from the waste package. The same kink shows up in the fracture/matrix release ratio. Variability in the seepage flux ratio dominates for the larger releases, variability in the breach area dominates for the smaller releases. For each percolation flux bin, a wider range of flow focusing tends to increase release and increase the fraction of releases entering the fracture system, but the differences are small relative to the spread in the distribution. The cumulative distribution over all bins is quite similar to the middle bin for seepage (not shown), release, and fracture/matrix release ratio.

06/24/10 Seepage effects on transient releases.



The previous entries explored the steady-state behavior of solubility-limited conservative radionuclides moving from a waste package through the invert and into the host rock. I used a highly abstracted approach to estimate transport, suitable for rapid calculations exploring the consequences of uncertainty and variability. The method captures essential aspects of the procedure sufficiently to understand the general controls on solubility-limited radionuclides. Partitioning between matrix and fracture systems is not completely resolved with the method, because retardation is not a factor under steady-state conditions but invert and matrix retardation clearly has an effect that favors release to the fracture system at early time. Further, the analysis did not consider dissolution-limited release.

The DOE approach considers a process-level model using GoldSim. The invert is represented by a single mixing cell, which implies that mass is available for release to the host rock immediate a transfer to the invert occurs. DOE represents the host rock with a network of matrix and fracture pathways extending 30 m below the host rock. The model apportions all dripping flux to the fracture continua and all imbibition flux to the matrix. If the background flux is larger than the dripping flux, the model uses the background flux for the fracture continuum. Note that

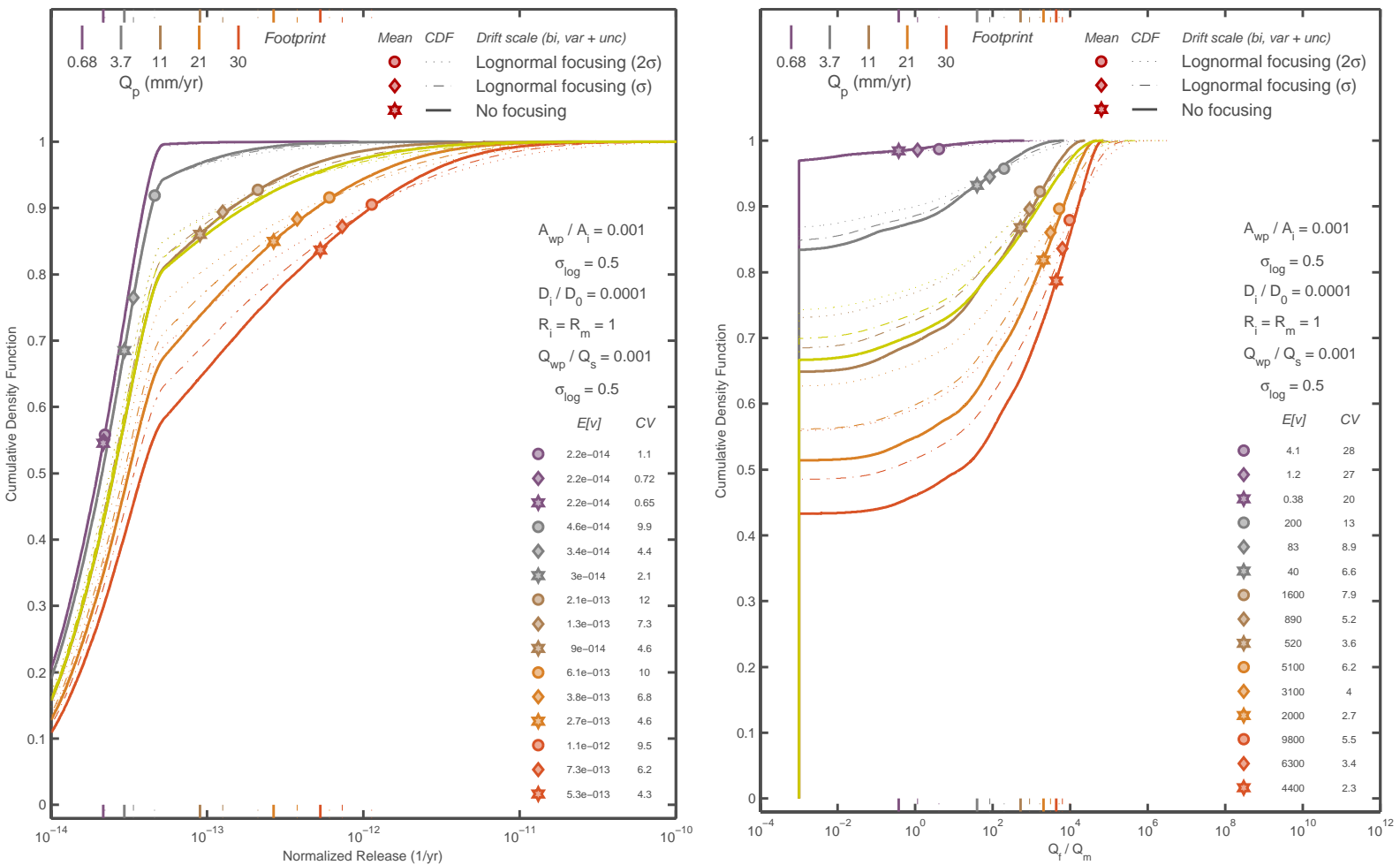


Figure 4-41: Steady-state release with small variable failed area, small invert diffusion coefficient, variable water through the waste package, and no retardation.

the DOE-calculated imbibition flux approaches zero after the thermal period ceases. The DOE model assumes that the background concentration at the bottom of the network is zero for both the matrix and fracture system.

I developed a transient method using the pdepe solver from *Matlab*. Again the concept is a single one-dimensional (1D) leg in the invert and a separate 1D leg for both the fracture and matrix. Based on the steady-state analysis, waste package details do not affect the partitioning between matrix and fracture but may affect the amount and timing of releases from the waste package to the invert. The focus of this analysis is on partitioning between matrix and fracture, so I only considered transport through the invert and host rock.

For this analysis, I discretized the invert into 10 cells over 1.8 m and the host rock into 43 cells over 36 m. Each cell represents a dual continuum (fracture and matrix). Within the invert, the two continua have the same properties and a large transfer coefficient, approximating a single continuum. I wasn't able to figure out a more graceful way of getting the pdepe routine to handle transferring fluxes from a single-continuum zone to a dual-continuum zone. The pdepe routine automatically selects a time step based on the solution.

I considered two types of host rock, represented by the Tptpll and Tptpmn units with nominal DOE fracture and matrix properties. The flux through the system represents seepage, which is partitioned within the host rock according to the unsaturated hydraulic properties to maintain the same pressure in the matrix and fracture. The Tptpll matrix (using the property set DOE calls TLL) is assigned a nominal saturated hydraulic conductivity of 11 and 10^5 mm/yr for matrix and fractures, respectively. The Tptpmn matrix (using the property set DOE calls TMN) is assigned a nominal saturated hydraulic conductivity of 0.14 and 2.8×10^5 mm/yr for matrix and fractures, respectively. This procedure assumes that seepage is at a constant rate so that the matrix and fracture system attains equilibrium. With the assumed hydraulic properties for the Tptpll unit, the water flux through the fracture system is 29, 2.7, 0.0012, and 6.710^{-7} times the water flux through the matrix. With the assumed hydraulic properties for the Tptpmn unit, the water flux through the fracture system is 920, 94, 8.8, and 0.88 times the water flux through the matrix.

All of the analyses assume that the effective diffusion coefficient is the molecular diffusion coefficient (2.310^{-9} m²/s) multiplied by an effective tortuosity (0.195, 0.025, and 0.0156 for invert, fracture, and matrix, respectively) representative of the Tptpll unit (Sandia National Laboratories, 2007, Section 7.3.1.3). Dispersion is assumed to be negligible. The area for diffusive transport in fractures is assumed to be 10^{-3} of the total area, which does not take into account the rapid

decrease in saturation as flux changes.

I considered three boundary conditions for the top boundary. Solubility-limited release is represented by a unit relative concentration. Dissolution-controlled release is represented by a unit relative flux, with the presumption that solubility does not constrain and the dissolution of the waste form provides a flux independent of conditions outside the waste package. Because the dissolution rate may decay over time, I also considered the possibility of an exponentially decaying waste dissolution rate with a characteristic half-life.

I implemented a mixed boundary condition at the bottom boundary, with zero concentration in the matrix and zero concentration gradient (advective outflow only) in the fracture. Imposing a zero-concentration condition in the fracture implies extremely steep and non-physical gradients near the bottom boundary for high fluxes, inducing numerical difficulty. Imposing a zero-gradient condition is more representative for advection-dominated conditions but shuts off release in diffusion-dominated conditions (*e.g.*, the matrix). The mixed condition balances the two concerns.

The analysis systematically varies several conditions: (i) retardation, (ii) source boundary condition, (iii) dripping flux, (iv) host rock, and (v) transfer between fracture and matrix. Each figure represents the concentration and flux in the matrix and fracture continua, as well as the ratio between matrix and fracture, for three levels of retardation. The same retardation coefficient is assigned to the matrix and invert, while the fracture continuum has no retardation. Note that not all combinations are plotted because of the large set of combinations.

Solubility-limited releases are typical for actinides, such as uranium, neptunium, and plutonium. Figure 4-42 displays the results from a solubility-limited release into the TLL host rock for extremely large dripping fluxes (100 mm/yr). Figures 4-43, 4-44, and 4-45 display the corresponding results for dripping fluxes of 10, 1, and 0.1 mm/yr, respectively.

Each figure has six columns and three rows. The columns are divided into two sets of three columns. The first set, the leftmost three columns, display calculated concentration. From left to right, these columns display normalized concentration in the fracture and matrix, and the fracture/matrix ratio of concentration. The leftmost (first) color scale is used for the first two columns and the second color scale is used for the third column. The second column set (*i.e.*, the rightmost three columns) is exactly analogous to the first set except that the columns display calculated mass flux given the upstream boundary condition.

The columns in the first set are labeled as normalized to the upstream boundary condition

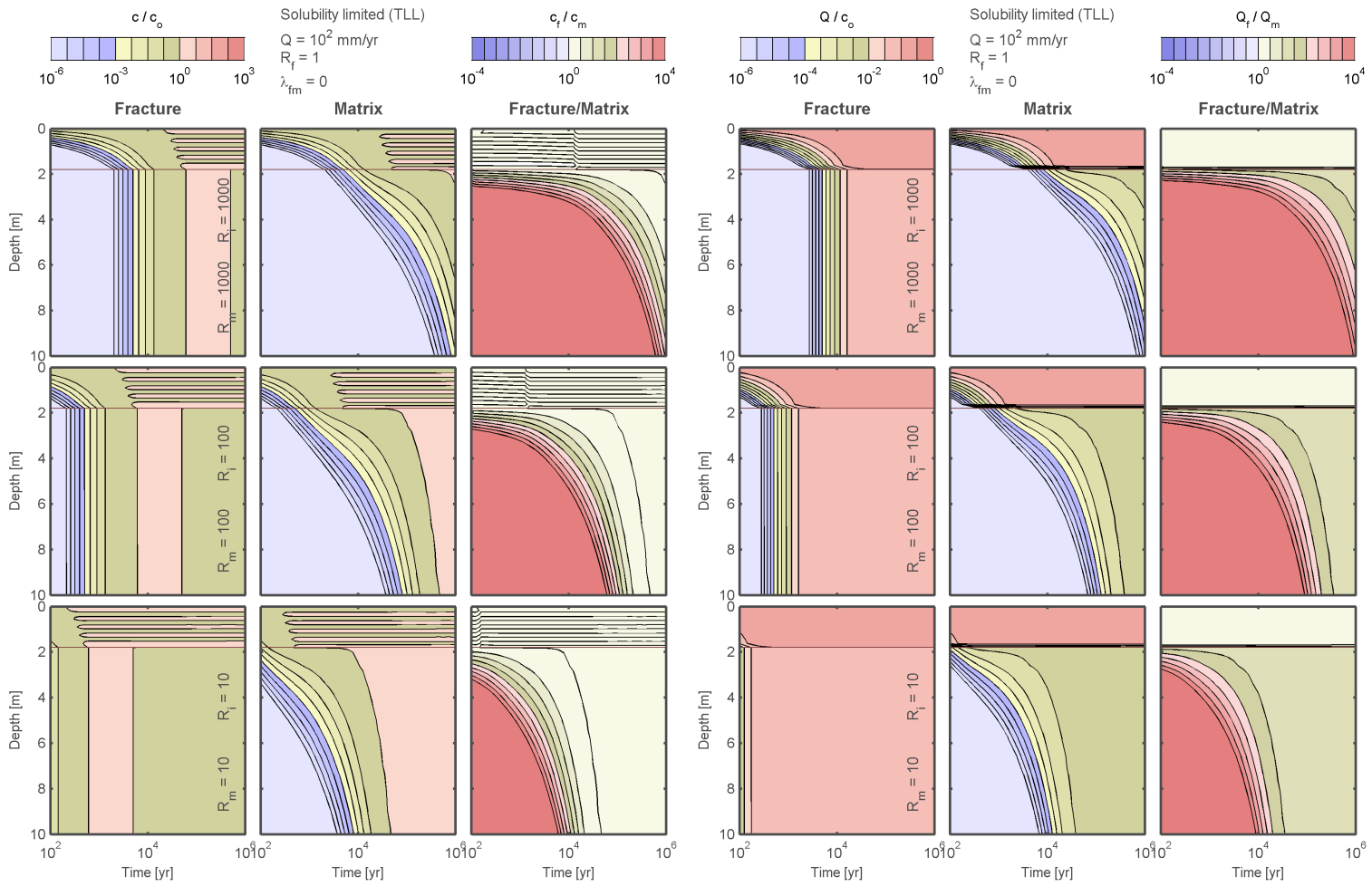


Figure 4-42: Transient solubility-limited release to the TLL drift shadow with 100 mm/yr dripping.

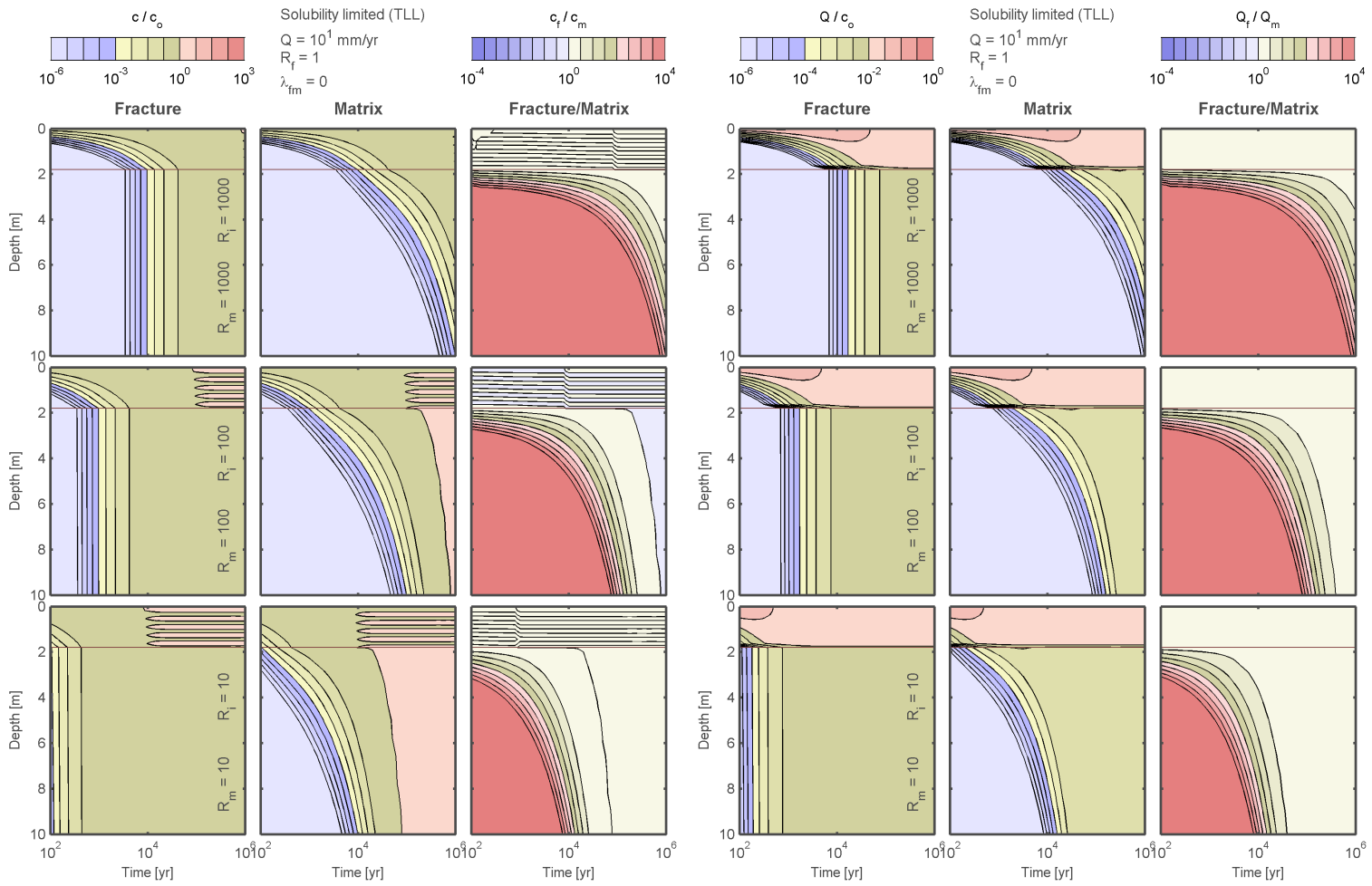


Figure 4-43: Transient solubility-limited release to the TLL drift shadow with 10 mm/yr dripping.

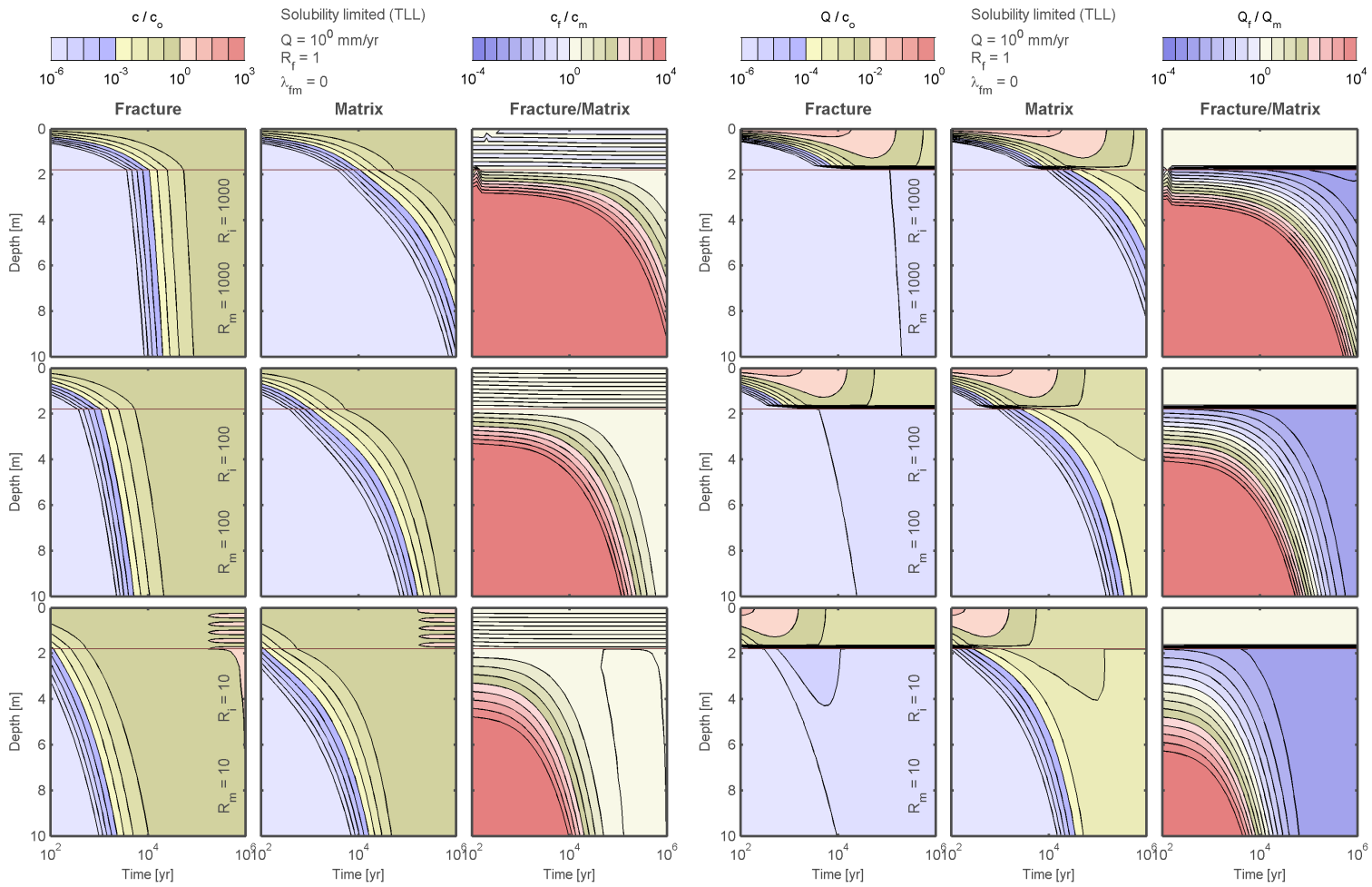


Figure 4-44: Transient solubility-limited release to the TLL drift shadow with 1 mm/yr dripping.

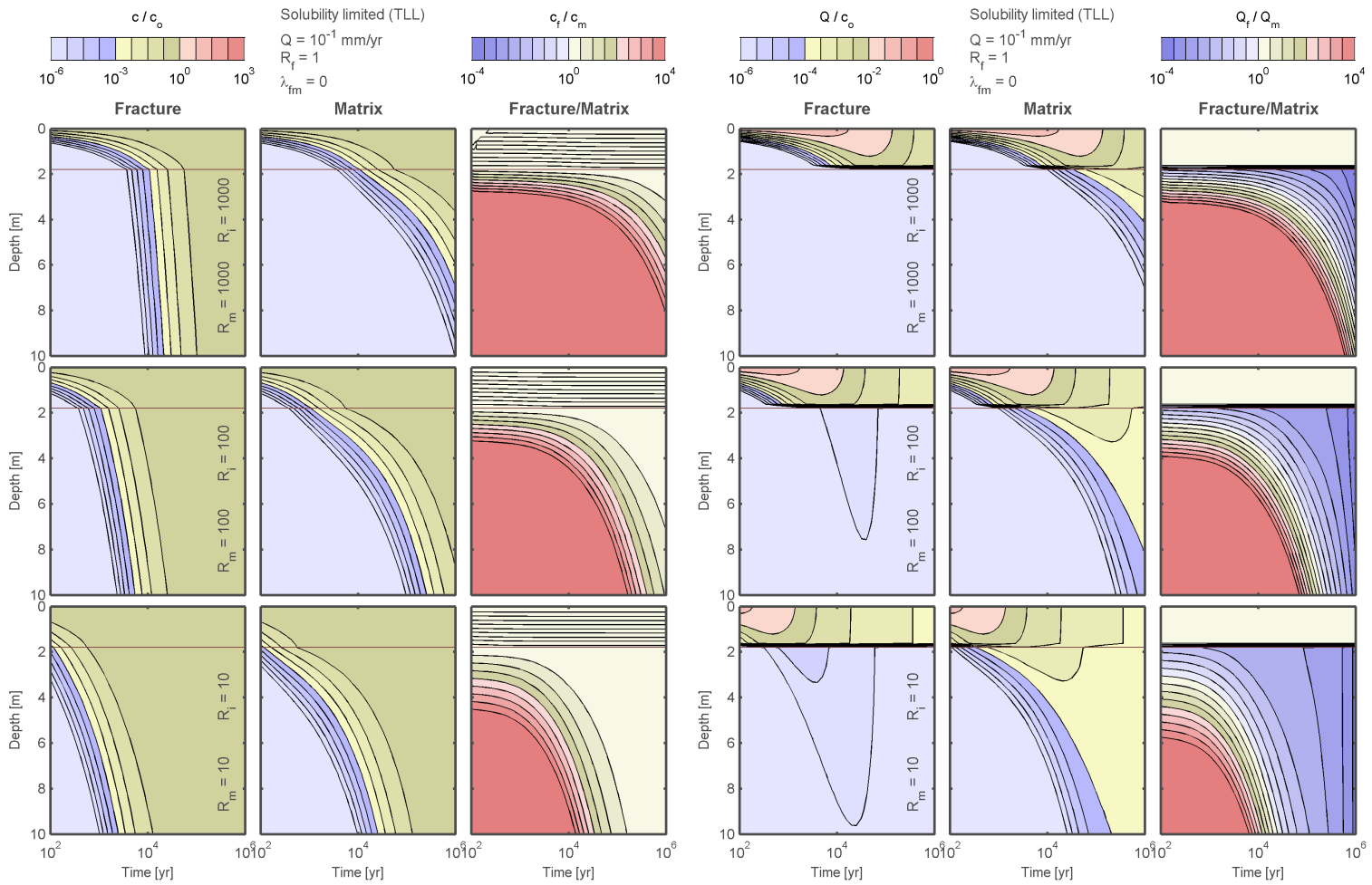


Figure 4-45: Transient solubility-limited release to the TLL drift shadow with 0.1 mm/yr dripping.

concentration (the concentration at the outside of the waste package) because the equations are linear (note that the boundary concentration for the simulations has a value of 1). These columns are labeled as normalized to the upstream boundary condition because a different upstream concentration would scale the mass fluxes proportionally. The proportional scaling would occur because (i) the transport problem is linear, (ii) advective transport is proportional to concentration, and (iii) diffusive transport is proportional to the concentration gradient and the downstream matrix concentration boundary condition is zero. In subsequent figures that display results based on a dissolution-controlled scenario, the column sets represent concentration and mass flux as well, but using the same rationale the concentration and mass flux are labeled as normalized to the initial mass flux (note that the initial mass flux has a value of 1 for the simulations).

The rows in the figure represent different retardation values within the matrix and invert (the fracture system is assumed nonretarding). DOE describes ^{99}Tc as nonsorbing; ^{237}Np , ^{235}U , and ^{233}U as moderately sorbing; and ^{241}Am , ^{239}Pu , ^{231}Pa , ^{229}Th , ^{226}Ra , ^{90}Sr , and ^{135}Cs as strongly sorbing under unsaturated conditions (SAR Section 2.3.8.4.3). Retardation is assumed the same for the matrix and invert for simplicity, but the retardation coefficient would likely be different for the two media because a nearly saturated tuff rock is likely to have a different specific surface area for sorption than relatively dry crushed tuff. The retardation coefficient in the invert would decrease with increasing dripping flux because the retardation coefficient decreases with increasing water content, which increases with flux under unsaturated conditions.

For context, SAR Table 2.3.8-2 reports sorption coefficient (K_d) values on the order of 0.1 to 1 mL/g for uranium and neptunium and on the order of 100 for plutonium. The retardation coefficient is calculated by

$$R = 1 + \frac{K_d \rho}{\theta} \quad (4-4)$$

where ρ is bulk density and θ is water content. Assuming $\rho = 2.5$ g/mL and $\theta = 0.1$, R is 3.5, 26, and 2500 for K_d values of 0.1, 1, and 100 mL/g. Therefore, the bottom row is more representative of moderately sorbing radionuclides such as uranium and neptunium and the top row is more representative of highly sorbing radionuclides such as plutonium. Note that SAR Table 2.3.8-2 lists K_d values for some elements that are more than 10 to more than 100 times larger than the plutonium values.

Figure 4-42 shows that the system response time increases proportionally to the retardation coefficient, just as expected. The figures in the middle row are essentially the same as the figures above and below, except offset in time by a factor of 10. The concentration figures indicate that the fracture system responds quickly relative to the matrix system, with respect to both concentration and flux. Once the system equilibrates, the concentration in the fracture and matrix

system is approximately the same so that the fracture/matrix concentration ratio approaches 1. The fracture/matrix mass flux ratio is approximately 10 at steady state, corresponding to a matrix saturated hydraulic conductivity that is approximately 1/10th of the percolation flux. Prior to steady state, the quick fracture system response relative to the matrix means that the ratio of fracture to matrix flow below the invert is very large (in the figures, the fracture/matrix ratio is clipped at 10^4 for both concentration and mass flux).

Invert concentration exhibits vertical oscillations as the system attains steady state. These small numerical oscillations are visually magnified because of a threshold contour exactly at the reference boundary condition value.

The Figures 4-42 through 4-45 sequence shows a number of significant characteristics.

- The fracture/matrix concentration ratio approaches 1 for all flux cases.
- Diffusion is important for transport within the invert at the lower fluxes, particularly the 1 and 0.1 mm/yr cases. This is evidenced by a decay over time for mass flux within the upper invert (10 mm/yr) and throughout the invert and host rock (1 and 0.1 mm/yr). Decay of release over time is typical of diffusion-dominated release with a fixed concentration boundary condition.
- The equilibrium fracture/matrix mass flux ratio drops with dripping flux. The fracture system has an equilibrium release only slightly greater than the matrix at 10 mm/yr, reflective of a calculated fracture flux that is 2.7 times larger than the matrix flux at hydraulic equilibrium. At lower fluxes, the matrix carries essentially all of the water and accordingly the fracture system carries essentially none of the release.
- Equilibrium occurs slightly later in the 10 mm/yr case than the 100 mm/yr case, because the flow through the matrix controls time to equilibrium in the matrix and flow through the matrix in the 10 mm/yr case is more than 80 percent of the 100 mm/yr case. The lower flow in the invert also slows transport through the invert, resulting in a later onset of release to the host rock.
- Equilibrium occurs substantially later in the 0.1 mm/yr case than the cases, because diffusion through the invert (rather than advection) becomes the dominant control at this low flow.

Figures 4-46, 4-47, 4-48, and 4-49 represent dissolution-controlled release for the same conditions. Dissolution-controlled release occurs when waste-form degradation occurs slowly enough that the radionuclide can escape without reaching its solubility limit. Technetium generally has a

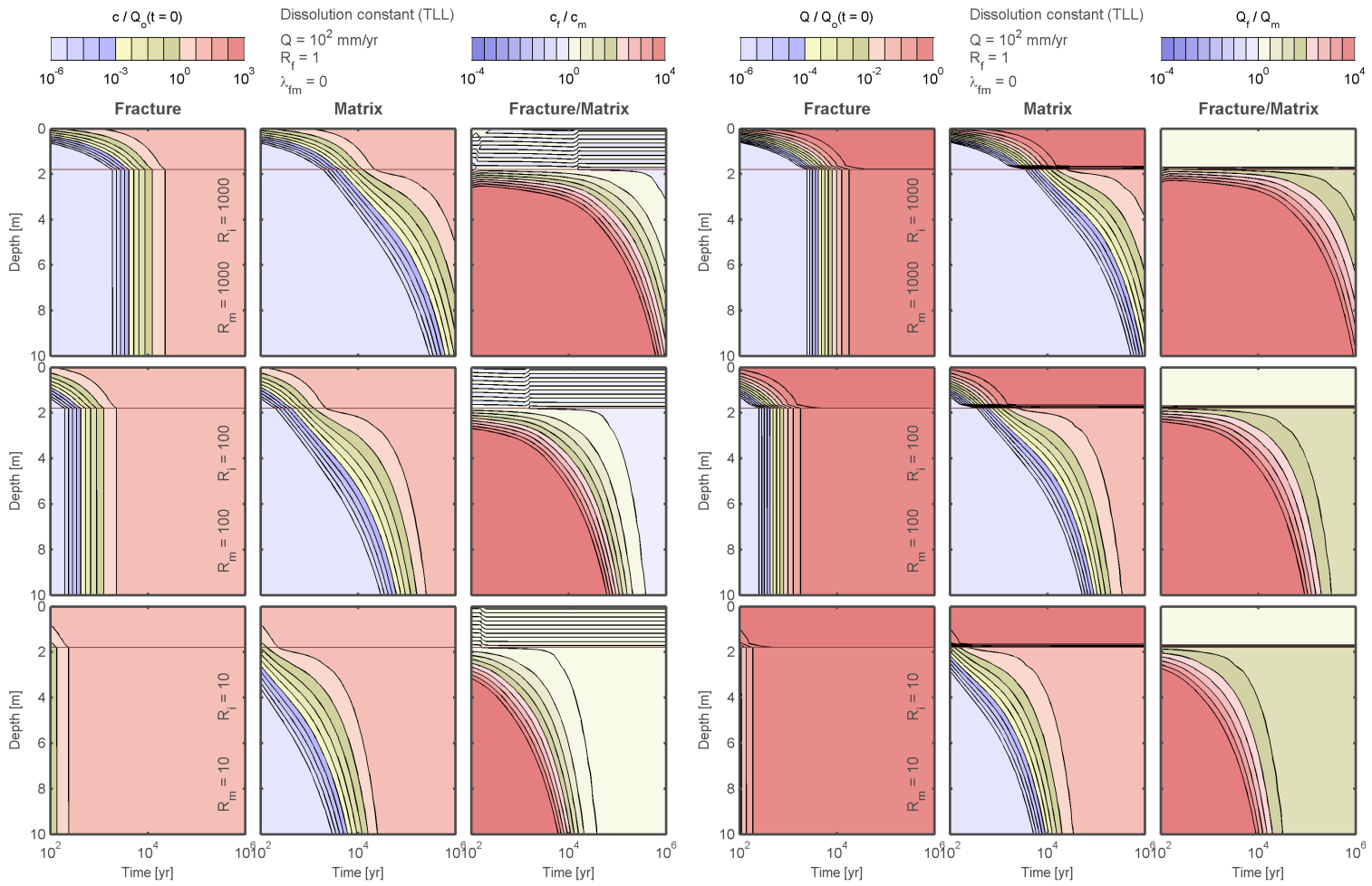


Figure 4-46: Transient dissolution-controlled release to the TLL drift shadow with 100 mm/yr dripping.

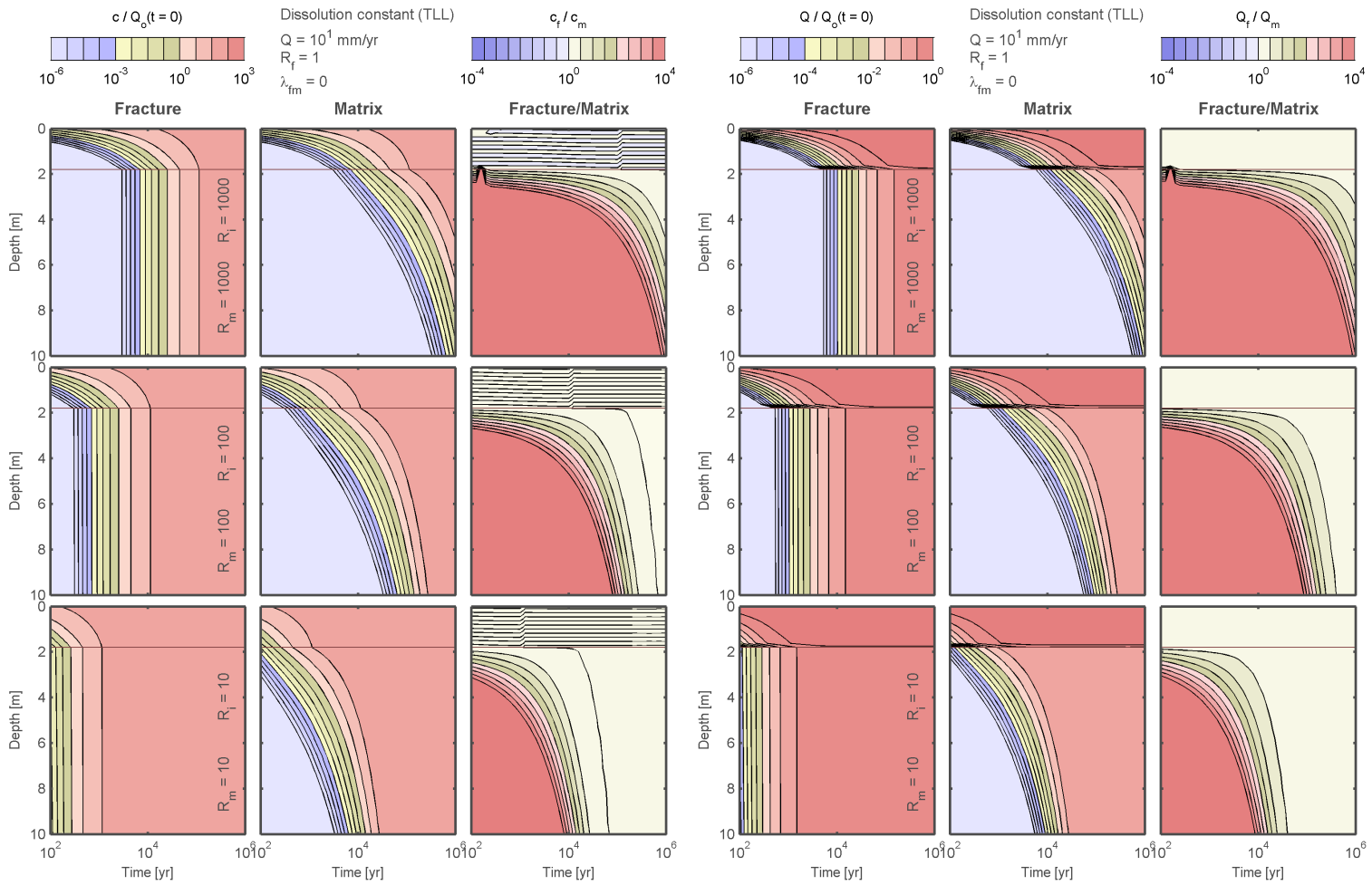


Figure 4-47: Transient dissolution-controlled release to the TLL drift shadow with 10 mm/yr dripping.

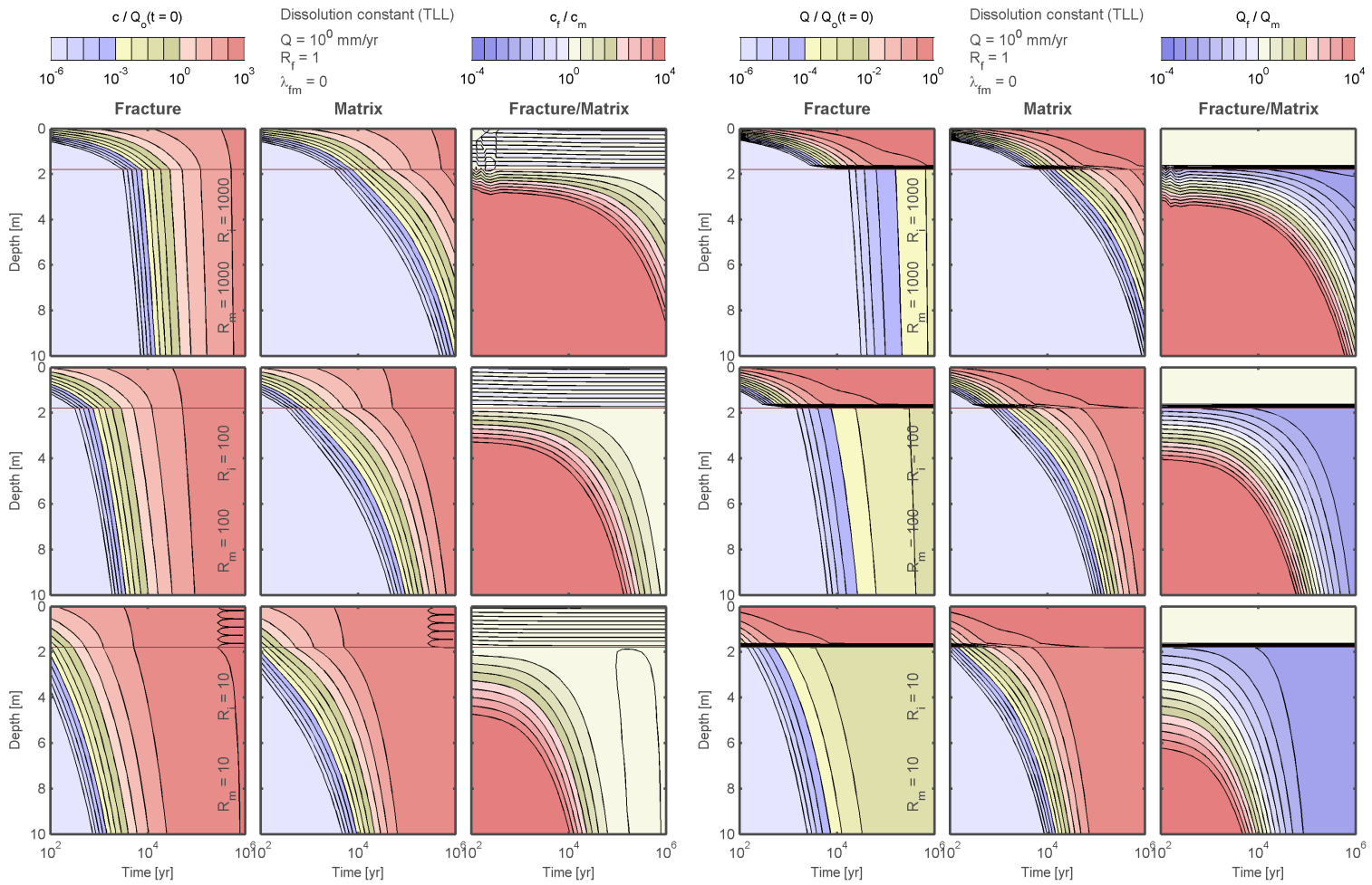


Figure 4-48: Transient dissolution-controlled release to the TLL drift shadow with 1 mm/yr dripping.

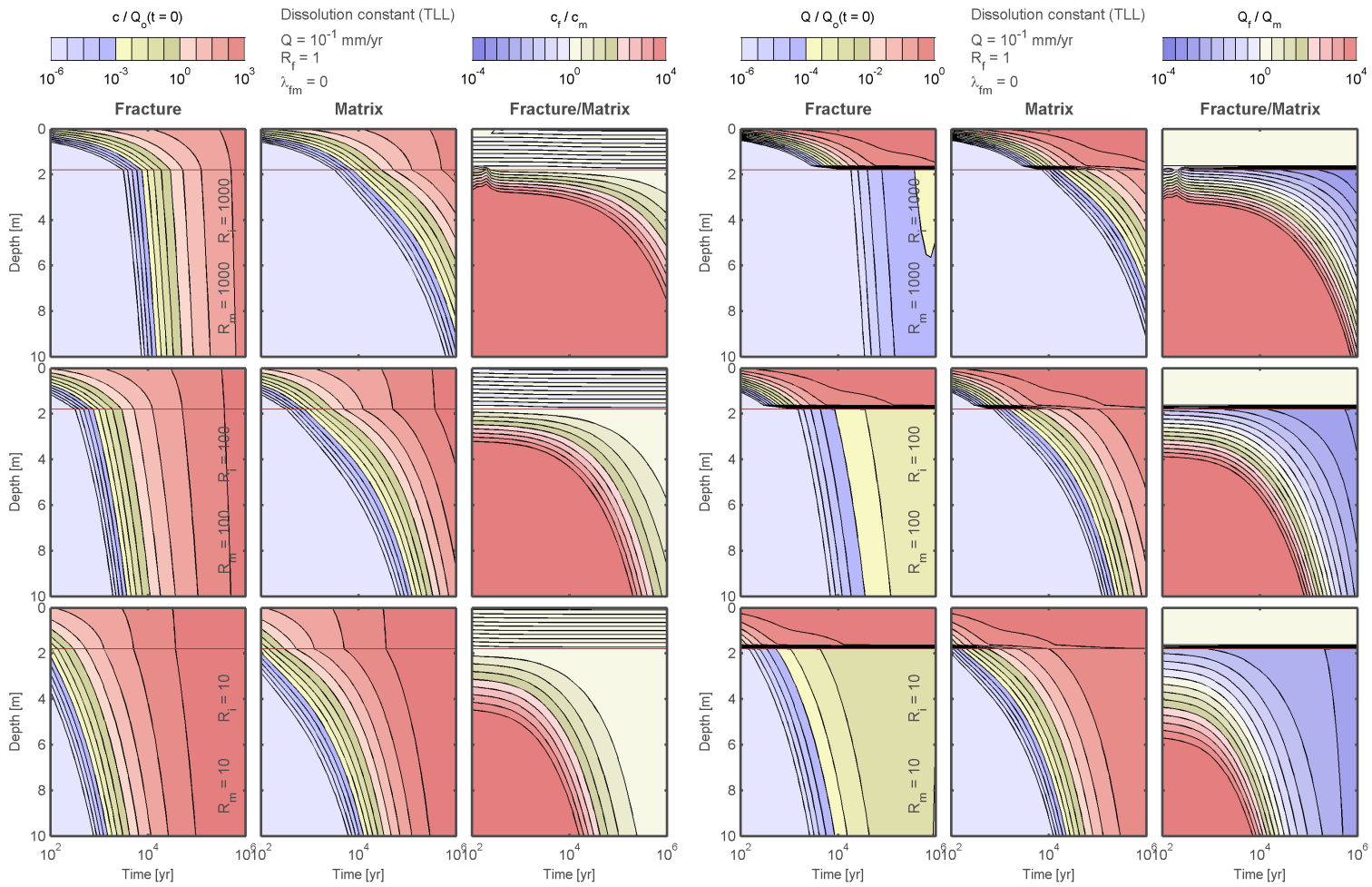


Figure 4-49: Transient dissolution-controlled release to the TLL drift shadow with 0.1 mm/yr dripping.

sufficiently large solubility limit that release rates are controlled by dissolution. Technetium is not considered significantly sorptive under the repository conditions, thus the retardation coefficient is close to one. The same sets of retardation coefficients are presented in these dissolution-controlled figures as the solubility-controlled figures to allow cross comparison of trends. A non-sorbing radionuclide would be closely represented by the bottom row in the figures, with the time axis shifted faster by one order of magnitude (100 years for a moderately sorbing element corresponds to 10 years for the non-sorbing element).

Partitioning between fracture and matrix is quite similar for the two release scenarios, as is the response time to equilibrium. The two scenarios differ in how the concentration changes over time. Dissolution-controlled concentrations monotonically increase over time to a limiting value regardless of flow rate. This also occurs for solubility-limited concentrations under advection-dominated conditions, but under diffusion-dominated conditions the concentrations reach a peak then decrease. Under sufficiently dry conditions, presumably a solubility limit would be reached even for dissolution-controlled conditions.

Figures 4-50, 4-51, 4-52, and 4-53 represent dissolution-controlled release for the same conditions except that the TMN properties (*i.e.*, for the Tptpmn unit) are used. The saturated hydraulic conductivity for the TMN matrix is approximately 0.1 mm/yr, two orders of magnitude smaller than for the TLL matrix. Accordingly, the fracture/matrix ratio for a given dripping flux is approximately the same as for the TLL set with a flux smaller by two orders of magnitude. For example, partitioning for the TMN set with a dripping flux of 0.1 mm/yr is similar to the partitioning for the TLL set with a dripping flux of 10 mm/yr. As a result, diffusion dominates advection within the TMN matrix regardless of dripping flux. Scaling TMN results according to dripping flux does not yield results that are completely analogous to the TLL results because the balance between diffusion and advection does not scale.

Figures 4-54, 4-55, 4-56, and 4-57 represent solubility-limited release with fracture-matrix transfer in the TLL host rock. Transfer flux is represented by

$$Q_{fm} = \lambda_{fm}(c_f - c_m) \quad (4-5)$$

where Q_{fm} is the transfer rate per unit length, λ_{fm} is the transfer conductance, and c is concentration. The transfer conductance is set to 10^{-4} . The effect of fracture/matrix transfer is to mix the two systems, so that the overall response is intermediate between the fracture and matrix responses occurring without fracture/matrix transfer.

Figures 4-58, 4-59, 4-60, and 4-61 represent dissolution-controlled release where the rate of dissolution slows exponentially with a half-life of 10^4 years. Again the TLL host rock properties are

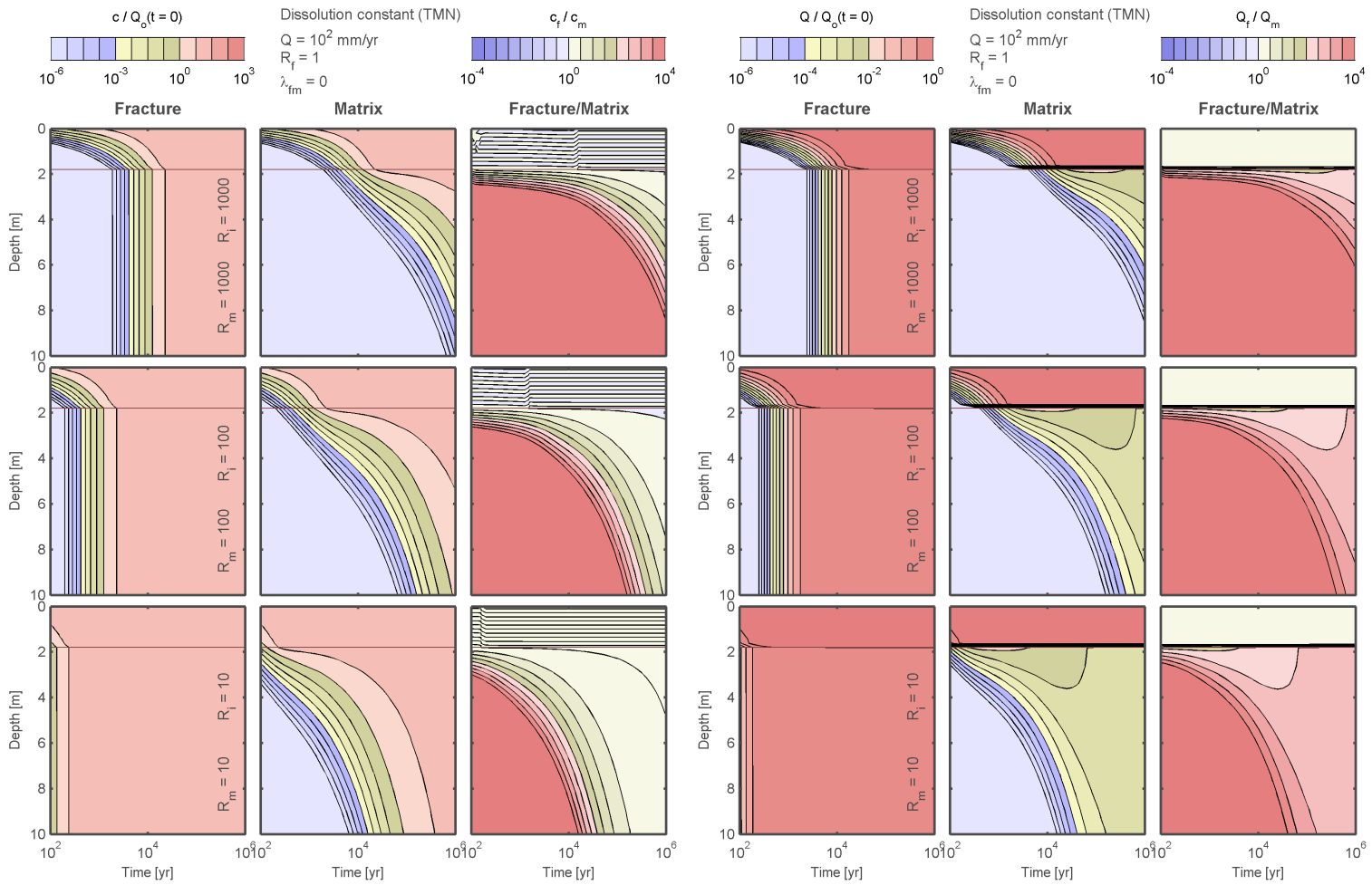


Figure 4-50: Transient dissolution-controlled release to the TMN drift shadow with 100 mm/yr dripping.

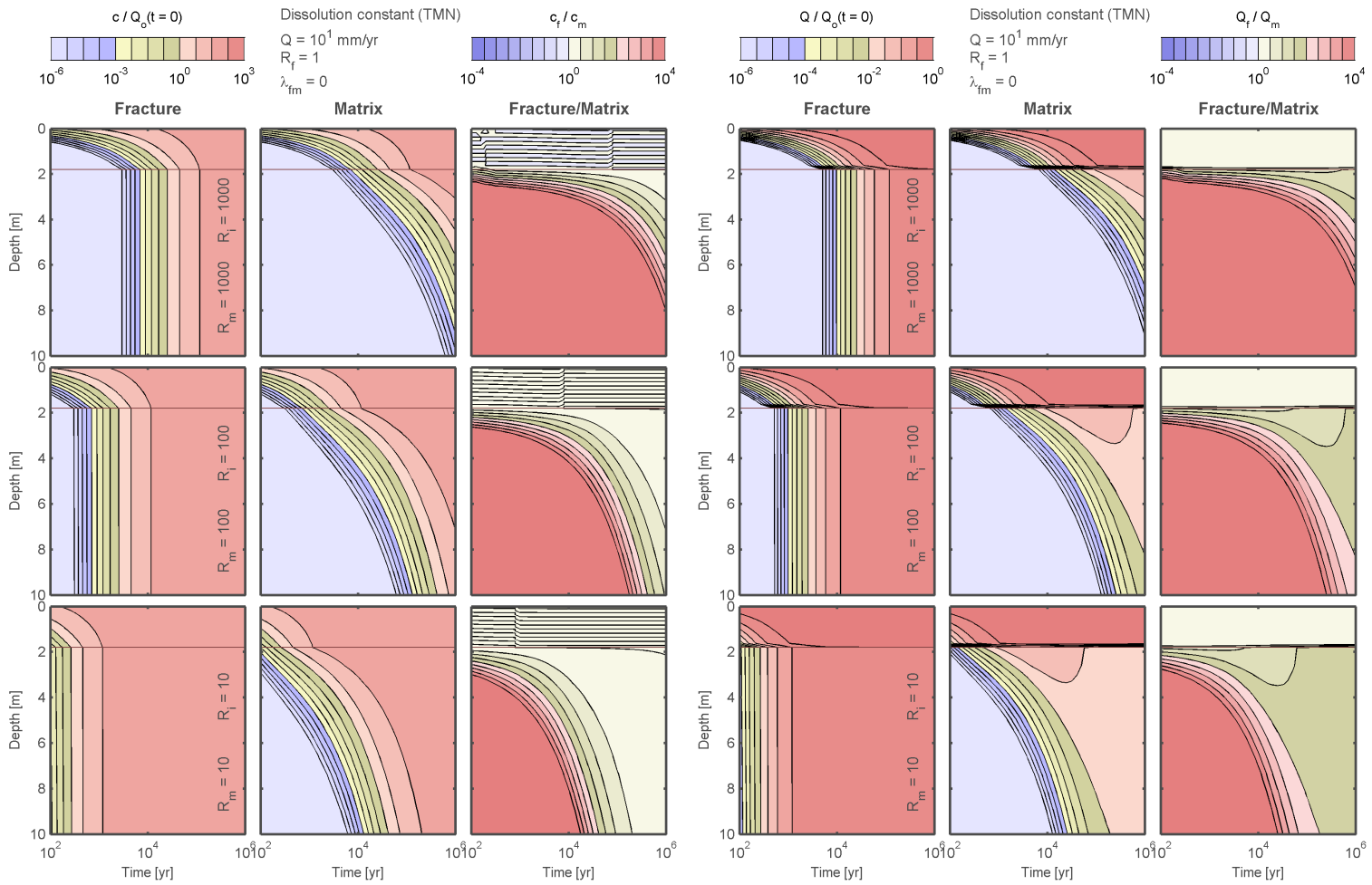


Figure 4-51: Transient dissolution-controlled release to the TMN drift shadow with 10 mm/yr dripping.

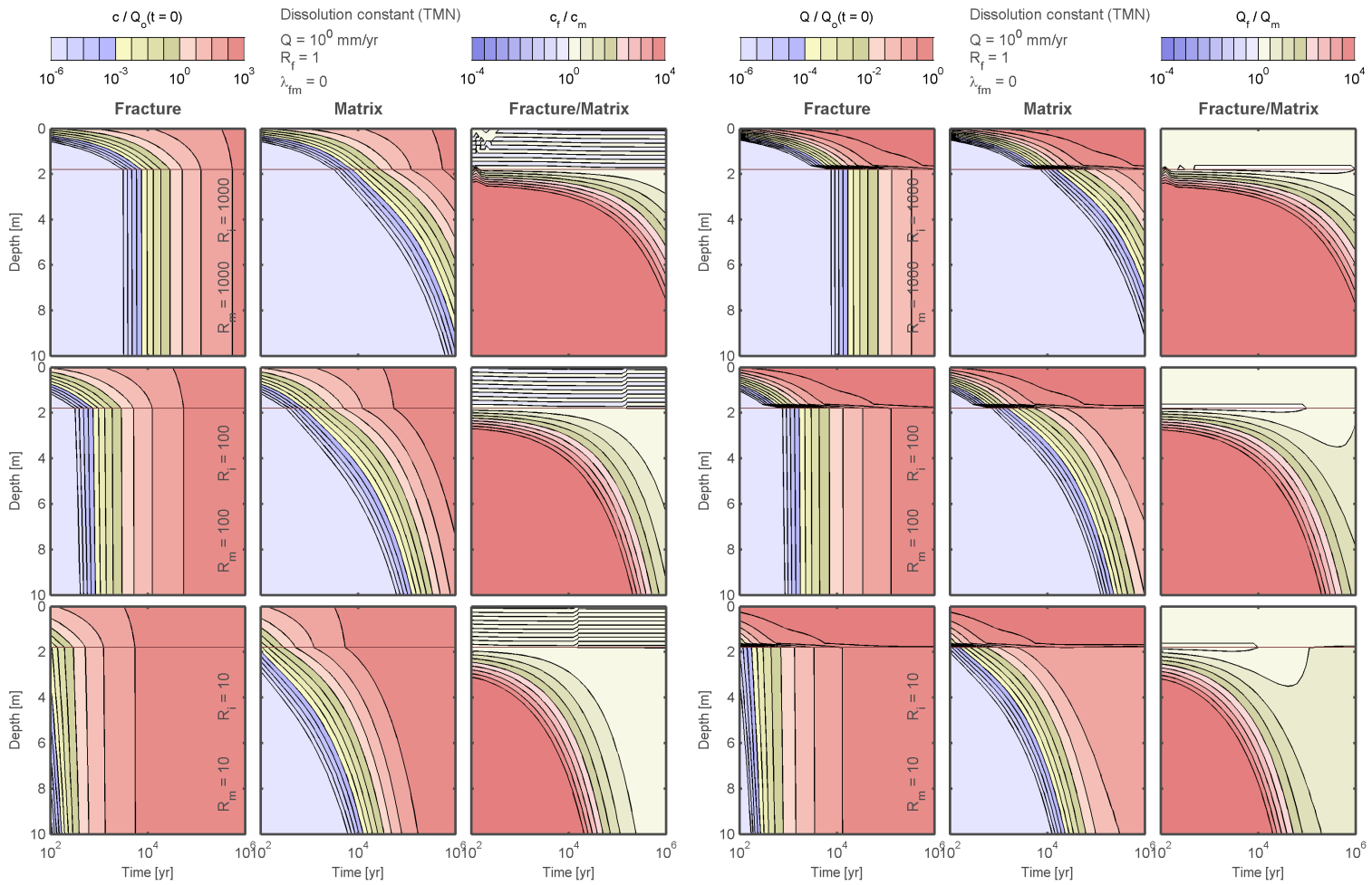


Figure 4-52: Transient dissolution-controlled release to the TMN drift shadow with 1 mm/yr dripping.

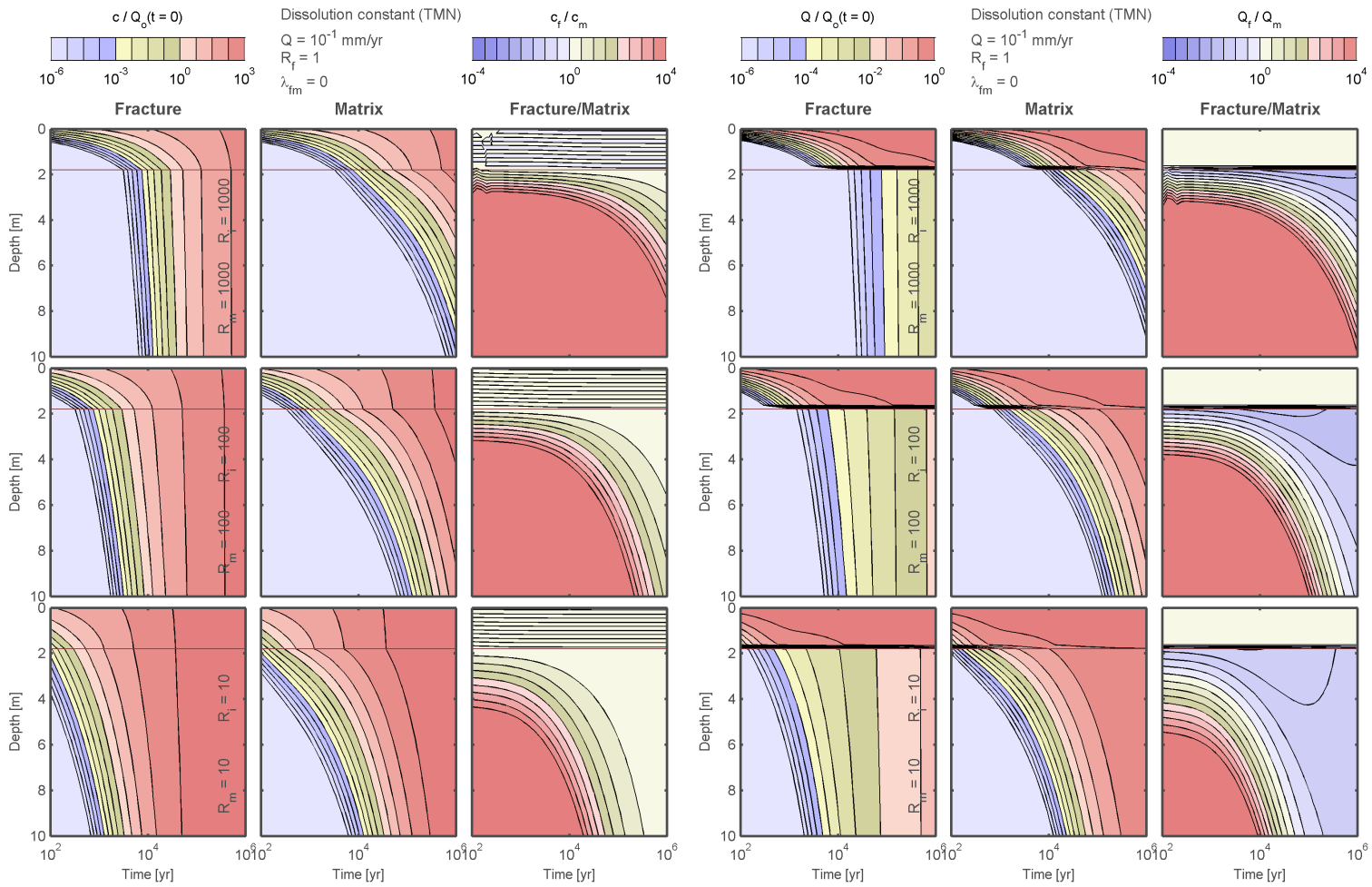


Figure 4-53: Transient dissolution-controlled release to the TMN drift shadow with 0.1 mm/yr dripping.

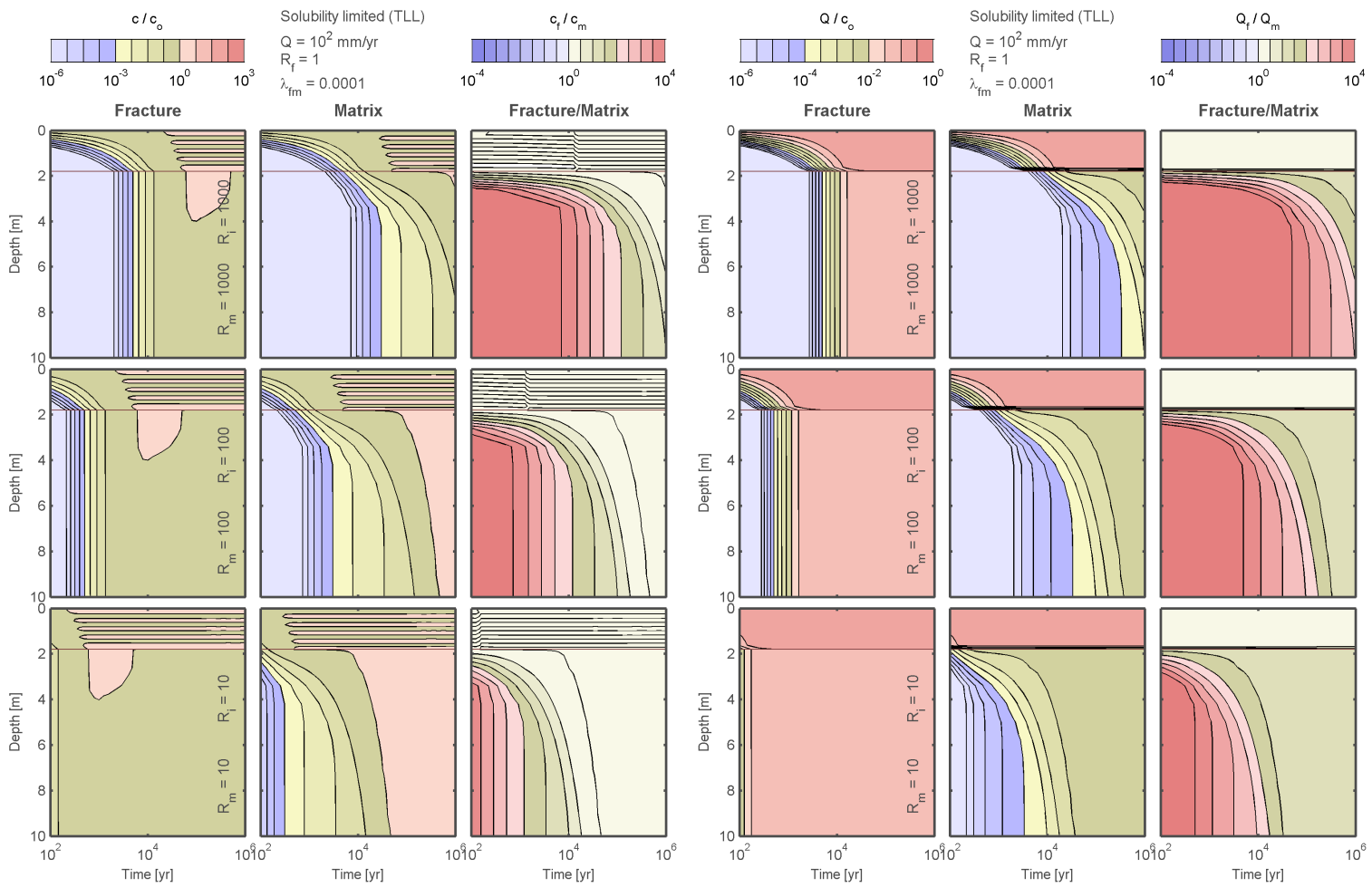


Figure 4-54: Transient solubility-limited release to the TLL drift shadow with 100 mm/yr dripping and matrix/fracture transfer.

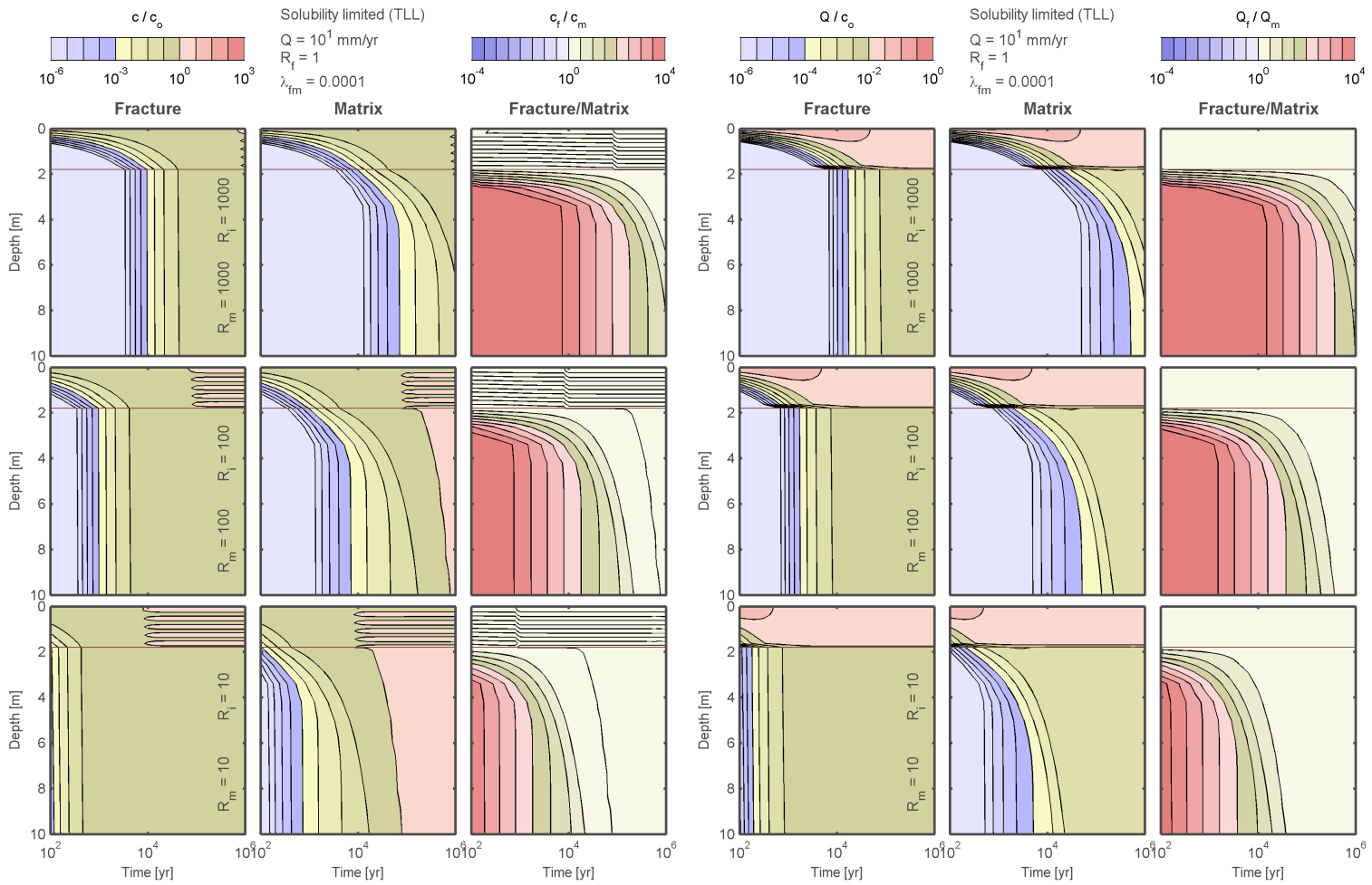


Figure 4-55: Transient solubility-limited release to the TLL drift shadow with 10 mm/yr dripping and matrix/fracture transfer.

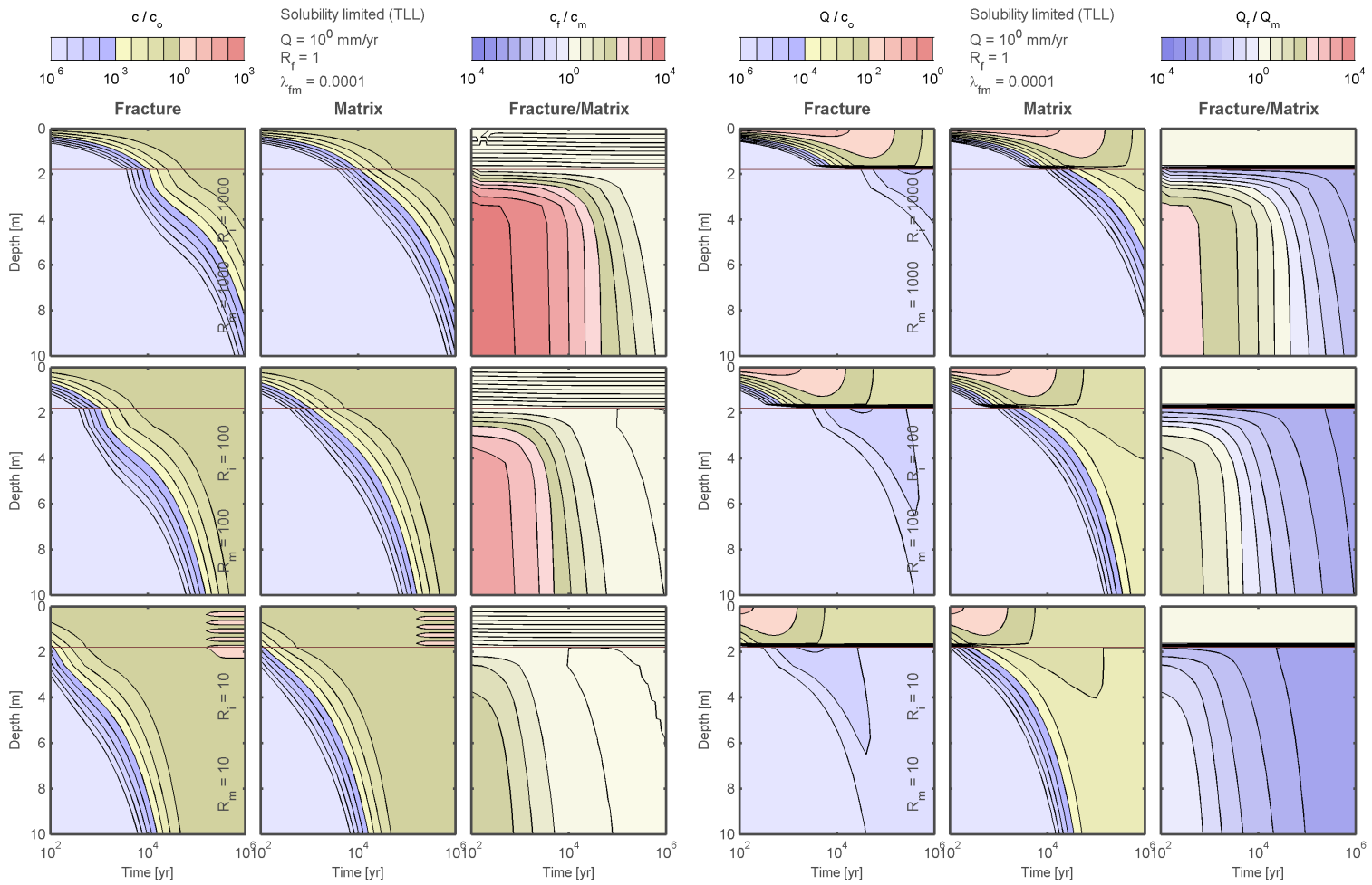


Figure 4-56: Transient solubility-limited release to the TLL drift shadow with 1 mm/yr dripping and matrix/fracture transfer.

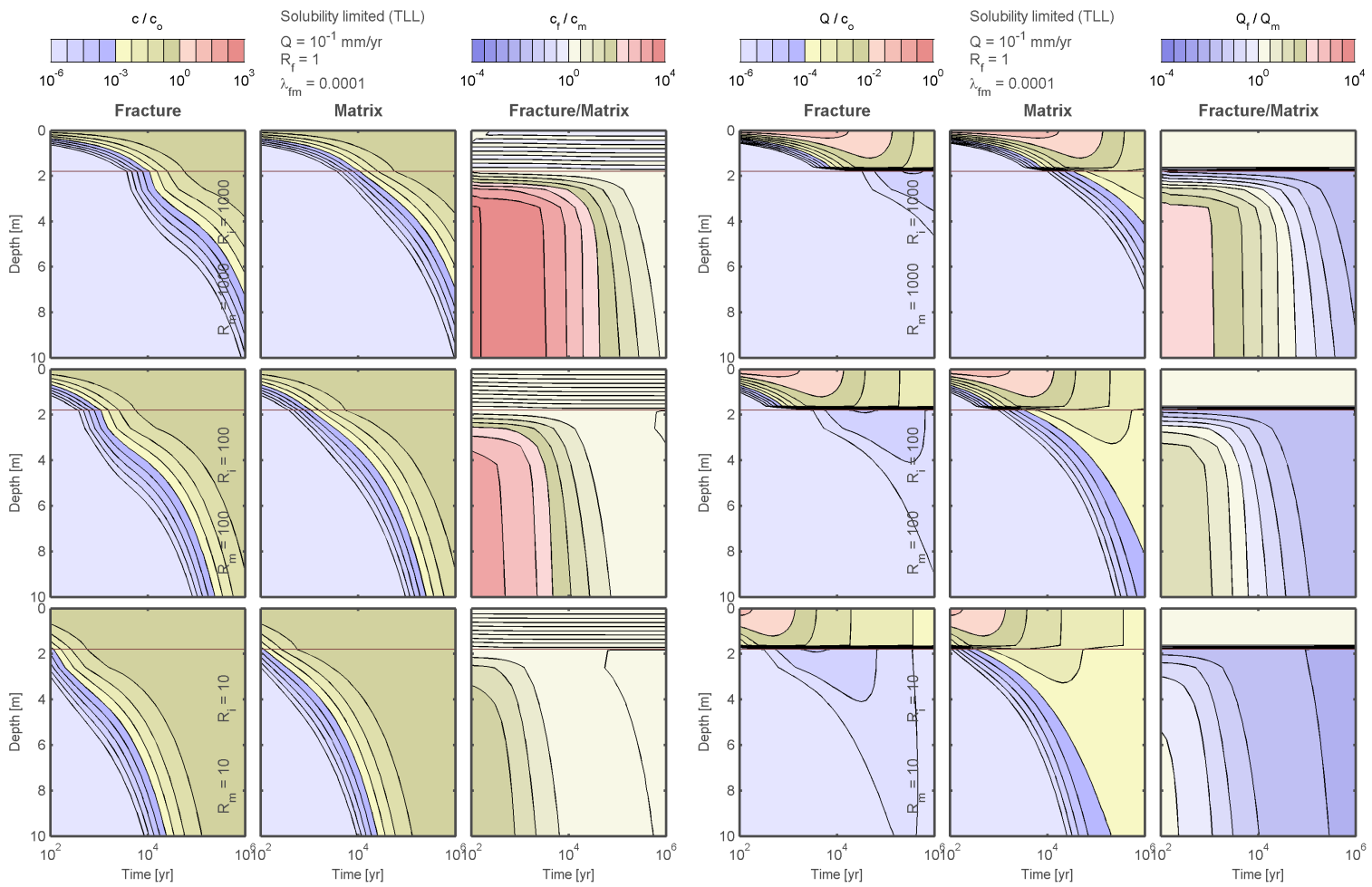


Figure 4-57: Transient solubility-limited release to the TLL drift shadow with 0.1 mm/yr dripping and matrix/fracture transfer.

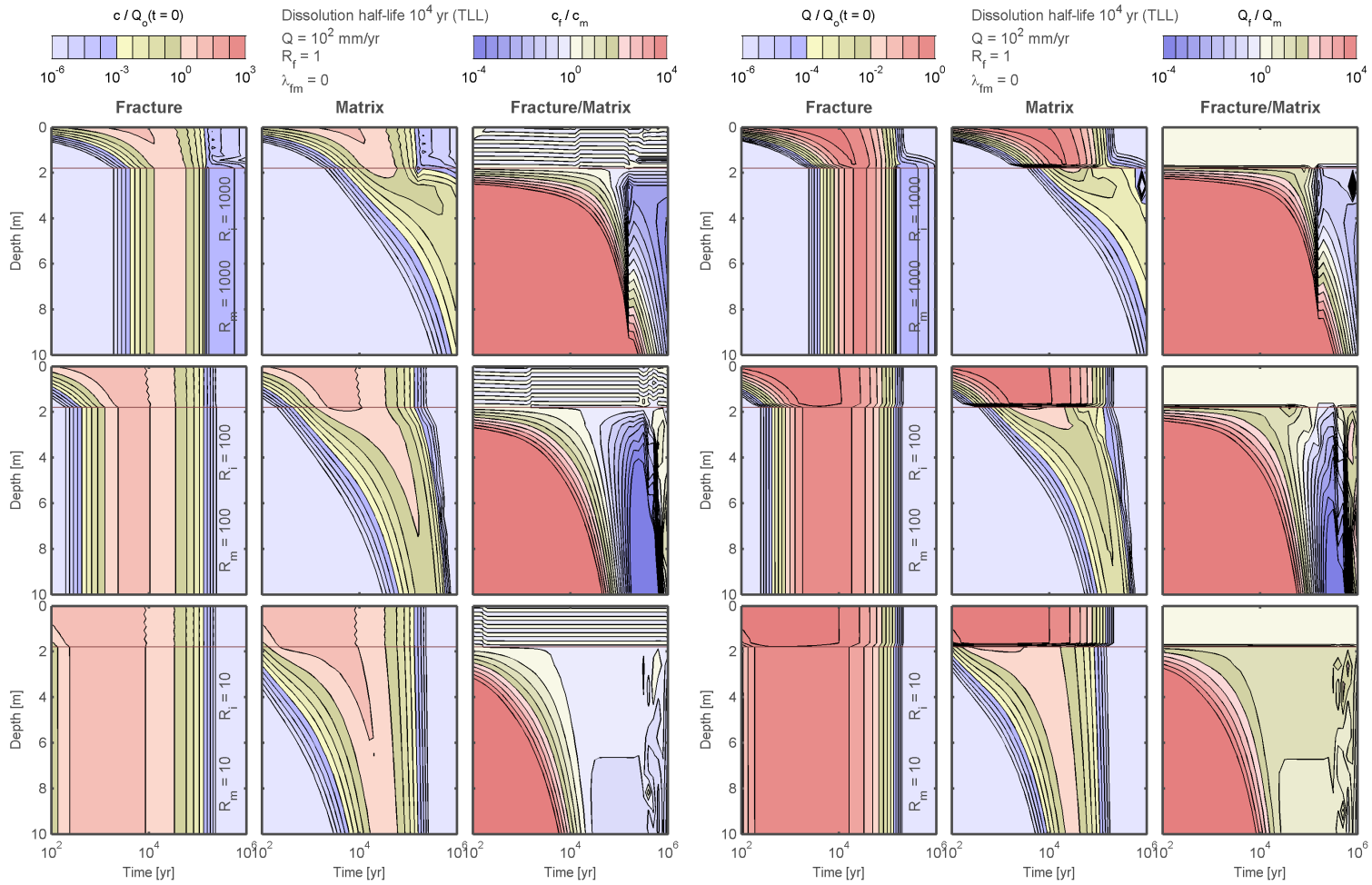


Figure 4-58: Transient decaying dissolution-controlled release to the TLL drift shadow with 100 mm/yr dripping.

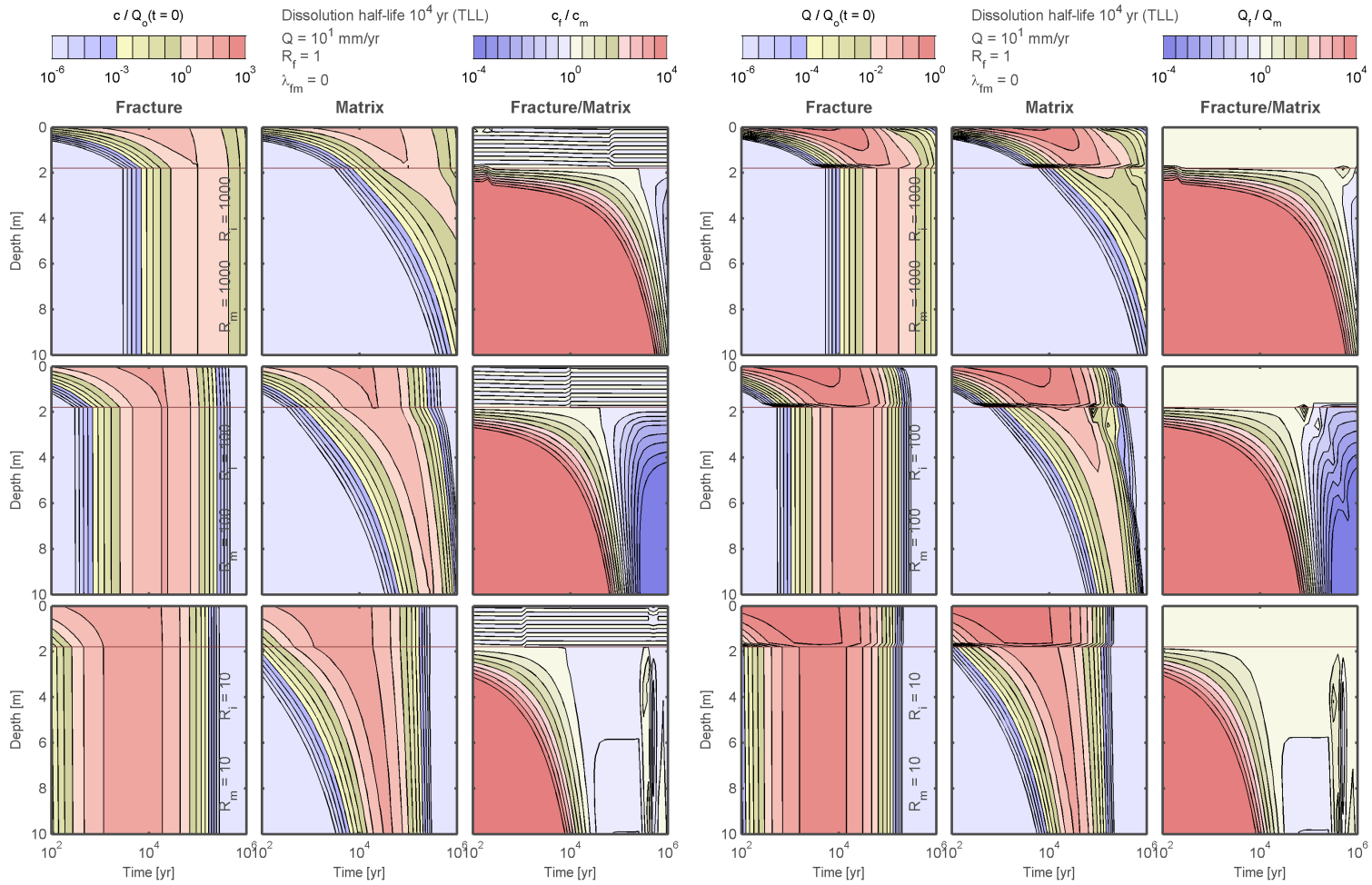


Figure 4-59: Transient decaying dissolution-controlled release to the TLL drift shadow with 10 mm/yr dripping.

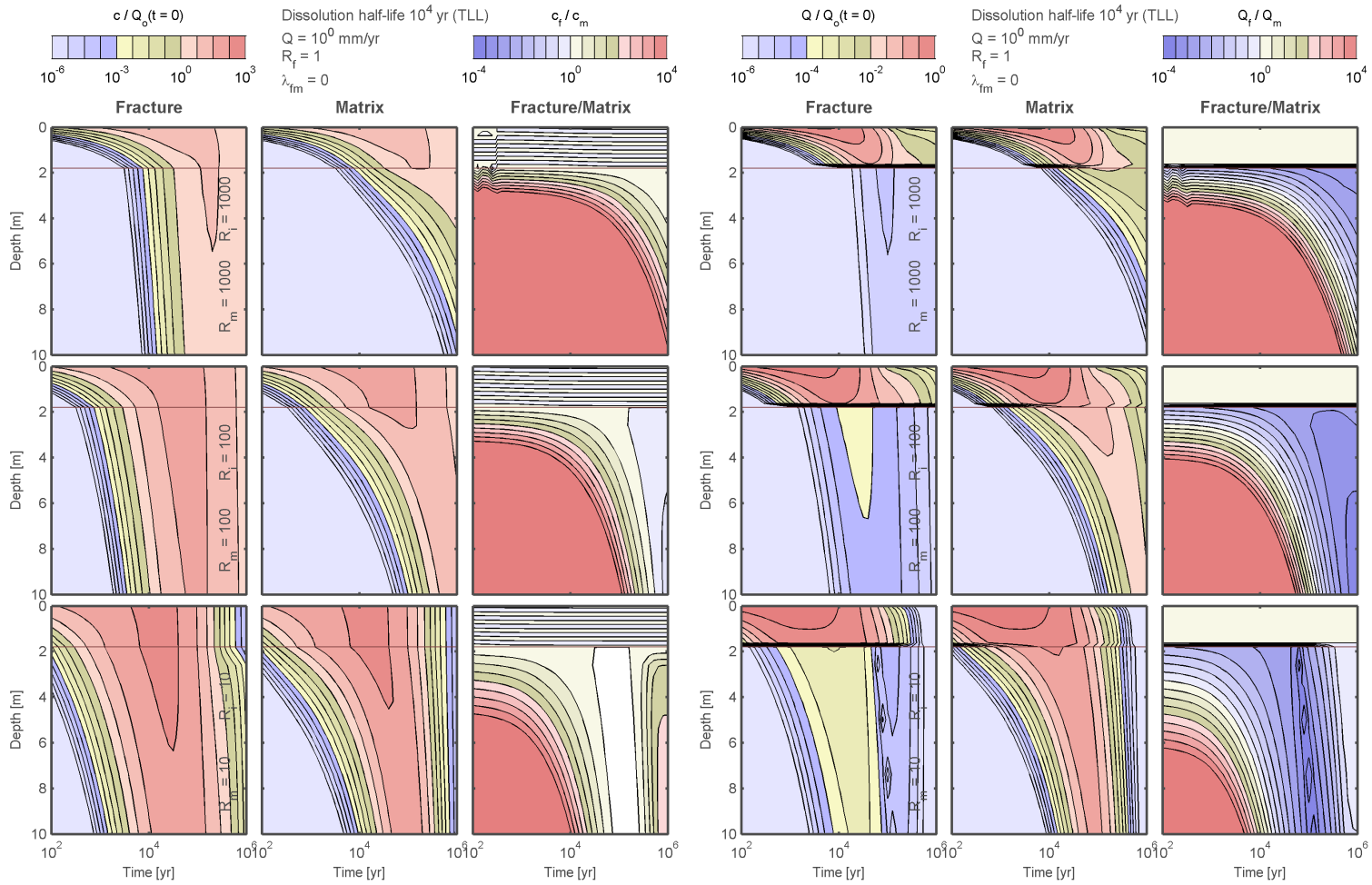


Figure 4-60: Transient decaying dissolution-controlled release to the TLL drift shadow with 1 mm/yr dripping.

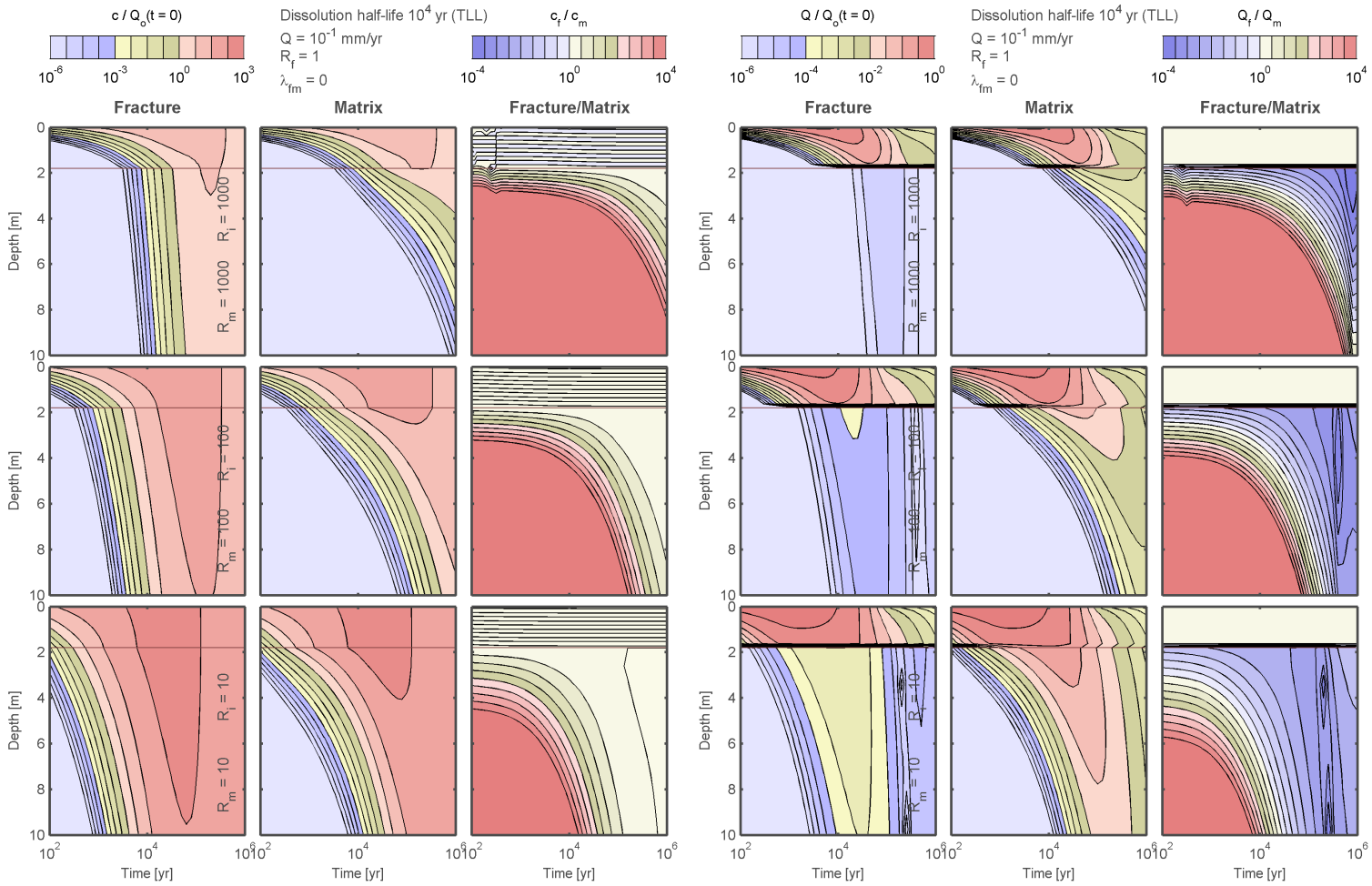


Figure 4-61: Transient decaying dissolution-controlled release to the TLL drift shadow with 0.1 mm/yr dripping.

used. As might be expected, the results are similar to the dissolution-controlled that is steady over time until the source rate substantially decays. Transport rates drop continually after that time, with releases less than 10^{-3} and 10^{-30} of the initial rate by 10^5 and 10^6 years, respectively, after the start. The fracture/matrix ratios become inaccurately calculated in the later period because of the small fracture fluxes.

06/26/10 Model effects on transient partitioning.



The transient release model results thus far are an approximation for release into a drift shadow, where all water flux in the host rock passes through the drift first. The DOE model calculating the partitioning between matrix and fracture systems differs in several ways, including: (i) the entire invert is one mixing cell, (ii) dripping water is assumed to partition into the fractures and imbibition water partitions into the matrix, (iii) the fracture system is assumed to have the maximum of the average background flux and the dripping flux, and (iv) an additional column is available on both sides of the drift for lateral diffusion.

The consequence of the mixing-cell assumption is clear: even though the time it takes to attain peak release from the invert probably won't change much, a fraction of the radionuclide mass entering the invert becomes instantaneously available for release (albeit at a low level). The figures documenting the series of transient analyses indicate that the mixing cell may speed up initial travel through the invert by 10^4 years or more for highly sorptive elements.

I look at implications of relaxing the drift shadow using the approximation that the fracture system has at least 10 mm/yr flux (a representative background flux) and the matrix has no flux (late-time imbibition into the invert drops close to zero). Figures 4-62, 4-63, 4-64, and 4-65 represent solubility-limited release with this approximation for the host-rock flux. Comparing these figures with Figures 4-42 through 4-45 reveals differences for all four levels of dripping flux.

In the current approximation, the behavior of the matrix remains almost the same regardless of dripping flux, with a slightly earlier response for the 100 mm/yr case as a result of rapid transport through the invert. The matrix features the characteristic diffusion-limited response of transport peaking as concentrations increase then declining as concentration gradients decrease. Matrix release in the current approximation is less than matrix release in the earlier drift-shadow approximation because there is no advective component. The behavior of the fracture system is essentially the same between the current approximation and the drift-shadow approximation when the dripping fluxes are greater than the background flux, but rather different for low dripping fluxes.

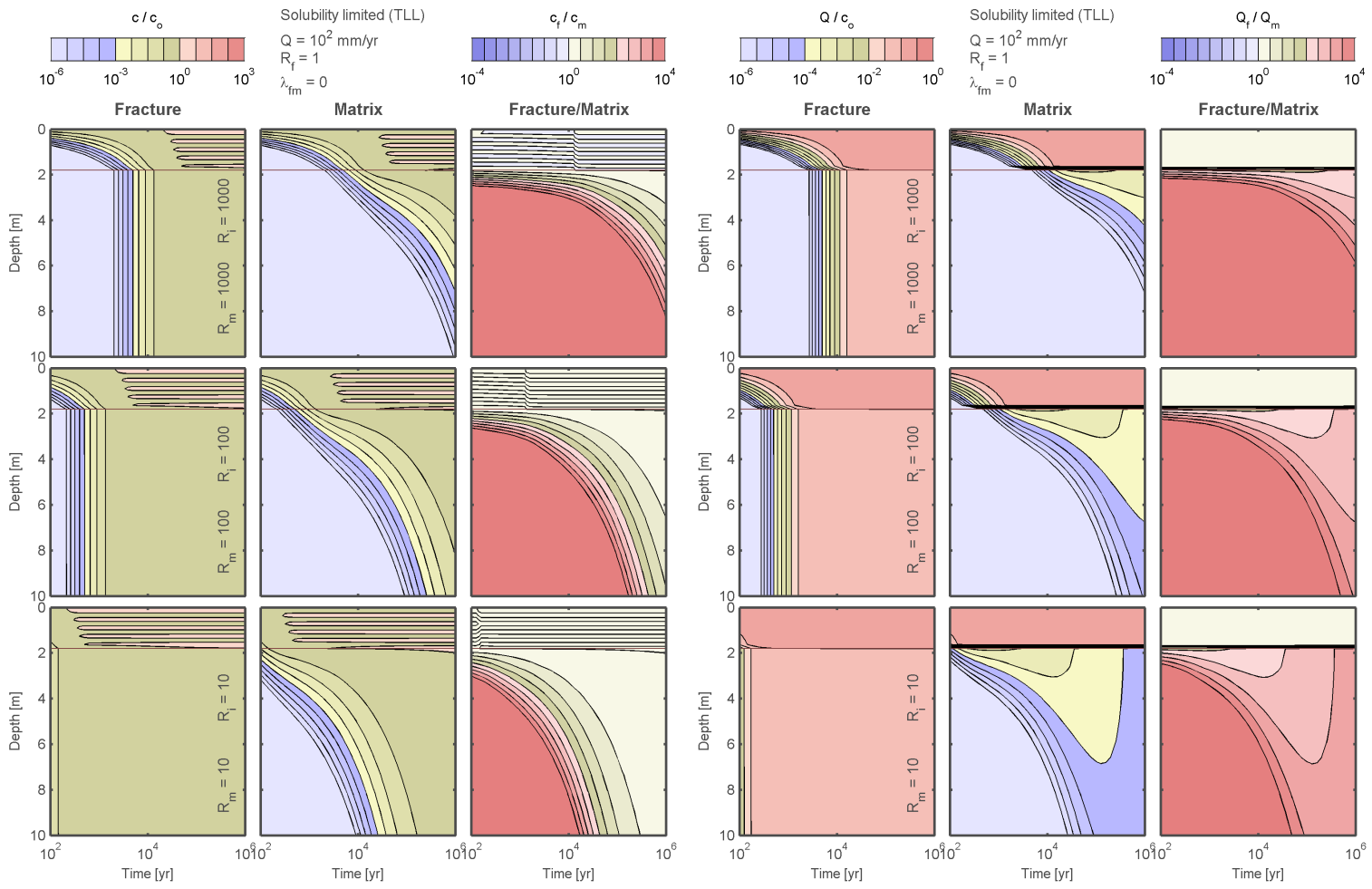


Figure 4-62: Transient solubility-limited release to the TLL drift shadow with 100 mm/yr dripping and host-rock percolation abstraction.

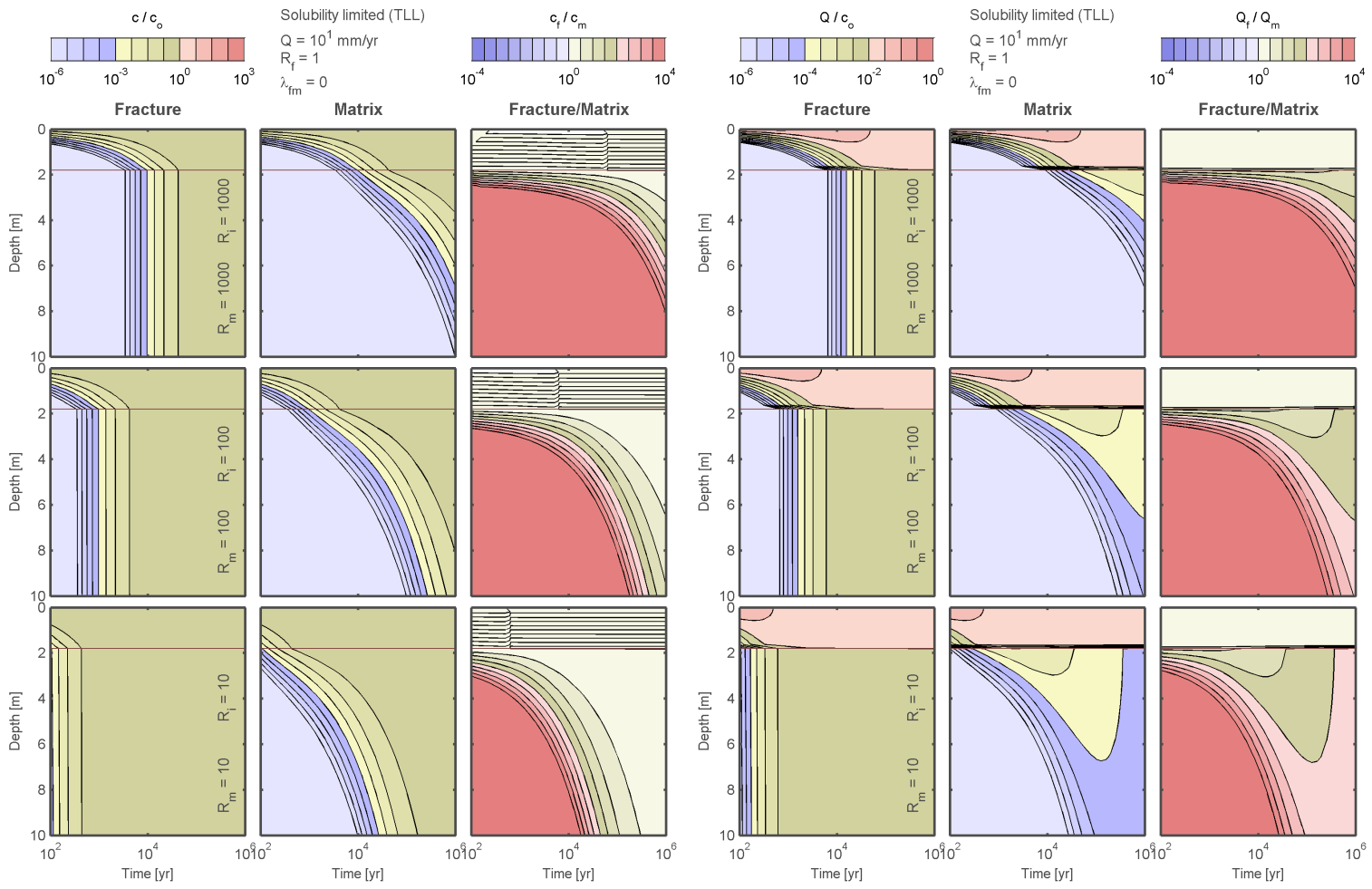


Figure 4-63: Transient solubility-limited release to the TLL drift shadow with 10 mm/yr dripping and host-rock percolation abstraction.

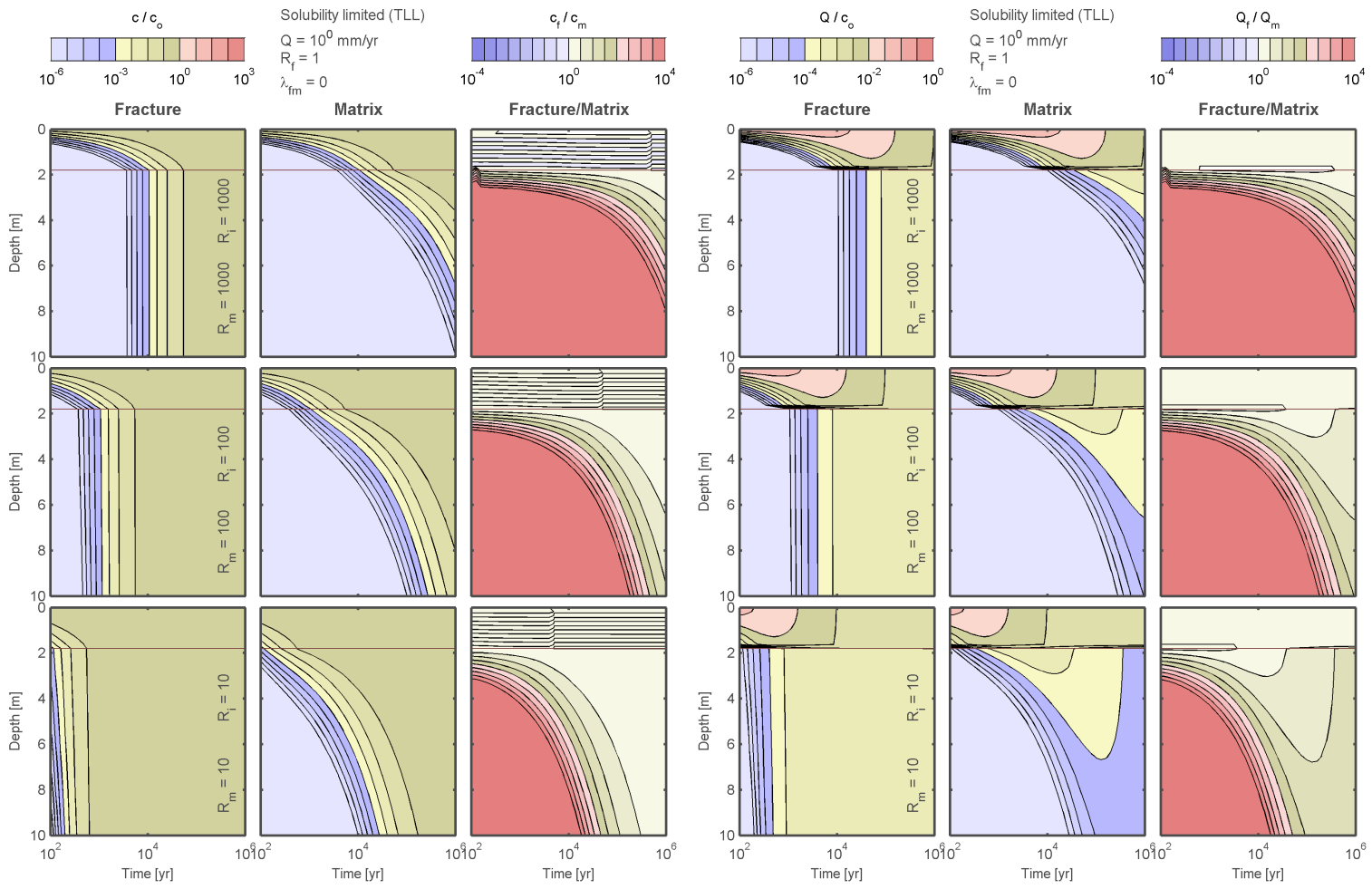


Figure 4-64: Transient solubility-limited release to the TLL drift shadow with 1 mm/yr dripping and host-rock percolation abstraction.

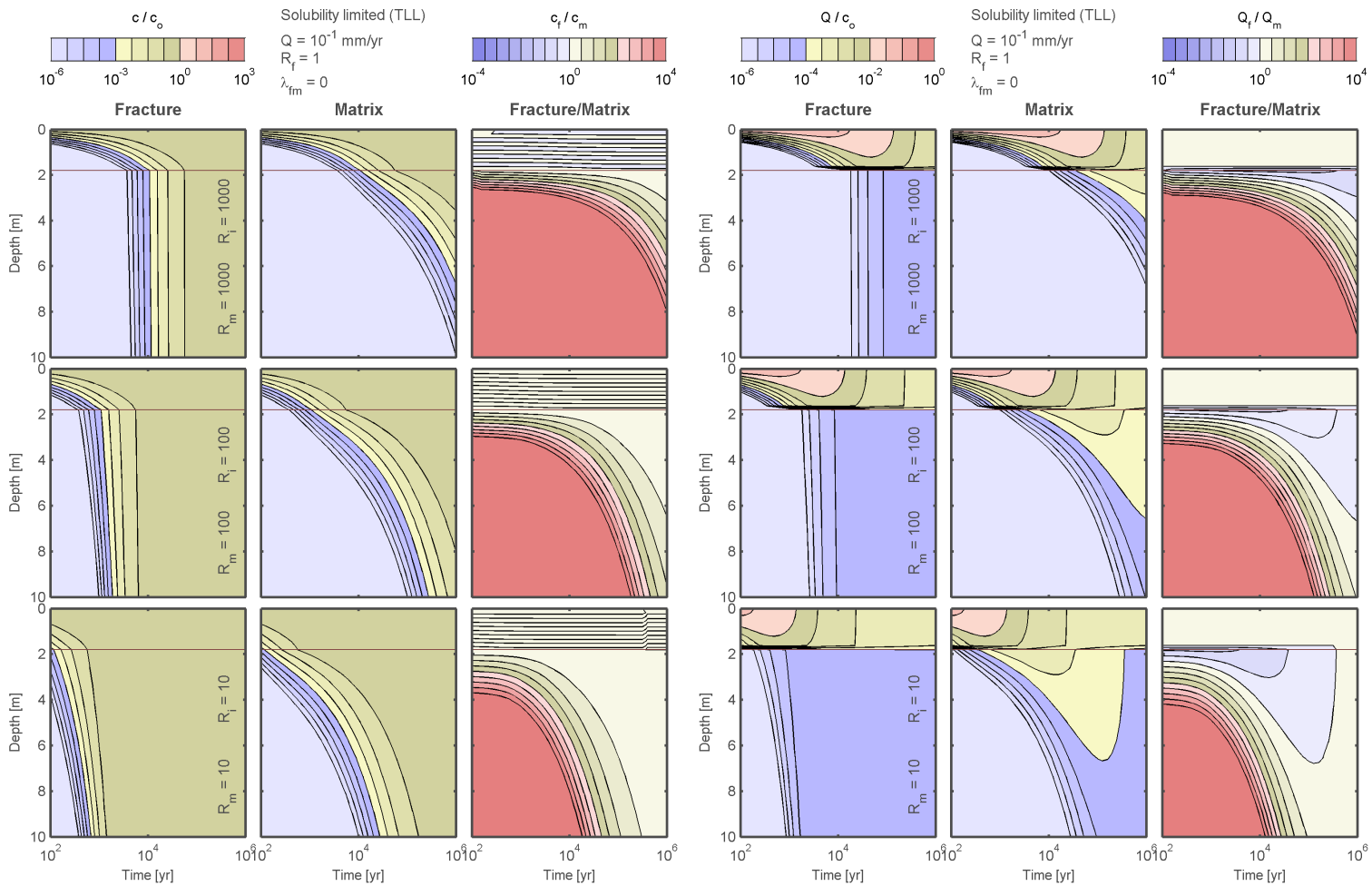
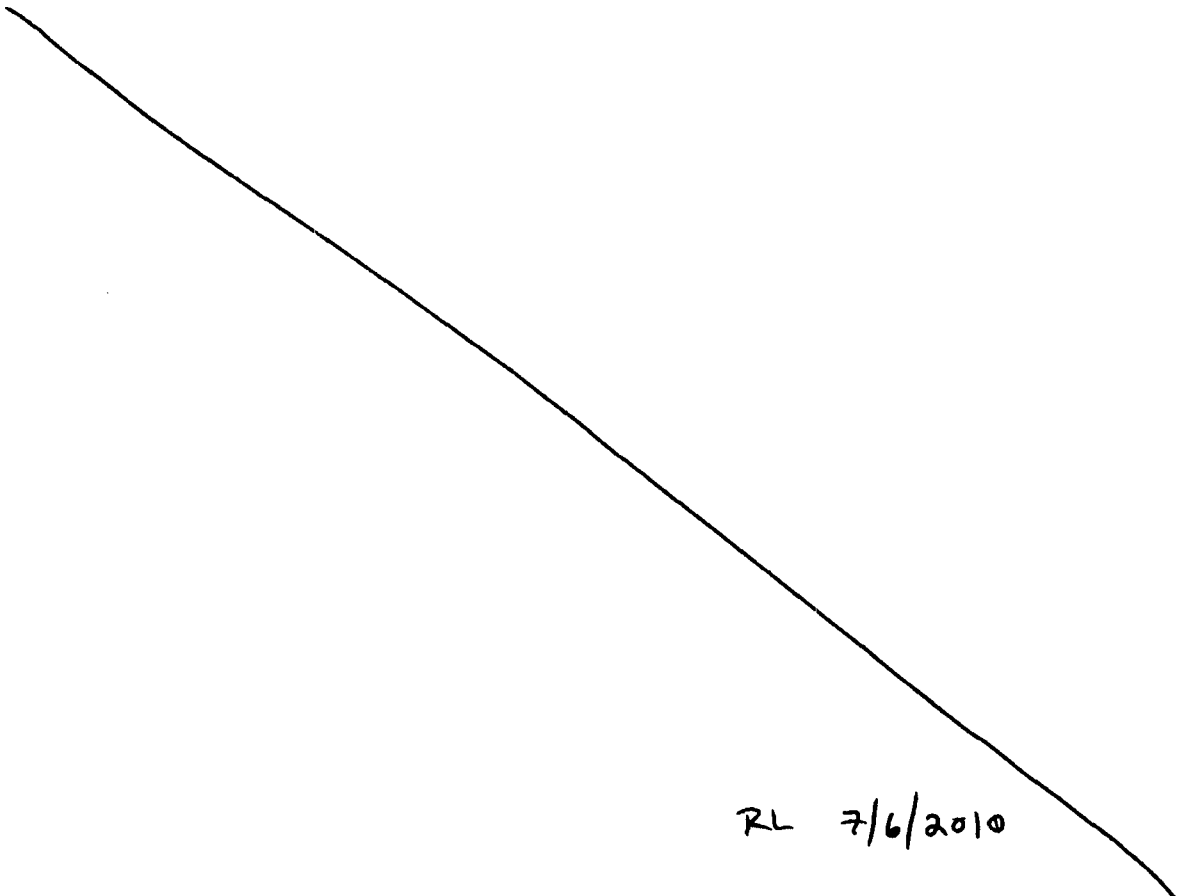


Figure 4-65: Transient solubility-limited release to the TLL drift shadow with 0.1 mm/yr dripping and host-rock percolation abstraction.

In the earlier drift-shadow approximation, the TLL matrix carries some (at high dripping rates) or almost all (at low dripping rates) of the dripping flux, which makes the matrix advection-dominated at high dripping rates and almost shuts off fracture release at low dripping.

The current approximation tends to increase the fracture/matrix release ratio by decreasing matrix releases at large dripping and increasing fracture releases at small dripping. As a result, the total calculated fracture release does not drop off as rapidly with dripping flux under the current approximation. At the 1 mm/yr dripping flux, there is no time in which matrix release is larger than fracture release, in contrast to the drift-shadow case where the steady state condition has matrix release at least three orders of magnitude larger than fracture release. At the 0.1 mm/yr dripping flux, there is a transient period when the fracture/matrix release ratio is less than 1, peaking at approximately one order of magnitude. In the drift-shadow approximation, the system responds so slowly that it never reaches equilibrium in 10^6 years but the ratio appears to be heading towards the ballpark of the 1 mm/yr case.



RL 7/6/2010

References

Bechtel SAIC Company, LLC. 2007. *Abstraction of Drift Seepage*. MDL-NBS-HS-000019 REV01 AD01, Bechtel SAIC Company, LLC, Las Vegas, NV.

Sandia National Laboratories. 2007. *EBS Radionuclide Transport Abstraction*. ANL-WIS-PA-000001 REV 03, Sandia National Laboratories, Las Vegas, NV.

RL 7/6/2010

5 Site-scale unsaturated zone flow model visualization

06/28/10 Supplemental information on percolation.



This entry collects supplemental information that I created earlier to visualize the percolation flux fields used in performance assessment calculations. These flux fields were calculated by the Site-Scale Unsaturated Zone Flow Model and were used in the licence application. The information is included for completeness.

The original flow files were included with the supplemental Environmental Impact Statement package. The visualization work occurred primarily in January and February, 2008. The work was intended to understand the particulars of the flow fields and how the mesh was constructed. I created *Matlab* routines to extract the mesh and flow fields from the original files. The figures in this entry are based on the original *Matlab* routines.

06/29/10 Infiltration and percolation redistribution.



Figure 5-1 displays the entire unsaturated zone site-scale flow model domain, which consists of 2,042 columns. The bottom elevation of the domain (DOE uses the water table) provides the color coding for each column.

The top and bottom polygons for the model are indicated in blue and red lines, respectively. In most columns the columns have identical horizontal shape from top to bottom, but DOE represents some of the faults with slanting columns.

The mesh file does not provide the polygons for the model. I used *Matlab*'s Voronoi gridding routines, which create polygons from the center point of each cell, to provide an indication of the mesh. DOE used similar techniques. I visually checked the grid with the DOE representation. Most *Matlab*-generated polygons appear very similar to the DOE plots, but some polygons have slightly differing shape (but preserve the number of sides).

I overlaid the proposed emplacement drift locations (pale blue lines) on the grid. Each mesh column contacting an emplacement drift is vertically oriented. Five faults represented by discrete features intersect at least one emplacement drift. From south to north, these include (i) the Sundance Fault, (ii) an unnamed splay from the Ghost Dance Fault, (iii) the Drillhole Wash Fault, (iv) the Pagany Wash Fault, and (v) the Sever Wash Fault. The Sundance fault intersects

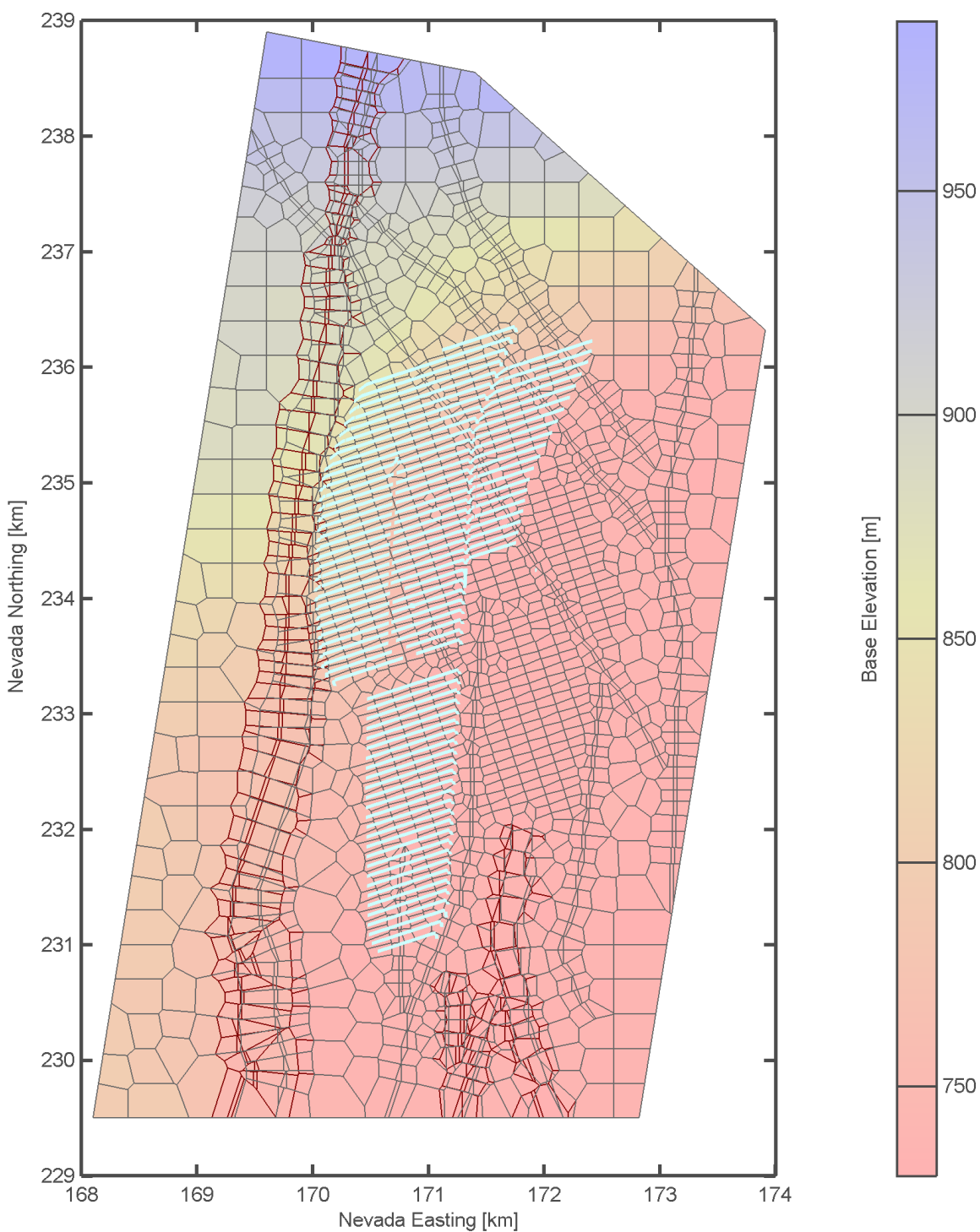


Figure 5-1: Voronoi polygons for the site-scale unsaturated zone flow model. Blue and red polygons represent the top and bottom of the model, respectively. Emplacement drifts are indicated in pale blue.

emplacement drifts in a contingency area and the small splay off the Ghost Dance fault intersects the drifts at the locations DOE plans to locate the accelerated thermal test drifts. Subsequent figures display the region surrounding the proposed emplacement drifts.

Figures 5-2, 5-3, 5-4, and 5-5 display upper boundary condition net infiltration on the top polygons of the mesh. Each figure displays the four infiltration maps corresponding to the 10th, 30th, 50th, and 90th percentile uncertainty maps.

Figures 5-6, 5-7, 5-8, and 5-9 each display one of the four present-day net infiltration maps. Each figure also displays three maps that track the changes in percolation flux relative to the top boundary condition. The subfigure labeled PtnM1 is the topmost layer in the PTn unit, the subfigure labeled TSWM5 is the primary repository layer in the TSw unit, and the subfigure labeled WT represents flow to the water table.

The additional figures display a normalized change in flux in the form

$$Q_n = \frac{I - Q_p}{|I|} \quad (5-1)$$

where Q_n is normalized flux, I is the top boundary condition flux, Q_p is the percolation flux, and $|I|$ is the areal-average value of the top boundary condition flux. The top color scale is used for the top boundary condition subfigure and the bottom scale is used for the other subfigures. The value for $|I|$ is indicated in the label for the bottom color scale. A value of 1 for Q_n indicates that $Q_p = 0$, a value of 0 indicates that $Q_p = I$ (no net change in percolation flux) and a value of -1 indicates that $Q_p \geq 2I$ (at least a doubling in flux).

The three Q_n maps in each of the present-day figures show a consistent pattern of increasing redistribution with depth through the repository horizon and much larger redistribution into focused areas below the repository horizon. Redistribution above the repository appears to be largely associated with lateral flow from ridges to washes and some downdip flow from Yucca Crest to the east. In the northern half of the repository, recharge to the water table is largely focused into discrete faults. In the southern half of the repository, recharge to the water table is also focused, associated with diversion to the edge of restrictive low-permeability units.

Despite the generally consistent patterns for the four percentiles, the patterns are somewhat affected by the top boundary condition. The pattern of relative redistribution from the top boundary into the PTn is quite consistent among the four maps, indicating generally vertical flow and local topography-induced redistribution. The pattern of redistribution at the repository horizon is more pronounced and more affected by the distribution of net infiltration, retaining the upper redistribution and adding downdip and fault-induced redistribution. The patterns below the repository

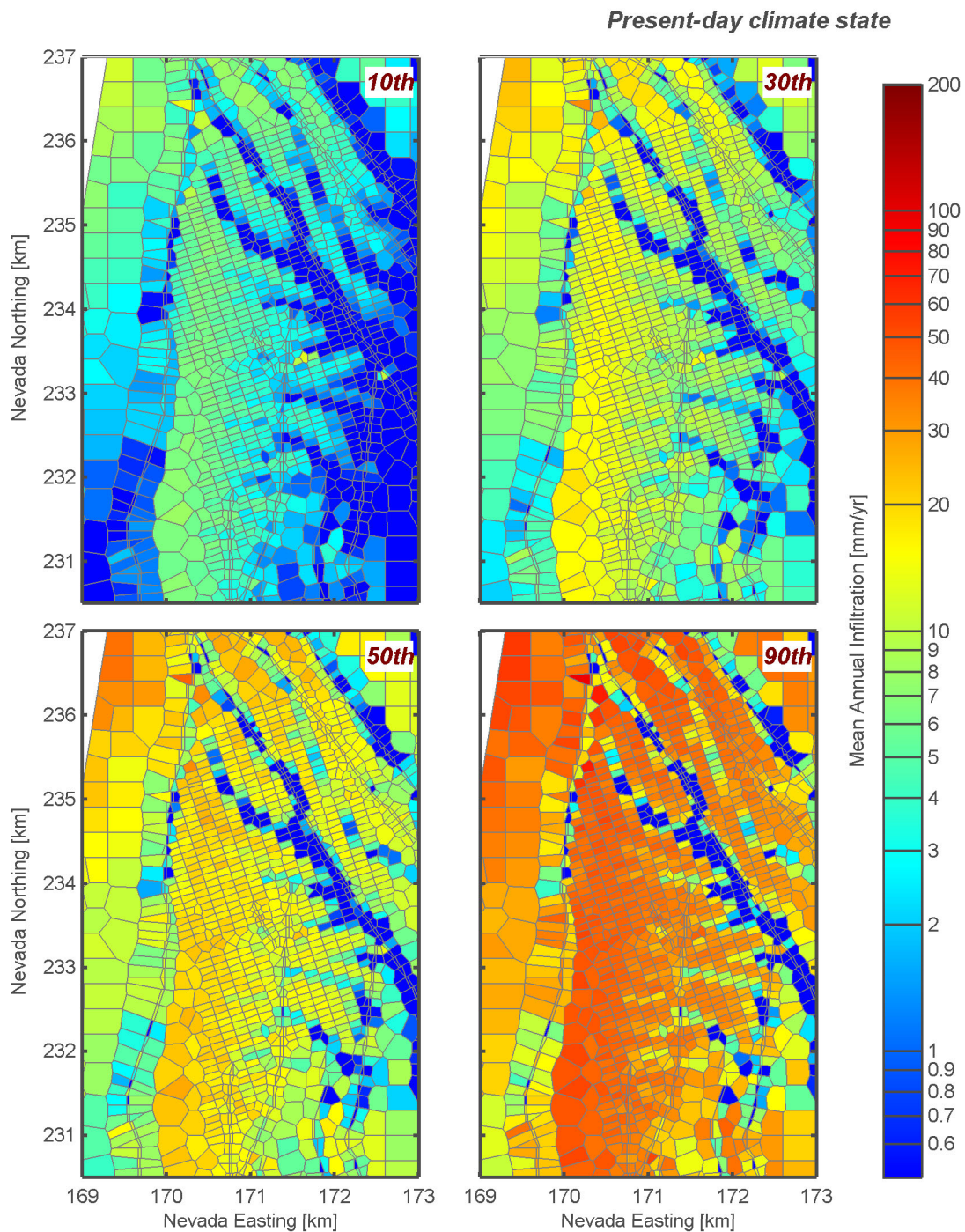


Figure 5-2: Upper boundary condition mean annual infiltration for the 10th, 30th, 50th, and 90th percentile maps under the present-day climate.

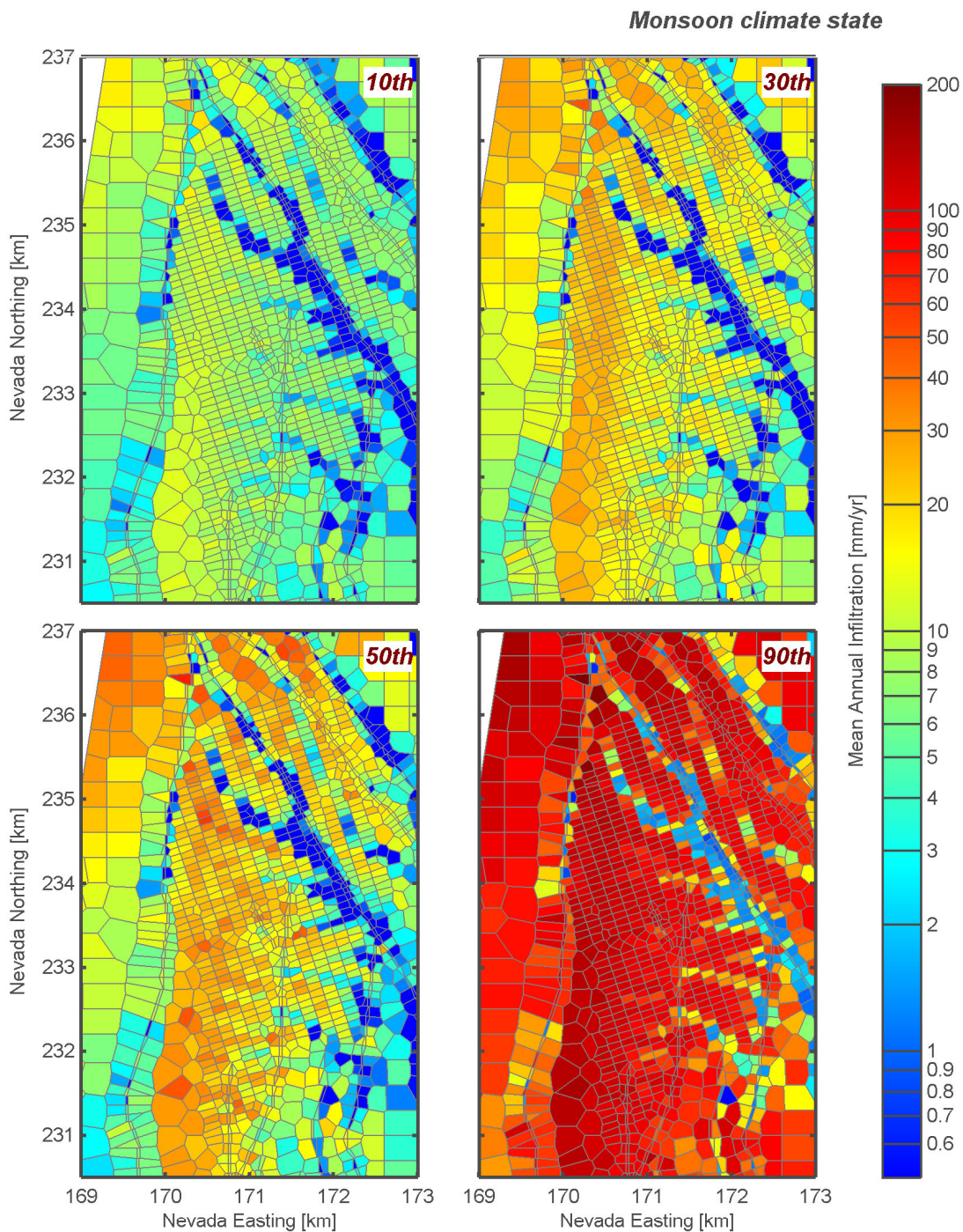


Figure 5-3: Upper boundary condition mean annual infiltration for the 10th, 30th, 50th, and 90th percentile maps under the monsoon climate.

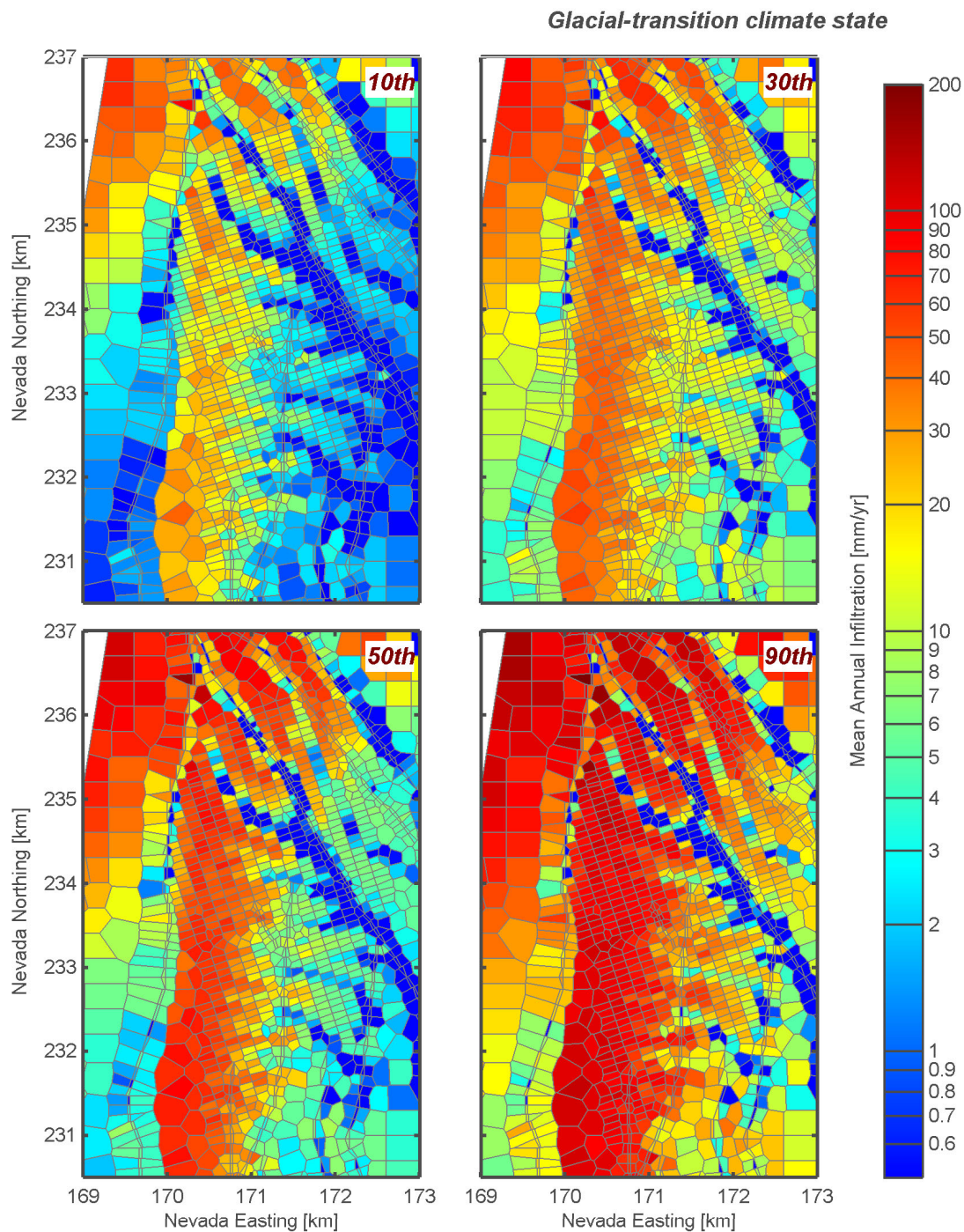


Figure 5-4: Upper boundary condition mean annual infiltration for the 10th, 30th, 50th, and 90th percentile maps under the glacial-transition climate.

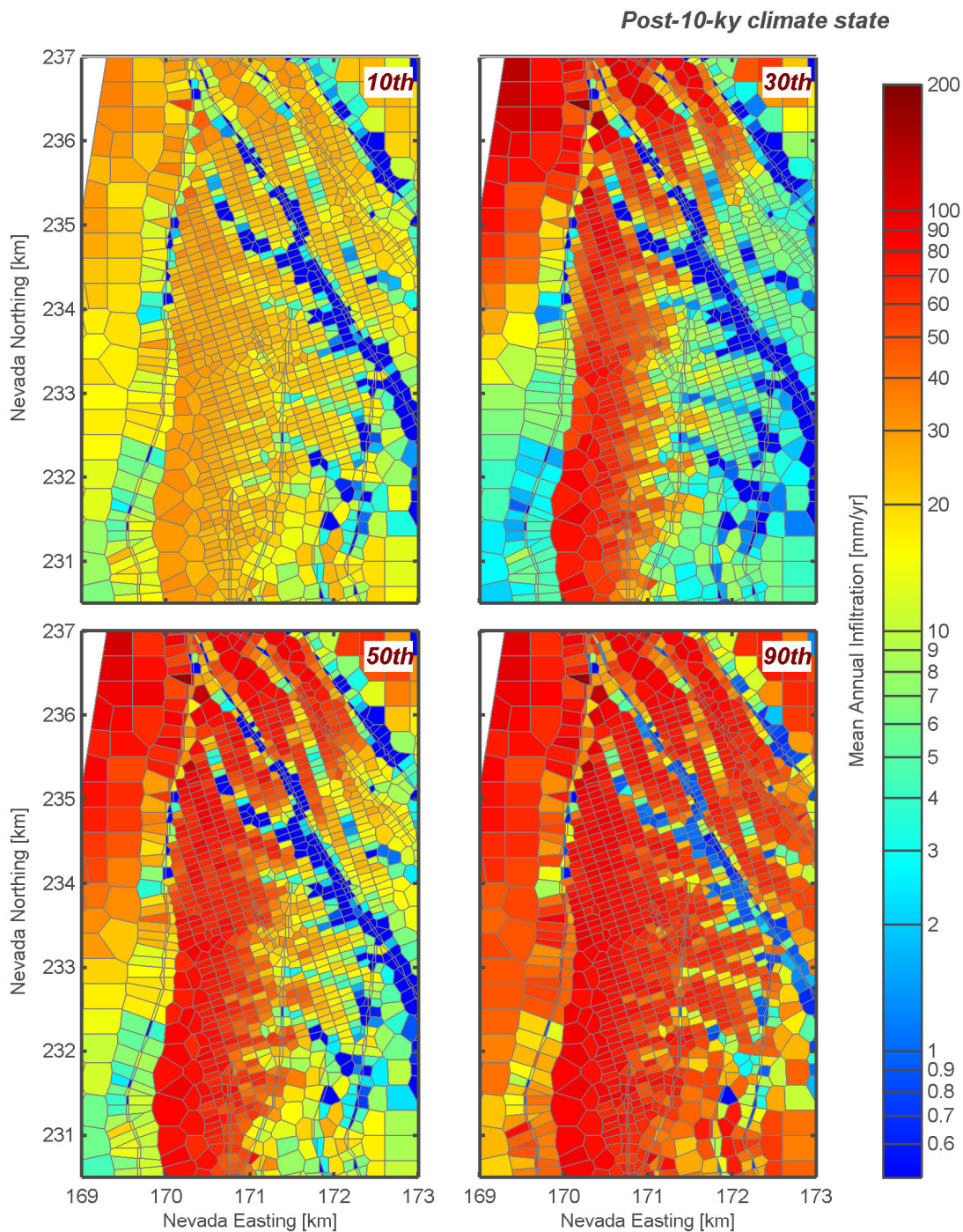


Figure 5-5: Upper boundary condition mean annual infiltration for the 10th, 30th, 50th, and 90th percentile maps under the post-10-ky climate.

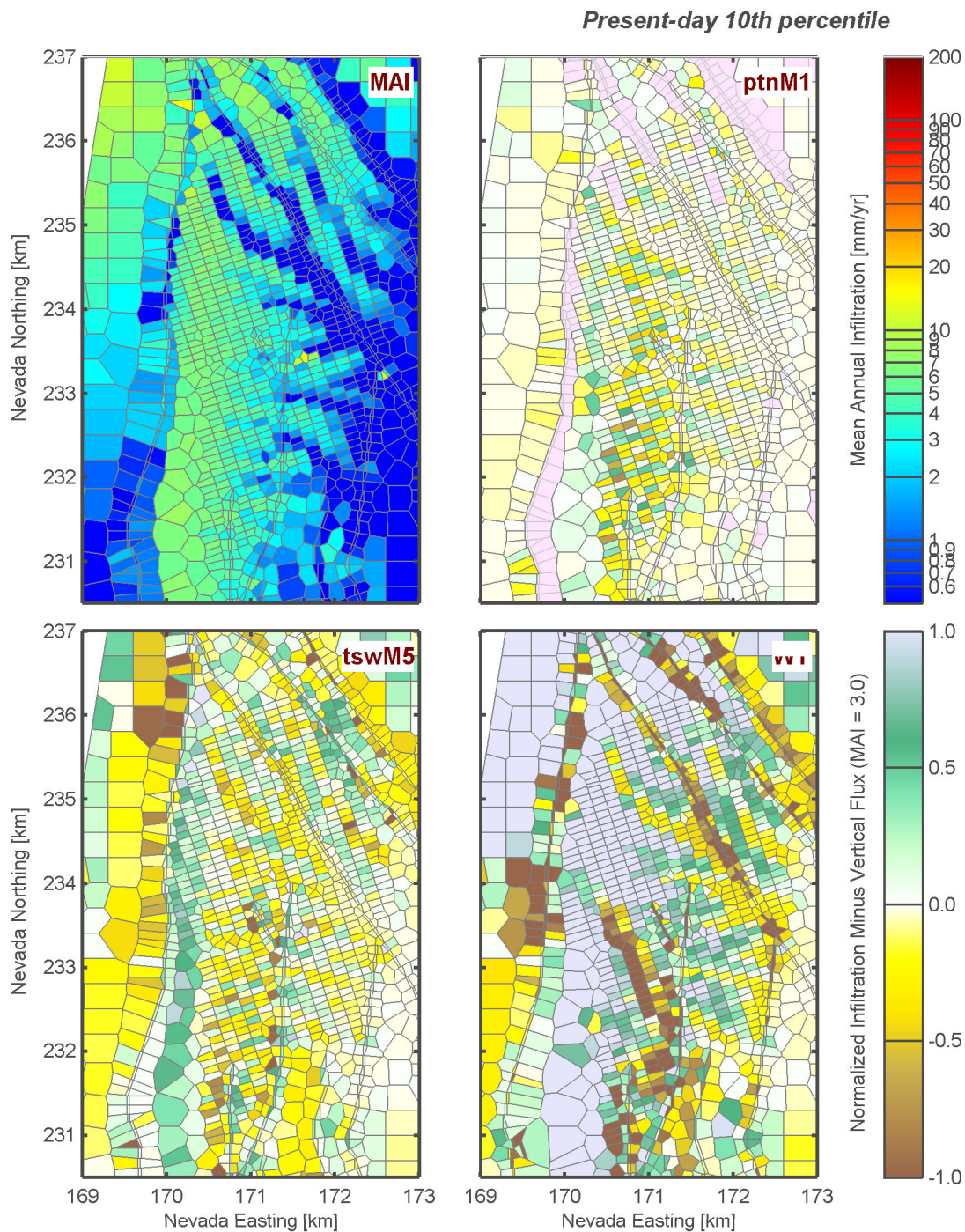


Figure 5-6: Upper boundary condition mean annual infiltration and relative changes to percolation flux in the PTn, TSw, and as recharge for the 10th percentile maps under the present-day climate.

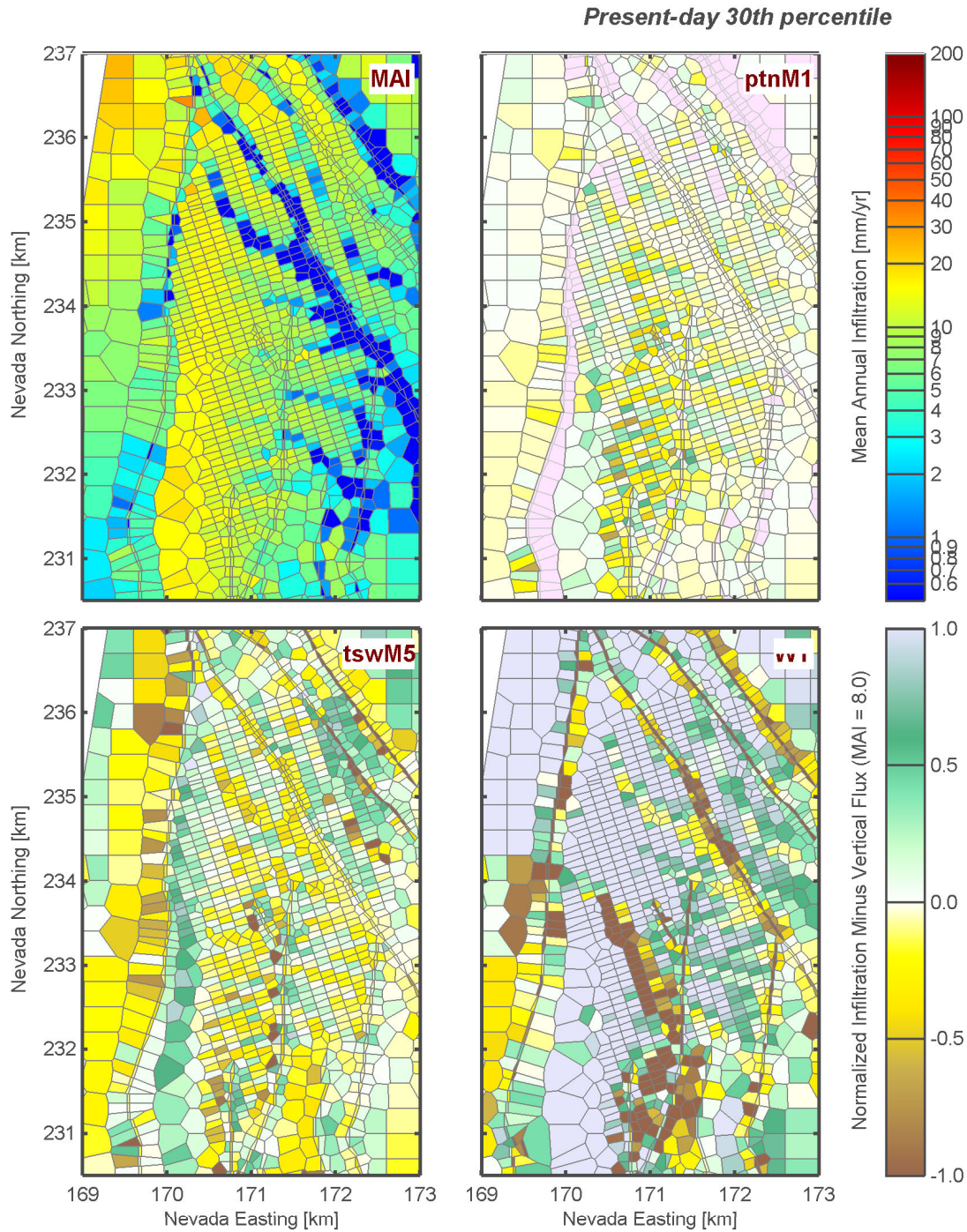


Figure 5-7: Upper boundary condition mean annual infiltration and relative changes to percolation flux in the PTn, TSw, and as recharge for the 30th percentile maps under the present-day climate.

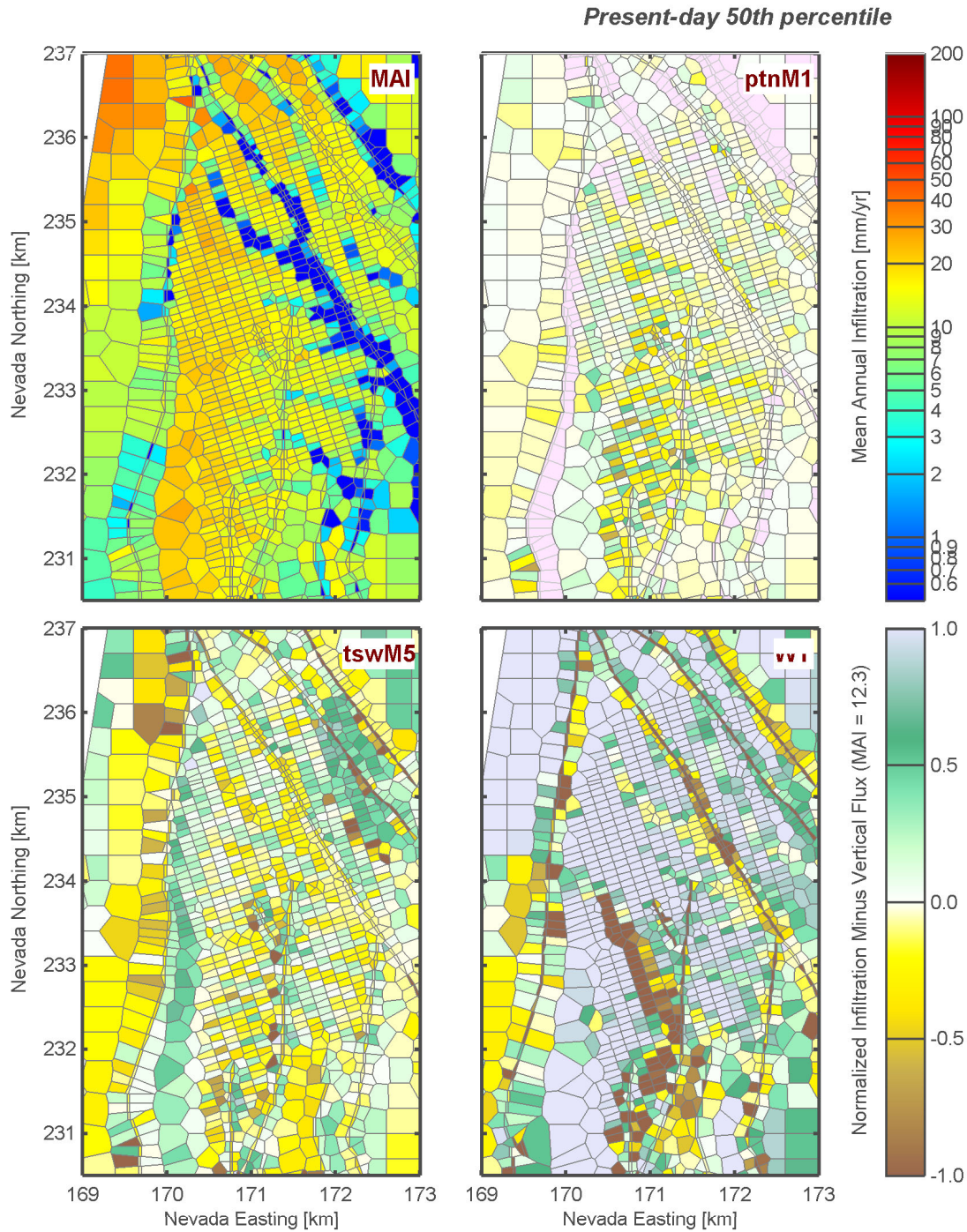


Figure 5-8: Upper boundary condition mean annual infiltration and relative changes to percolation flux in the PTn, TSw, and as recharge for the 50th percentile maps under the present-day climate.

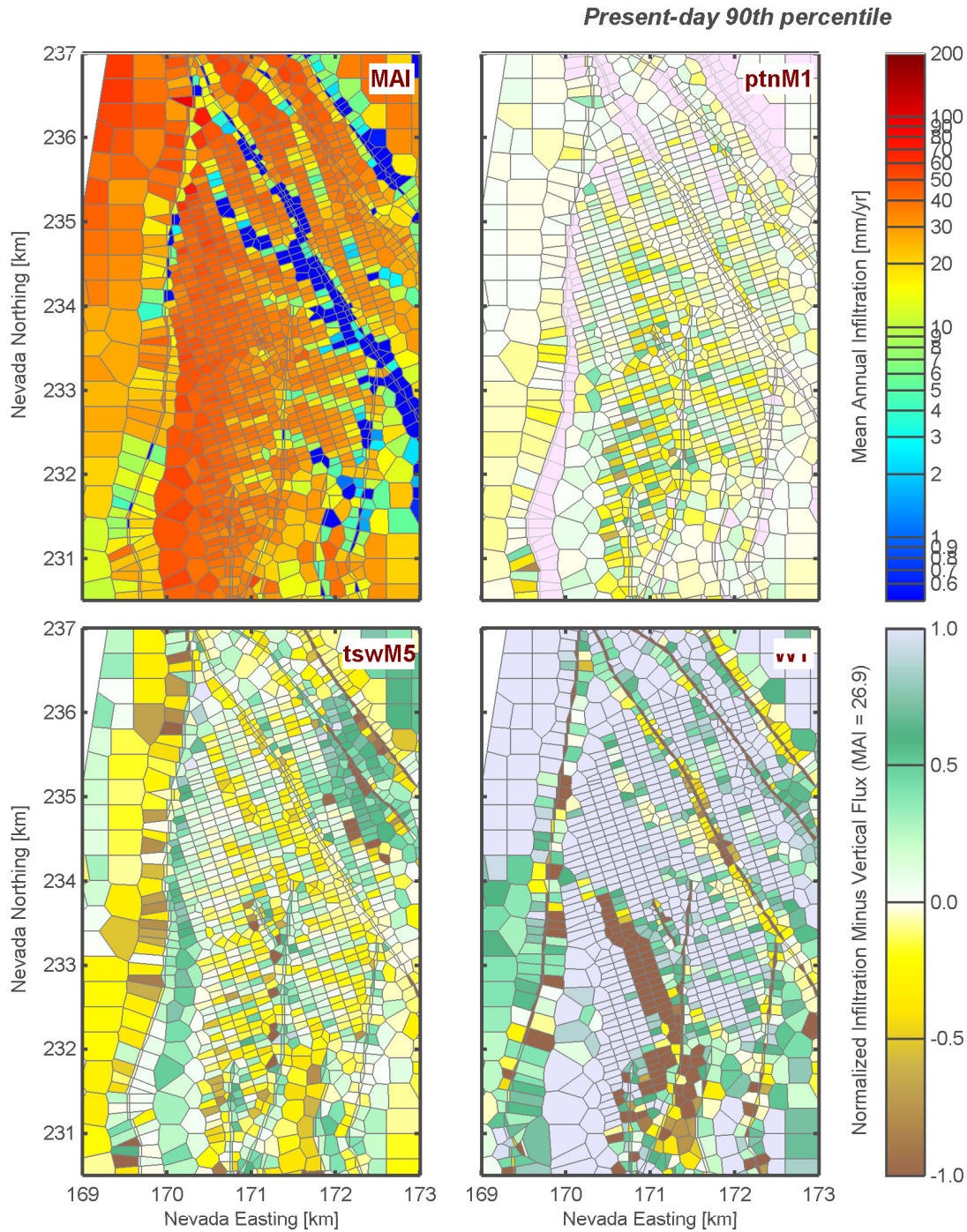
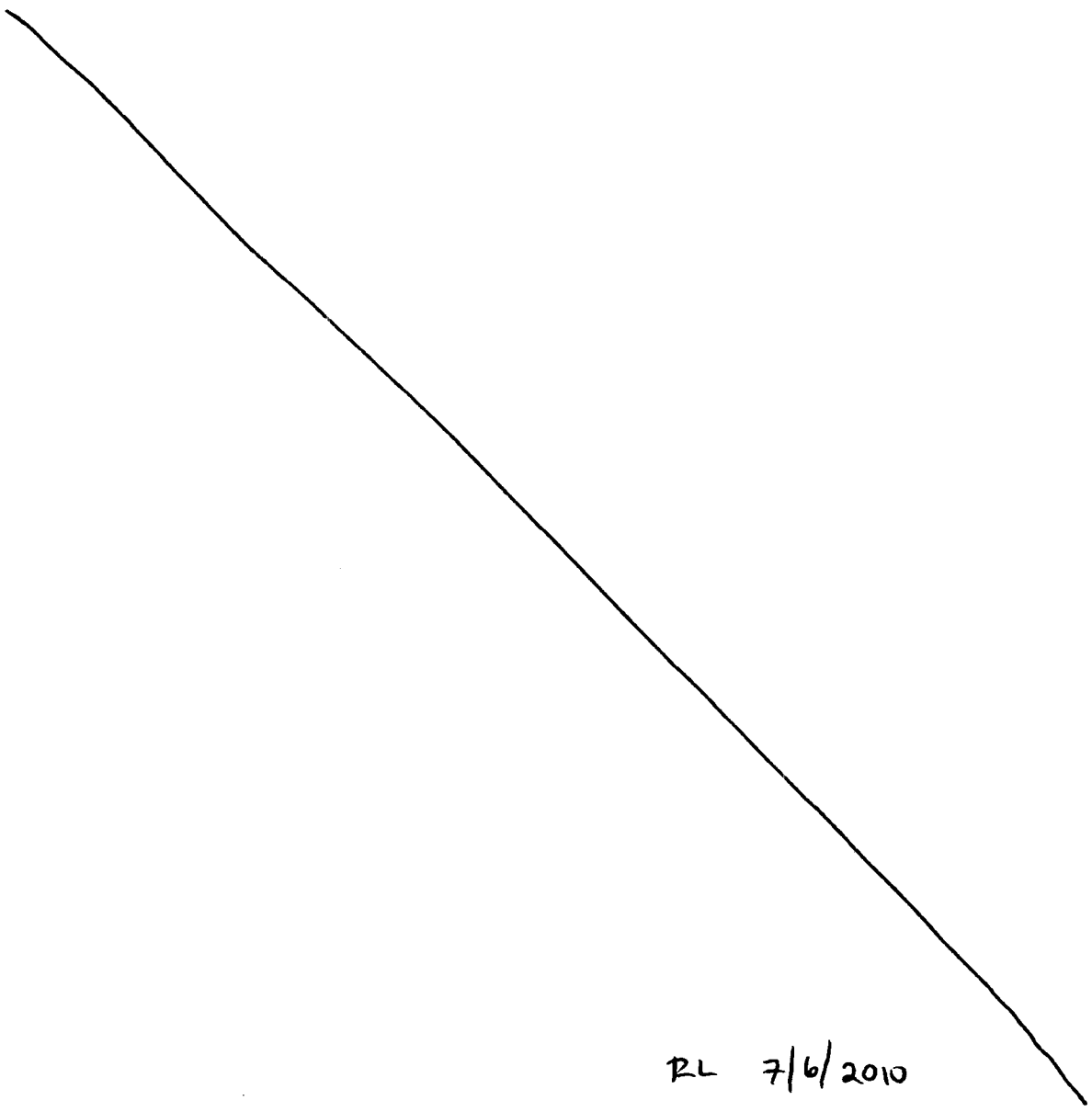


Figure 5-9: Upper boundary condition mean annual infiltration and relative changes to percolation flux in the PTn, TSw, and as recharge for the 90th percentile maps under the present-day climate.

are the most affected by the top boundary condition.

Figures 5-10, 5-11, 5-12, and 5-13 each display one of the four monsoon net infiltration maps. Figures 5-14, 5-15, 5-16, and 5-17 each display one of the four glacial-transition net infiltration maps. Figures 5-18, 5-19, 5-20, and 5-21 each display one of the four post-10-ky net infiltration maps. The general redistribution patterns are similar among all 16 flow fields.



RL 7/6/2010

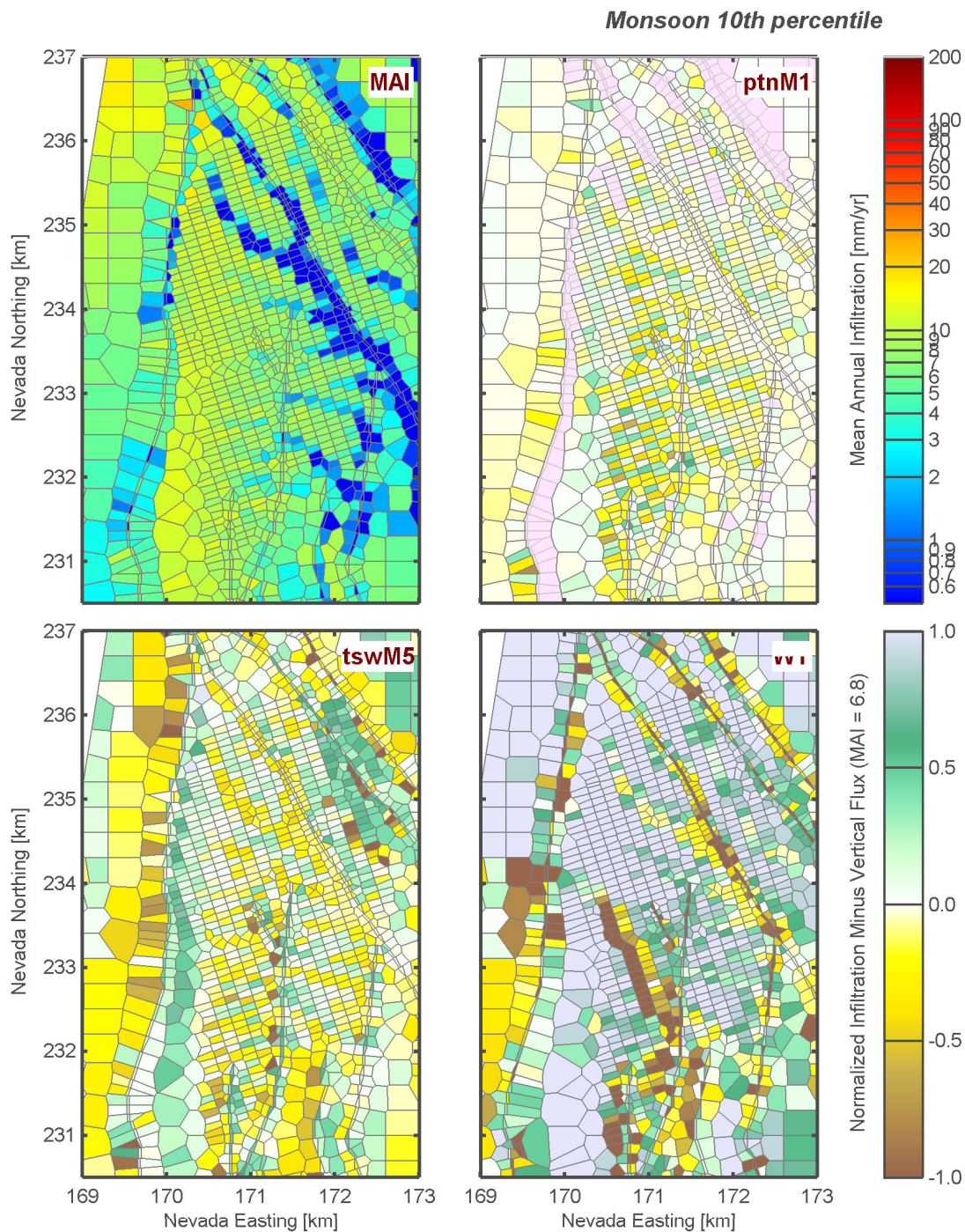


Figure 5-10: Upper boundary condition mean annual infiltration and relative changes to percolation flux in the PTn, TSw, and as recharge for the 10th percentile maps under the monsoon climate.

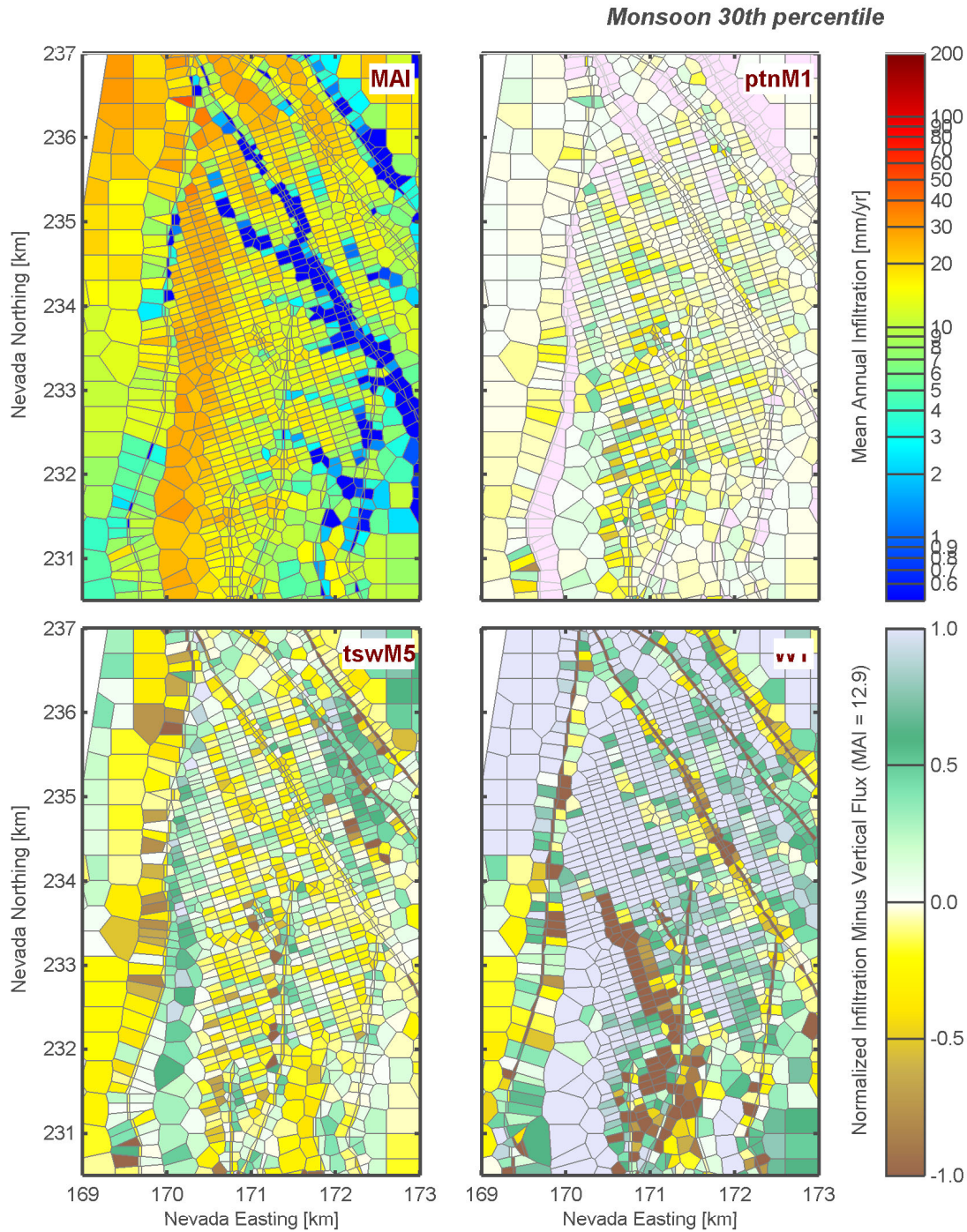


Figure 5-11: Upper boundary condition mean annual infiltration and relative changes to percolation flux in the PTn, TSw, and as recharge for the 30th percentile maps under the monsoon climate.

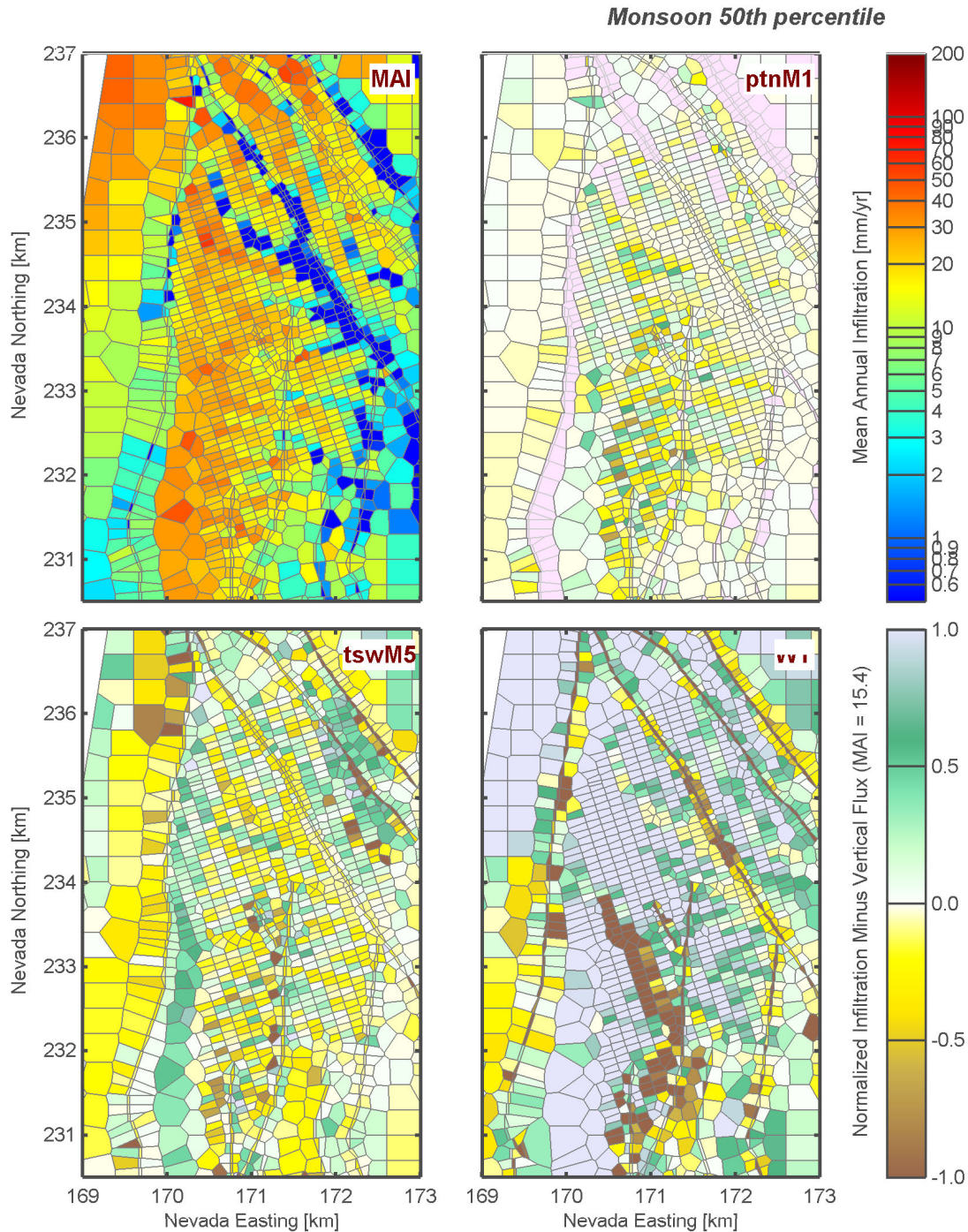


Figure 5-12: Upper boundary condition mean annual infiltration and relative changes to percolation flux in the PTn, TSw, and as recharge for the 50th percentile maps under the monsoon climate.

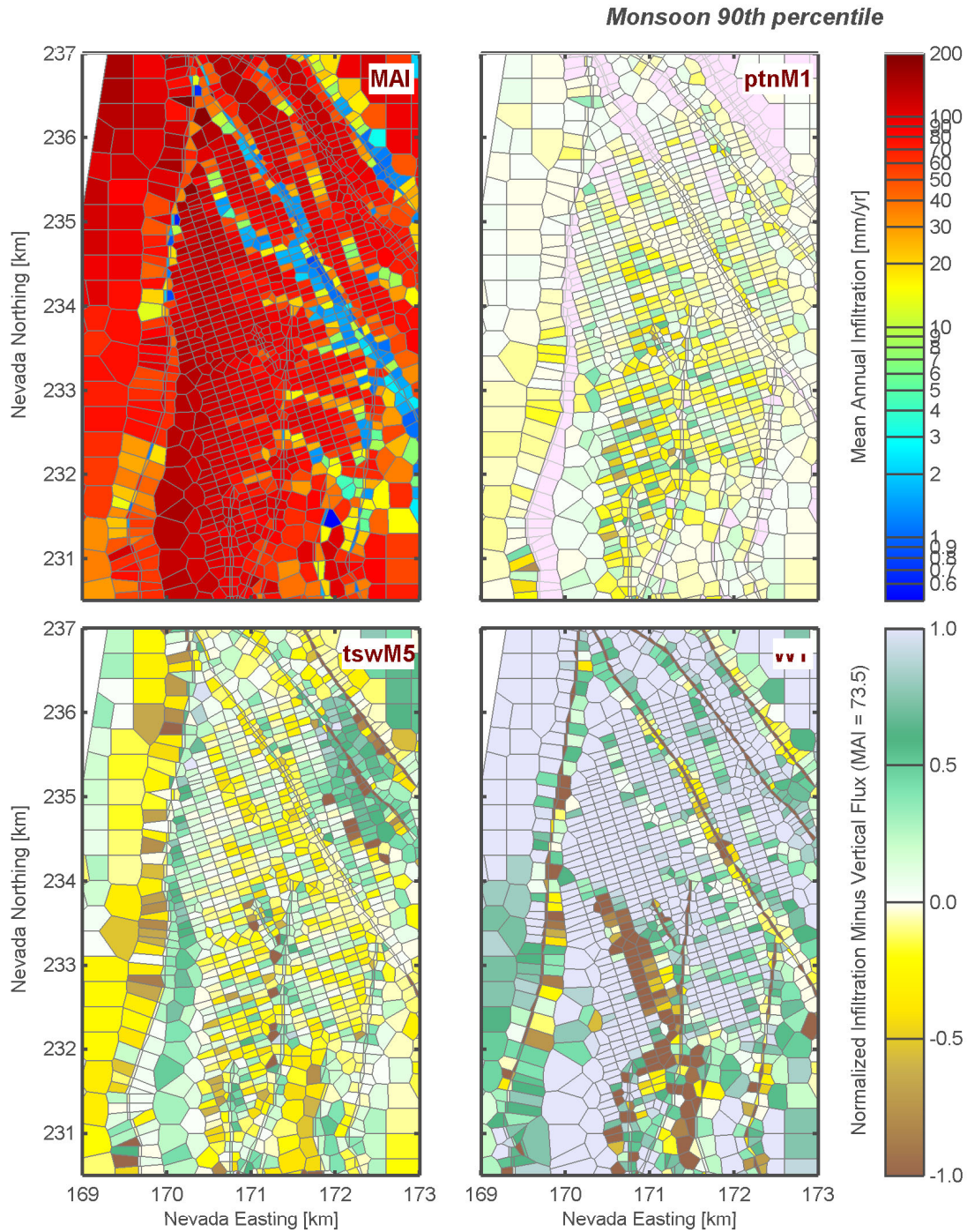


Figure 5-13: Upper boundary condition mean annual infiltration and relative changes to percolation flux in the PTn, TSw, and as recharge for the 90th percentile maps under the monsoon climate.

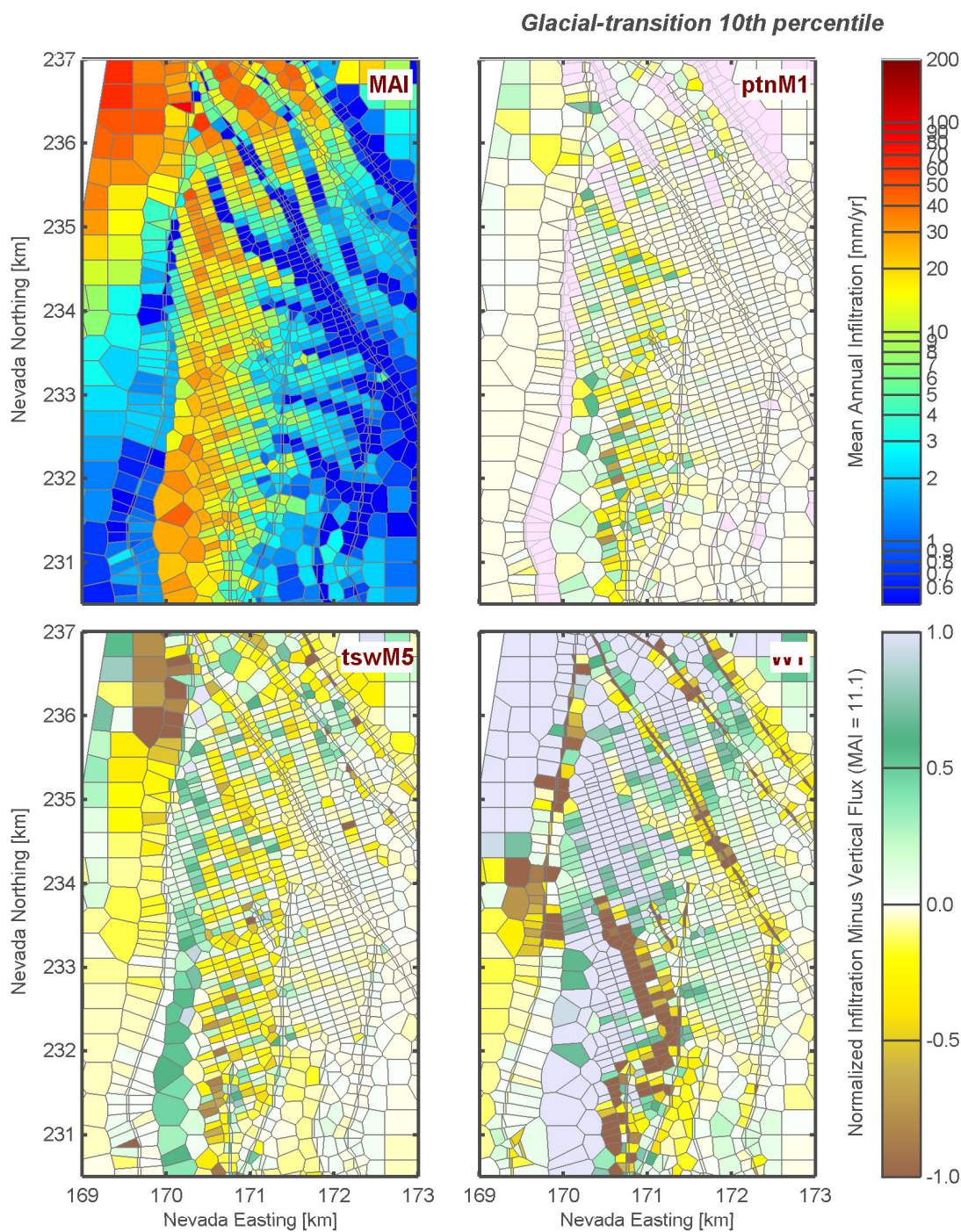


Figure 5-14: Upper boundary condition mean annual infiltration and relative changes to percolation flux in the PTn, TSw, and as recharge for the 10th percentile maps under the glacial-transition climate.

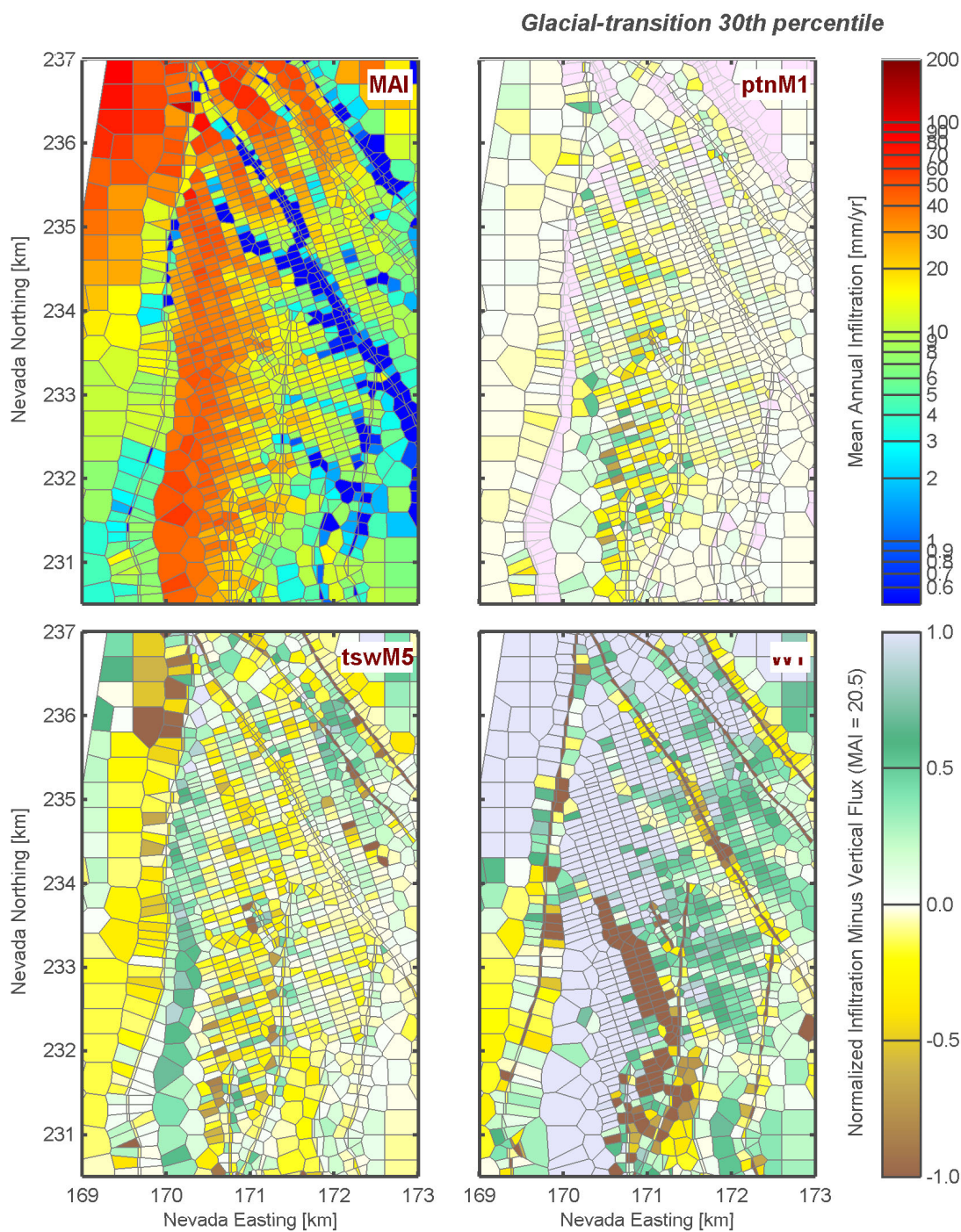


Figure 5-15: Upper boundary condition mean annual infiltration and relative changes to percolation flux in the PTn, TSw, and as recharge for the 30th percentile maps under the glacial-transition climate.

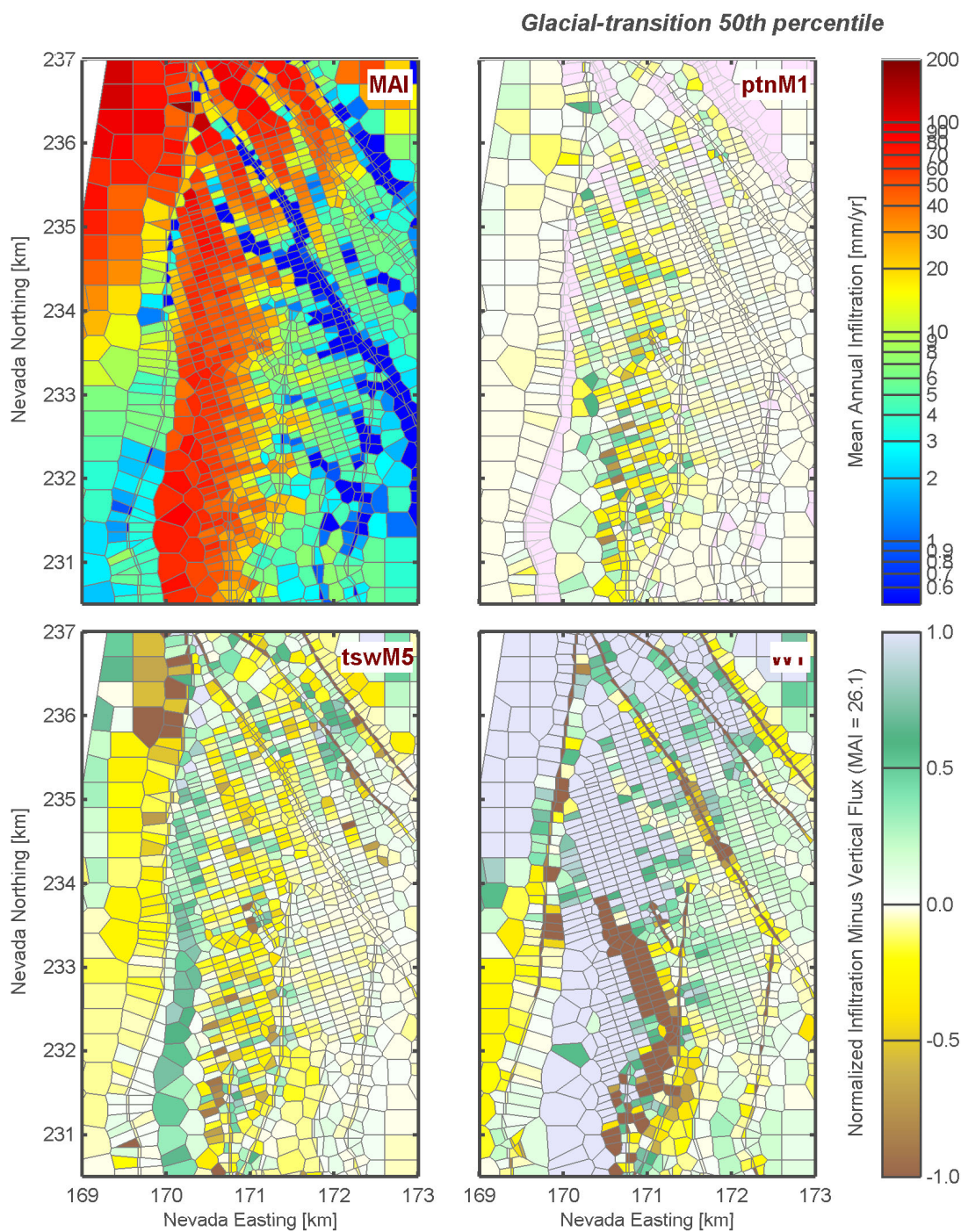


Figure 5-16: Upper boundary condition mean annual infiltration and relative changes to percolation flux in the PTn, TSw, and as recharge for the 50th percentile maps under the glacial-transition climate.

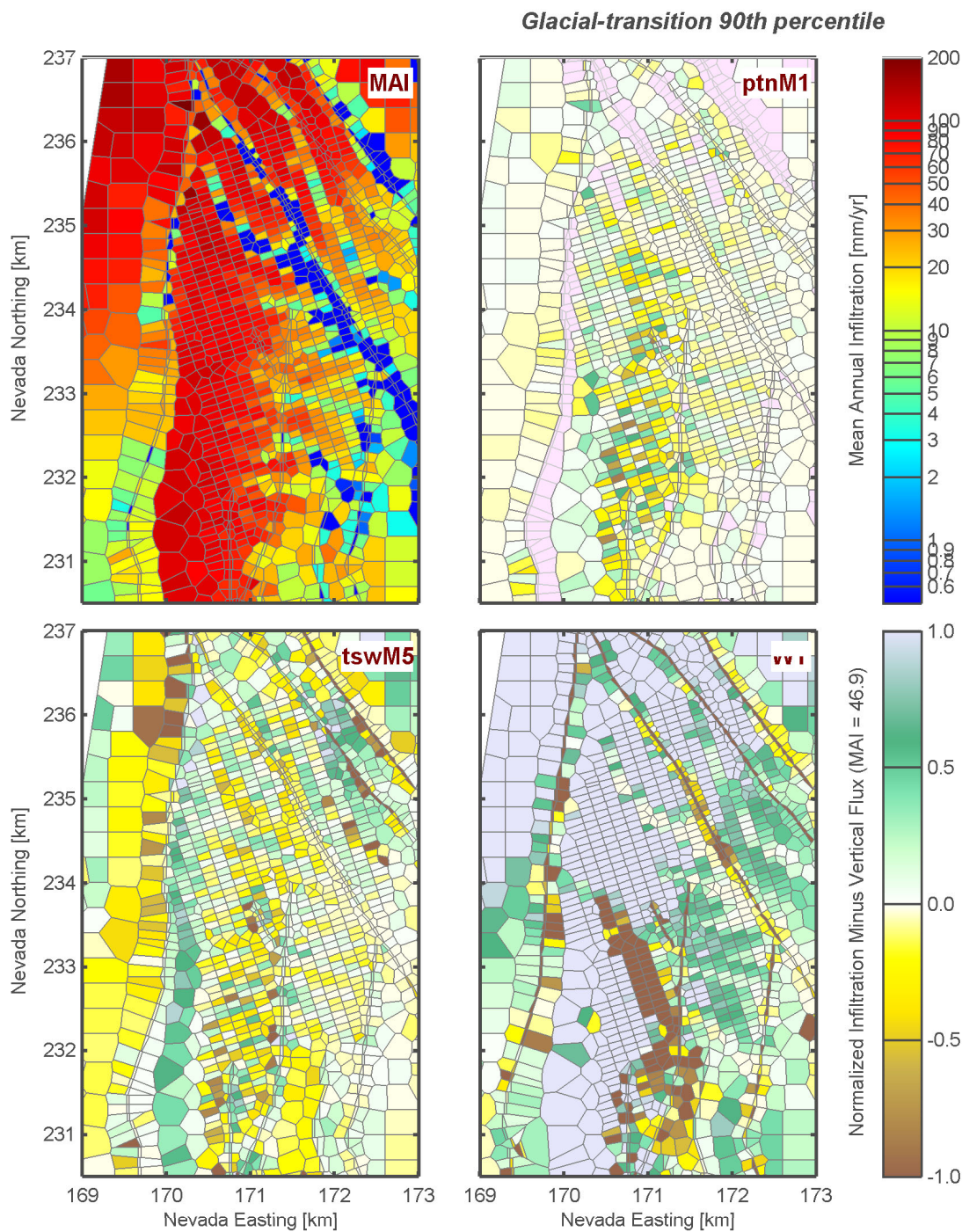


Figure 5-17: Upper boundary condition mean annual infiltration and relative changes to percolation flux in the PTn, TSw, and as recharge for the 90th percentile maps under the glacial-transition climate.

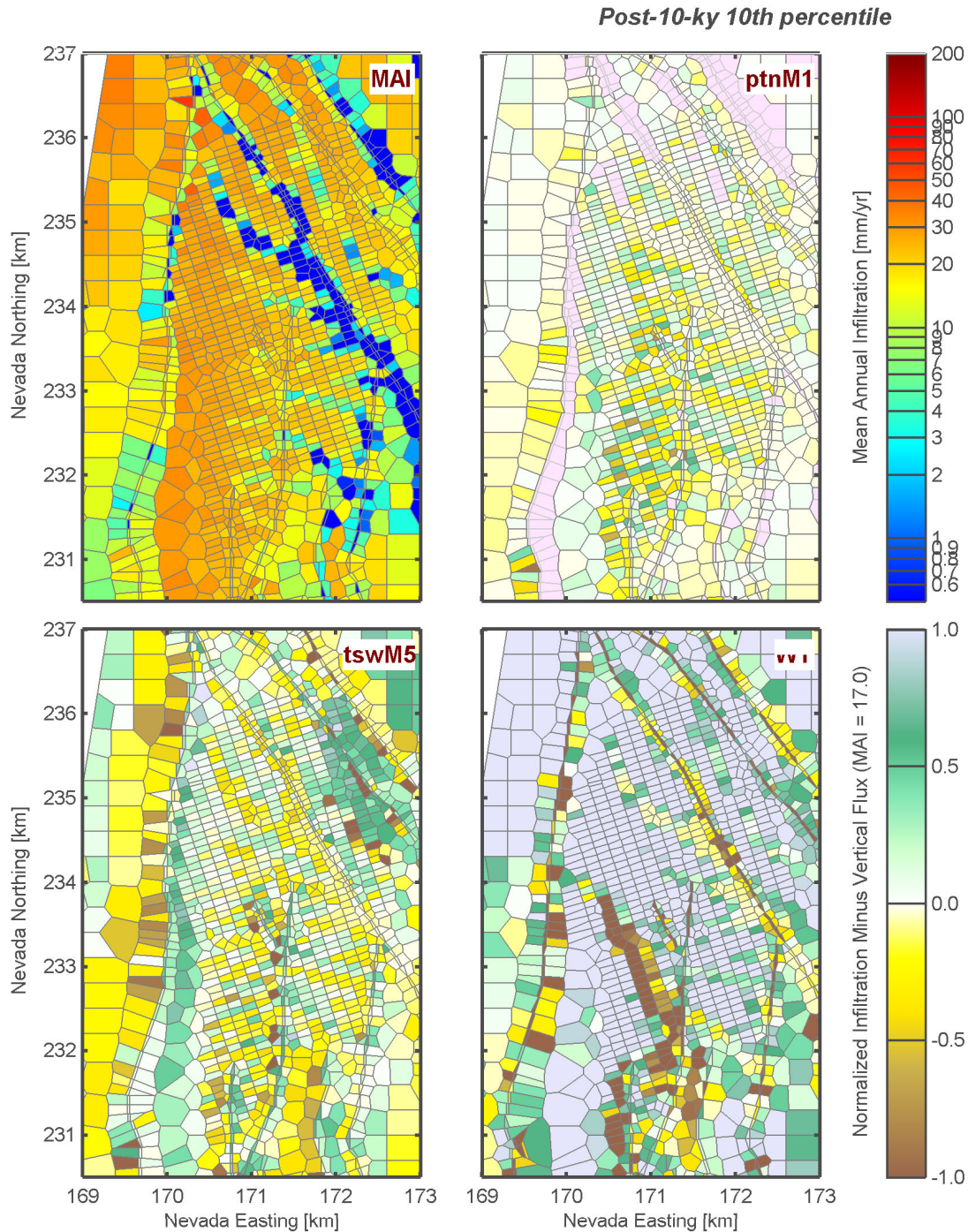


Figure 5-18: Upper boundary condition mean annual infiltration and relative changes to percolation flux in the PTn, TSw, and as recharge for the 10th percentile maps under the post-10-ky climate.

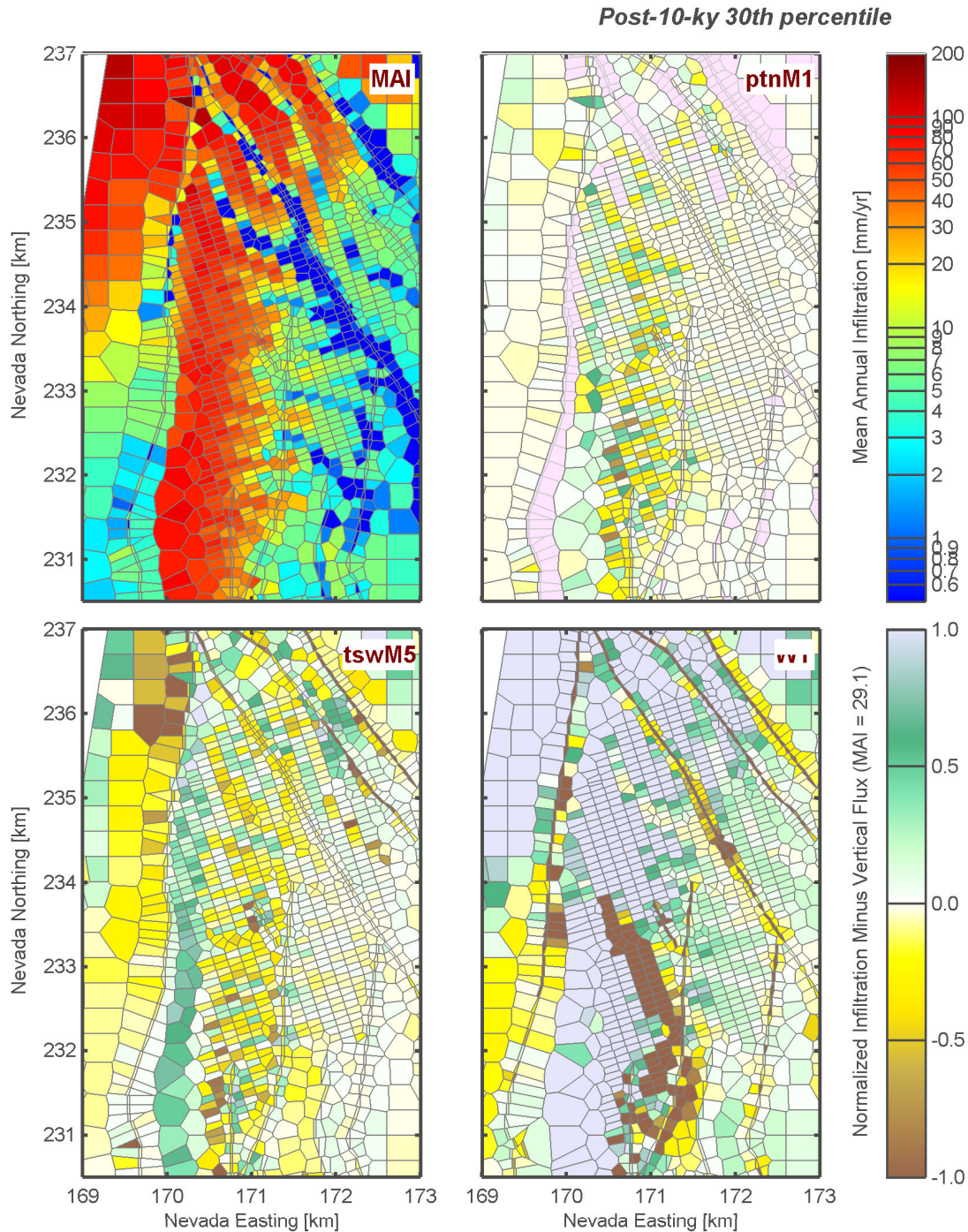


Figure 5-19: Upper boundary condition mean annual infiltration and relative changes to percolation flux in the PTn, TSw, and as recharge for the 30th percentile maps under the post-10-ky climate.

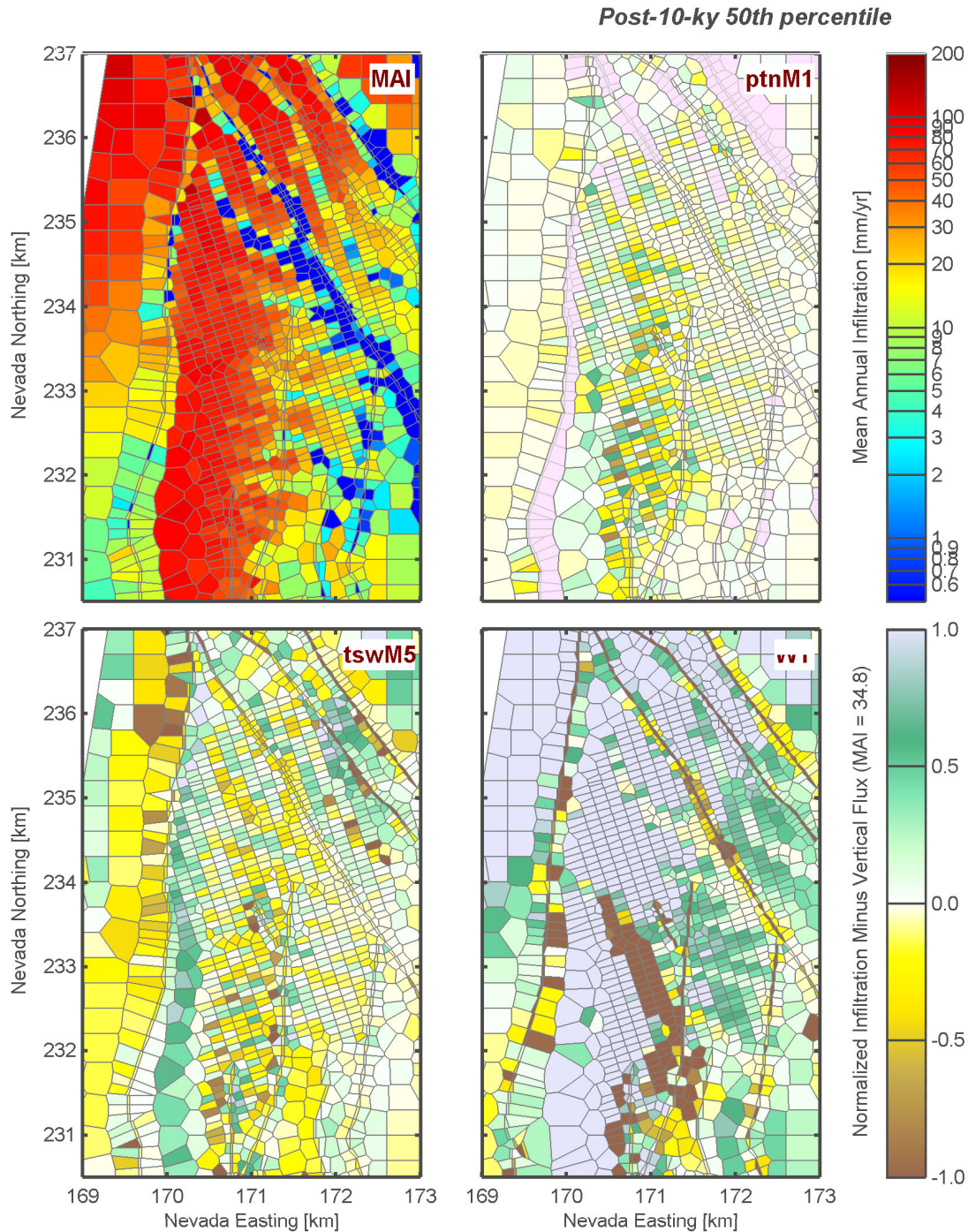


Figure 5-20: Upper boundary condition mean annual infiltration and relative changes to percolation flux in the PTn, TSw, and as recharge for the 50th percentile maps under the post-10-ky climate.

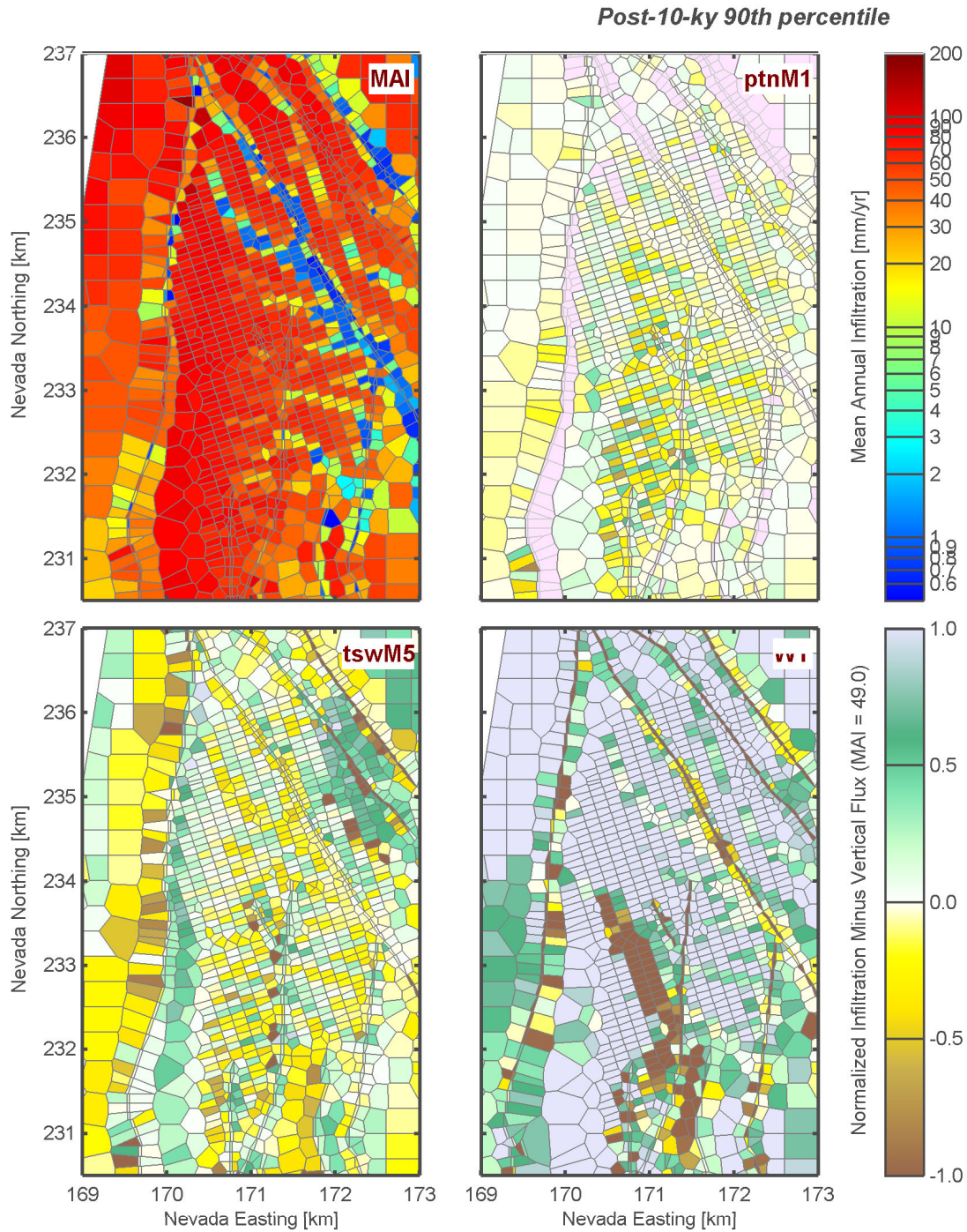


Figure 5-21: Upper boundary condition mean annual infiltration and relative changes to percolation flux in the PTn, TSw, and as recharge for the 90th percentile maps under the post-10-ky climate.

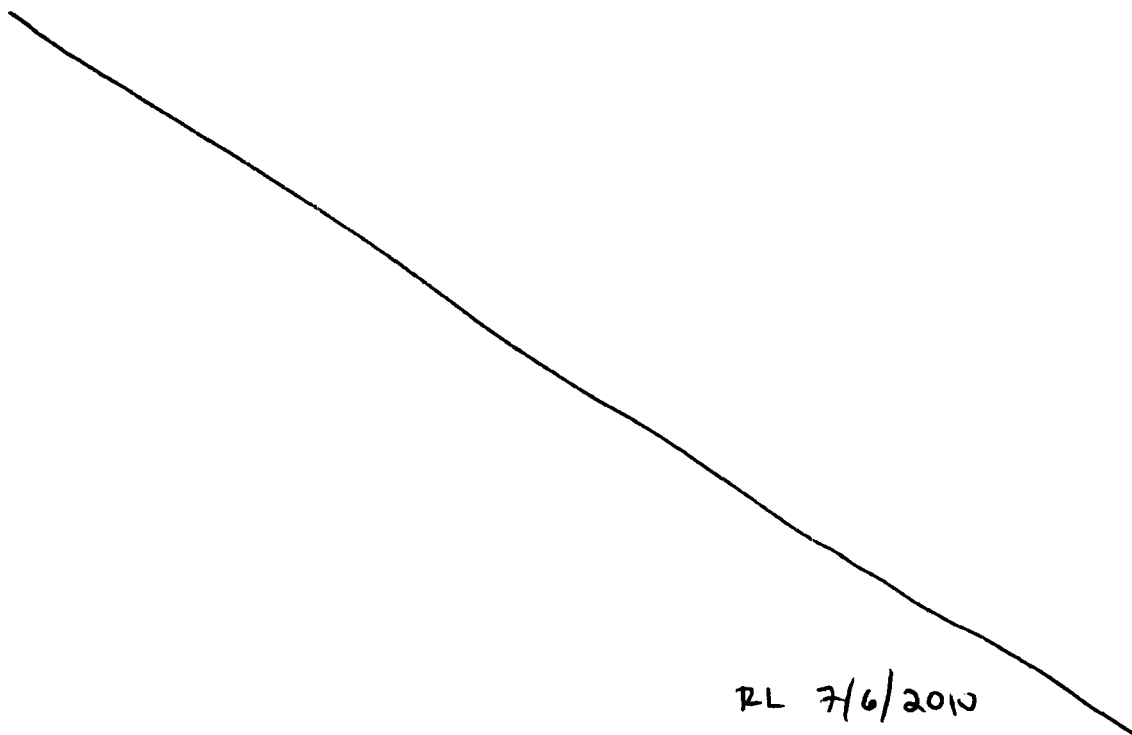
06/30/10 Percolation and saturation slices.

SAS

I was able to extract and plot quantities defined for each grid cell in the mesh, such as saturation and fracture-matrix transfer fluxes. Likewise, I was able to readily extract fluxes defined for columns, because the grid mesh is organized so that cells in columns are contiguous. I did not extract horizontal fluxes, because significant coding would be necessary to calculate fluxes on the unstructured grid.

Figures 5-22, 5-23, 5-24, and 5-25 plot cell-centered values for cells located in east-west swaths in a sequence from the southern to the northern end of the proposed footprint. Each swath extends 100 m north and south of the nominal northing. These figures illustrate vertical fluxes, transfers between matrix and fractures, and saturations for the 10th percentile boundary condition of the present-day climate. Figures 5-26, 5-27, and 5-28 display the same parameters for a sequence of swaths from west to east. Welded, nonwelded, and perched layers are readily visible based on contrasts in saturation and vertical matrix flux, as well as fluxes between the fracture and matrix.

Figures 5-29, 5-30, 5-31, 5-32, 5-33, 5-34, and 5-35 display the corresponding swaths and parameters for the 30th percentile glacial-transition climate.



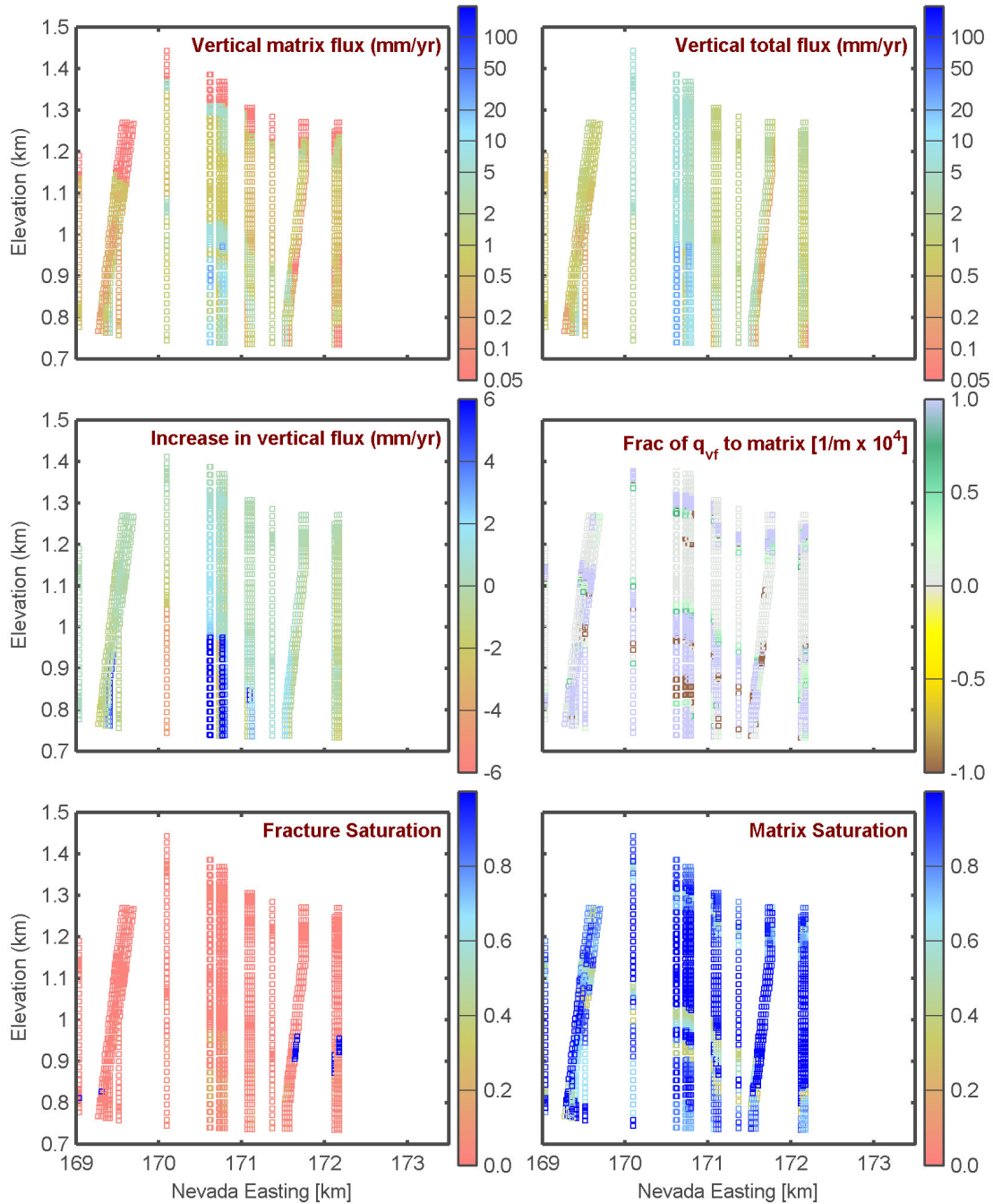
Present-day 10th percentile: Northing 231.0 km

Figure 5-22: Southern east-west cross-section of fluxes and saturations for the 10th percentile boundary condition under the present-day climate.

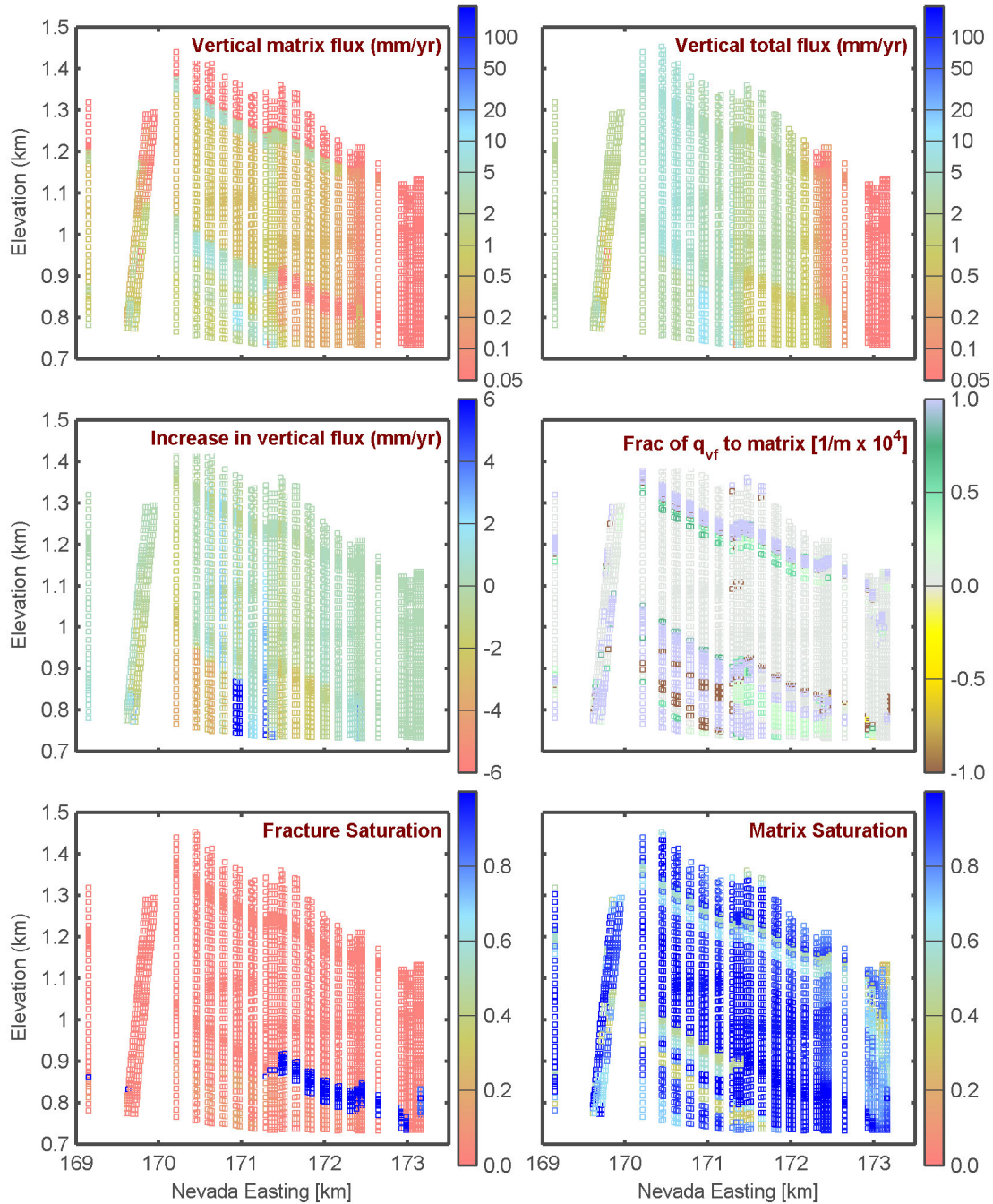
Present-day 10th percentile: Northing 232.6 km

Figure 5-23: South-central east-west cross-section of fluxes and saturations for the 10th percentile boundary condition under the present-day climate.

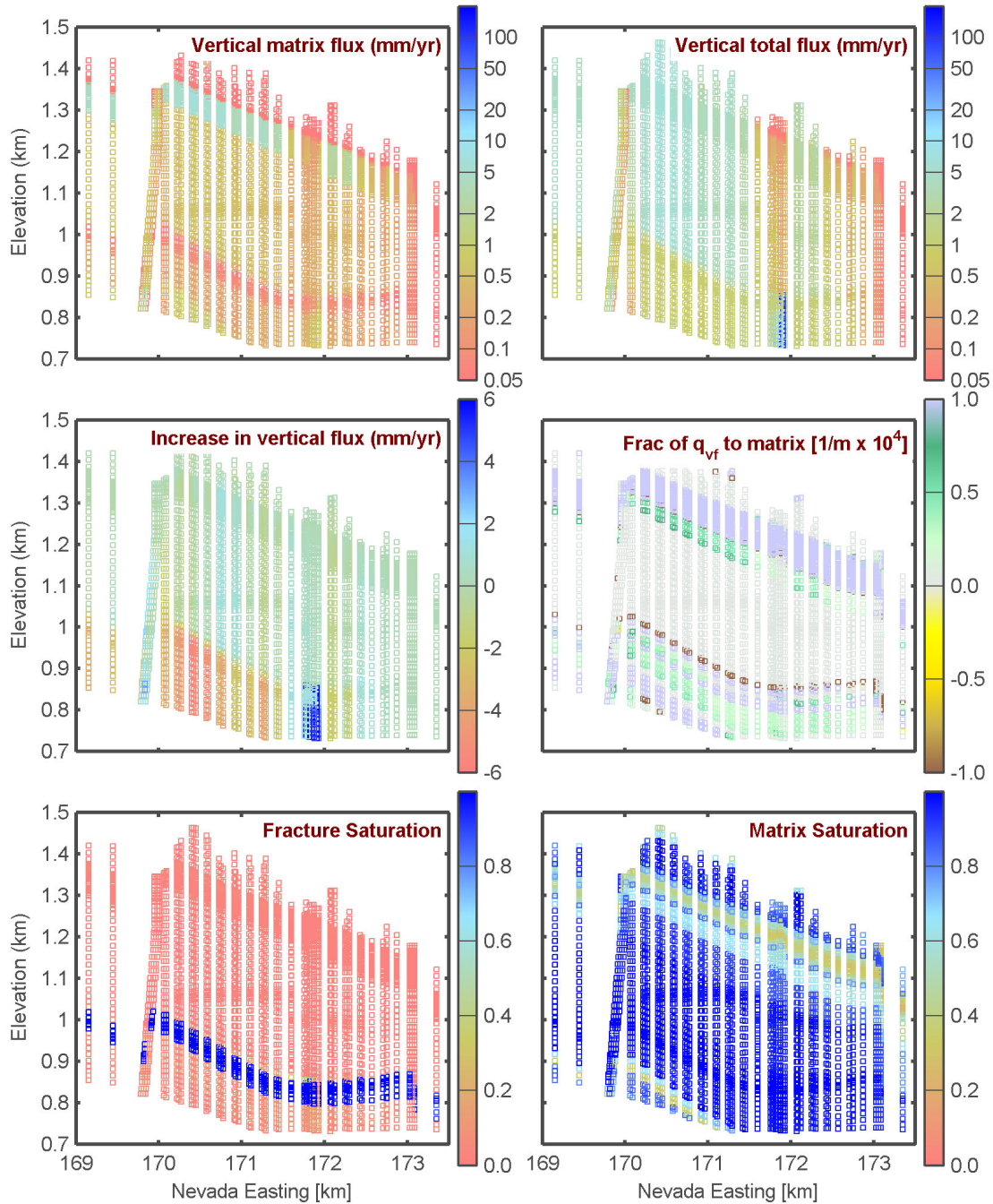
Present-day 10th percentile: Northing 234.4 km

Figure 5-24: North-central east-west cross-section of fluxes and saturations for the 10th percentile boundary condition under the present-day climate.

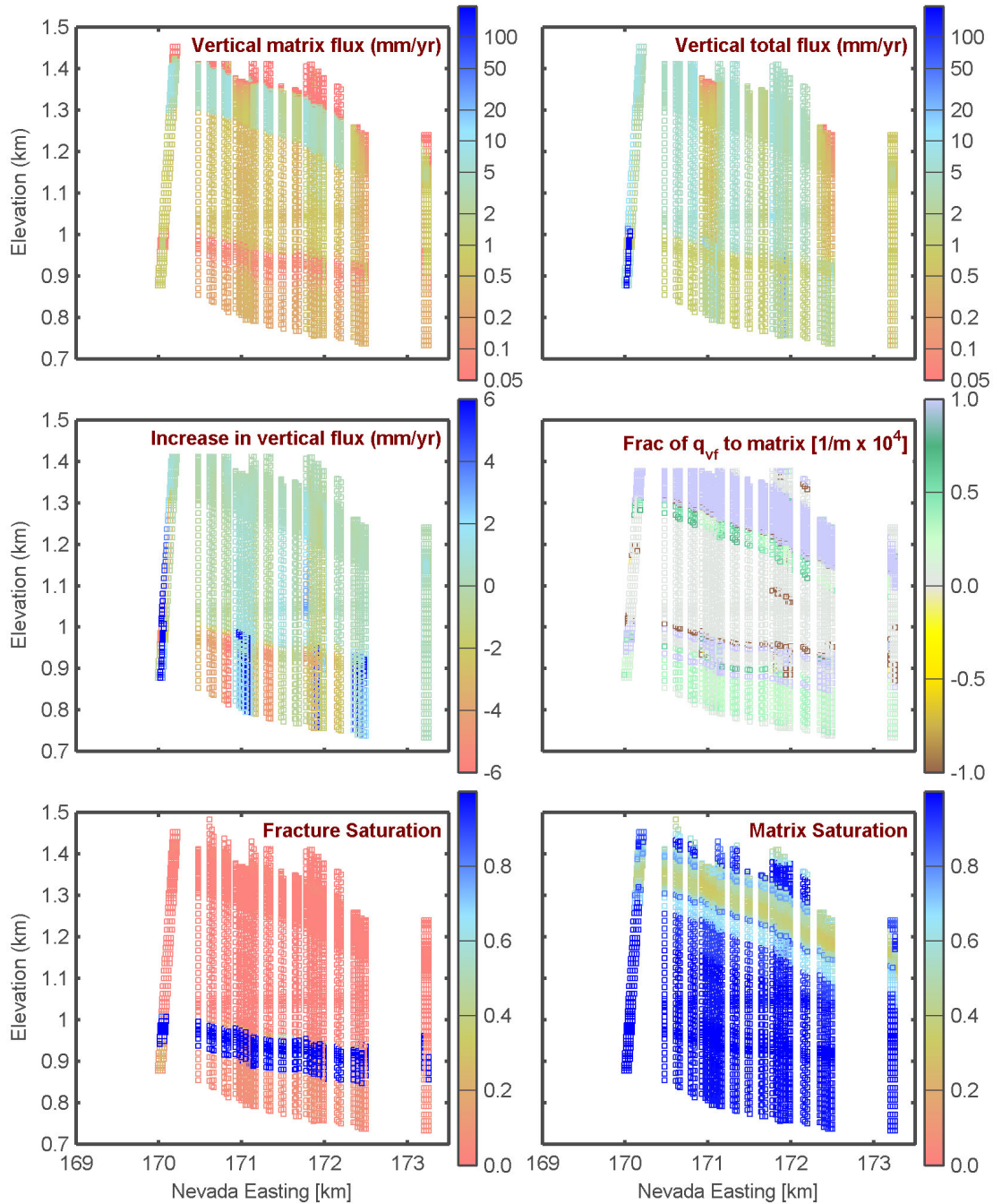
Present-day 10th percentile: Northing 235.8 km

Figure 5-25: Northern east-west cross-section of fluxes and saturations for the 10th percentile boundary condition under the present-day climate.

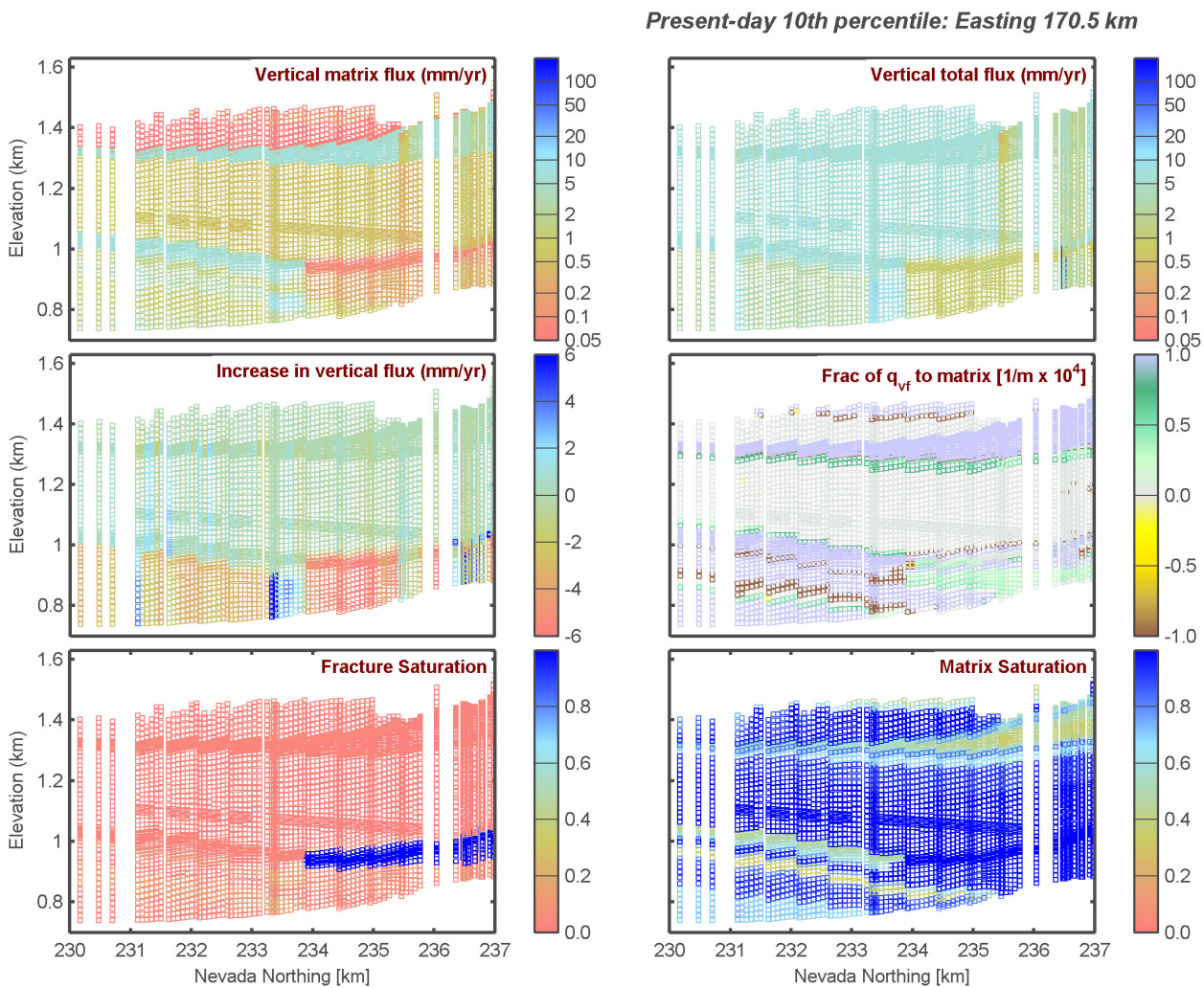


Figure 5-26: Western north-south cross-section of fluxes and saturations for the 10th percentile boundary condition under the present-day climate.

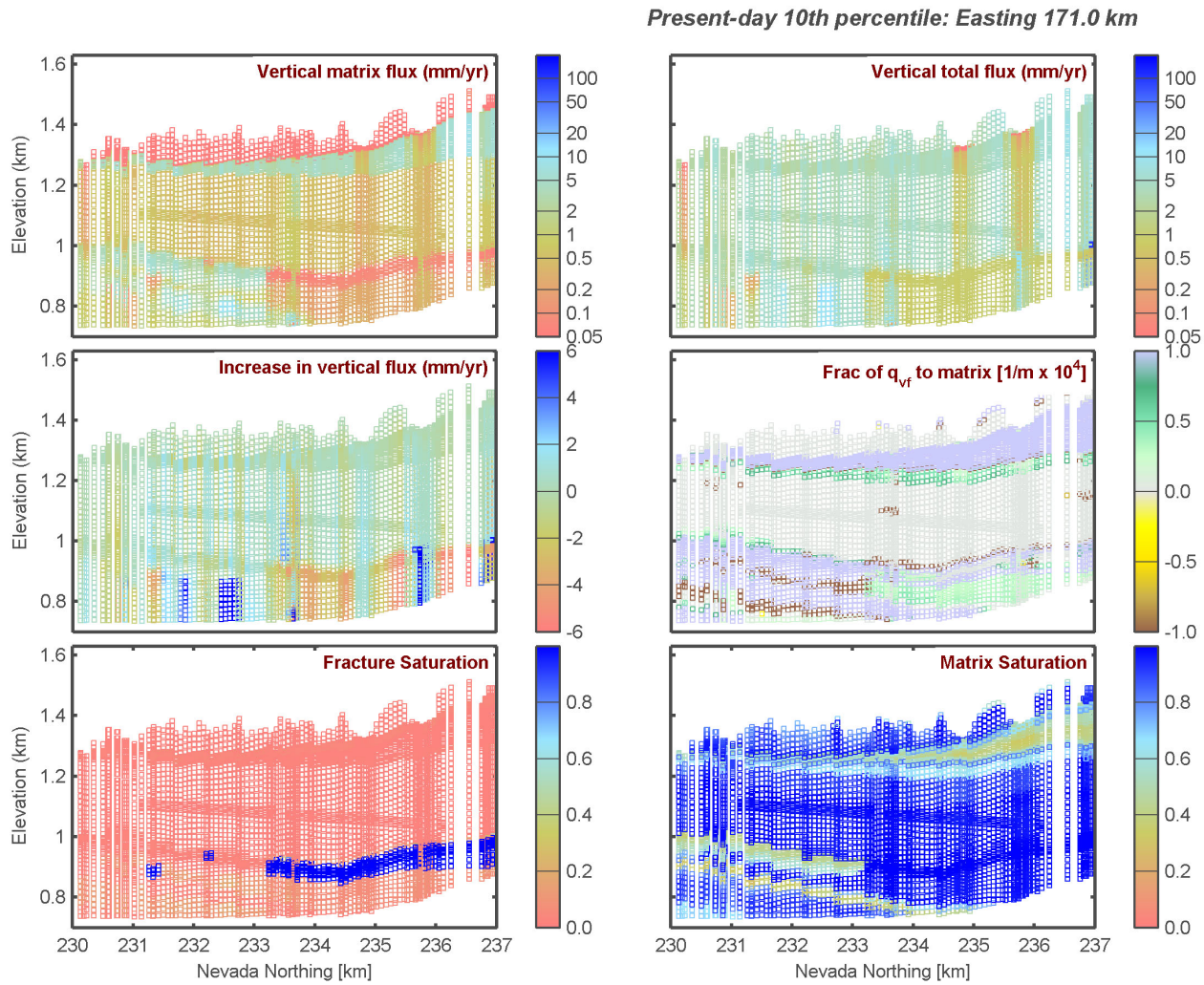


Figure 5-27: Central north-south cross-section of fluxes and saturations for the 10th percentile boundary condition under the present-day climate.

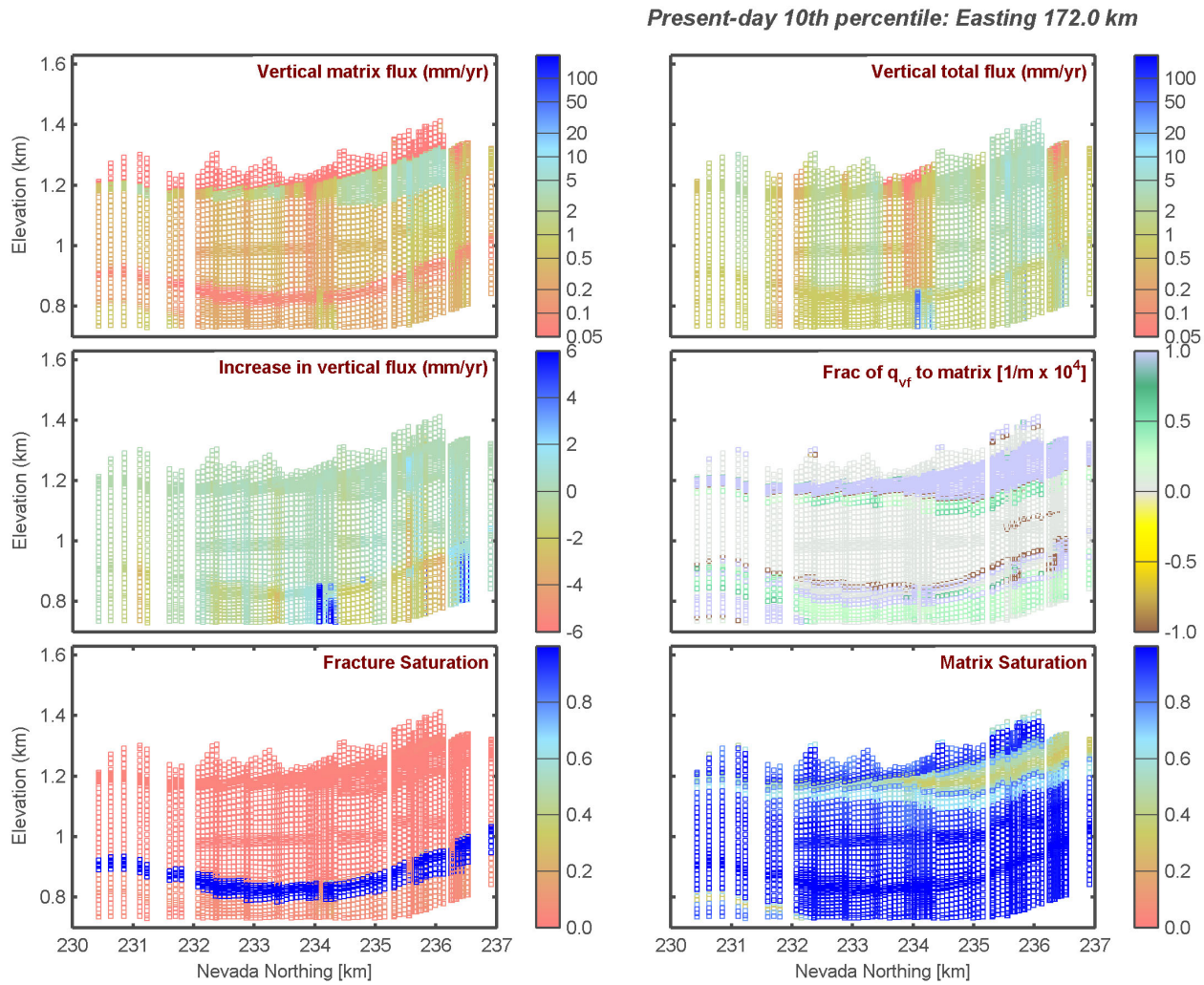


Figure 5-28: Eastern north-south cross-section of fluxes and saturations for the 10th percentile boundary condition under the present-day climate.

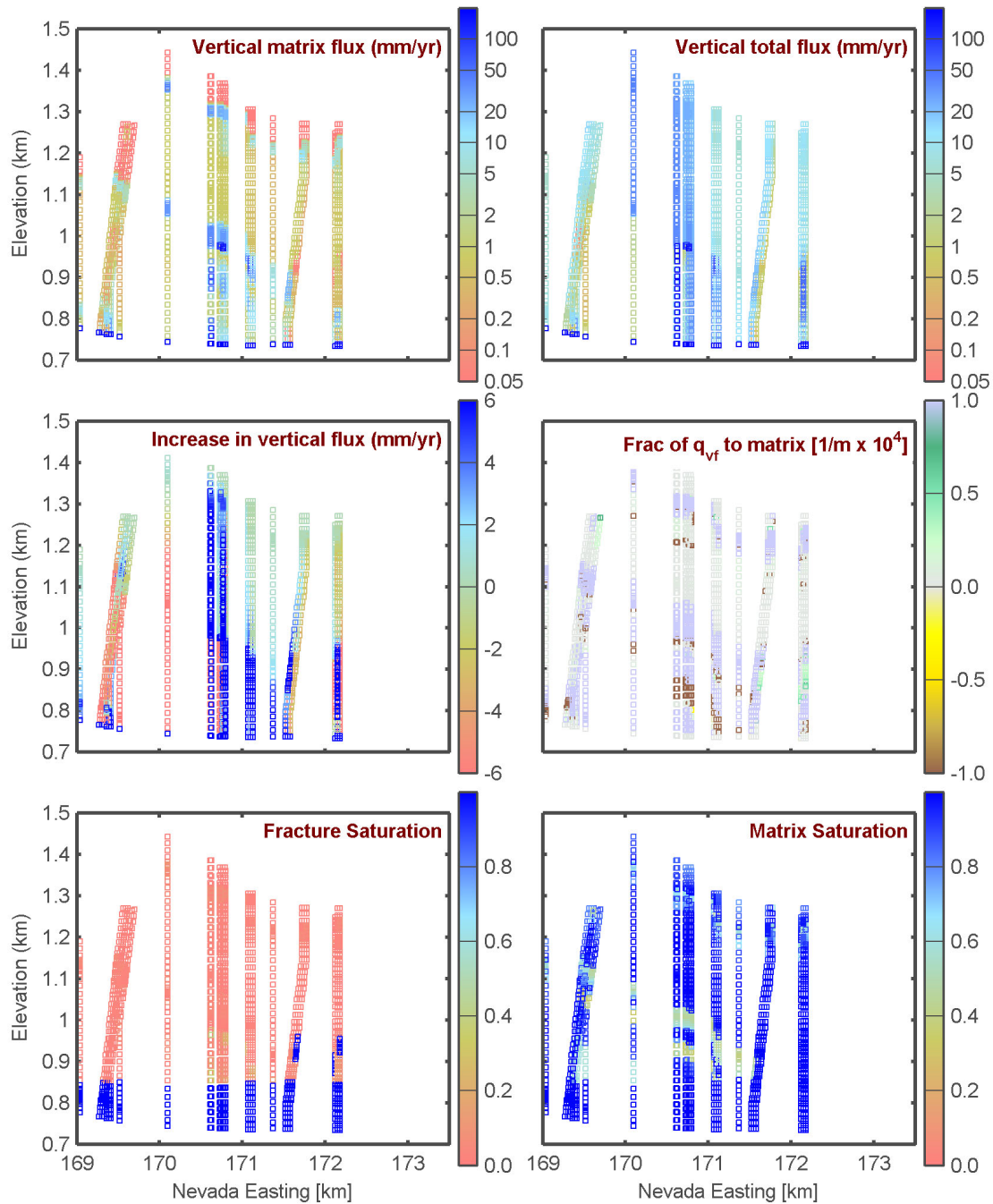
Glacial-transition 30th percentile: Northing 231.0 km

Figure 5-29: Southern east-west cross-section of fluxes and saturations for the 30th percentile boundary condition under the glacial-transition climate.

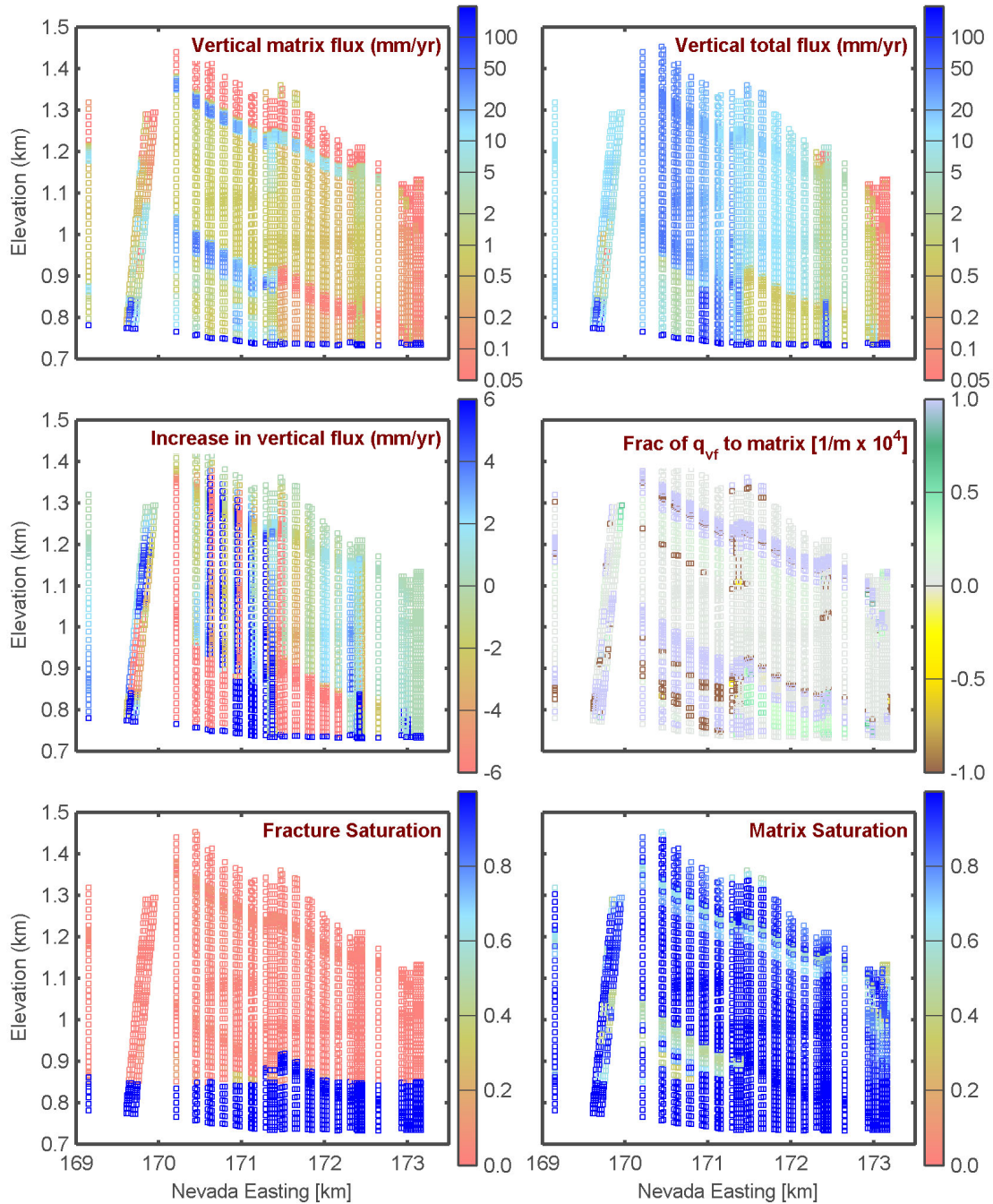
Glacial-transition 30th percentile: Northing 232.6 km

Figure 5-30: South-central east-west cross-section of fluxes and saturations for the 30th percentile boundary condition under the glacial-transition climate.

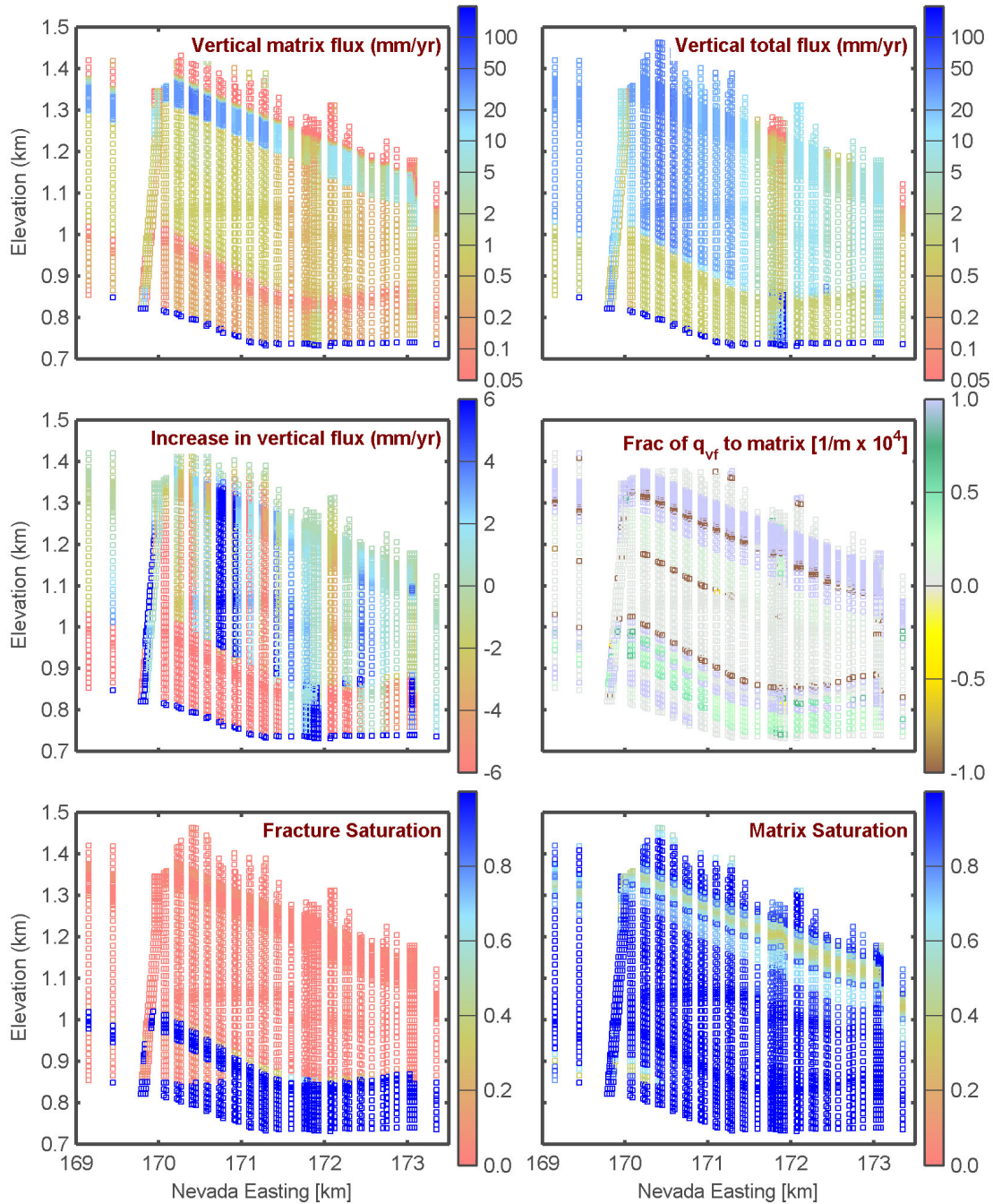
Glacial-transition 30th percentile: Northing 234.4 km

Figure 5-31: North-central east-west cross-section of fluxes and saturations for the 30th percentile boundary condition under the glacial-transition climate.

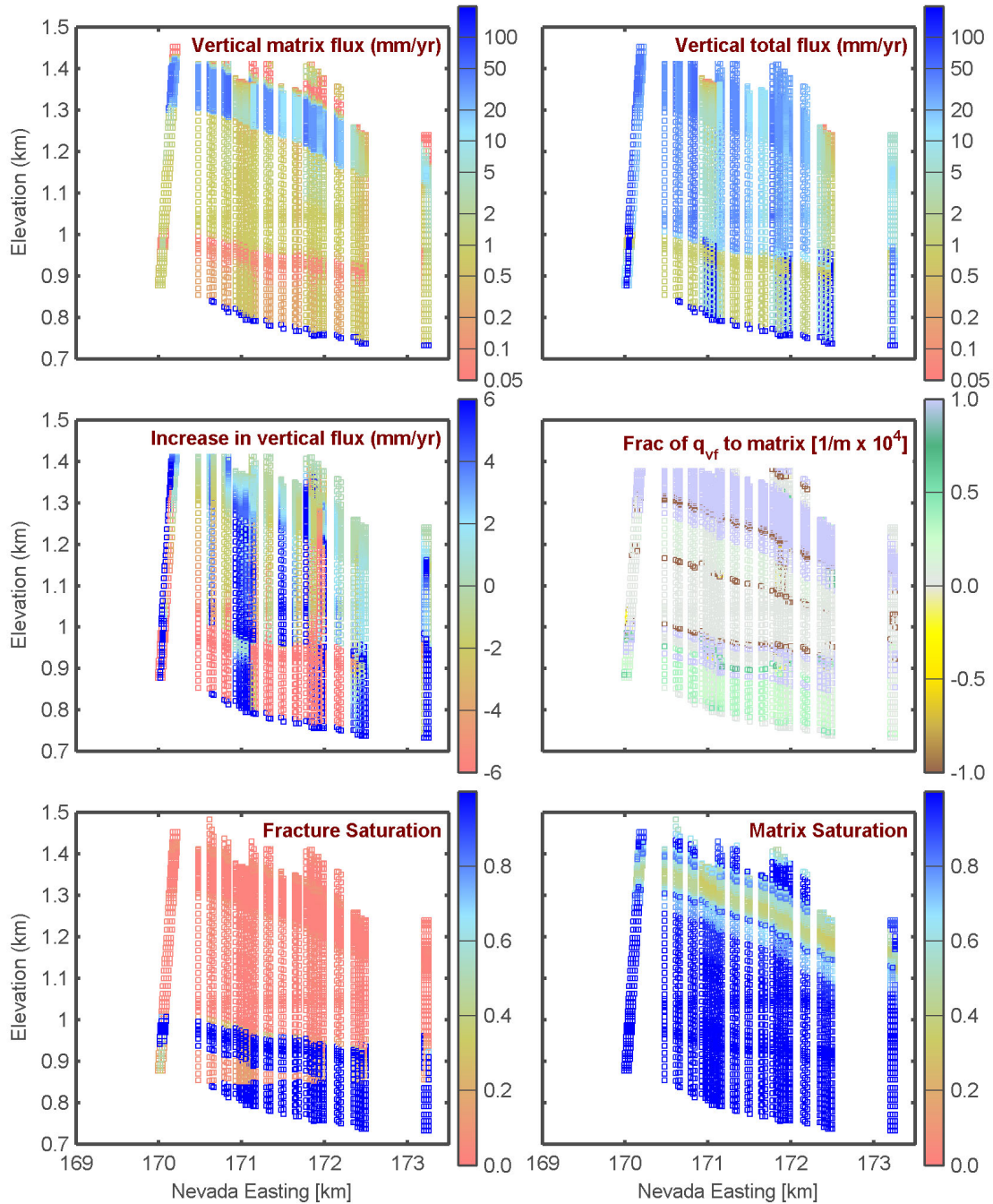
Glacial-transition 30th percentile: Northing 235.8 km

Figure 5-32: Northern east-west cross-section of fluxes and saturations for the 30th percentile boundary condition under the glacial-transition climate.

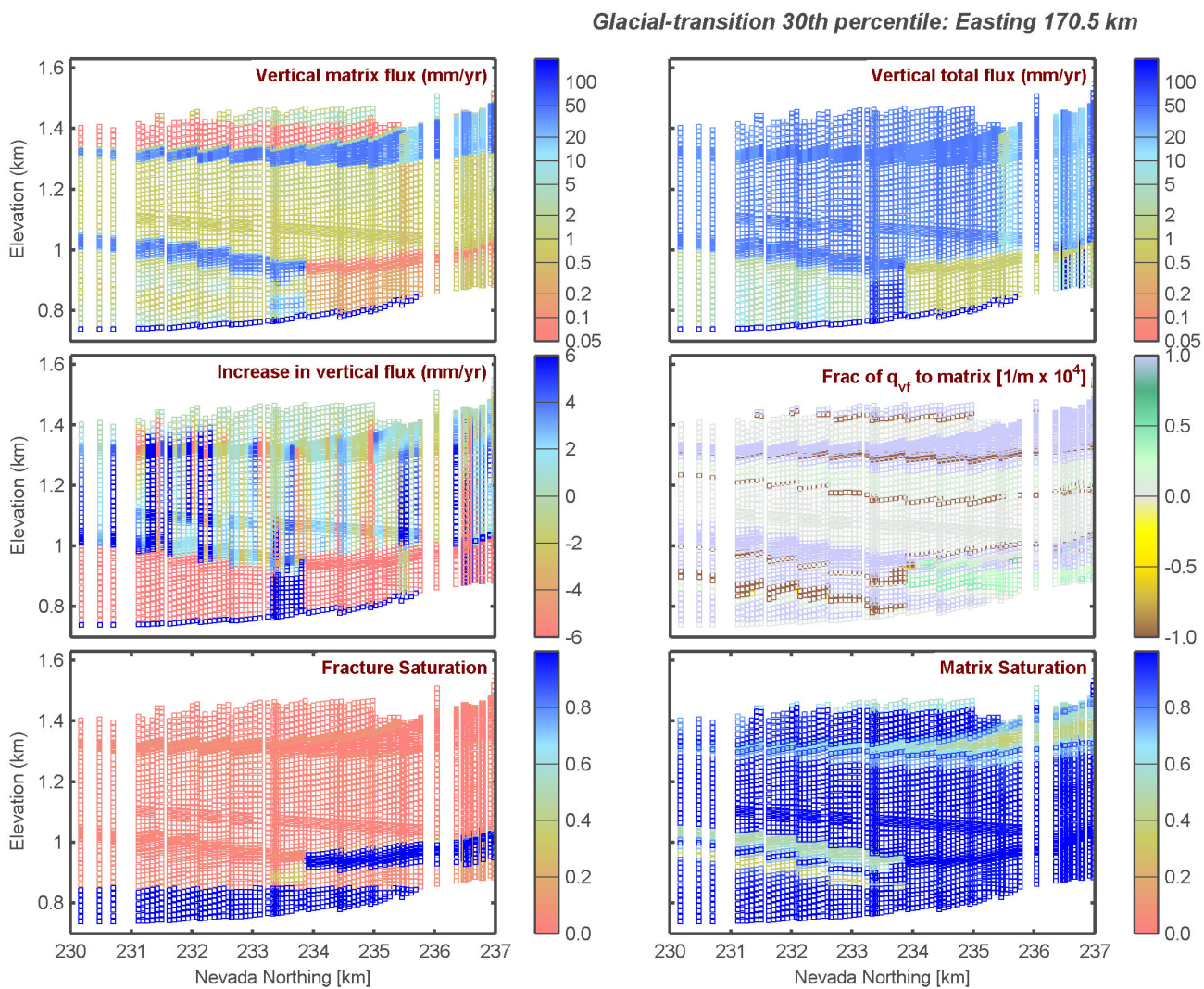


Figure 5-33: Western north-south cross-section of fluxes and saturations for the 30th percentile boundary condition under the glacial-transition climate.

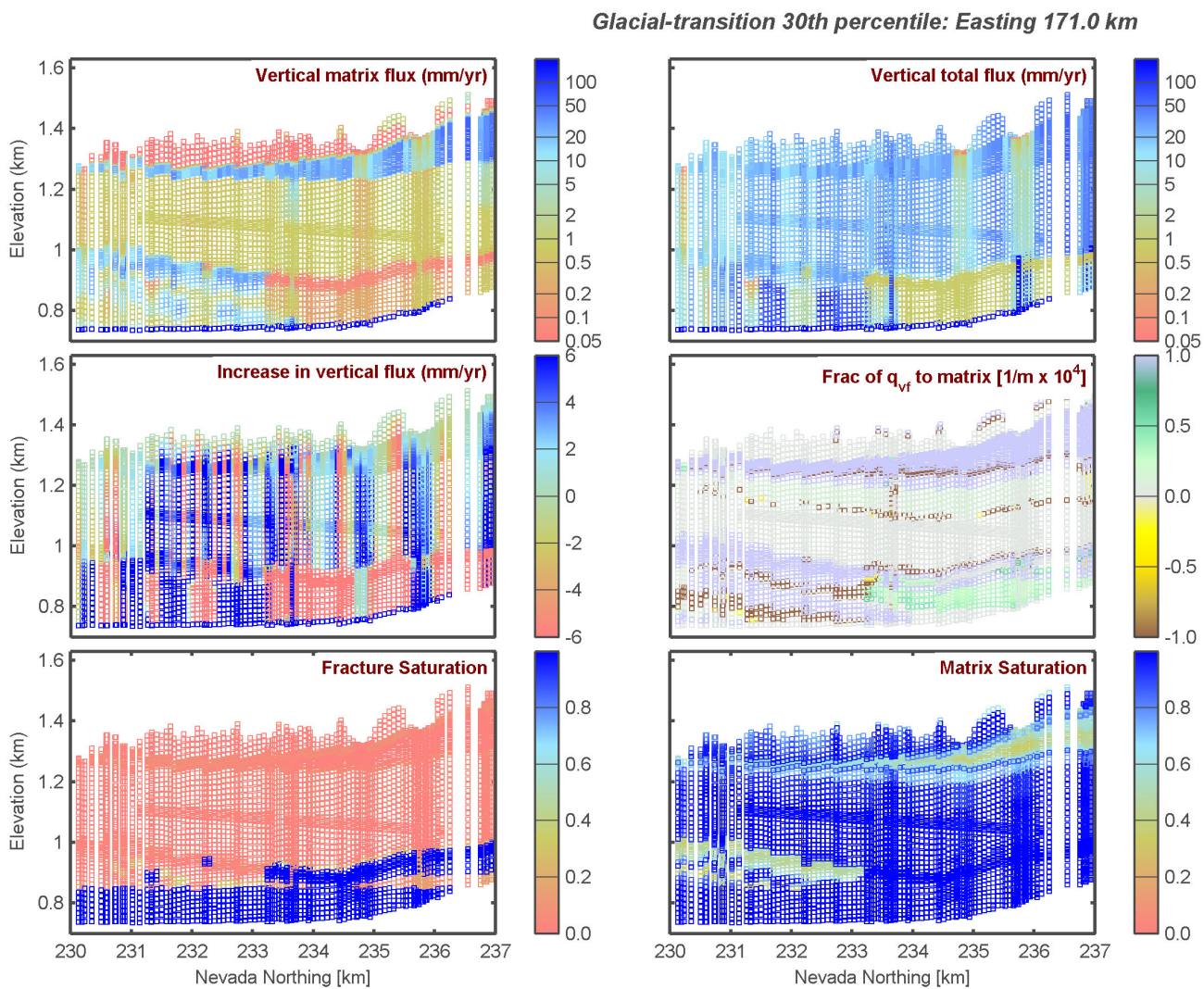


Figure 5-34: Central north-south cross-section of fluxes and saturations for the 30th percentile boundary condition under the glacial-transition climate.

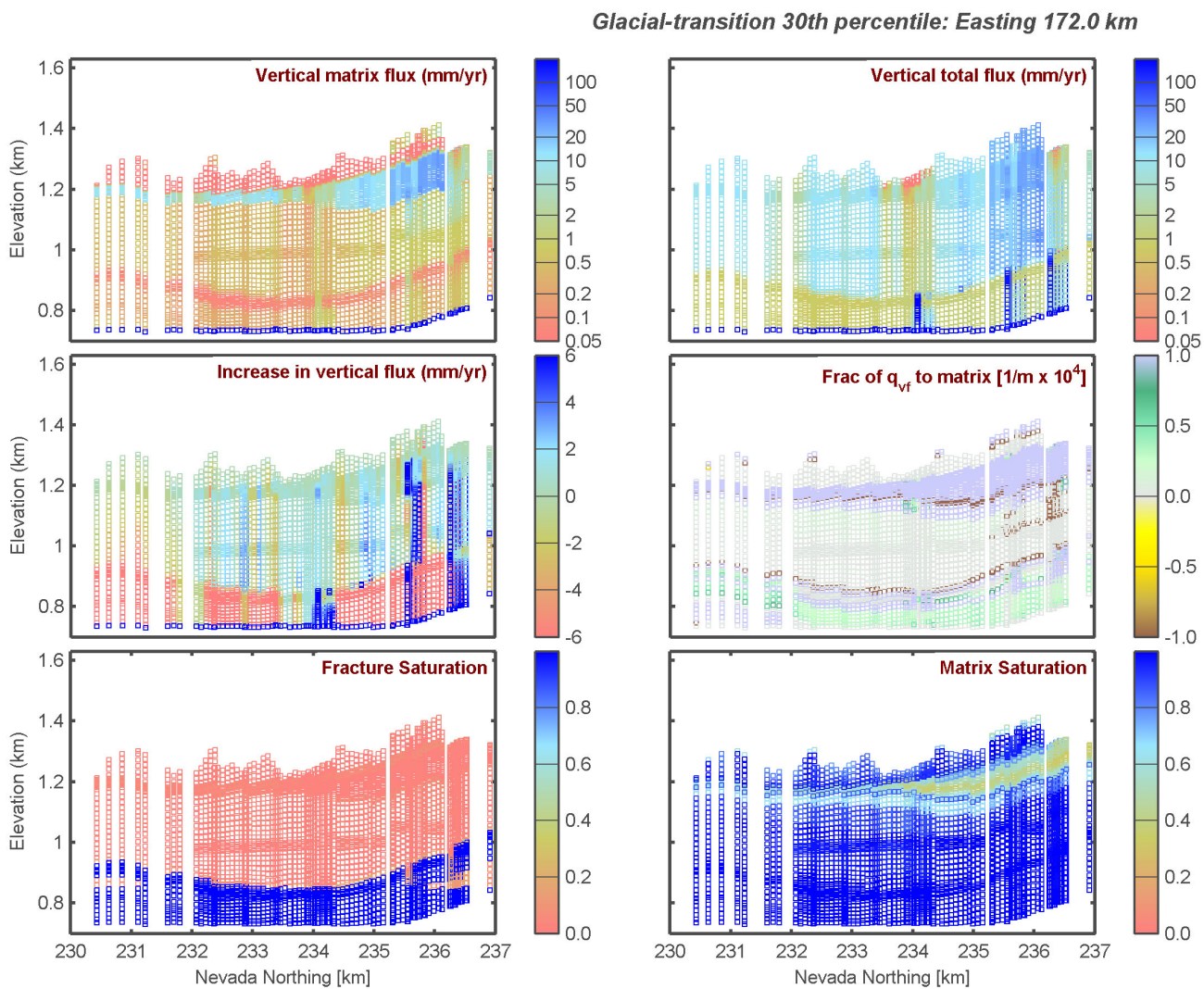
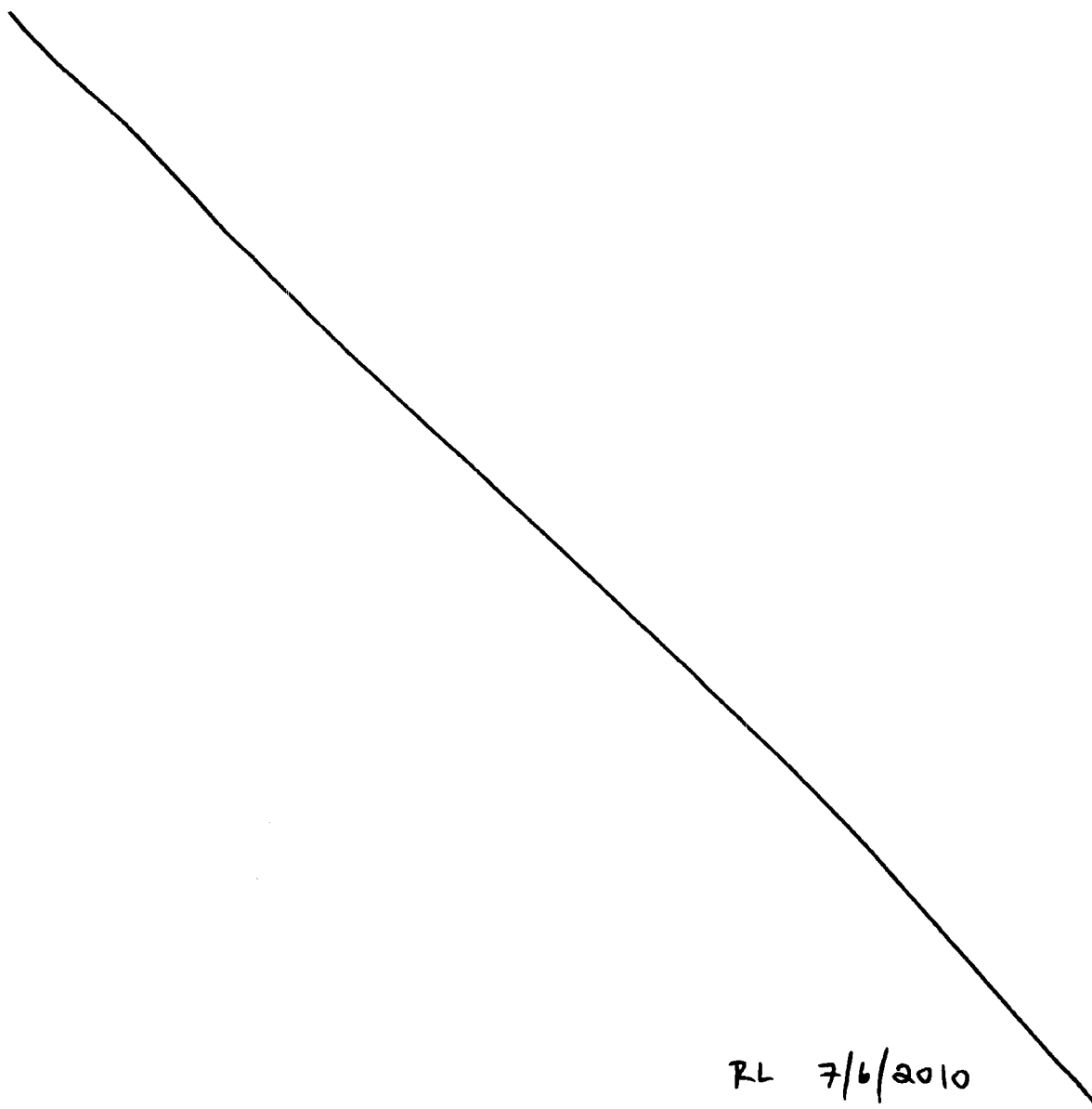


Figure 5-35: Eastern north-south cross-section of fluxes and saturations for the 30th percentile boundary condition under the glacial-transition climate.

Code listing appendix for infiltration, percolation, and seepage**04/21/10 test_DOE_seepratecurve.m.**

The following *Matlab* program is used to calculate the effects of variability on seepage as reported in the entry dated 4/20/10.



RL 7/6/2010

```
1 function test_DOE_seepratecurve(varargin)
2 % test DOE seep rate curve (RAI 3.2.2.1.1-002)
3
4 % coefficient of variation sampling
5
6 %zcase = 'norm';           % normal distribution
7 %zcase = 'lognorm';       % lognormal distribution
8 %zcase = 'bimode';        % bimodal
9
10 ccase = {'bimode' 'norm' 'lognorm'};
11
12 % percolation flux mean
13 % GT MAI [mm/yr] (10/30/50/90 percentile)
14 % from RAI 3.2.2.1.2.1-5-005, Tables 2 & 3
15
16 Pa00 = 10;
17 Pamd = [1.22 2.63 3.62 6.97];
18 cPamd = {'10th' '30th' '50th' '90th'};
19
20 % percolation flux coefficient of variation
21
22 PaCV = [0 0.2 0.5 0.8 2.5];
23 Pasd = sqrt(log(PaCV.^2 + 1));
24
25 nval = 1e6;               % number of samples
26
27 WParea = 5.1 * 5.5;       % WP length * drift diameter (m2)
28 densw = 1000;            % kg/m3
29
30 % plotting options
31
32 xlfsz = 8;
33 xlfwt = 'norm';
34 xlfcl = 0.3 .* [1 1 1];
35
36 for it1 = 1:2:length(varargin)
37     eval([varargin{it1} '= varargin{it1+1};']);
38 end
39 ppargs = {'fonts' xlfsz, 'fontw' xlfwt, 'labcol' xlfcl};
40
41 path('D:\My Files\Matlab\Util', path);
```

```

42
43 fSsc      = 1000 / (WParea * densw);           % kg/WP (mm/m) (WP/m2) (m3/kg) => mm
44
45 nmd       = length(Pamd);
46 nsd       = length(Pasd);
47
48 Par       = randn([nval nsd]);
49 [Pmr,Parv] = deal(randn([nval nsd]));
50
51 [Prmna,Srmna,Srmda] = deal(zeros([nmd nsd]));
52
53 for itC = 1 : length(ccase)
54
55     zcase  = ccase{itC};
56
57     for it0 = 1:nmd
58
59         Pa0    = Pa00 * Pamd(it0);
60
61         switch (zcase)
62         case 'lognorm'
63             for it1 = 1:nsd
64                 Parv(:,it1) = exp(Par(:,it1).*Pasd(it1));
65                 Parv(:,it1) = Pa0 .* Parv(:,it1) ./ mean(Parv(:,it1));
66             end
67         case 'norm'
68             for it1 = 1:nsd
69                 CV        = PaCV(it1);
70                 if (CV > 0.8) CV        = NaN; end
71                 Parv(:,it1) = Par(:,it1) .* (CV * Pa0);
72                 Parv(:,it1) = max(0, Pa0 + Parv(:,it1));
73             end
74         case 'bimode'
75             for it1 = 1:nsd
76                 CV        = PaCV(it1);
77                 if (CV > 0.8) CV        = NaN; end
78                 Parv(:,it1) = sign(Par(:,it1)) .* (CV * Pa0);
79                 Parv(:,it1) = max(0, Pa0 + Parv(:,it1));
80             end
81     end
82     Prmn    = mean(Parv);

```

```

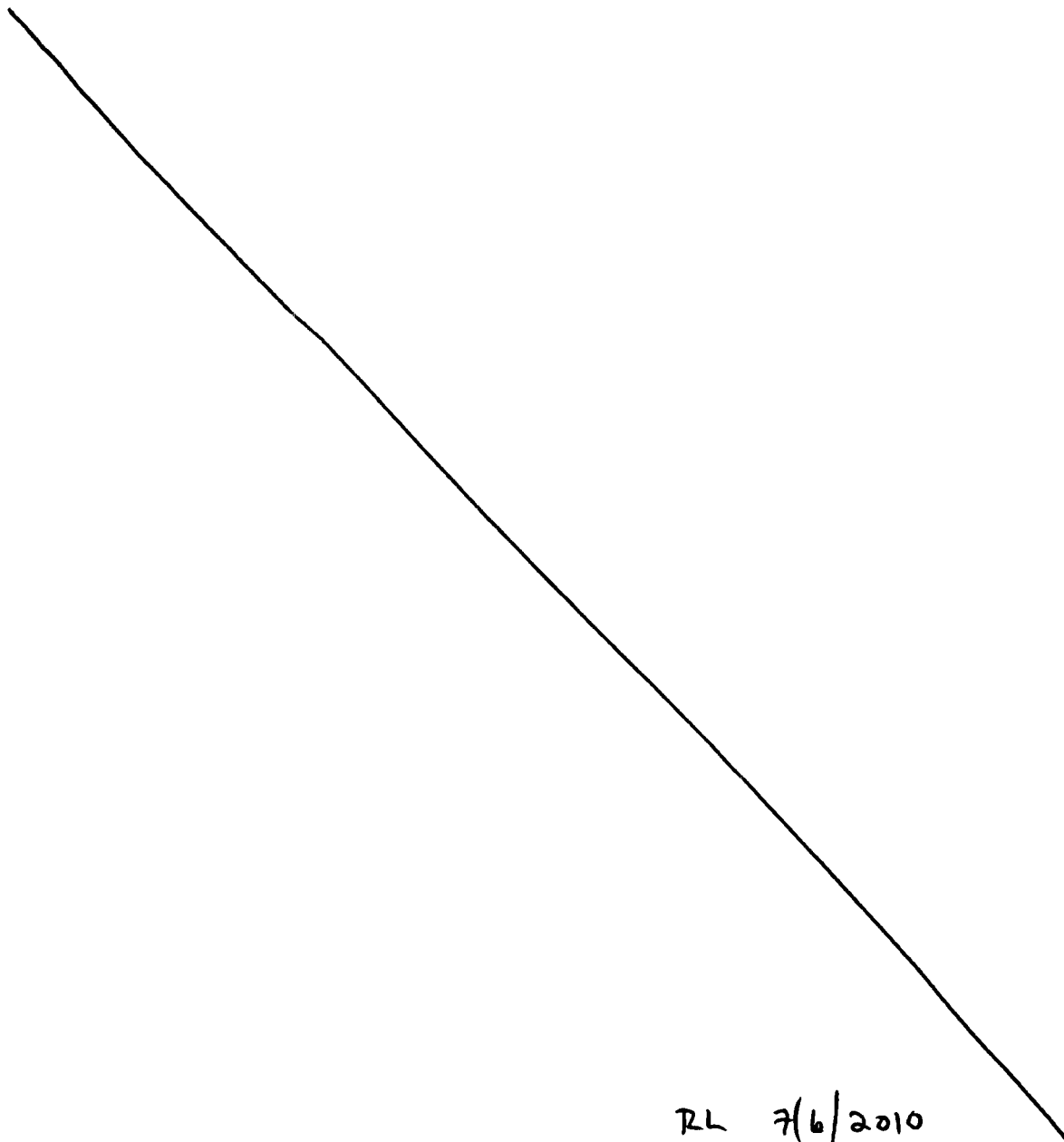
83
84 Sr      = funcrate(Parv);
85 Srmn     = mean(Sr);
86 Srmd     = median(Sr);
87
88 Prmna(it0,:) = Prmn;
89 Srmna(it0,:) = Srmn;
90 Srmna(it0,:) = Srmd;
91
92 end
93
94 vr      = [.2 .2 .3 .3];
95 vG      = [0.6186    0.1569    0.1649    0.0596];
96
97 Crmna    = Srmna ./ Srmna(:,ones([1 size(Srmna,2)]));
98 fprintf('Seepage ratio for sampling case %s\n', zcase);
99 for it1 = 1:nmd
100     fprintf('%s\t', cPamd{it1});
101     fprintf('%.3g', Prmna(it1,1));
102     fprintf('\t%.4g', Crmna(it1,:));      fprintf('\n');
103 end
104 fprintf('%s\t', 'GLUE-wt');
105 fprintf('%.3g', vG * Srmna(:,1));
106 fprintf('\t%.4g', (vG * Srmna) ./ (vG * Srmna(:,1)));  fprintf('\n');
107
108 end      % itC
109
110
111 function [S,Fs] = funcrate(Pa)
112 % rate curve given by RAI 3.2.2.1.1-002, Section 1.2
113
114 H      = ones(size(Pa));
115 H(Pa < 1)      = 0;
116 S      = H .* (0.2 .* exp(-0.003 .* Pa) .* (Pa - 1).^1.69 ...
117             + 28.05 .* (1 - exp(-0.001 .* Pa)) .* Pa);
118
119 Fs      = mean(H);

```

04/23/10 test_massif_precip.m.



The following *Matlab* program is used to calculate sequences of daily precipitation and analyze seasonal characteristics as reported in the entry dated 4/22/10.



RL 7/6/2010

```
1 function test_massif_precip(zop, zclim, varargin)
2 % test seasonal values for precipitation
3
4 if (nargin < 1) zop      = 'nominal';    end
5 if (nargin < 2) zclim    = 'monsoon';    end
6
7 xlfsz  = 8;
8 xlfwt  = 'norm';
9 xlfcl  = 0.3 .* [1 1 1];
10
11 zsim    = 'run';
12 ypr     = ~1;
13
14 zfigdir = 'Figure';
15
16 switch (zop)
17 case 'sample', nsamp    = 100;
18 otherwise,     nsamp    = 1;
19 end
20
21 ny      = 1000;
22 nd      = 365;
23
24 for it1 = 1:2:length(varargin)
25     eval([varargin{it1} '= varargin{it1+1};']);
26 end
27
28 cafter  = {[[] [] [] zfigdir]};
29 ppargs  = {'fonts' xlfsz, 'fontw' xlfwt, 'labcol' xlfcl};
30 d       = 1 : nd;
31 dp      = (2 * pi / nd) .* d;
32
33 path('D:\My Files\Matlab\Util',path);
34
35 switch (zsim)
36
37 % run a simulation
38
39 case 'run'
40
41     switch (zclim)
```



```
42
43 % statistics from SNL (2007), Simulation of Net Infiltration for
44 % Present-Day and Potential Future Climates, Table F-22
45
46     case 'present'
47
48 % nominal
49
50         aP00    = [.934 .027 -1.31];
51         aP10    = [.58 .06 -1.5];
52         aL      = [5.2 .7 2.5];
53         aM      = [.78 .15 2.4];
54
55 % lower bound
56
57         aP00l   = aP00 - [.01 .003 .09];
58         aP10l   = aP10 - [.08 .03 .4];
59         aLl     = aL - [1.2 .2 .7];
60         aMl     = aM - [.28 .04 .4];
61
62 % upper bound
63
64         aP00u   = aP00 + [.01 .003 .09];
65         aP10u   = aP10 + [.07 .04 .4];
66         aLu     = aL + [1.3 .2 .7];
67         aMu     = aM + [.29 .04 .4];
68
69     case 'monsoon'
70
71 % nominal
72
73         aP00    = [.92 .02 2];
74         aP10    = [.58 -.02 1.8];
75         aL      = [6.5 1.6 -1.6];
76         aM      = [.9 .1 -1.48];
77
78 % lower bound
79
80         aP00l   = [.896 -.03 1.74];
81         aP10l   = [.5 -.13 1.4];
82         aLl     = [4 -1.3 -2];
```

```

83         aMl      = [.5 -.3 -1.78];
84
85 % upper bound
86
87         aP00u    = [.944 .07 2.25];
88         aP10u    = [.67 .1 2.3];
89         aLu      = [9 4.5 -1.1];
90         aMu      = [1.3 .5 -1.17];
91
92         case 'glacial'
93
94 % nominal
95
96         aP00     = [.84 .066 -1.12];
97         aP10     = [.54 .07 -.93];
98         aL       = [3.8 .6 NaN];
99         aM       = [.7 .12 NaN];
100
101 % lower bound
102
103         aP00l    = [.74 .028 -1.22];
104         aP10l    = [.47 .02 -.93-.84];
105         aLl      = [3.1 .1 -pi];
106         aMl      = [.48 .08 -pi];
107
108 % upper bound
109
110         aP00u    = [.89 .104 -1.02];
111         aP10u    = [.62 .11 -.93+.84];
112         aLu      = [4.5 1 pi];
113         aMu      = [.92 .16 pi];
114
115     end
116
117     Pdy      = zeros([nsamp nd]);
118
119     fn       = {'aP00l' 'aP10l' 'aLl' 'aMl' 'aP00u' 'aP10u' 'aLu' 'aMu'};
120     for it1 = 1:length(fn)
121         Ssamp.(fn{it1}) = eval(fn{it1});
122     end
123     [Ssamp.aP00,Ssamp.aP10,Ssamp.aL,Ssamp.aM]      = deal(zeros([nsamp 3]));

```

```

124
125     for it0 = 1:nsamp
126
127         switch (zop)
128         case 'nominal'
129         case 'lower'
130             aP00 = aP00l;      aP10 = aP10l;
131             aL = aLl;  aM = aMl;
132         case 'lower'
133             aP00 = aP00u;      aP10 = aP10u;
134             aL = aLu;  aM = aMu;
135         case 'sample'
136             f = rand([1 12]);
137             aP00 = aP00l + f(0+[1:3]) .* (aP00u - aP00l);
138             aP10 = aP10l + f(3+[1:3]) .* (aP10u - aP10l);
139             aL = aLl + f(6+[1:3]) .* (aLu - aLl);
140             aM = aMl + f(9+[1:3]) .* (aMu - aMl);
141         end
142
143         P00d = max(0, min(1, aP00(1) + aP00(2).*sin(aP00(3) + dp)));
144         P10d = max(0, min(1, aP10(1) + aP10(2).*sin(aP10(3) + dp)));
145         Ld = aL(1) + aL(2).*sin(aL(3) + dp);
146         Md = aM(1) + aM(2).*sin(aM(3) + dp);
147         for it1 = 1:10
148             if (any(log(Ld) <= Md))
149                 aL = aLl + rand([1 3]) .* (aLu - aLl);
150                 aM = aMl + rand([1 3]) .* (aMu - aMl);
151                 Ld = aL(1) + aL(2).*sin(aL(3) + dp);
152                 Md = aM(1) + aM(2).*sin(aM(3) + dp);
153             end
154         end
155
156         Ssamp.aP00(it0,:) = aP00;
157         Ssamp.aP10(it0,:) = aP10;
158         Ssamp.aL(it0,:) = aL;
159         Ssamp.aM(it0,:) = aM;
160
161         Sd = sqrt(2 .* (log(Ld) - Md));
162
163         Pw = 1 - P10d ./ (1 - P00d + P10d);
164

```

```

165     [yw1,P1]      = deal(zeros([1 ny]));
166
167     for it1 = 1:ny
168         R          = rand([1 nd]);
169         Pd          = P_invexp(Md, Sd, rand([1 nd]));
170         Pdi         = ones(size(Pd));
171         if (R(1) > Pw(1))      Pdi(1) = 0;      end;
172
173         yw1(it1)      = ~Pdi(1);
174         P1(it1) = Pd(1);
175
176         for it2 = 2 : nd
177             if (Pdi(it2 - 1) == 0)
178                 if (R(it2) < P00d(it2)) Pdi(it2)      = 0;      end
179             else
180                 if (R(it2) < P10d(it2)) Pdi(it2)      = 0;      end
181             end
182         end
183
184         Pdy(it0,:)      = Pdy(it0,:) + Pd .* Pdi;
185
186     end
187
188     end      % it0
189
190     Pdy      = Pdy .* (1/ny);
191
192     julm      = cumsum([0 31 28 31 30 31 30 31 31 30 31 30 31]);
193     imon      = d;
194     for it1 = 12 : -1 : 1
195         imon(julm(it1) < d & d < julm(it1+1))      = it1;
196     end
197
198     Pmy      = zeros([size(Pdy,1) 12]);
199     for it1 = 1:12
200         Pmy(:,it1)      = sum(Pdy(:,imon == it1), 2);
201     end
202
203     Pmy(imag(Pmy(:)) ~= 0)      = NaN;
204
205     zf      = sprintf('%s_%d', zclim, nsamp);

```

```

206 %      save(zf, 'Pdy', 'Pmy', 'imon', 'Ssamp');
207      save(zf, 'Pmy', 'imon', 'Ssamp');
208
209 case 'load'
210     zf      = sprintf('%s_%d', zclim, nsamp);
211     S      = load(zf);
212     fn      = fieldnames(S);
213     for it1 = 1:length(fn)
214         eval([fn{it1} '= S.(fn{it1});']);
215     end
216 end
217
218 imo      = 1 : 12;
219 mPmy     = mean(Pmy,1);
220 sPmy     = std(Pmy,1);
221 vPmy     = [mPmy-sPmy; mPmy; mPmy+sPmy];
222
223 if (0)
224     figure(1)
225     plot(imo, mPmy, 'o', imo([1 1],:), vPmy([1 3],:), '-');
226 %      bar([mPmy-sPmy; mPmy; mPmy+sPmy]')
227     fprintf('MAP = %.1f\n', sum(mean(Pmy,1)));
228 end
229
230 if (0)
231
232     figure(gcf)
233     clf
234
235     drive_plot('set_paper_size', 'halpage');
236     drive_plot('set_screen_to_paper_size');
237
238     nmap   = 32;
239     cmap   = jet(nmap) .* 0.3 + (1 - 0.3);
240     MAP    = sum(Pmy,2);
241     vMAP   = [min(MAP) max(MAP)];
242     vi     = linspace(vMAP(2), vMAP(1), nmap)';
243     vmap   = interp1(vi, cmap, MAP);
244
245     c      = {
246         vPmy(2,:)      3.5      0.4 .* [1 1 1]      'Mean'

```

```

247         vPmy(1,:)      2.5      0.7 .* [1 .5 .5]      'Mean-Std'
248         vPmy(3,:)      2.5      0.7 .* [.5 .5 1]      'Mean+Std'
249     };
250
251     for it1 = 1:nsamp
252         lw      = 0.5;
253         if (any(MAP(it1) == vMAP))      lw      = 1.5; end
254         plot(imo, Pmy(it1,:), '- ', 'color', vmap(it1,:), 'linewidth', lw);
255         hold on
256     end
257 %     plot(imo, mPmy, 'o', imo([1 1],:), vPmy([1 3],:), '- ');
258
259     for it1 = 1:size(c,1)
260         plot(imo, c{it1,1}, '- ', 'linewidth', c{it1,2}, 'color', c{it1,3});
261     end
262 %     plot(imo, vPmy(2,:), '- ', 'linewidth', 3.5, 'color', 0.4 .* [1 1 1]);
263 %     plot(imo, vPmy(1,:), '- ', 'linewidth', 2.5, 'color', 0.7 .* [1 .5 .5]);
264 %     plot(imo, vPmy(3,:), '- ', 'linewidth', 2.5, 'color', 0.7 .* [.5 .5 1]);
265     set(gca, 'xlim', [0.5 12.5], 'xtick', imo, ...
266         'xtickl', {'J' 'F' 'M' 'A' 'M' 'J' 'J' 'A' 'S' 'O' 'N' 'D'}, ...
267         'yminortick', 'on');
268
269     drive_plot('pretty_plot', 'Month', 'Precipitation [mm]', ppargs{:});
270
271     drive_plot('legend_axis', 'make');
272
273     xl      = 0.04 + [0 0.04 0.07];
274     yl      = 0.94;
275     dyl     = -0.06;
276     for it1 = 1:size(c,1)
277         plot(xl(1:2), yl([1 1]), '- ', 'linewidth', c{it1,2}, 'color', c{it1,3});
278         hold on
279         text(xl(3), yl, c{it1,4}, 'color', xlfcl);
280         yl      = yl + dyl;
281     end
282
283     switch (zclim)
284     case 'present', z      = 'Interstadial';
285     case 'monsoon', z      = 'Monsoon';
286     case 'glacial', z      = 'Glacial Transition';
287     end

```



```

288     text(0.95, 0.94, z, 'color', xlfcl, 'horiz', 'r', 'fontw', 'b', 'fonta', 'obl');
289
290     zf      = sprintf('hairsP_%s%g', zclim(1:3), nsamp);
291     drive_plot('after_plot', ypr, zf, cafter{:});
292
293 end
294
295 if (0)
296
297     figure(gcf)
298     clf
299
300     drive_plot('set_paper_size', 'halfpage');
301     drive_plot('set_screen_to_paper_size');
302
303     nmap    = 32;
304     cmap    = jet(nmap) .* 0.3 + (1 - 0.3);
305     MAP     = sum(Pmy,2);
306     Fmy     = Pmy ./ MAP(:,ones([1 12])));
307
308     mFmy    = mean(Fmy,1);
309     sFmy    = std(Fmy,1);
310     vFmy    = [mFmy-sFmy; mFmy; mFmy+sFmy];
311
312     vMAP    = [min(MAP) max(MAP)];
313     vi      = linspace(vMAP(2), vMAP(1), nmap)';
314     vmap    = interp1(vi, cmap, MAP);
315
316     c      = {
317         vFmy(2,:)      3.5      0.4 .* [1 1 1]      'Mean'
318         vFmy(1,:)      2.5      0.7 .* [1 .5 .5]    'Mean-Std'
319         vFmy(3,:)      2.5      0.7 .* [.5 .5 1]    'Mean+Std'
320     };
321
322     for it1 = 1:nsamp
323         lw      = 0.5;
324         if (any(MAP(it1) == vMAP))      lw      = 1.5; end
325         plot(imo, Fmy(it1,:), '-','color', vmap(it1,:), 'linewidth', lw);
326         hold on
327     end
328 %     plot(imo, mPmy, 'o', imo([1 1],:), vPmy([1 3],:), '-');

```

```

329
330     for it1 = 1:size(c,1)
331         plot(imo, c{it1,1}, '-', 'linewidth', c{it1,2}, 'color', c{it1,3});
332     end
333 %     plot(imo, vPmy(2,:), '-', 'linewidth', 3.5, 'color', 0.4 .* [1 1 1]);
334 %     plot(imo, vPmy(1,:), '-', 'linewidth', 2.5, 'color', 0.7 .* [1 .5 .5]);
335 %     plot(imo, vPmy(3,:), '-', 'linewidth', 2.5, 'color', 0.7 .* [.5 .5 1]);
336     set(gca, 'xlim', [0.5 12.5], 'xtick', imo, ...
337         'xtickl', {'J' 'F' 'M' 'A' 'M' 'J' 'J' 'A' 'S' 'O' 'N' 'D'}, ...
338         'yminortick', 'on');
339
340     drive_plot('pretty_plot', 'Month', 'Precipitation Fraction', ppargs{:});
341
342     drive_plot('legend_axis', 'make');
343
344     xl      = 0.04 + [0 0.04 0.07];
345     yl      = 0.94;
346     dyl     = -0.06;
347     for it1 = 1:size(c,1)
348         plot(xl(1:2), yl([1 1]), '-', 'linewidth', c{it1,2}, 'color', c{it1,3});
349         hold on
350         text(xl(3), yl, c{it1,4}, 'color', xlfcl);
351         yl      = yl + dyl;
352     end
353
354     switch (zclim)
355     case 'present', z      = 'Interstadial';
356     case 'monsoon', z      = 'Monsoon';
357     case 'glacial', z      = 'Glacial Transition';
358     end
359     text(0.95, 0.94, z, 'color', xlfcl, 'horiz', 'r', 'fontw', 'b', 'fonta', 'obl');
360
361     zf      = sprintf('hairsF_%s%g', zclim(1:3), nsamp);
362     drive_plot('after_plot', ypr, zf, cafter{:});
363
364 end
365
366 % total precipitation
367
368 if (1)
369 %     figure(3)

```

```

370     figure(gcf)
371     clf
372     drive_plot('set_paper_size', 'halfpage');
373     drive_plot('set_screen_to_paper_size');
374
375     c      = {
376             sort(sum(Pmy(:,[1:3 11:12]),2)) 1.5      [0 0 1]      'Nov - Mar'
377             sort(sum(Pmy(:,[6:9]),2))      1.5      [0.7 0 0]    'Jun - Sep'
378             sort(sum(Pmy(:,2),2))          1.5      0.4.*[1 1 1]  'Annual'
379     };
380
381     vcdf    = linspace(0,1,nsamp);
382     ylim    = [-0.05 1.05];
383     vim     = zeros([1 size(c,1)]);
384     for it1 = 1 : size(c,1)
385         v      = c{it1,1};
386         plot(v, vcdf, '-','linewidth', c{it1,2}, 'color', c{it1,3});
387         hold on
388         vm     = mean(v);
389         vi     = interp1(v, vcdf, vm);
390         vim(it1) = mean(vi);
391         plot(vm, vi, 'o', 'linewidth', c{it1,2}, ...
392             'markeredgecolor', c{it1,3}, ...
393             'markerfacecolor', c{it1,3}.*0.3 + [1 1 1].*(1-0.3));
394         plot(vm+[0 0], ylim(1)+[0 0.03].*diff(ylim), '-',' ...
395             'linewidth', c{it1,2}, 'color', c{it1,3});
396         plot(vm+[0 0], ylim(1)+[0 0.03].*diff(ylim), '-',' ...
397             'linewidth', 2.5, 'color', c{it1,3});
398
399         fprintf('%s:\t%.1f\t%.1f\t%.1f\n', c{it1,4}, vm, min(v), max(v));
400     end
401     set(gca, 'ylim', ylim, 'xminortick', 'on');
402     xlim    = get(gca, 'xlim');
403     for it1 = 1 : size(c,1)
404         plot(xlim(1)+[0 0.03].*diff(xlim), vim(it1)+[0 0], '-',' ...
405             'linewidth', 2.5, 'color', c{it1,3});
406     end
407     drive_plot('pretty_plot', 'Precipitation [mm]', 'Cumulative Frequency', ppargs{:});
408
409     drive_plot('legend_axis', 'make');
410

```

```

411     xl      = 0.78 + [0 0.04 0.07];
412     yl      = 0.16;
413     dyl     = 0.06;
414     for it1 = 1:size(c,1)
415         plot(xl(1:2), yl([1 1]), '-','linewidth', c{it1,2}, 'color', c{it1,3});
416         hold on
417         text(xl(3), yl, c{it1,4}, 'color', xlfcl);
418         yl    = yl + dyl;
419     end
420
421     switch (zclim)
422     case 'present', z      = 'Interstadial';
423     case 'monsoon', z      = 'Monsoon';
424     case 'glacial', z      = 'Glacial Transition';
425     end
426     text(0.95, 0.06, z, 'color', xlfcl, 'horiz', 'r', 'fontw', 'b', 'fonta', 'obl');
427
428     zf      = sprintf('WScdf_%s%g', zclim(1:3), nsamp);
429     drive_plot('after_plot', ypr, zf, cafter{:});
430
431 end
432
433 % annual fraction
434
435 if (0)
436 %     figure(3)
437     figure(gcf)
438     clf
439     drive_plot('set_paper_size', 'halfpage');
440     drive_plot('set_screen_to_paper_size');
441
442     va      = sum(Pmy(:, :), 2);
443     c      = {
444         sort(sum(Pmy(:, [1:3 11:12])), 2) ./ va      1.5      [0 0 1]      'Nov - Mar'
445         sort(sum(Pmy(:, [6:9])), 2) ./ va      1.5      [0.7 0 0]      'Jun - Sep'
446     };
447
448     vcdf    = linspace(0, 1, nsamp);
449     ylim    = [-0.05 1.05];
450     for it1 = 1 : size(c, 1)
451         v    = c{it1, 1};

```

```

452         plot(v, vcdf, '-', 'linewidth', c{it1,2}, 'color', c{it1,3});
453         hold on
454         vm      = mean(v);
455         plot(vm, interp1(v, vcdf, vm), 'o', 'linewidth', c{it1,2}, ...
456             'markeredgecolor', c{it1,3}, ...
457             'markerfacecolor', c{it1,3}.*0.3 + [1 1 1].*(1-0.3));
458         plot(vm+[0 0], ylim(1)+[0 0.03].*diff(ylim), '-', ...
459             'linewidth', c{it1,2}, 'color', c{it1,3});
460     end
461     set(gca, 'ylim', ylim, 'xminortick', 'on');
462     drive_plot('pretty_plot', 'Precipitation [mm]', 'Cumulative Frequency', ppargs{:});
463
464     drive_plot('legend_axis', 'make');
465
466     xl      = 0.78 + [0 0.04 0.07];
467     yl      = 0.16;
468     dyl     = 0.06;
469     for it1 = 1:size(c,1)
470         plot(xl(1:2), yl([1 1]), '-', 'linewidth', c{it1,2}, 'color', c{it1,3});
471         hold on
472         text(xl(3), yl, c{it1,4}, 'color', xlfcl);
473         yl    = yl + dyl;
474     end
475
476     switch (zclim)
477     case 'present', z      = 'Interstadial';
478     case 'monsoon', z      = 'Monsoon';
479     case 'glacial', z      = 'Glacial Transition';
480     end
481     text(0.95, 0.06, z, 'color', xlfcl, 'horiz', 'r', 'fontw', 'b', 'fonta', 'obl');
482
483     zf      = sprintf('WSfcd_f_%s%g', zclim(1:3), nsamp);
484     drive_plot('after_plot', ypr, zf, cafter{:});
485
486 end
487
488 if (0)
489 %     figure(3)
490     figure(gcf)
491     clf
492     drive_plot('set_paper_size', 'halpage');

```

```

493     drive_plot('set_screen_to_paper_size');
494
495     va      = sum(Pmy(:, :), 2);
496     vw      = sum(Pmy(:, [1:3 11:12]), 2);
497     vs      = sum(Pmy(:, [6:9]), 2);
498     c      = {
499         [va vw] 2.5      [0 0 1]      'Nov - Mar'
500         [va vs] 2.5      [0.7 0 0]    'Jun - Sep'
501         [vw vs] 2.5      [0.7 0.7 0]  'Win/Sum'
502     };
503
504     % vcdf = linspace(0,1,nsamp);
505     % ylim = [-0.05 1.05];
506     % vam  = mean(va);
507     i1     = 1:5:nsamp;
508     for it1 = 1 : size(c,1)
509         v      = c{it1,1};
510         plot(v(i1,1), v(i1,2), '.', 'linew', c{it1,2}, 'color', c{it1,3});
511         hold on
512     end
513     set(gca, 'xminortick', 'on', 'yminortick', 'on');
514     if (1)
515         set(gca, 'xsc', 'lo', 'ysc', 'lo');
516         clim = get(gca, {'xlim' 'ylim'});
517         xlim = clim{1};      ylim = clim{2};
518         xmr  = exp(log(xlim(1)) + [0 0.03].*diff(log(xlim)));
519         ymr  = exp(log(ylim(1)) + [0 0.03].*diff(log(ylim)));
520     else
521         clim = get(gca, {'xlim' 'ylim'});
522         xlim = clim{1};      ylim = clim{2};
523         xmr  = xlim(1) + [0 0.03].*diff(xlim);
524         ymr  = ylim(1) + [0 0.03].*diff(ylim);
525     end
526     for it1 = 1 : size(c,1)
527         vm      = mean(c{it1,1});
528         plot(vm(1), vm(2), 'o', 'linew', c{it1,2}, ...
529             'markersize', 10, ...
530             'markeredgecolor', c{it1,3}.*0.5 + [0 0 0].*(1-0.5), ...
531             'markerfacecolor', c{it1,3}.*0.3 + [1 1 1].*(1-0.3));
532         plot(xmr, vm(2)+[0 0], '-', ...
533             'linew', c{it1,2}, 'color', c{it1,3});

```



```

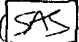
534         plot(vm(1)+[0 0], ymr, '- ', ...
535               'linewidth', c{it1,2}, 'color', c{it1,3});
536     end
537
538     drive_plot('pretty_plot', 'Annual Precipitation [mm]', ...
539               'Seasonal Precipitation [mm]', ppargs{:});
540
541     drive_plot('legend_axis', 'make');
542
543     xl      = 0.04 + [0 0.04 0.07];
544     yl      = 0.94;
545     dyl     = -0.06;
546     for it1 = 1:size(c,1)
547 %         plot(xl(1:2), yl([1 1]), '- ', 'linewidth', c{it1,2}, 'color', c{it1,3});
548         plot(mean(xl(1:2)), yl, 'o', 'linewidth', c{it1,2}, ...
549               'markersize', 10, ...
550               'markeredgecolor', c{it1,3}.*0.5 + [0 0 0].*(1-0.5), ...
551               'markerfacecolor', c{it1,3}.*0.3 + [1 1 1].*(1-0.3));
552         hold on
553         text(xl(3), yl, c{it1,4}, 'color', xlfcl);
554         yl      = yl + dyl;
555     end
556
557     switch (zclim)
558     case 'present', z      = 'Interstadial';
559     case 'monsoon', z      = 'Monsoon';
560     case 'glacial', z      = 'Glacial Transition';
561     end
562     text(0.95, 0.06, z, 'color', xlfcl, 'horiz', 'r', 'fontw', 'b', 'fonta', 'obl');
563
564     zf      = sprintf('WScor_%s%g', zclim(1:3), nsamp);
565     drive_plot('after_plot', ypr, zf, cafter{:});
566
567 end
568
569 return
570
571
572 %>>>>>>
573 function P      = P_invexp(M, S, R)
574 % calculate precipitation levels from lognormal distribution


```


```
575
576 u      = inormcdf(R);
577
578 P      = exp(M + S .* u);
```

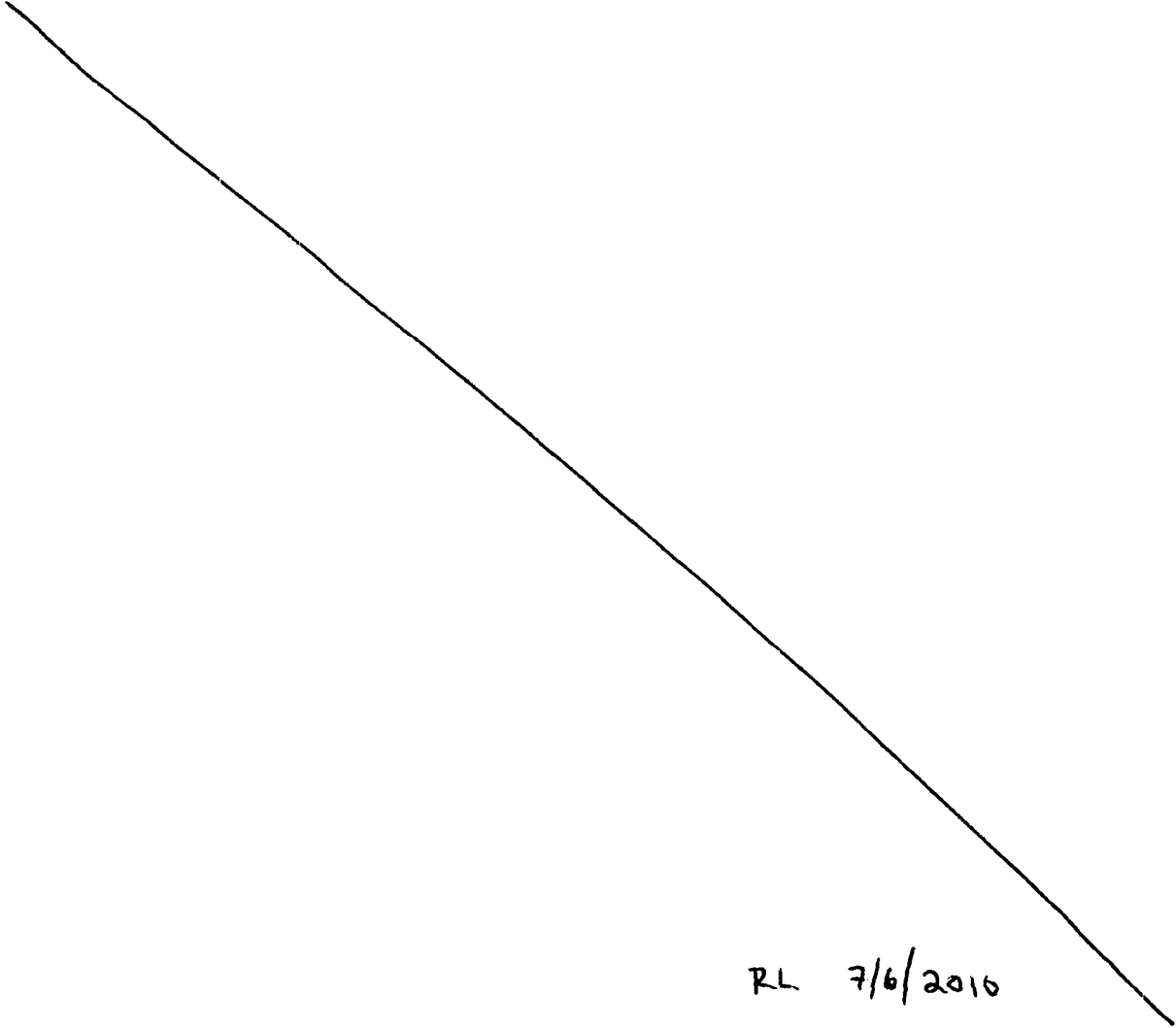
RL 7/6/2010

Final QA Information

Entries into Scientific Notebook 1005E for the period August 31, 2009, to June 30, 2010, have been made by Stuart Stothoff (; June 30, 2010).

No original text entered into this Scientific Notebook has been removed (; June 30, 2010).

The final entry date for this Scientific Notebook is June 30, 2010 and the notebook is closed (; June 30, 2010).



RL 7/6/2010

ADDITIONAL INFORMATION FOR SCIENTIFIC NOTEBOOK NO. 1005E

Document Date:	08/24/2009
Availability:	Southwest Research Institute® Center for Nuclear Waste Regulatory Analyses 6220 Culebra Road San Antonio, Texas 78228
Contact:	Southwest Research Institute® Center for Nuclear Waste Regulatory Analyses 6220 Culebra Road San Antonio, TX 78228-5166 Attn.: Director of Administration 210.522.5054
Data Sensitivity:	<input checked="" type="checkbox"/> "Non-Sensitive" <input type="checkbox"/> Sensitive <input type="checkbox"/> "Non-Sensitive - Copyright" <input type="checkbox"/> Sensitive - Copyright
Date Generated:	7/22/2010 & 7/21/2010
Operating System: (including version number)	Windows
Application Used: (including version number)	
Media Type: (CDs, 3 1/2, 5 1/4 disks, etc.)	2 CD
File Types: (.exe, .bat, .zip, etc.)	xls, zip, dbf, tex, jpg, doc
Remarks: (computer runs, etc.)	Notebook supplemental material

Description of scientific notebook #1005E contents

S. Stothoff

Scientific notebook #1005E was issued August 31, 2009, to document confirmatory analyses supplementing review of the SAR with respect to (i) climate and infiltration and (ii) unsaturated zone flow. The notebook is limited to analyses related to DOE models and does not contain conclusions regarding adequacy of DOE work or contentions that might be related to the same models.

Section 1 looks at precipitation as implemented in the DOE infiltration model. It is not cited in the SER. Some contentions are related to precipitation issues.

Section 2 looks at the DOE model for seepage and potential consequences of some of the assumptions. It is not cited in the SER. There are contentions related to seepage issues.

Section 3 contains four analyses specifically cited in the SER. There are contentions related to the subject matter for each of the four topics analyzed.